V. 122, NO. 2
MARCH 2025

ACI MATERIALS JOURNAL

A JOURNAL OF THE AMERICAN CONCRETE INSTITUTE

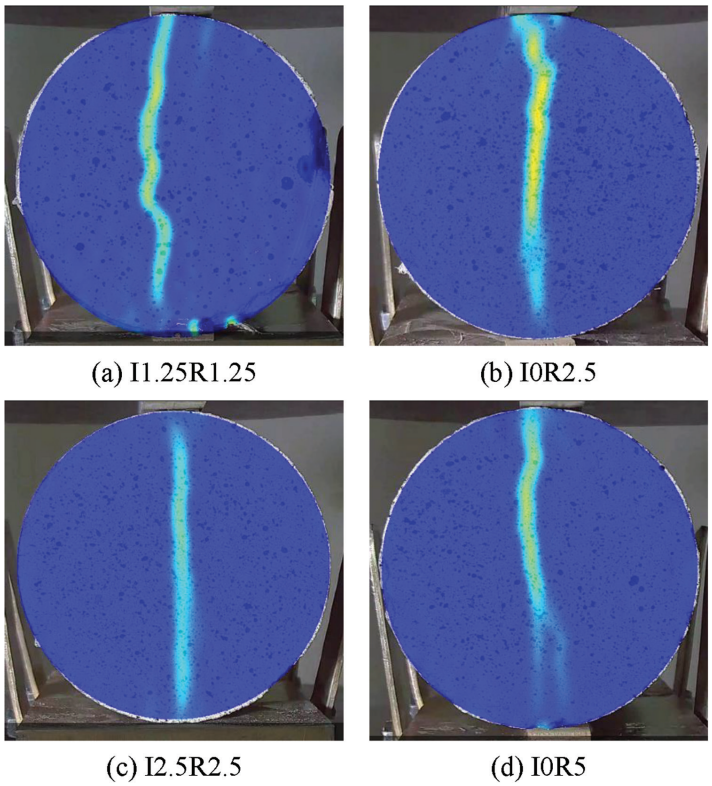

(a) I1.25R1.25 (b) I0R2.5

(c) I2.5R2.5 (d) I0R5

American Concrete Institute

CONTENTS

PRINTED WITH SOY INK

ACI MATERIALS JOURNAL

MARCH 2025, V. 122, NO. 2

A JOURNAL OF THE AMERICAN CONCRETE INSTITUTE
AN INTERNATIONAL TECHNICAL SOCIETY

The *ACI Materials Journal* (ISSN 0889-325x) is published bimonthly by the American Concrete Institute. Publication office: 38800 Country Club Drive, Farmington Hills, MI 48331. Periodicals postage paid at Farmington, MI, and at additional mailing offices. Subscription rates: $210 per year, payable in advance. POSTMASTER: Send address changes to: *ACI Materials Journal*, 38800 Country Club Drive, Farmington Hills, MI 48331.

Canadian GST: R 1226213149.

Direct correspondence to 38800 Country Club Drive, Farmington Hills, MI 48331. Telephone: +1.248.848.3700.
Website: http://www.concrete.org.

MEETINGS

APRIL 2025

13-16—2025 ICRI Spring Convention, Austin, TX, www.icri.org/event/2025-icri-spring-convention

14-16—The Masonry Society 2025 Spring Meeting, Spokane, WA, https://masonrysociety.org/event/2025-spring-meeting

14-17—International Conference on Advances in Structural and Geotechnical Engineering (ICASGE'25), Hurghada, Egypt, https://icasge.conferences.ekb.eg

21-22—2025 Slag Cement School, Houston, TX, www.slagcement.org/school

24—Concrete Durability and Structural Integrity, Beirut, Lebanon, https://acts-int.com/conferences/Concrete-Durability-and-Structural-Integrity

MAY 2025

2-3—2025 ACPA Spring Board Meeting, Nashville, TN, www.concretepumpers.com/content/2025-acpa-spring-board-meeting

4-7—2025 PTI Spring Convention, Phoenix, AZ, www.post-tensioning.org/events/conventions.aspx

4-8—2025 IEEE-IAS/PCA Cement Conference, Birmingham, AL, https://portlandcement.swoogo.com/2025CementConference

5-6—2nd International Geotechnical Innovation Conference (IGIC 2025), Jeddah, the Kingdom of Saudi Arabia, https://geotechnicalinnovationconference.com

14-16—2025 International *fib* Symposium on Conceptual Design of Structures, Rio de Janeiro, Brazil, https://fib.abece.com.br

19-21—NPCA Committee Week 2025, Indianapolis, IN, https://precast.org/events/committeeweek

20-22—Sustainable Construction in Africa 2025 (SCA25), Nairobi, Kenya, https://sca25.org

JUNE 2025

16-18—Concrete Solutions 9th International Conference on Concrete Repair, Durability and Technology, Lisbon, Portugal, https://concrete-solutions.org

16-18—*fib* Symposium 2025 – Concrete Structures: Extend Lifespan, Limit Impacts, Antibes, France, https://fibsymposium2025.sciencesconf.org

23-25—3rd International Workshop on Calcium Sulfoaluminate Cements (CSA 2025), Leeds, UK, https://eps.leeds.ac.uk/events-39/doc/3rd-international-workshop-calcium-sulfoaluminate-cements

ACI CONCRETE CONVENTION: FUTURE DATES

2025—Oct. 26-29, Hilton Baltimore & Baltimore Marriott Inner Harbor, Baltimore, MD
2026—Mar. 29-Apr. 1, Hyatt Regency O'Hare Chicago, Rosemont/Chicago, IL
2026—Oct. 11-14, Hilton Atlanta, Atlanta, GA
2027—Mar. 21-24, Caesars Palace Las Vegas, Las Vegas, NV

For additional information, contact:
Event Services, ACI
38800 Country Club Drive
Farmington Hills, MI 48331
Telephone: +1.248.848.3795
email: conventions@concrete.org

ON FRONT COVER: 122-M08, p. 24, Fig. 15—Effect of fiber content and hybridization on crack properties.

Contributions to *ACI Materials Journal*

The *ACI Materials Journal* is an open forum on concrete technology and papers related to this field are always welcome. All material submitted for possible publication must meet the requirements of the "American Concrete Institute Publication Policy" and "Author Guidelines and Submission Procedures." Prospective authors should request a copy of the Policy and Guidelines from ACI or visit ACI's website at **www.concrete.org** prior to submitting contributions.

Papers reporting research must include a statement indicating the significance of the research.

The Institute reserves the right to return, without review, contributions not meeting the requirements of the Publication Policy.

All materials conforming to the Policy requirements will be reviewed for editorial quality and technical content, and every effort will be made to put all acceptable papers into the information channel. However, potentially good papers may be returned to authors when it is not possible to publish them in a reasonable time.

Discussion

All technical material appearing in the *ACI Materials Journal* may be discussed. If the discussion is received within four months of the paper's print publication, it will appear in the issue dated ten months from this journal's date. Discussion material received after specified dates will be considered individually for publication or private response. ACI Standards published in ACI Journals for public comment have discussion due dates printed with the Standard. Discussion should be complete and ready for publication, including finished, reproducible illustrations. Discussion must be confined to the scope of the paper and meet the ACI Publication Policy.

Follow the style of the current issue. Discussions should not exceed 1800-word equivalents (illustrations and tables count as 300 words each). References should be complete. Do not repeat references cited in original paper; cite them by original number. Numbering of additional references, figures, tables, and equations should follow sequentially from the original manuscript throughout the discussion. The discusser must indicate the month, year, volume number, issue number, authors' names, and manuscript number of the original manuscript. Closures responding to a single discussion should not exceed 1800-word equivalents in length, and to multiple discussions, approximately one half of the combined lengths of all discussions. Closures are published together with the discussions.

Discuss the paper, not some new or outside work on the same subject. Use references wherever possible instead of repeating available information.

Discussion offered for publication should offer some benefit to the general reader. Discussion which does not meet this requirement will be returned or referred to the author for private reply.

Send manuscripts to:
http://mc.manuscriptcentral.com/aci

Send discussions to:
Journals.manuscripts@concrete.org

ACI MATERIALS JOURNAL TECHNICAL PAPER

Title No. 122-M07

Uncertainty of Models for Modulus of Elasticity of Concrete in Colombian Code

by Albert R. Ortiz and Julian Carrillo

The modulus of elasticity of concrete is typically estimated using numerical models that consider factors such as the compressive strength of the concrete, aggregate properties, unit weight of concrete, and water-cement ratio. The most-used equation depends on the relationship between the compressive strength of the concrete and its modulus of elasticity. However, this simplified formula may provide an inaccurate estimate of the modulus of elasticity of concrete containing different types of aggregates under varying loading conditions. More sophisticated models can be used to accurately estimate the modulus of elasticity for specific applications, such as expressions involving the unit weight of concrete. This study presents a probabilistic update to the expressions used for estimating the modulus of elasticity of concrete based on an extensive database of over 2600 experimental tests from 20 different studies. Bayesian inference was used to update the currently proposed models, allowing for the determination of the expressions representing the trends of the current database along with their associated uncertainties. The updated expressions were formulated considering either the compressive strength of concrete or both the compressive strength and the unit weight as input parameters. Expressions for estimating the modulus of elasticity, considering the aggregate's origin, were also updated. This comprehensive approach enhances the accuracy and reliability of predicting the modulus of elasticity, providing valuable insights and tools for concrete structures' design and structural reliability analysis.

Keywords: aggregates; Bayesian model updating; modulus of elasticity; uncertainty quantification.

INTRODUCTION

The modulus of elasticity of concrete (E_c) represents a key parameter for estimating the response of reinforced concrete (RC) structures because it strongly influences the structure's flexibility for serviceability and ultimate limit states.[1] Concrete is a heterogeneous material; therefore, its mechanical properties depend on many factors, such as aggregate type, water-cement ratio, curing process, and constituent material proportions, which may change with age. Therefore, the heterogeneity of concrete affects the modulus of elasticity, making it harder to provide a constant or unique value during any construction stage of a structure.

The estimation of E_c is typically derived from other concrete parameters defined in the design stage, which are practical to define, even though they may not be highly correlated.[2] Codes and guidelines from the American Concrete Institute (ACI),[3] Eurocode (European Committee for Standardization),[4] and others (Asociación Colombiana de Ingeniería Sísmica)[5] prescribe different equations to obtain the values of E_c as functions of compressive strength f_c' and concrete unit weight w_c. Materials' nominal or specified mechanical properties are required for code-based design and the structural analysis of RC buildings. Therefore, a design tool consists of deriving other concrete parameters as functions of these properties used in the design stage. In the case of concrete materials, the high variability in the modulus of elasticity is of great importance because it influences the stiffness and corresponding deformations of structures. Traditionally, the estimation of E_c follows a deterministic approach, considering single values of random variables such as the maximum concrete compressive strength, unit weight, and type of coarse aggregates.

Uncertainty quantification of the expressions used in structural engineering is essential for estimating the structures' safety. However, previously published studies have not deeply assessed the error in estimating key parameters such as E_c. These studies have been primarily focused on updating the expression as a function of experimental data sets and finding an optimal value. Other studies have included new parameters such as porosity, curing history, or chemical components of the cement.[6-11] For example, E_c strongly affects the lateral displacements or story drifts and may motivate changes in the lateral resistance system of the building, mainly in countries with high seismic demands.[12] In other types of structures different from buildings, such as railroad ties, studying the concrete modulus of elasticity is essential in terms of durability.[13]

In 2010, the current Colombian building code for earthquake-resistance construction (NSR-10[5]) introduced a new set of equations following the functional form of ACI 318-19.[3] The constants of these equations were updated by a local study in 1994 by Farias,[14] which used 180 samples from the Bogotá region. From 1994 to today, experimental data from new studies of the concrete modulus of elasticity propose different values of these constants. These studies came from different country regions and used diverse data analysis methodologies. The variability in construction methods and tests affects a generalization model of the modulus, even when the available data of these studies offer a more extensive and varied sample than that used in the equations currently proposed in NSR-10. Because of the variability in tests and methodologies, this study presents a

ACI Materials Journal, V. 122, No. 2, March 2025.

MS No. M-2023-241.R2, doi: 10.14359/51745620, received October 28, 2024, and reviewed under Institute publication policies.

general model to estimate the modulus of elasticity of the concrete involving Bayesian statistical analysis methods.

The paper has four sections. The following section ("Models for Predicting Modulus of Elasticity of Concrete") discusses the models behind the calculus of the E_c under different material parameters proposed by different codes worldwide. This section also introduces two models for updating E_c based on the current trends from experimental data. The section "Bayesian Model Updating" presents a background of the methodology for updating the models. This methodology is based on Bayesian inference (BI), the results of which, beyond a maximum likelihood, present the posterior distribution of the updated constants and the model's standard deviation. The "Database" section presents the posterior distribution of the updated parameters and proposes new models for estimating the E_c based on the total samples. Finally, the section "Results and Discussion" presents an overview of the paper and remarks on some critical conclusions regarding the calculus and uncertainties of the E_c.

RESEARCH SIGNIFICANCE

Traditionally, studies for estimating E_c focus on optimizing model parameters beyond quantifying distributions. Using Bayesian statistical analysis, this paper presents and discusses the quantification of uncertainty in expressions used to estimate the modulus of elasticity of concrete in Colombia. These equations may serve as tools for updating the new version of the building code for earthquake-resistant concrete structures in Colombia.

MODELS FOR PREDICTING MODULUS OF ELASTICITY OF CONCRETE

Design codes worldwide prescribe the parameters to be used for predicting the behavior of concrete structures. Codes proposed by Eurocode and ACI are among the most common and serve as references for other design codes in other regions of the world, such as Colombia.[15] Parameter specifications at the design stage are difficult to predict because there are no experimental data, and all information relies on models. In particular, for concrete, most parameters rely on the most common and known specified parameters, such as the maximum compressive strength, and in other cases, adding a second parameter related to the unit weight of the concrete.

The modulus of elasticity of concrete is defined in ACI 318 based on the work of Pauw in 1960.[6] The modulus is defined as the slope of the line drawn from zero stress to a compressive stress of 45% of the compressive strength and is also called the secant modulus. This value tries to approximate the elastic behavior of the material following a typical linear strain-stress relationship. The secant modulus diverges from the tangent modulus, which may also be used in the concrete industry when high strengths are considered and highly nonlinear effects may occur. Models for estimating the concrete's secant modulus of elasticity have been proposed by several authors in the last century and adopted from codes, considering the simplicity and preventing laborious experimental testing. A list of 11 equations proposed in the literature was introduced by Puttbach et al.[1] They all rely on the f_c'; however, the error, or how uncertain the equations are, is not presented.

Table 1—Values of proportional constants reported in NSR-10, MPa

Origin of aggregate	k_1	k_2
Igneous	5500	0.047
Metamorphic	4700	0.041
Sedimentary	3600	0.031
Without distinguishing	3900	0.031

The relationship between the modulus of elasticity of concrete (E_c) and the maximum compressive strength of concrete (f_c') is commonly expressed as proportional to the square root of the latter, as shown in Eq. (1). For reference purposes, this model will be called Model 1. Because the modulus of elasticity of lightweight aggregate concrete may be considerably lower than the values of normalweight concrete of comparable compressive strength, Pauw[6] also proposed that the modulus of elasticity can also be calculated considering the unit weight of concrete w_c, with an additional parameter corresponding to the cubic root of the density squared, as shown in Eq. (2). This model will be called Model 2. In both models, the terms k_1 and k_2 correspond to adjustment factors that vary according to the manufacturing conditions and characteristics of the aggregates, so it is common to find differences between regions or countries

$$E_c = k_1\sqrt{f_c'} \tag{1}$$

$$E_c = w_c^{1.5}k_2\sqrt{f_c'} \tag{2}$$

For the case of Colombia, the local code (NSR-10) proposes the value of $k_1 = 3900$ for Eq. (1) and $k_2 = 0.034$ for Eq. (2). These constants' values are applied when units of E_c and f_c' are MPa. When the origin of the coarse aggregate is discriminated, NSR-10 prescribes different values of the proportional constants k_1 and k_2. Table 1 summarizes the values reported in Section 8.5 of Section C of NSR-10.

BAYESIAN MODEL UPDATING

Beck and Katafygiotis[16] and Jaynes[17] explain specific concepts to understand the BI methodology applied in this study. Uncertainty in modeling intricate systems can be categorized as either epistemic or aleatory. Epistemic uncertainty arises from a lack of knowledge and can be reduced through enhanced data and modeling techniques, while aleatory uncertainty stems from inherent variability or randomness and is irreducible. Hence, implementing BI in structural models aims to diminish epistemic error. BI is founded on Bayes' theorem,[18] which is defined as follows

$$P(A|B) = \frac{P(B|A) \cdot P(A)}{P(B)} \tag{3}$$

where the term $P(A|B)$ represents the probability of the occurrence of an event A given that event B has occurred. In this context, Bayes' theorem is rooted in the fundamental principle where the laws of probability guide rational

belief. Within BI, probabilities represent degrees of belief rather than frequencies or long-term averages. This methodology offers a framework for updating beliefs as more experimental evidence or information becomes available, starting with prior beliefs and using Bayes' rule to derive a posterior probability distribution. Therefore, BI provides a flexible approach for complex modeling through data and inference.[19]

Bayesian methods have been extensively used in engineering for model updating and uncertainty quantification due to their capability to handle various challenges, such as missing data, hierarchical structures, nonlinear relationships, and model uncertainty.[20-23] BI, in particular, offers a flexible and robust statistical modeling approach, making it well-suited for complex engineering problems. The most common form of Bayes' theorem in this context can be expressed as

$$P(\theta|D,M_j) = \frac{P(D|\theta,M_j) \cdot P(\theta|M_j)}{P(D)} \quad (4)$$

where $P(\theta|D, M_j)$ represents the posterior probability density function (PDF) of the parameter vector θ for the model M_j, given the observation D; $P(\theta|M_j)$ denotes the prior probability distribution, representing the initial belief regarding the parameters; $P(D|\theta, M_j)$ is the likelihood of observing evidence D given the parameters θ evaluated in the model M_j; and the model evidence $P(D)$ acts as a normalizing constant, ensuring the posterior distribution integrates into one. Specifically, the term M_j represents any of the models described through Eq. (1) and (2) ($j = 1$ or $j = 2$) (recall that k_1 and k_2 are tuning parameters and are associated with Model 1 and Model 2, respectively). D represents the observations (that is, experimental data) used to update the model.

In the context of BI, the marginal likelihood becomes more complex as the number of model parameters and data points increases, resulting in computational challenges. The complexity of the likelihood function used in the model can also impact the marginal likelihood. As it does not affect the shape of the posterior distribution, it is common to work with the unnormalized posterior distribution, which is proportional to the product of the prior distribution and the likelihood function.[24]

$$P(\theta|D,M_j) \propto P(D|\theta,Mj) \cdot P(\theta|Mj) \quad (5)$$

Likelihood function definition

In the context of BI, the likelihood function is a crucial component that represents the probability of observing a specific data set given a set of model parameters. A probabilistic relationship between the model predictions and the experimental data must be assumed to formulate the likelihood function, accounting for both aleatory and epistemic uncertainty.[25] Different prediction error equations may be used for each parameter type depending on the data's characteristics. The likelihood function, typically characterized by a normal distribution, accommodates multiple observations of the same structure and comprehensively characterizes the associated errors beyond the updated parameters. Thus, the likelihood function $\phi(x)$ is defined as follows

$$\phi(x) = \left(\frac{1}{2\pi}\right)^{\frac{p}{2}} |\Sigma|^{-\frac{1}{2}} e^{-\frac{1}{2}(x-\mu)^T\Sigma^{-1}W(x-\mu)} \quad (6)$$

where μ and x represent the experimental and model data, respectively. The likelihood function reaches its maximum value when the vector x equals the vector μ. p is the dimension of the normal distribution. The weight matrix W assigns different values to the obtained information from the tests, providing relative importance to different parts of the model or measurement data. The weight matrix can reflect confidence levels in different parts of the data or measurement accuracy levels. Therefore, the Bayesian model updating approach enables a more robust estimation of the model parameters by considering the weight matrix, measurements, and information.

In the context of the updating process proposed in this work, the likelihood function allows for estimating uncertainty in the model. As there is only one type of observation, all observations of the modulus of elasticity are organized into a vector of size $n \times 2$, where n represents the number of tests ($n = 2618$), and the columns represent the specified and measured values of f_c' and E_c, respectively. Therefore, the likelihood takes the form of a normal distribution with dimension $p = 1$, as shown in Eq. (7). The standard deviation of the likelihood, denoted as σ in Eq. (7), is a parameter to be updated. This implies that the parameters being updated are $\theta = (k_1, \sigma)$ for Model 1 and $\theta = (k_2, \sigma)$ for Model 2.

$$f(x) = \frac{1}{\sqrt{2\pi\sigma^2}} e^{-\frac{(x-\mu)^2}{2\sigma^2}} \quad (7)$$

DATABASE

A total of 22 studies carried out in Colombia were identified to provide original experimental data on the modulus of elasticity of concrete. Using original data is essential as the analysis relies on data directly obtained from these experimental sources rather than relying on factors derived from other authors. The studies used to obtain experimental information for this analysis are summarized in Table 2.[26-47] Furthermore, Fig. 1 shows the relationship between the secant modulus of elasticity of concrete and the compressive strength, considering variations related to the source of the aggregates.

As shown in Table 2, data come from 11 different states in the country, including the major cities of Bogotá, Cali, and Barranquilla. Figure 2 shows a continental map of Colombia with the space distribution of samples. Regions with more samples are Bogotá, Santander, Tolima, and Valle del Cauca.

The functions found in the literature for calculating E_c are proportional to the square or cubic root of the maximum compressive strength of concrete. However, there is no substantial change in the correlation factor of the expression and the data when a linear, square, or cubic approximation obtains the modulus. For example, a poor correlation factor is seen in other expressions, such as those adopted by Eurocode, which used parameters proportional to the cubic root

Table 2—Documents used as source of original data for estimating E_c

Year	Authors	City/Origin	Data
1987	Cajas and Hernández[26]	Bogotá/unreported	77
1991	Roa[27]	Bogotá/sedimentary	348
1992	Farias[28]	Bogotá/sedimentary	180
1993	Moya[29]	Cali/sedimentary	47
1993	Vásquez and Barbosa[30]	Villavicencio/ metamorphic	60
1993	Valencia and Murcia[31]	Cali/igneous	100
1993	Padrón and de Jesús Gonzalez[32]	Cartagena/sedimentary	88
1993	Padilla José Antonio et al.[33]	Bogotá/sedimentary	532
1993	Campos[34]	Ibagué/sedimentary	139
1993	Salas and Cabrales[35]	Montería/sedimentary	69
1994	Valdez[36]	Barranquilla/ sedimentary	80
1994	Cuervo[37]	Tunja/sedimentary	100
1994	Albán and Serrano[38]	Bucaramanga/ sedimentary	240
1994	Silva[39]	Neiva/igneous	99
1994	Pimienta[40]	Valledupar/igneous	69
1994	Barreto[41]	Guamo/sedimentary	124
2001	Montejo and López[42]	Cali/igneous	35
2001	Luna and Sandino[43]	Cali/igneous	34
2006	La Rosa and Dede[44]	Santa Marta/ metamorphic	65
2012	Barragán[45]	Bucaramanga/ unreported	30
2015	Murcia[46]	Bogotá/unreported	60
2016	Pineda[47]	Bogotá/sedimentary	42

of the f_c'. Figure 3 shows the E_c samples collected in this study plotted against f_c', $\sqrt{f_c'}$, and $\sqrt[3]{f_c'}$. If a linear relationship is assumed between E_c and f_c', the correlation coefficient is 0.40. When the relationship between those parameters is transformed to the square root ($\sqrt{f_c'}$), the correlation increases to 0.42. If the cubic root is used instead, the correlation factor moves to 0.43. Beyond this discussion, the model used in this work follows the form proportional to the square root of maximum compressive strength ($\sqrt{f_c'}$).

RESULTS AND DISCUSSION

The models presented in Eq. (1) and (2) were adjusted using the Bayes model updating methodology described earlier. The updating process described previously was implemented in the PyMC library of Python, which allows users to build Bayesian models and fit them using Markov chain Monte Carlo methods.[48] The prior distributions are defined as non-informative priors, with the initial value of the chain equal to the value defined by the Colombian Code, as specified in Table 1. The posterior distributions were sampled using the importance sampling algorithm, a Markov chain Monte Carlo used in Bayesian analysis. A thousand realizations were enough for the chain to reach convergence, which was checked using the Geweke algorithm, also implemented in PyMC.

The updating process was divided into categories by aggregate origin. Each category characterizes the PDF for the constant k_1, which is obtained for the model involving only the maximum compressive strength, and k_2, which is obtained for the models that include the unit weight of the concrete and its maximum compressive strength. Along with the PDF of these constants, a posterior PDF of the standard deviation of the likelihood is also introduced. This value describes the standard deviation of the model based on the experimental data used during the updating process. Ultimately, all samples are combined to propose a general PDF

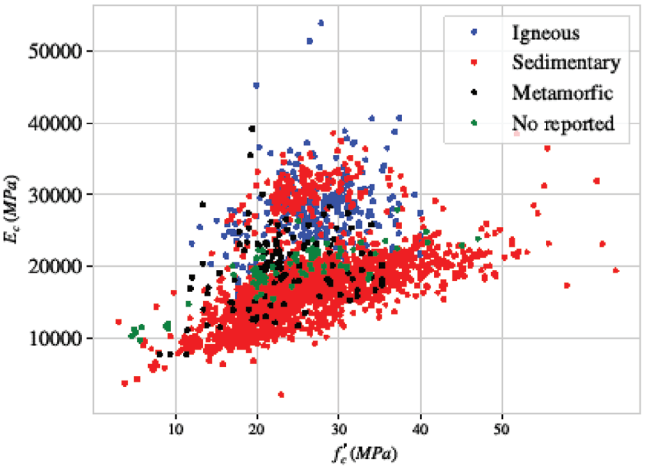

Fig. 1—Concrete modulus of elasticity (E_c) and compressive strength (f_c') for samples by source.

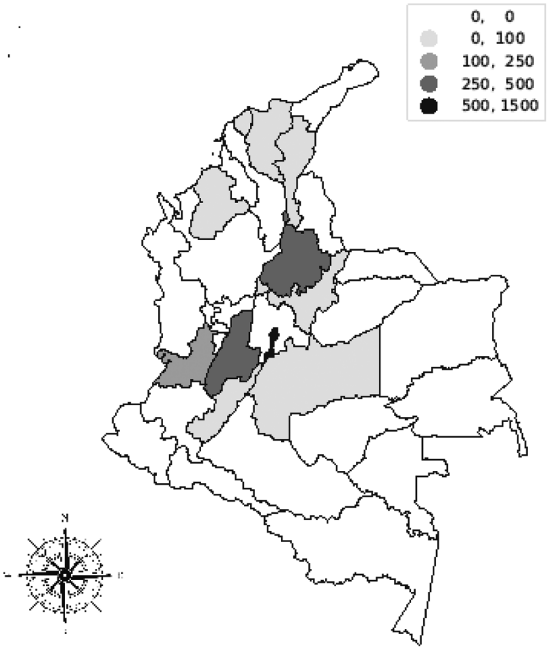

Fig. 2—Number of experimental samples per state in Colombia.

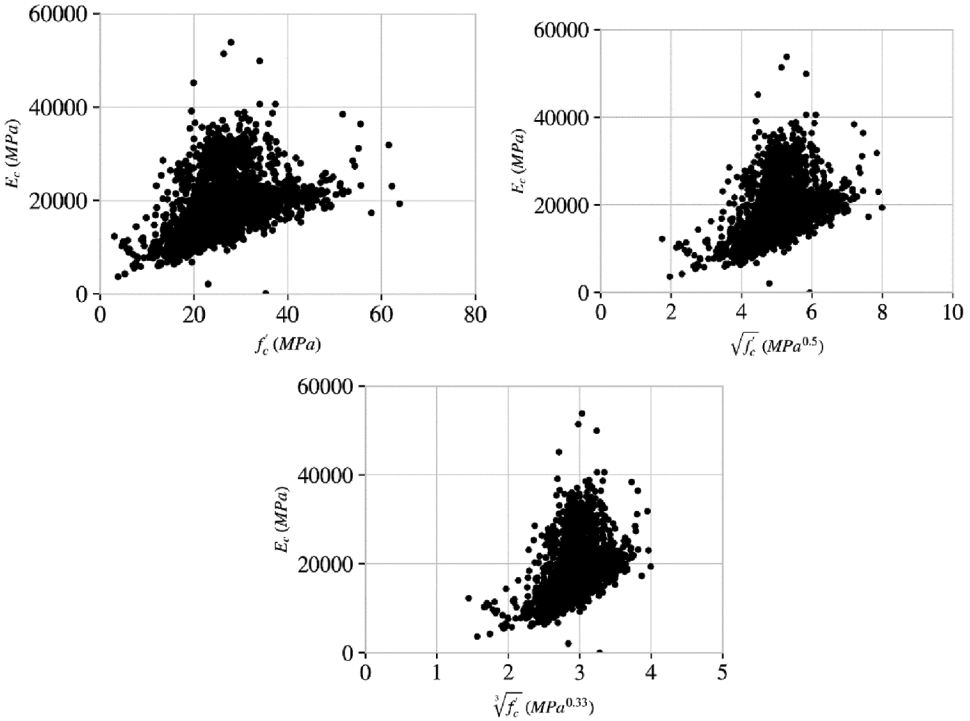

Fig. 3—Relationship between E_c *and* f_c' *for all samples used in this study: (a)* E_c, $f_c'E_c$, *and square root of* f_c'; *and (b)* E_c *and cubic root of* f_c'.

for k_1 and k_2 and a PDF for the model error disregarding the aggregate's origin.

Results by aggregate's origin

Igneous—The updating process of the E_c model based on Models 1 and 2 involved 337 samples, corresponding to 12.81% of the total samples obtained in this study. Figure 4 shows the results of the updating process for Model 1. Figure 5 shows the PDF of k_2 and σk_2, respectively, when the unit weight of the concrete is considered. The figures present the posterior distribution of the parameters and the 95% high-density interval (HDI). The 95% HDI is the range of values containing 95% of the total mass, where all points within the interval have a higher probability density than those outside.

Sedimentary—The updating process for the expression used to calculate the E_c of sedimentary aggregates involved 2225 samples, which accounted for 84.6% of the total samples obtained in this study. The results of the updating process for Model 1, which solely relies on the maximum compressive strength of concrete to estimate the E_c, are illustrated in Fig. 6(a) and (b). Figures 7(a) and (b) present the posterior PDFs of k_2 and σk_2, respectively, when the unit weight of the concrete is considered.

Metamorphic—In the process of updating the expression used to calculate the E_c of metamorphic aggregates, a total of 115 samples were involved, representing 5.16% of all the samples obtained in this study. The results of this updating process, specifically for Model 1, which exclusively uses the maximum compressive strength of concrete to estimate the E_c, are visualized in Fig. 8(a) and (b). Results including the unit weight of concrete, involved in updating Model 2, are presented in Fig. 9(a) and (b).

Results without distinction of aggregate origin

The samples introduced in Table 2 were updated using BI, disregarding the aggregate's origin. The use of a general expression without this aggregate's differentiation is popular at the design stage when suppliers of concrete are unknown and therefore the aggregate's origin is unspecified. The parameters k_1 and σk_1 are presented in Fig. 10(a) and (b). The updating process was also performed for Model 2, including the unit weight of concrete. Figures 11(a) and (b) present the posterior distributions for the model involving w_c and f_c'.

Table 3 summarizes the previous results and shows the standard deviation obtained for the model involving each aggregate type. The table includes the values of the 94% confidence interval and the mean value. The table shows that all the posteriors fit normal distributions; therefore, the maximum a posteriori (MAP) value is near the results' mean value. It is also shown in the table that the standard deviation σ of general expressions without introducing aggregates produces a MAP of 5637 and 5462 MPa for Models 1 and 2, respectively. These σ values correspond to a coefficient of variation of 24.2% and 24.0%, respectively, when concrete with $f_c' = 28$ MPa is used. In contrast, the coefficient of variation for models involving aggregate origin ranges from 16.6 to 21.8%. Equations (8) and (9) present the MAP value of constants k_1 and k_2 in the probabilistic general expressions without aggregate differentiation.

$$E_c \sim N\left(\mu = 4402\sqrt{f_c'}, \sigma = 5637\right) \quad (8)$$

$$E_c \sim N\left(\mu = w_c^{1.5}\,0.039\sqrt{f_c'}, \sigma = 5461\right) \quad (9)$$

Compared to the current regulation, the values found in this study are slightly higher than those prescribed in the

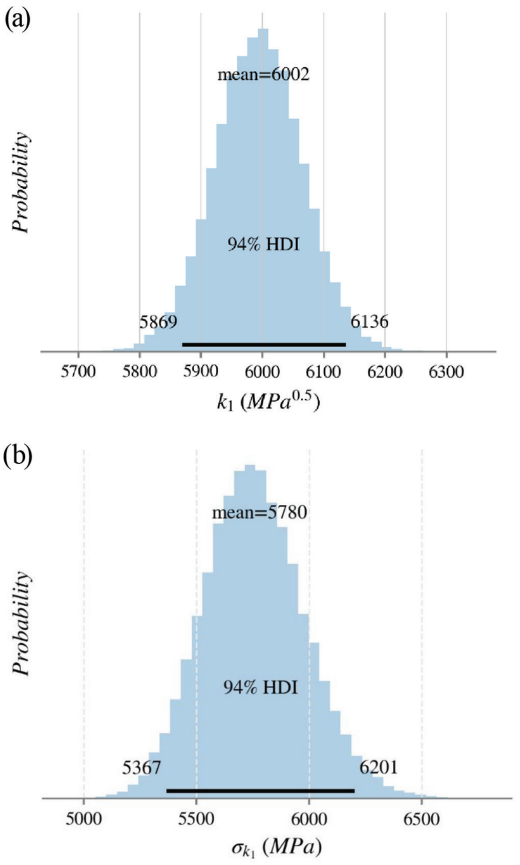

Fig. 4—Posterior PDF for: (a) k_1; and (b) σk_1 for igneous aggregates.

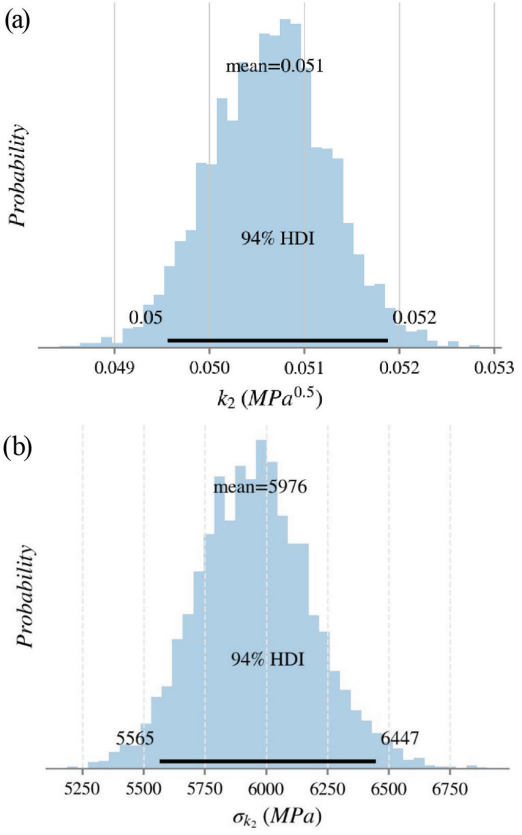

Fig. 5—Posterior PDF for: (a) k_2; and (b) σk_2 for igneous aggregates.

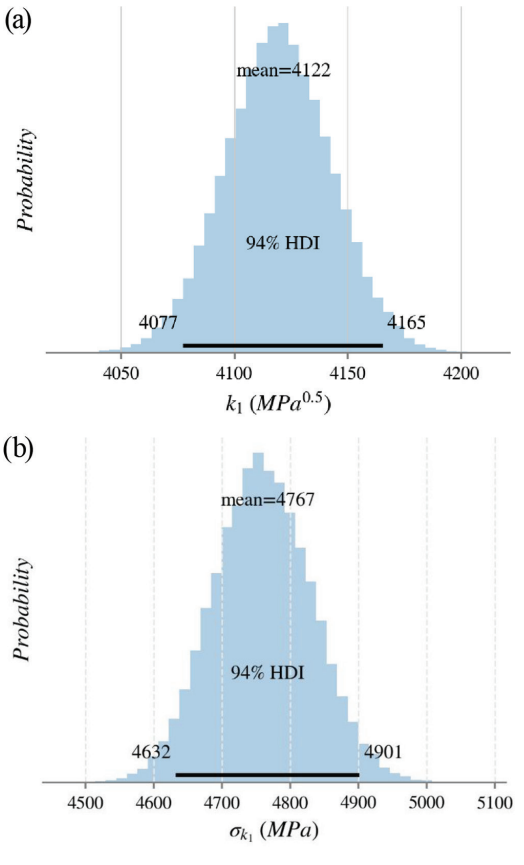

Fig. 6—Posterior PDF for: (a) k_1; and (b) σk_1 for sedimentary aggregates.

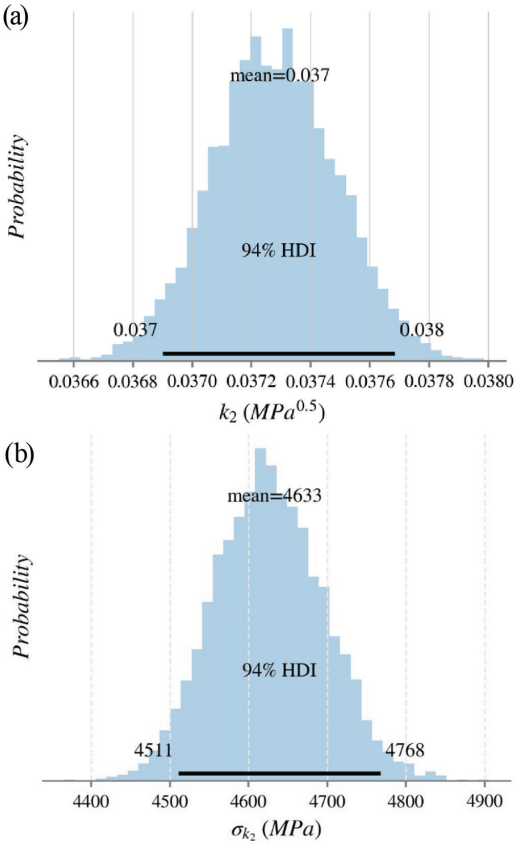

Fig. 7—Posterior PDF for: (a) k_2; and (b) σk_2 for sedimentary aggregates.

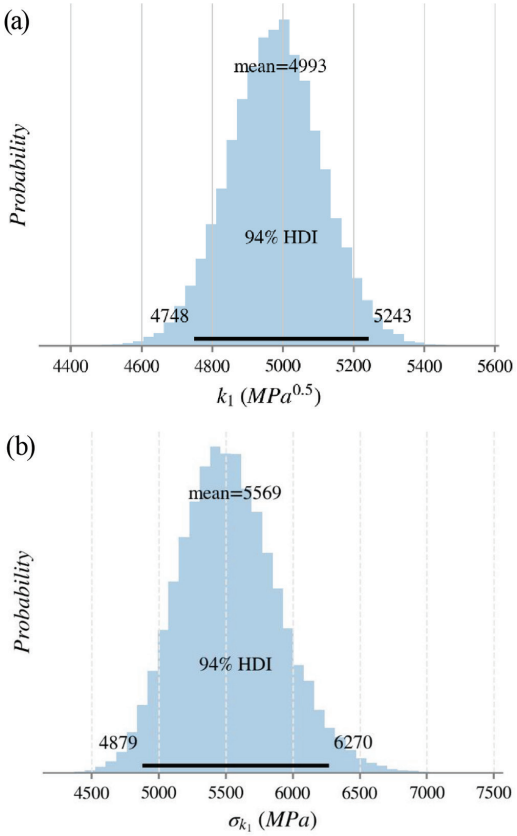

Fig. 8—Posterior PDF for: (a) k_1; and (b) σk_1 for metamorphic aggregates.

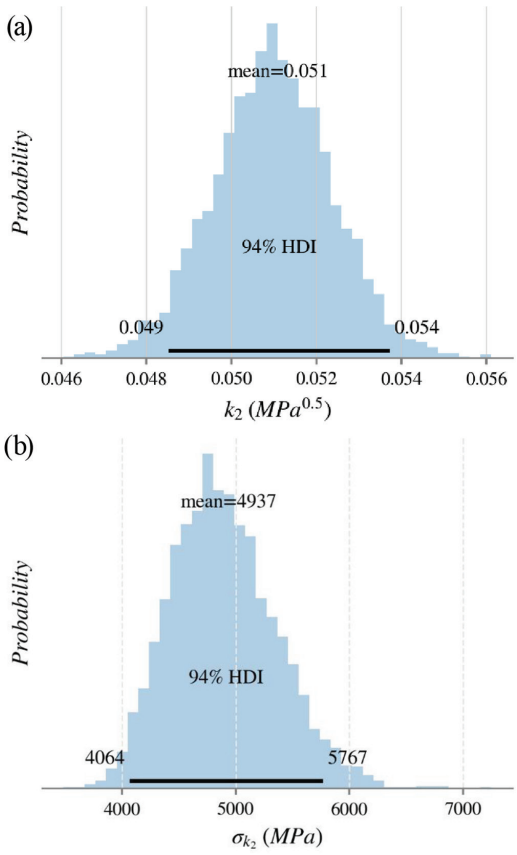

Fig. 9—Posterior PDF for: (a) k_2; and (b) σk_2 for metamorphic aggregates.

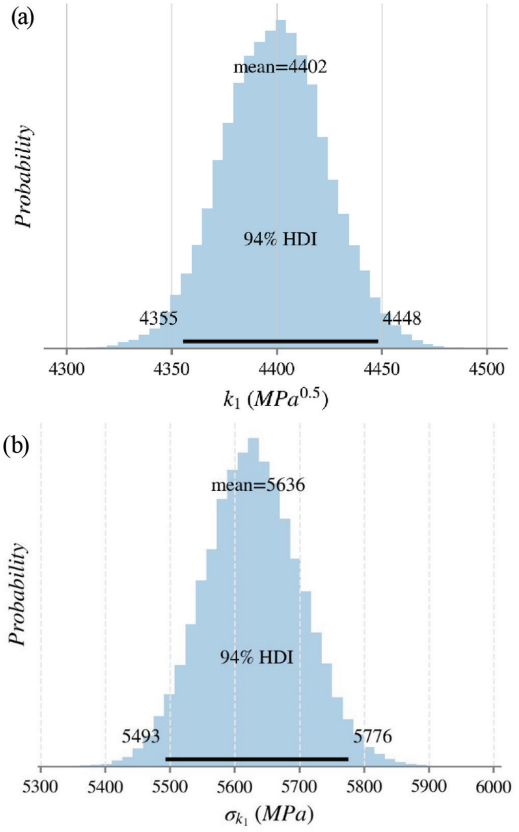

Fig. 10—Posterior PDF for: (a) k_1; and (b) σk_1 for all samples.

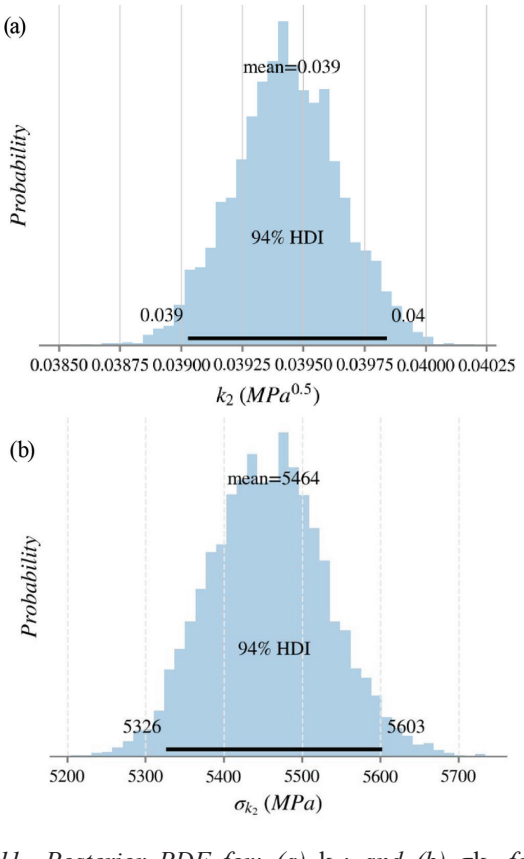

Fig. 11—Posterior PDF for: (a) k_2; and (b) σk_2 for all samples.

Table 3—Summary of constants found for different aggregates

Model parameters	Aggregate	k constant, $MPa^{0.5}$	94% confidence interval of k, $MPa^{0.5}$	σ, MPa	94% confidence interval of σ, MPa
f_c'	All	4402	[4356, 4448]	5637	[5494, 5777]
f_c', w_c		0.039	[0.039, 0.04]	5461	[5309, 5597]
f_c'	Igneous	6002	[5865, 6134]	5779	[5358, 6199]
f_c', w_c		0.051	[0.049, 0.052]	5976	[5530, 6388]
f_c'	Sedimentary	4122	[4078, 4166]	4767	[4634, 4905]
f_c', w_c		0.037	[0.037, 0.038]	4636	[4502, 4773]
f_c'	Metamorphic	4994	[4749, 5247]	5571	[4860, 6272]
f_c', w_c		0.051	[0.049, 0.054]	4947	[4097, 5846]

Table 4—Comparison of constants found in this study to current Colombian specification

Model parameters	Aggregate	MAP, $MPa^{0.5}$	NSR-10 current value, $MPa^{0.5}$	% increase to NSR-10
f_c'	All	4402	3900	4.6
f_c', w_c		0.039	0.034	14.7
f_c'	Igneous	6002	5500	9.1
f_c', w_c		0.051	0.047	8.5
f_c'	Sedimentary	4122	3600	14.5
f_c', w_c		0.037	0.031	19.4
f_c'	Metamorphic	4994	4700	6.3
f_c', w_c		0.051	0.041	24.4

current Colombian Code specifications. However, these values are still lower than the value prescribed by ACI in its current specification, where the constant's value is 4700. Table 4 compares the values found in this study with the current building codes and the percentage increment in the proposed values.

For the general expression without aggregate distinction (Model 1), Fig. 12 to 14 present the posterior predictive check of the updated models. The figures present the simulation of the variability of the E_c taking into account the k_i constant and the deviation σ of the model. The figures were obtained using three commercial concrete compressive strengths of 21, 28, and 35 MPa. The figures include the deterministic modulus calculated using expressions from ACI 318-19 and NSR-10. In all compressive strength scenarios, the 95% confidence intervals range from 10,000 to 35,000 MPa, which shows the need to understand the uncertainty beyond a deterministic value of the modulus.

CONCLUSIONS

In this work, Bayesian inference (BI) was applied to estimate the uncertainty in the models used to describe the modulus of elasticity of concrete. The analysis focused on studying the variation in the modulus of elasticity of concrete as a function of the concrete's compressive strength and weight and the coarse aggregate's origin. The analysis included studies from 1987 to 2016, comprising a total of 2618 samples taken in several cities of Colombia (Barranquilla, Villavicencio, Cali, Tunja, Cartagena, Bucaramanga, Bogotá, Neiva, Valledupar, Ibagué, Montería, Guamo, and Santa Marta).

In the general expression of the modulus of elasticity as a function of the concrete strength, the constant k_1 yields a symmetrical distribution with an average and maximum a posteriori (MAP) value of 4402 (in terms of MPa). When the unit weight is included in the equation (as in Eq. (2), k_2), the k_2 constant yields 0.039. Both values are higher than those proposed by NSR-10 but lower than those proposed by ACI 318-19. In both cases, the coefficient of variation yields approximately 25%.

Coarse aggregates affect the MAP of constants k_1 and k_2. In all three cases, aggregates from igneous origin provided a high stiffness in concrete, increasing the constant value to 6002. Otherwise, aggregates from sedimentary origin (k_1 = 4121) provide less-rigid concrete and a lower modulus of elasticity than metamorphic (k_1 = 4994) and igneous aggregates. The uncertainties associated with the expressions involving a specific aggregate's origin are lower than when using a general equation without that differentiation. It means that information regarding the aggregate's origin may reduce the uncertainty in the expressions used to estimate the concrete modulus by roughly 20%.

Including the concrete's unit weight fails in reducing the uncertainty in the expression (Eq. (2)) and produces almost the same standard deviation. This study focused on normalweight concrete from samples varying from 1510 to 3178 kgf/m^3; however, 90% of data have unit weights ranging from 2382 to 2540 kgf/m^3. The use of Model 2 in lightweight concrete must still be revised in detail for concrete outside the study's range.

Including the variability in concrete allows for estimating more realistic scenarios of the mechanical behavior of

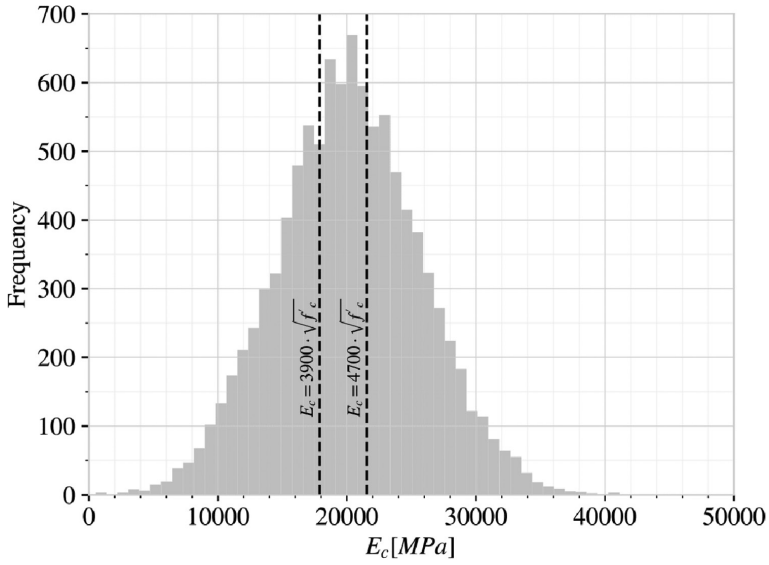

Fig. 12—Probability density function of modulus of elasticity for $f_c' = 21$ *MPa without distinction of aggregates or unit weight.*

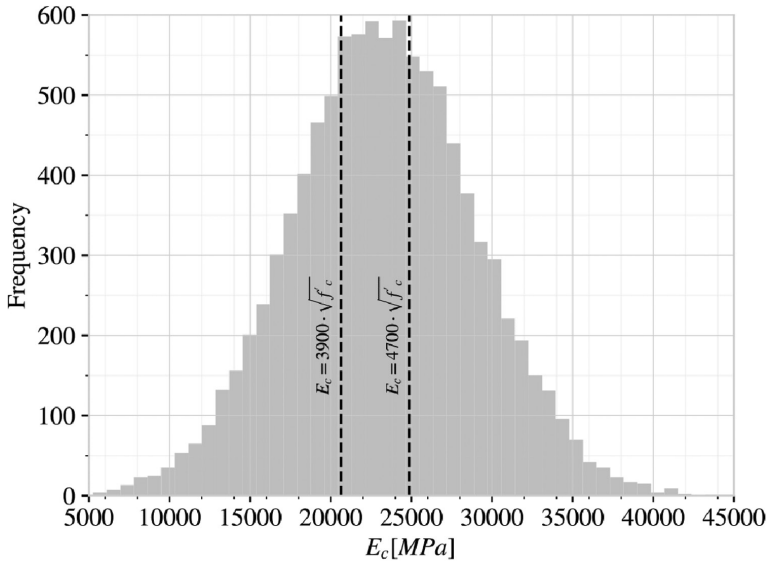

Fig. 13—Probability density function of modulus of elasticity for $f_c' = 28$ *MPa without distinction of aggregates or unit weight.*

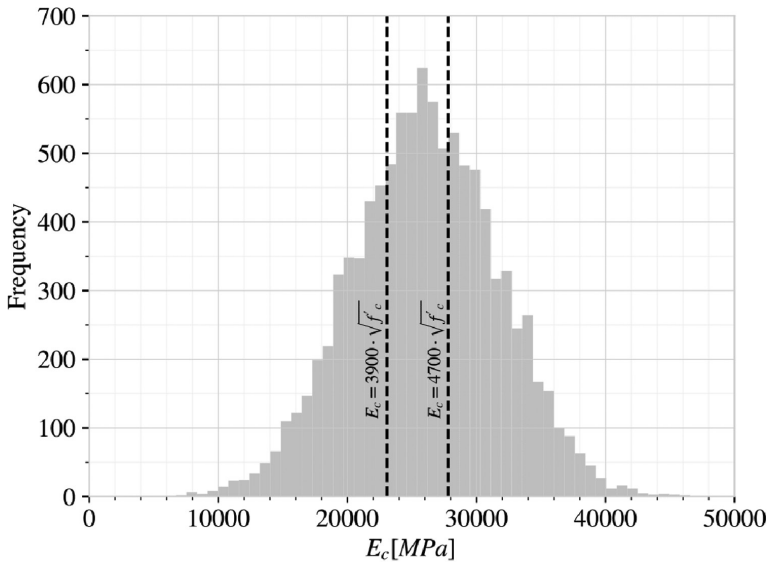

Fig. 14—Probability density function of modulus of elasticity for $f_c' = 35$ *MPa without distinction of aggregates or unit weight.*

concrete structures. The information proposed in this study could suit an extensive program for reliability analysis of structures in Colombia, leading to updating design factors and avoiding using imported factors from different latitudes that may not reproduce the behavior of Colombian materials. The proposed equations have been developed to be included in conventional force-based design, performance-based seismic design, and probabilistic risk assessment. Finally, the outcome of this research could contribute to developing more accurate models and guidelines for improving current provisions by adopting the equations proposed herein.

AUTHOR BIOS

Albert R. Ortiz *is a Professor and Chair in the School of Civil Engineering and Geomatics at the Universidad del Valle, Cali, Colombia. He is also a member of the Colombian Earthquake Engineering Research Network (CEER). His research interests include uncertainty quantification and structural reliability in the behavior and design of reinforced concrete structures.*

ACI member **Julian Carrillo** *is a Professor in the Department of Civil Engineering at the Universidad Militar Nueva Granada, Bogotá, Colombia, and a member of CEER. He is a member of ACI Committees 133, Disaster Reconnaissance; 314, Simplified Design of Concrete Buildings; 318S, Spanish Translation; 369, Seismic Repair and Rehabilitation; and 374, Performance-Based Seismic Design of Concrete Buildings; and Joint ACI-ASCE Subcommittee 445-B, Shear & Torsion-Seismic Shear. His research interests include the behavior and design of reinforced concrete structures under seismic actions.*

ACKNOWLEDGMENTS

The Universidad del Valle financially supported this work (Grant No. 21185: "Structural reliability evaluation of reinforced concrete elements subjected to bending and shear").

REFERENCES

1. Puttbach, C.; Prinz, G. S.; and Murray, C. D., "A Detailed Review of Equations for Estimating Elastic Modulus in Specialty Concretes," *Journal of Materials in Civil Engineering*, ASCE, V. 35, No. 6, 2023, p. 03123001. doi: 10.1061/JMCEE7.MTENG-14699

2. Sun, R. W., and Fanourakis, G. C., "An Assessment of Factors Affecting the Elastic Modulus of Concrete," *Structural Concrete*, V. 23, No. 1, 2022, pp. 593-603. doi: 10.1002/suco.202000553

3. ACI Committee 318, "Building Code Requirements for Structural Concrete (ACI 318-19) and Commentary (ACI 318R-19) (Reapproved 2022)," American Concrete Institute, Farmington Hills, MI, 2019, 624 pp.

4. EN 1998-1:2019, "Eurocode 8: Design of Structures for Earthquake Resistance – Part 1: General Rules, Seismic Actions and Rules for Buildings," European Committee for Standardization, Brussels, Belgium, 2019.

5. NSR-10, "Reglamento Colombiano de Construcción Sismo Resistente," Asociación Colombiana de Ingeniería Sísmica, Bogotá, Colombia, 2010.

6. Pauw, A., "Static Modulus of Elasticity of Concrete as Affected by Density," *ACI Journal Proceedings*, V. 57, No. 12, Dec. 1960, pp. 679-688.

7. Harsh, S.; Shen, Z.; and Darwin, D., "Strain-Rate Sensitive Behavior of Cement Paste and Mortar in Compression," *ACI Materials Journal*, V. 87, No. 5, Sept.-Oct. 1990, pp. 508-516.

8. Klink, S. A., "Cement and the Elastic Constants of Concrete," *Cement and Concrete Research*, V. 22, No. 5, 1992, pp. 761-768. doi: 10.1016/0008-8846(92)90099-H

9. Lydon, F. D., and Balendran, R. V., "Some Observations on Elastic Properties of Plain Concrete," *Cement and Concrete Research*, V. 16, No. 3, 1986, pp. 314-324. doi: 10.1016/0008-8846(86)90106-7

10. Popovics, S., "Verification of Relationships between Mechanical Properties of Concrete-Like Materials," *Materials and Structures*, V. 8, No. 3, 1975, pp. 183-191.

11. Kameswara Rao, C. V. S.; Swamy, R. N.; and Mangat, P. S., "Mechanical Behaviour of Concrete as a Composite Material," *Materials and Structures*, V. 7, No. 4, 1974, pp. 265-271.

12. Korkmaz, K. A.; Tekeli, H.; and Demir, F., "Determination of Elastic Moduli Effects on Storey-Drifts by Fuzzy Logic Algorithm," *Civil Engineering and Environmental Systems*, V. 26, No. 3, 2009, pp. 249-262. doi: 10.1080/10286600802080748

13. Ortiz, A. R.; Caicedo, J. M.; and Rizos, D., "Finite Element Model of High Strength Reduced Modulus High Performance Concrete," *ASME/IEEE Joint Rail Conference Proceedings*, Columbia, SC, 2016, 6 pp.

14. Farias, S., "Recopilación de la Información de los Ensayos sobre el Módulo de Elasticidad del Concreto en Diferentes Ciudades del País," MSc thesis, Universidad de los Andes, Bogotá, Colombia, 1994.

15. Tabsh, S. W., "Comparison between Reinforced Concrete Designs Based on the ACI 318 and BS 8110 Codes," *Structural Engineering and Mechanics*, V. 48, No. 4, 2013, pp. 467-477. doi: 10.12989/sem.2013.48.4.467

16. Beck, J. L., and Katafygiotis, L. S., "Updating Models and Their Uncertainties. I: Bayesian Statistical Framework," *Journal of Engineering Mechanics*, ASCE, V. 124, No. 4, 1998, pp. 455-461. doi: 10.1061/(ASCE)0733-9399(1998)124:4(455)

17. Jaynes, E. T., *Probability Theory: The Logic of Science*, Cambridge University Press, Cambridge, UK, 2003.

18. Bayes, T., and Hume, D., "Bayes's Theorem," *Proceedings of the British Academy*, V. 113, 1763, pp. 91-109.

19. Joyce, J., "Bayes' Theorem," Stanford Encyclopedia of Philosophy, 2003, https://plato.stanford.edu/entries/bayes-theorem/. (last accessed Feb. 17, 2025)

20. Denison, D. G. T.; Holmes, C. C.; Mallick, B. K.; and Smith, A. F. M., *Bayesian Methods for Nonlinear Classification and Regression*, John Wiley & Sons, Inc., New York, 2002.

21. MacLehose, R. F., and Hamra, G. B., "Applications of Bayesian Methods to Epidemiologic Research," *Current Epidemiology Reports*, V. 1, No. 3, 2014, pp. 103-109. doi: 10.1007/s40471-014-0019-z

22. Ma, Z.; Lai, Y.; Kleijn, W. B.; Song, Y.-Z.; Wang, L.; and Guo, J., "Variational Bayesian Learning for Dirichlet Process Mixture of Inverted Dirichlet Distributions in Non-Gaussian Image Feature Modeling," *IEEE Transactions on Neural Networks and Learning Systems*, V. 30, No. 2, 2019, pp. 449-463. doi: 10.1109/TNNLS.2018.2844399

23. Zhang, Y.-M.; Wang, H.; Bai, Y.; Mao, J.-X.; and Xu, Y.-C., "Bayesian Dynamic Regression for Reconstructing Missing Data in Structural Health Monitoring," *Structural Health Monitoring*, V. 21, No. 5, 2022, pp. 2097-2115. doi: 10.1177/14759217211053779

24. Zhang, E. L.; Feissel, P.; and Antoni, J., "A Comprehensive Bayesian Approach for Model Updating and Quantification of Modeling Errors," *Probabilistic Engineering Mechanics*, V. 26, No. 4, 2011, pp. 550-560. doi: 10.1016/j.probengmech.2011.07.001

25. Argyris, C.; Papadimitriou, C.; Panetsos, P.; and Tsopelas, P., "Bayesian Model-Updating Using Features of Modal Data: Application to the Metsovo Bridge," *Journal of Sensor and Actuator Networks*, V. 9, No. 2, 2020, Article No. 27. doi: 10.3390/jsan9020027

26. Cajas, F. A., and Hernández, L. M., "Evaluación del Módulo de Elasticidad Estático Secante del Hormigón," thesis, Universidad Nacional de Colombia, Bogotá, Colombia, 1987.

27. Roa, O. A., "Módulo Secante de Elasticidad del Concreto," MSc thesis, Universidad de los Andes, Bogotá, Colombia, 1991.

28. Farias, S. L., "Aproximación a la Obtención del Módulo de Elasticidad del Concreto," MSc thesis, Pontificia Universidad Javeriana, Bogotá, Colombia, 1992.

29. Moya, S. L. C., "Evaluación del Módulo de Elasticidad del Concreto para la Ciudad de Cali," thesis, Universidad del Valle, Cali, Colombia, 1993.

30. Vásquez, C. H. C., and Barbosa, I. D., "Ciclo Investigativo para la Obtención del Módulo de Elasticidad del Concreto en la Ciudad de Villavicencio," thesis, Pontificia Universidad Javeriana, Bogotá, Colombia, 1993.

31. Valencia, R., and Murcia, L. C., "Ciclo Investigativo para la Obtención del Módulo de Elasticidad del Concreto en la Ciudad de Cali," thesis, Pontificia Universidad Javeriana, Bogotá, Colombia, 1993.

32. Padrón, A. M., and de Jesús Gonzalez, J., "Ciclo Investigativo para la Obtención del Módulo de Elasticidad del Concreto en la Ciudad de Cartagena," thesis, Pontificia Universidad Javeriana, Bogotá, Colombia, 1993.

33. Padilla José Antonio, A. L.; Cortés, A.; Fernando, C.; and Polo, A. J. F., "Ciclo Investigativo para la Obtención del Módulo de Elasticidad del Concreto en la Ciudad de Bogotá (Segunda Parte)," thesis, Pontificia Universidad Javeriana, Bogotá, Colombia, 1993.

34. Campos, A. P. A., "Ciclo Investigativo para la Obtención del Módulo de Elasticidad del Concreto en la Ciudad de Ibagué," PhD thesis, Pontificia Universidad Javeriana, Bogotá, Colombia, 1993.

35. Salas, A., and Cabrales, E., "Ciclo Investigativo para la Obtención del Módulo de Elasticidad del Concreto en la Ciudad de Montería," PhD thesis, Pontificia Universidad Javeriana, Bogotá, Colombia, 1993.

36. Valdez, J. L. R. C. C. E. B., "Ciclo Investigativo para la Obtención del Módulo de Elasticidad del Concreto en la Ciudad de Barranquilla," MSc thesis, Pontificia Universidad Javeriana, Bogotá, Colombia, 1994.

37. Cuervo, G. A. S. A. A. S., “Ciclo Investigativo para la Obtención del Módulo de Elasticidad del Concreto en la Ciudad de Tunja,” MSc thesis, Pontificia Universidad Javeriana, Bogotá, Colombia, 1994.

38. Albán, R. E., and Serrano, M. F., “Ciclo Investigativo para la Obtención del Módulo de Elasticidad del Concreto en la Ciudad de Bucaramanga,” MSc thesis, Pontificia Universidad Javeriana, Bogotá, Colombia, 1994.

39. Silva, J. E. V. M. F., “Ciclo Investigativo para la Obtención del Módulo de Elasticidad del Concreto en la Ciudad de Neiva,” MSc thesis, Pontificia Universidad Javeriana, Bogotá, Colombia, 1994.

40. Pimienta, A. O. M., “Ciclo Investigativo para la Obtención del Módulo de Elasticidad del Concreto en la Ciudad de Valledupar,” MSc thesis, Pontificia Universidad Javeriana, Bogotá, Colombia, 1994.

41. Barreto, E. D., “Ciclo Investigativo para la Obtención del Módulo de Elasticidad del Concreto en el Guamo,” MSc thesis, Pontificia Universidad Javeriana, Bogotá, Colombia, 1994.

42. Montejo, L. A., and López, H., “Determinación de las Propiedades Mecánicas del Concreto Endurecido Usados en el Diseño Estructural para los Concretos Elaborados en la Ciudad de Cali con Materiales Elaborados de la Región,” MSc thesis, Universidad del Valle, Cali, Colombia, 2001.

43. Luna, D. A. O., and Sandino, C., “Determinación de las Propiedades Mecánicas del Concreto Endurecido Usados en el Diseño Estructural para los Concretos Elaborados en la Ciudad de Cali con Materiales Elaborados de la Región,” thesis, Universidad del Valle, Cali, Colombia, 2001.

44. La Rosa, H., and Dede, D. D., “Determinación del Módulo de Elasticidad para Concretos Estructurales Utilizados en la Ciudad de Santa Marta,” thesis, Universidad del Magdalena, Santa Marta, Colombia, 2006.

45. Barragán, E. A. G. B. M. F. C., “Comparación de los Módulos de Elasticidad de Concreto Normal, con el Ensayo de Compresión y el Ensayo de Flexió,” thesis, Universidad Pontificia Bolivariana, Medellín, Colombia, 2012.

46. Murcia, R. A. B., “Obtención del Módulo de Elasticidad y la Relación de Poisson, para Concretos de 21 y 28 MPa en Seis Diferentes Obras Ubicadas en la Zona Occidental de Bogotá,” thesis, Universidad La Gran Colombia, Bogotá, Colombia, 2015.

47. Pineda, J. M. O., “Determinación de la Relación de Poisson y Módulo de Elasticidad para Concretos de 21 y 28 Megapascales en Concretos de la Ciudad de Villavicencio,” thesis, Universidad La Gran Colombia, Bogotá, Colombia, 2016.

48. Abril-Pla, O.; Andreani, V.; Carroll, C.; Dong, L.; Fonnesbeck, C. J.; Kochurov, M.; Kumar, R.; Lao, J.; Luhmann, C. C.; Martin, O. A.; Osthege, M.; Vieira, R.; Wiecki, T.; and Zinkov, R., “PyMC: A Modern, and Comprehensive Probabilistic Programming Framework in Python,” *PeerJ Computer Science*, V. 9, 2023, Article No. e1516. doi: 10.7717/peerj-cs.1516

CALL FOR ACTION

ACI Invites You To...

Share your expertise

Do you have EXPERTISE in any of these areas?

- BIM
- Chimneys
- Circular Concrete Structures Prestressed by Wrapping with Wire and Strand
- Circular Concrete Structures Prestressed with Circumferential Tendons
- Concrete Properties
- Demolition
- Deterioration of Concrete in Hydraulic Structures
- Electronic Data Exchange
- Insulating Concrete Forms, Design, and Construction
- Nuclear Reactors, Concrete Components
- Pedestal Water Towers
- Pipe, Cast-in-Place
- Strengthening of Concrete Members
- Sustainability

Become a Reviewer for the ACI Journals

Then become a REVIEWER for the *ACI Structural Journal* or the *ACI Materials Journal*.

How to become a Reviewer:

1. Go to: **http://mc.manuscriptcentral.com/aci;**
2. Click on "Create Account" in the upper right-hand corner; and
3. Enter your E-mail/Name, Address, User ID and Password, and Area(s) of Expertise.

Update your Manuscript Central user account information

Did you know that the database for MANUSCRIPT CENTRAL, our manuscript submission program, is separate from the ACI membership database?

How to update your user account:

1. Go to **http://mc.manuscriptcentral.com/aci;**
2. Log in with your current User ID & Password; and
3. Update your E-mail/Name, Address, User ID and Password, and Area(s) of Expertise.

QUESTIONS?

E-mail any questions to Journals.Manuscripts@concrete.org.

American Concrete Institute

Always advancing

ACI MATERIALS JOURNAL TECHNICAL PAPER

Title No. 122-M08

Split Tensile Behavior of Recycled Steel Fiber-Reinforced Concrete

by T. Asheghi Mehmandari, M. Shokouhian, M. Imani, K. F. Tee, and A. Fahimifar

This study investigates the behavior of recycled steel fibers (RSFs) recovered from waste tires and industrial hooked-end steel fibers (ISF) in two single and hybrid reinforcement types with different volume content, incorporating microstructural and macrostructural analyses. Scanning electron microscopy (SEM) is used to study the microstructure and fractures, focusing on crack initiation in the fiber interface transition zone (FITZ). The macrostructural analysis involves using digital image correlation (DIC) software, Ncorr, to analyze the split tensile behavior of plain and fiber-reinforced concrete (FRC) specimens, calculating strain distribution and investigating crack initiation and propagation. The SEM study reveals that, due to the presence of hooked ends, industrial fibers promoted improved mechanical interlocking; created anchors within the matrix; added frictional resistance during crack propagation; significantly improved load transfer; and had better bonding, crack bridging, and crack deflection than recycled fibers. RSFs significantly delay crack initiation and enhance strength in the pre-peak zone. The study suggests hybridizing recycled fibers from automobile tires with industrial fibers as an optimum strategy for improving tensile performance and using environmentally friendly materials in FRC.

Keywords: digital image correlation (DIC); fiber interface transition zone (FITZ); recycled steel fibers (RSFs); scanning electron microscopy (SEM); split tensile behavior; sustainable fiber-reinforced concrete (FRC).

INTRODUCTION

Concrete is widely recognized as the most popular construction material on a global scale. The exponential rise in the use of concrete can be attributed to the expansion of infrastructure projects and the corresponding expansion of the population.[1] One of the main disadvantages of concrete is its relatively low tensile strength compared to its compressive strength. This observation suggests that concrete exhibits a tendency to crack and fail when subjected to tensile stress, while demonstrating resilience against compression. For the past 30 years, experimental and computational evidence has shown that fiber-reinforced concrete (FRC) improves reinforced concrete (RC) constructions. Energy-absorbing FRC weighs more than normal concrete. Continuous aligned fibers[2] and randomly oriented short fibers[3,4] have improved cementitious material's brittle tensile qualities in academic studies. Annually, simple cement-based composites need 60 million tons of fibers.[5] Using waste-based fibers not only reduces environmental impacts, but also lowers construction costs. Numerous studies have been conducted to evaluate the viability of incorporating waste materials derived from diverse sources into concrete.[6-10] In this context, it has been observed that recycled steel fibers (RSFs) derived from automobile tires have demonstrated a significant enhancement in the mechanical characteristics and impact resistance of reinforced mixture compositions. This increase can be attributed to the rehardening ability of RSFs under stress, as evidenced by Caggiano et al.[11,12] and Martinelli et al.[13] The significant environmental advantages of recycled tire steel fiber (RTSF) are supported by empirical evidence from life cycle assessment (LCA) studies,[14] which indicate that the manufacturing process of RTSF consumes approximately 5% of the energy required for producing conventional industrial steel fibers (ISFs). Therefore, the use of RSFs obtained from tires for reinforcing concrete not only leads to a reduction in construction expenses and adverse environmental effects but also provides substantial enhancements in the tensile behavior of plain concrete. The use of fiber hybridization has been identified as an effective method for enhancing the performance of concrete in comparison to the use of a single fiber type or size.[15-18] This occurs because of the well-mixed design and selection of fibers. Furthermore, understanding crack initiation and propagation in construction materials is directly linked to the effectiveness of fiber hybridization in enhancing concrete performance. Understanding the processes by which cracks initiate and propagate in construction materials is crucial for ensuring the structural stability and long-term resilience of various infrastructures.[19,20]

Microcracks play a crucial role in the initiation of crack formation, demonstrating the capacity to undergo fast expansion during seismic events or gradual growth over an extended period. It is worth mentioning that even cracks leading to sudden structural failure arise from these microscopic cracks. Moreover, the process of crack expansion indicates a continuous progression, whereby a minuscule microcrack that is first undetectable progressively transforms into a significant crack, possessing the potential to do extensive harm to structures of considerable magnitude.[19,21-25] The conventional belief suggests that the initiation of cracks in concrete commonly occurs at the interface where aggregates and the cement paste meet. Indeed, the separation of aggregates from the cement paste frequently occurs prior to their actual fragmentation.[26] The interfacial transition zone (ITZ) is a spatial region situated at a distance of approximately

ACI Materials Journal, V. 122, No. 2, March 2025.

MS No. M-2023-293.R4, doi: 10.14359/51744375, received October 9, 2024, and reviewed under Institute publication policies.

30 to 50 µm from aggregates. The presence of a significant number of microcracks in this particular zone necessitates the implementation of measures to effectively delay the detachment between the cement paste and aggregates.[27] The fiber interface transition zone (FITZ) is a strip present in FRC, roughly 30 µm wide, surrounding the fibers.[27] The present region is prone to the occurrence of separating between the concrete matrix and the steel fibers, which may occur prior to the failure of the material. The FITZ plays a crucial role in the study of microcracks that form at the interface between fibers and surrounding concrete material. Acquiring a thorough comprehension of this region holds considerable significance in the field of FRC research, because the occurrence of fracture formation inside the FITZ frequently leads to concrete failures and subsequent elimination of fibers.[28-30] Scanning electron microscopy (SEM) is employed for the examination of the microstructure and morphology of the ITZ and FITZ in FRC. It offers valuable insights into the bond quality, porosity, and interface properties among aggregate particles, fibers, and cement paste, hence enhancing comprehension of the performance of FRC. The principal role of fibers is to serve as structural components that span over cracks and redirect the concentrated tensile stresses, which have the potential to cause cracking in concrete toward alternative regions within the composite material. As a consequence, there is a greater frequency and distribution of fracture, which is visually distinguished by improved ductility and a higher quantity of smaller cracks within the composite material. The deformation mechanism of a fiber is dependent upon the bond between the fiber and the matrix. This mechanism can manifest in two ways: the fiber being pulled out from the matrix or, less frequently, the fiber experiencing rupture.[31] To obtain a comprehensive understanding of plain and FRC specimens' tensile behavior, it is imperative to examine it from a fracture mechanical perspective. Consequently, in this study, the split tensile test for concrete was thoroughly evaluated, with a primary focus on fracture mechanics principles. To ensure accurate analysis of crack initiation and propagation during the test, digital image correlation (DIC) technology was employed. DIC technology offers a non-contact, full-field measurement approach, enabling precise tracking and analysis of surface deformations and crack development in brittle materials.[32-34] By capturing high-resolution images during the split tensile test, DIC algorithms effectively correlated displacement and strain fields between consecutive frames, facilitating accurate crack detection and monitoring. The use of DIC in this study aimed to offer comprehensive insights into crack initiation and propagation, encompassing vital parameters such as crack opening, crack length, and strain evolution. These parameters hold significant importance in gaining insights into the failure mechanisms of brittle materials subjected to tensile loading.

RESEARCH SIGNIFICANCE

This study investigates the split tensile behavior of concrete reinforced with a hybrid mixture of recycled and industrial steel fibers. Using DIC technology, it examines crack initiation and propagation under the split tensile test, enhancing understanding of crack behavior and failure mechanisms. The dual-level analysis of microstructural properties and macroscopic performance aims to improve material split tensile strength and sustainability. The findings highlight the practical application of hybrid FRC for eco-friendly, cost-effective construction solutions. This research contributes to FRC development, providing insights into creating resilient and sustainable infrastructure and optimizing material properties.

Table 1—Chemical, physical, and mechanical properties of cement used

Chemical properties	CaO	63.7%
	Free CaO	1.19%
	SiO_2	20.46%
	Al_2O_3	5.57%
	Fe_2O_3	3.65%
	MgO	1.32%
	SO_3	1.84%
	K_2O	0.32%
	Na_2O	0.49%
	IR	0.46%
	LOI	0.95%
Physical properties	Initial setting time	195 min
	Final setting time	230 min
	Specific gravity	3.05 g/cm^3
	Belin number	2580 cm^2/g
	Passing of 45 µm sieve	88.32%
Compressive strength, MPa	After 7 days	50.6
	After 28 days	61.6

Note: LOI is loss on ignition; IR is insoluble residue.

EXPERIMENTAL INVESTIGATION

Material properties

The present investigation employed portland cement as the primary material, using CEM I 52.5 N,[35] which was manufactured by a cement industry company located in southwestern Iran. The provided information in Table 1 outlines the characteristics of the cement as provided by the manufacturer. The high-range water-reducing admixture (HRWRA) used in this study was a polycarboxylic ether-based product. It was added to the mixture in amounts ranging from 0.2 to 2% by weight of cementitious material, in accordance with the manufacturer's recommendations. All the mixtures consisted of crushed limestone aggregate, with a maximum particle size of 19 mm. The material was obtained from a mine located in Raziabad, Tehran. ASTM C136/C136M-19 was employed to conduct a sieve analysis of the sediments.[36] Two types of fibers were used in the investigation, including industrial five-dimensional hooked-end steel fibers (ISFs) and RTSF. Figure 1 displays the raw materials employed in the production of concrete within the scope of this study. Additionally, Table 2 provides information regarding the geometric and strength characteristics of the fibers used. It

Table 2—Geometrical and mechanical properties of fibers[37]

Type	Length, mm	Diameter, mm	Aspect ratio (length/diameter)	Tensile strength, MPa	Specific gravity	Elastic modulus, GPa
ISF	35	0.4	87.5	2830	7.8	210
RSF	20 to 40	0.35	57 to 114	3120	6.9	210

Table 3—Mixture proportions of control and FRC mixtures, kg/m³

Mixture description	C	W	CS	FS	ISF	RSF	HRWRA
PC	500	174.36	671.2	1013.4	0	0	2.8
$I_{2.5}R_0$	500	174.36	671.2	1009.5	19.5	0	2.8
$I_{1.25}R_{1.25}$	500	174.36	671.2	1009.5	9.75	8.63	2.8
$I_0R_{2.5}$	500	174.36	671.2	1009.5	0	17.25	2.8
I_5R_0	500	174.36	666.2	1005.8	39	0	3.3
$I_{2.5}R_{2.5}$	500	174.36	666.2	1005.8	19.5	17.25	3.3
I_0R_5	500	174.36	666.2	1005.8	0	34.5	3.3

Note: C is cement; W is water; CS is coarse sand; FS is fine sand.

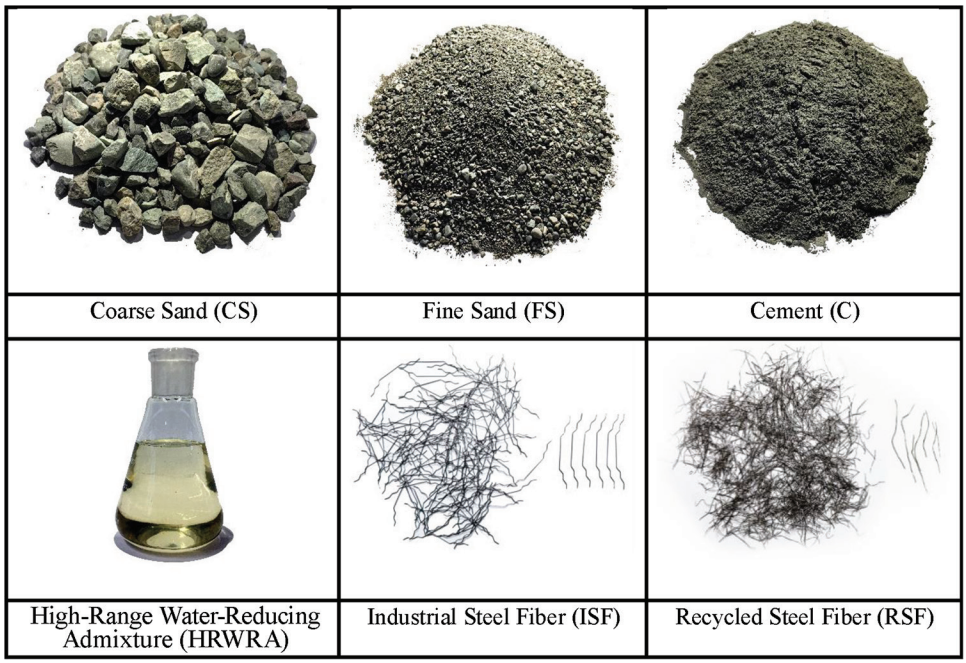

Fig. 1—Raw materials used.

is worth noting that these characteristics are provided by the manufacturer.[37] Moreover, the observed difference in specific gravity between ISF (7.8) and RTSF (6.9) can be attributed to the recovery process of RSFs from waste tires. During this process, some fibers acquire a very thin plastic coating, which reduces their specific gravity.

Mixture design

Table 3 presents the mixture ratios for seven different concrete mixtures. These mixtures include plain concrete (PC), four single-type fiber-reinforced mixtures, and two hybrid types of fiber-reinforced mixtures. Hybrid mixtures in this study are mixtures that contain similar volumetric proportions of both RSF and ISF. The water-binder ratio (w/b) for all mixtures is 0.340. In this study, the fiber content in the reinforced mixtures is either 0.25% or 0.5% V_f, representing low-volume and high-volume percentages, respectively. The term PC is used to refer to plain concrete, which is a mixture design that does not contain any fibers. Other mixtures incorporate either ISF, RTSF, or a combination of both. Additionally, out of the six mixture designs analyzed, three of them are characterized as having a low fiber content, with only 0.25% fiber used. Conversely, the remaining three mixture designs are classified as having a high fiber content, with 0.5% fiber incorporated into these combinations. Six different mixtures were prepared to study the effects of fiber content and reinforcement type. Two fiber contents were used for each of two reinforcement types (hybrid and single-fiber), resulting in six unique mixtures. This allows for a direct comparison of the effects of fiber content and reinforcement approach. It is important to acknowledge that the percentages mentioned are volumetric in nature. In addition, it should be noted that the letters I and R used in the descriptions of the mixtures correspond to

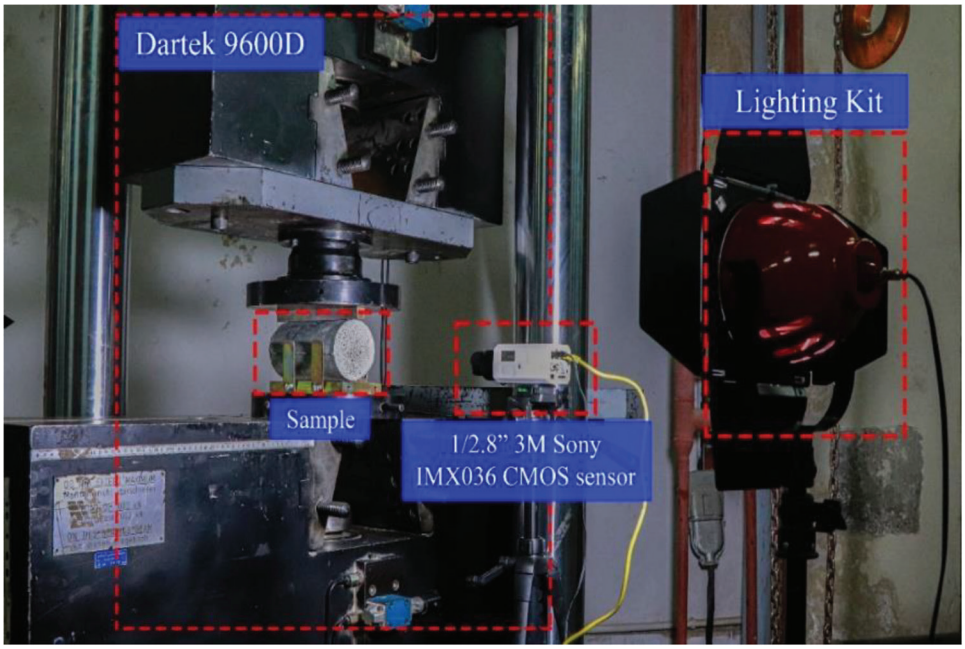

Fig. 2—Test setup and DIC equipment.

industrial and recycled fiber, respectively. Furthermore, the numerical value assigned to each letter (for example, 0, 1.25, and 2.5) represents the proportion of fiber in the mixture, expressed as a tenth of a percent. An example of this is the composition "I1.25R1.25," which combines recycled and industrial fibers. This composition includes 0.125% of RTSF and 0.125% of ISF, resulting in a total volume percentage of 0.25%. Hence, this combination is sometimes referred to as being low in fiber. The objective of this study was to assess the split tensile strength properties of concrete. This was achieved by conducting laboratory experiments using plain and FRC mixtures containing concrete aggregates of standard size. HRWRA was incorporated into concrete mixtures at a dosage range of 0.5 to 1% of the weight of cement. Laboratory-controlled samples of concrete were made using a pan mixer. The target tensile strength for samples with 0.25% and 0.5% fiber content was set at 5 and 6 MPa, respectively. Among samples with the same fiber content, single-ISF was expected to outperform hybrid and single-RSF in terms of mechanical properties.

To evaluate the split tensile strength and slump characteristics, standardized concrete mixtures were prepared in accordance with the specifications indicated in Table 3 within controlled laboratory conditions. To assess the workability of plain concrete and FRC combinations, experiments were conducted to measure the unit weight and slump of the fresh concrete.[38,39] Cement and fine and coarse aggregate were initially combined in a dry condition for approximately 2 minutes to make the concrete mixtures. The HRWRA additive and water were then added to the concrete mixture for 3 minutes. Finally, the fibers were added to the mixtures, and the mixing procedure was repeated for another 3 minutes to ensure that the fibers were well incorporated into the concrete. The freshly mixed concrete was then placed in cylinder molds and subjected to external vibration using a shake table. After being inserted into the molds for 24 hours, the extracts were cured in water at 20 ± 2°C for 28 days. Each mixture specimen was made and evaluated for split tensile strength using three cylinder specimens (200 x 100 mm). Furthermore, all the tests were carried out using the servo-control devices available in the Rock Mechanics Laboratory at Amirkabir University of Technology. As a result, specimens were subjected to the split tensile strength test under controlled laboratory circumstances.

Test methods

DIC measurement—DIC, an optical, high-precision, and non-contact measurement technique, was used to observe the formation and propagation of cracks and to back-calculate the strain distribution throughout the specimen. To achieve high-quality digital images and accurate results, specific sample preparation techniques were employed. To enhance visibility and facilitate observation, the cross section of the split tensile test specimen was randomly marked with contrasting black and white regions. Moreover, sections of compression and tension specimens were sprayed in a random pattern. A professional digital camera with a high-resolution complementary metal-oxide semiconductor (CMOS) camera, a 3-megapixel sensor, 1/2.8 in. format, and high resolution was fixed on a sturdy tripod to minimize disturbances. The camera operated at 30 frames per second (FPS) with a resolution of 2048 x 1536 pixels to capture the entire loading process. For DIC measurements, images were extracted at a rate of two per second, with critical moments (such as peak load moments) having more than two images per second extracted. Despite conducting all tests in daylight, a projector with adjustable light intensity, as shown in Fig. 2, was used to ensure consistent light contrast. Video recording began simultaneously with the test, capturing the entire loading process from start to finish.

The common parameter in both experimental and DIC methods is time. By using the loading speed of the test setup,

Fig. 3—SEM device.

the correlation between time and each point on the load-deflection curve was determined. Then, using the camera's FPS, the correlation between time and each extracted image was established. This allows for the connection between the load-deflection curve, and subsequently the stress-strain curve, and each image. It is worth noting that the strain of each sample at any moment equals the ratio of deflection to sample diameter (100 mm).

After the test, the video was edited with editing software, and 200 pictures were extracted from each video for analysis. The resulting digital images were analyzed using Ncorr,[40] a free, high-quality, and flexible DIC software, to calculate the strain distribution and investigate the formation and propagation of cracks.

SEM analysis—SEM contains various sequential steps. The initial step in preparing the FRC sample involves the use of cutting, polishing, or fracturing techniques to expose the specific surface of concern. Subsequently, a thin conductive layer is applied to cover the sample. Afterward, the prepared sample is fixed onto a sample holder or stub and put into the SEM chamber. To ensure the stability of the electron beam, the chamber is exposed to a high level of vacuum evacuation. The generation of an electron beam involves the use of an electron source, such as a tungsten filament or a field-emission gun (FEG), which is then directed onto the surface of the sample. The interaction between the electron beam and the sample leads to the emission of secondary electrons, backscattered electrons, and characteristic X-rays. These emissions offer valuable insights into the surface morphology, composition, and crystal structure of the sample. This procedure facilitates the study of crack patterns and the interaction between concrete and fibers. Through the application of SEM images, scholars have the ability to study the courses taken by cracks as they propagate; identify occurrences of fiber pullout, debonding, and bridging events; and acquire valuable knowledge regarding the mechanical characteristics shown by FRCs. The detectors present within the SEM are responsible for collecting the emitted electrons or X-rays. These collected particles are subsequently transformed into electrical signals, which are then shown on a screen for observation. The sample surface is imaged at a high resolution, enabling a collection of detailed visual information. Additionally, specialized software facilitates the execution of quantitative analysis of the collected images. SEM testing was performed on all six FRC samples, with three images taken from different locations on each sample. Figure 3 depicts the approach employed for doing SEM analysis.

EXPERIMENTAL RESULTS

SEM analysis result

FITZ—The FITZ is a crucial region within FRC, approximately 30 µm wide around the surface of each fiber, where the bonding and interaction between the fibers and the matrix material occur.[22] The transitional microstructure possesses distinctive characteristics that set it apart from both the surrounding bulk concrete and the fibers themselves. The features and behaviors of the FITZ can have a substantial impact on the overall performance of FRC. Gaining a comprehensive understanding of the properties and behavior of the FITZ is crucial to enhancing the structural design and performance of FRC. The presence of the FITZ in this investigation is visually depicted in Fig. 4.

The FITZ contains the phenomenon known as concrete-fiber detachment, which denotes the act of separation or detachment happening between the concrete matrix and the embedded fibers. The phenomenon of detachment might manifest over the whole length of the fibers, suggesting a breakdown in the bonding between the concrete and the fibers. Fibers are usually mixed into concrete as they improve its mechanical characteristics, notably its tensile strength and resistance to cracking. Nevertheless, the detachment of concrete and fibers in the FITZ may happen as a result of multiple variables, including stress concentrations, differential characteristics, and fiber pullout. The phenomenon of

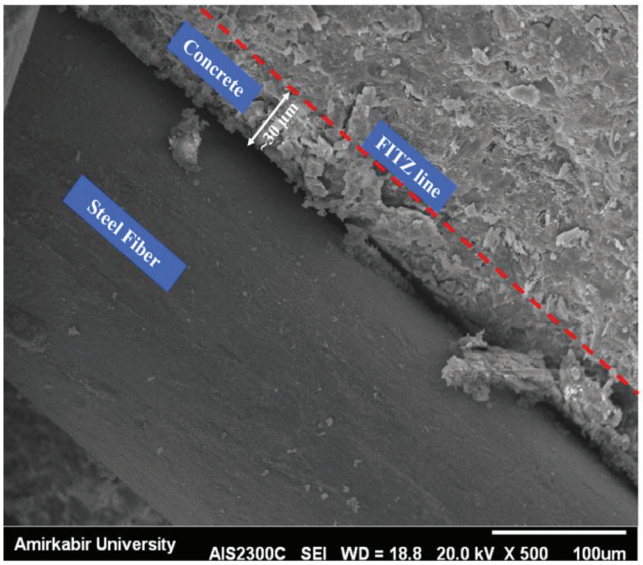

Fig. 4—Fiber interface transition zone (FITZ).

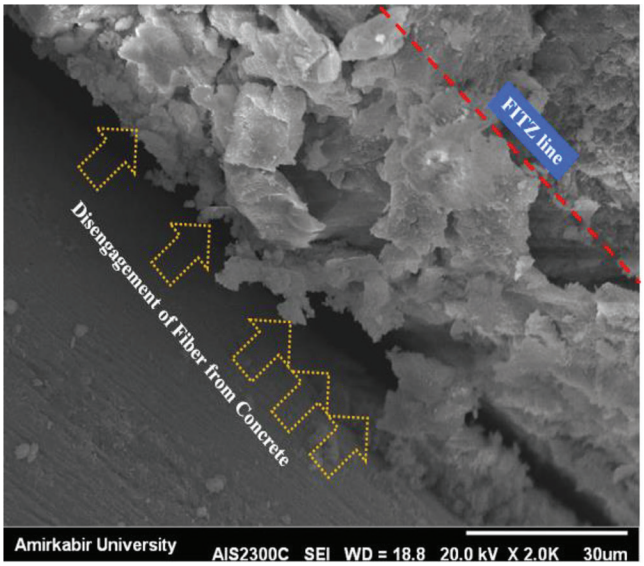

Fig. 5—Disengagement of fiber from concrete in FITZ.

detachment can be visually identified as cracks or gaps that exist between the individual fibers and the encompassing matrix of concrete. SEM pictures obtained from the FITZ reveal the presence of cracks that have developed in the vicinity of the steel fibers, suggesting a deterioration of the bonding connection in those particular areas. The separation of concrete fibers within the FRC in the FITZ has potential consequences for the overall performance and durability of the material. The load-transfer mechanism between the fibers and the matrix may be impacted, potentially leading to a decrease in the efficacy of the fiber reinforcement. Moreover, the existence of detached fibers can potentially facilitate the penetration of moisture, hence resulting in degradation and diminished durability. The occurrence of an inadequate bond between the fibers and the concrete is evident, as illustrated in Fig. 5. This figure offers a clearer illustration of this disengagement. When conducting a comparison between recycled and industrial steel fibers in relation to FITZ crack characteristics, various elements must be taken into consideration.

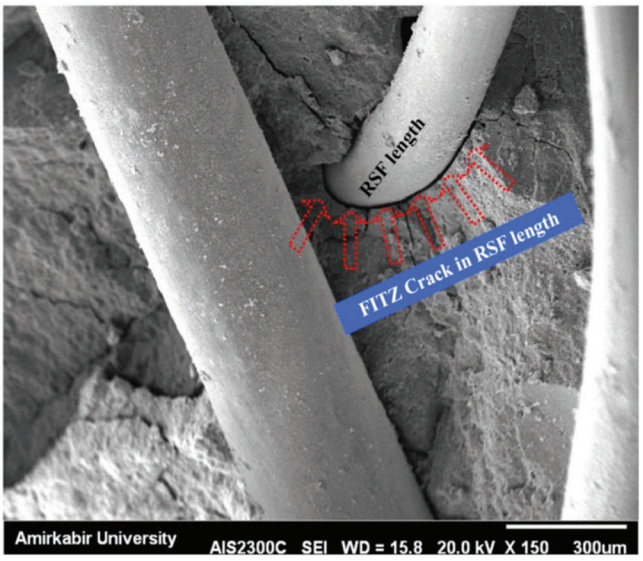

Fig. 6—Length of RSF.

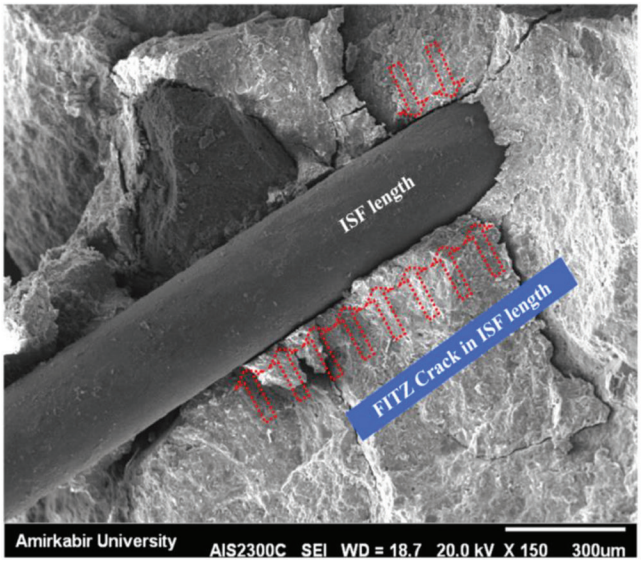

Fig. 7—Length of ISF.

These criteria include FITZ bonding and debonding, FITZ crack depth, FITZ crack shape, and FITZ crack length.

FITZ bonding and debonding—The bonding and debonding of fibers are defined and assessed along their straight length and at their hooked ends. It is notable that hooked ends are only ISF's feature. The results of the SEM study, as depicted in Fig. 6 and 7, indicate that there is not a significant difference in the bonding of fibers along their length in the FRC specimens. Nevertheless, when conducting a comparative examination, it was shown that the industrial fibers, which were supplied with ISF's hooked ends, displayed a notable improvement in bonding within their FITZ. This finding can be observed in Fig. 8 and 9. The presence of increased bonding significantly influenced the crack morphology within the FITZ, leading to apparent patterns that differed from those observed in specimens containing recycled fibers. The inclusion of hooked ends inside the industrial fibers played an essential part in promoting efficient crack bridging and enhanced crack

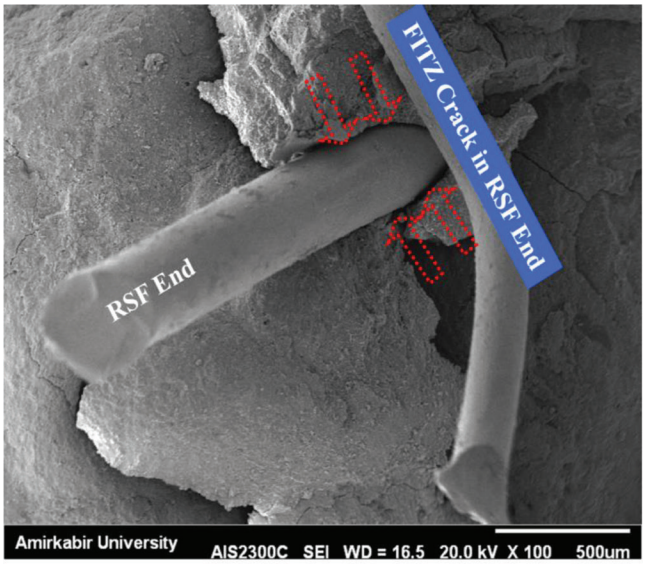

Fig. 8—End of RSF.

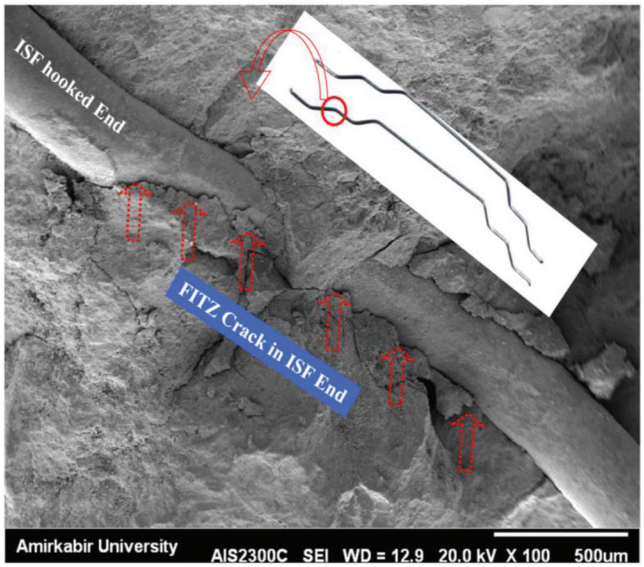

Fig. 9—End of ISF.

deflection, ultimately resulting in a more controllable and uniform crack pattern. The enhanced crack control within the FITZ is of significant value for the mechanical properties and durability of FRC structures. It significantly improves load transfer, mitigates crack propagation, and contributes to overall enhanced structural performance and increased resistance to crack growth. Furthermore, the impact of the presence of hooked ends in industrial fibers on crack behavior encompasses a wide range of factors. First, they serve as anchors within the matrix, effectively connecting and dispersing stresses along the surfaces of propagating cracks. This phenomenon facilitates the closing of cracks and diminishes crack opening, therefore improving the crack resistance and upholding the structural integrity of the FRC. In addition, the existence of hooked-end fibers alters the direction of crack propagation and introduces crack tortuosity, leading to deviations from linear crack trajectories and alignment with the fiber contours. Crack tortuosity describes the intricate and winding path a crack follows as it spreads

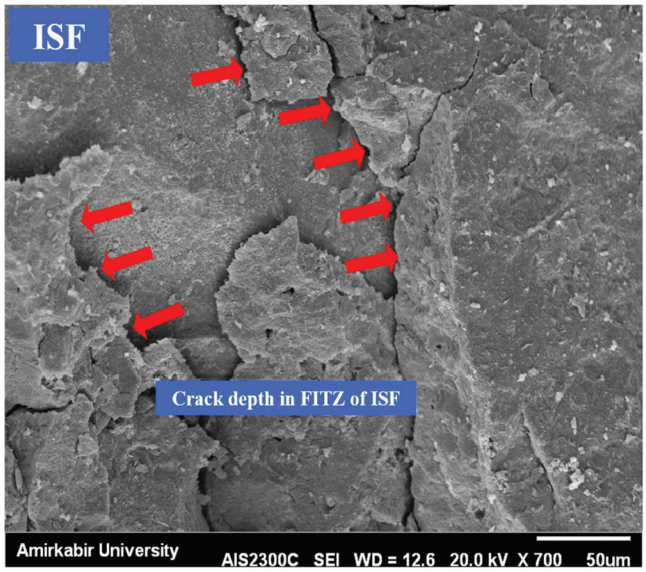

Fig. 10—Crack depth in FITZ near ISF.

through a material. Higher tortuosity indicates increased toughness and crack resistance, as the fibers deflect and bridge the cracks, creating a more convoluted path. In other words, it leads to an increase in the minimum crack length necessary for failure of the FRC. Moreover, the presence of hooked ends enhances the interfacial shear-transfer mechanism between the fibers and the surrounding concrete matrix. This in turn facilitates a more efficient distribution of loads across the FRC specimen and reduces the occurrence of localized stress concentrations. In the end, the inclusion of hooked ends in a material serves to restrict the propagation of cracks and prevent the spread of wide cracks. This characteristic is advantageous in FRC applications, where proper control of crack width is crucial. This is especially relevant in structures that necessitate minimal water or environmental penetration. Collectively, the results highlight the need to take into account the characteristics of fibers, specifically the existence of hooked ends, when making FRC mixtures with the objective of achieving superior crack control and improved mechanical features. The aforementioned explanation of enhanced bonding and its consequent impact on crack behavior highlights the possibility of including industrial fibers with hooked ends as a beneficial reinforcement component in FRC. This development facilitates the realization of more durable and solid concrete applications.

SEM analysis of FITZ crack depth in FRC—The SEM images of recycled FRC (RFRC), industrial FRC (IFRC), and hybrid FRC (HFRC) offer significant insights into their crack behavior. Figures 10 to 12 highlight a notable difference in cracking depth between industrial and recycled fiber specimens. This difference is attributed to several factors. Industrial fibers exhibit superior quality and homogeneity, leading to better bonding with the matrix and enhanced crack-bridging efficiency. In industrial fibers, in addition to hooking—which promotes interlocking, crack bridging, and deflection—surface treatments with coatings applied during production can enhance the bond strength between the cement paste and fibers. In contrast, recycled fibers often have irregular forms, variations in aspect ratios, and lack

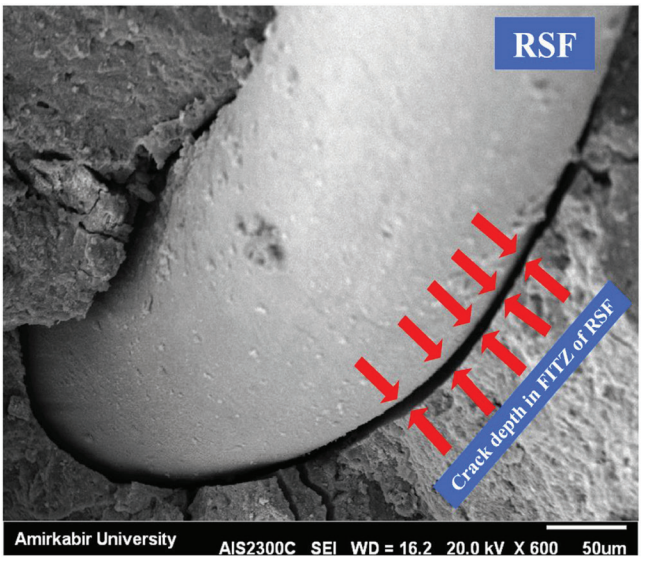

Fig. 11—Crack depth in FITZ near RSF.

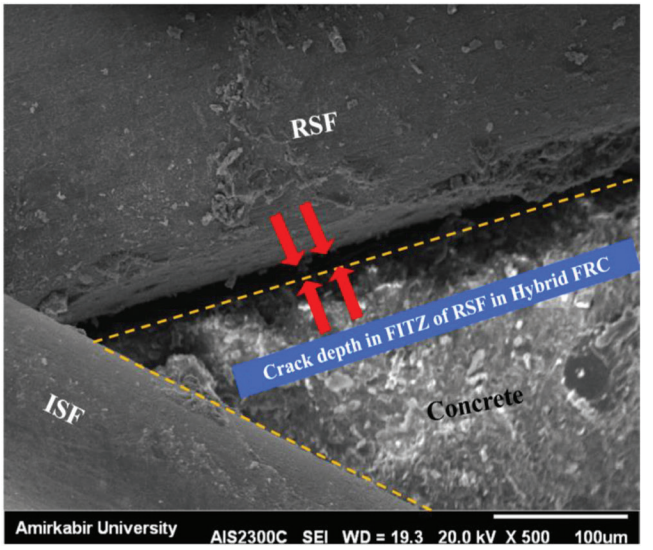

Fig. 12—Crack depth in FITZ in HFRC.

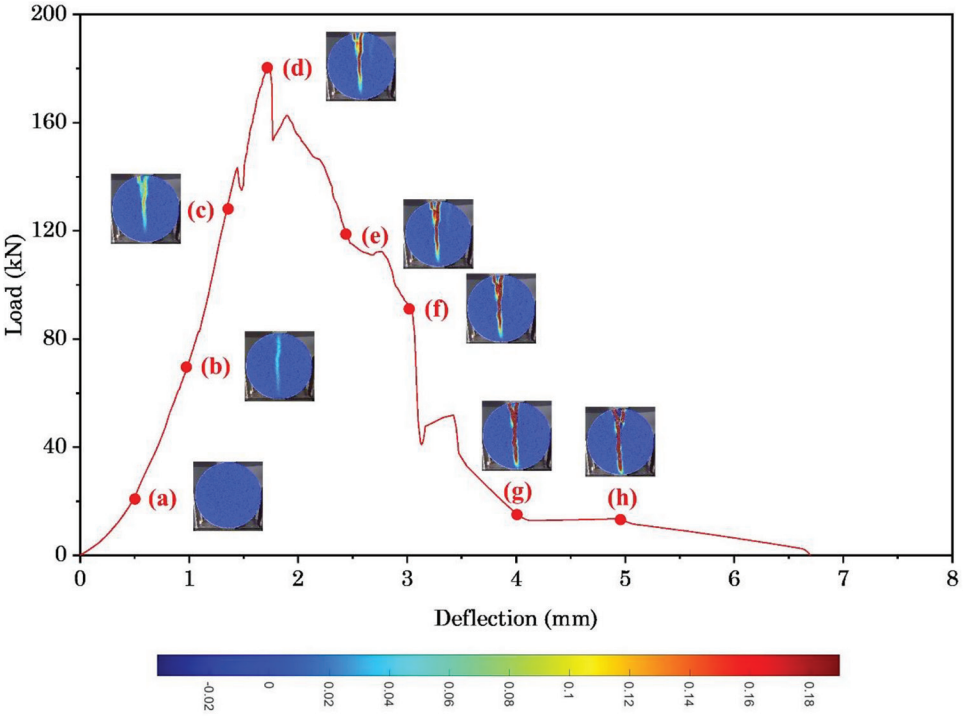

Fig. 13—Depiction of DIC analysis in I2.5R0.

hooks, which prevent interlocking and make them susceptible to pullout. Consequently, these characteristics reduce their crack-bridging efficiency and lead to deeper crack penetration. Their random curves and shapes hinder proper alignment in the bridging direction, decreasing overall effectiveness. The superior bonding and mechanical interlocking of industrial fibers provide more effective load transfer and stress redistribution, contributing to lower crack depth. Additionally, the regulated fiber content and distribution in industrial FRC ensure uniform dispersion throughout the matrix, enhancing crack control and stress transfer and further reducing crack depth.

Results of image processing analysis

Crack propagation pattern—The crack propagation pattern seen in all specimens was unified, wherein the main crack propagated in a downward direction from the upper part of the specimen during the tensile test. Figure 13 shows a depiction of the DIC analysis performed at eight distinct points in the I2.5R0 sample. Within this set of points, four are specifically dedicated to the examination of crack morphology before reaching the peak load, while the remaining four concentrate on the post-peak crack morphology. The DIC analysis offers significant insights into the start, propagation, and behavior of cracks during the entirety of the tensile test, encompassing both stages. Figure 14 depicts the crack propagation pattern seen in

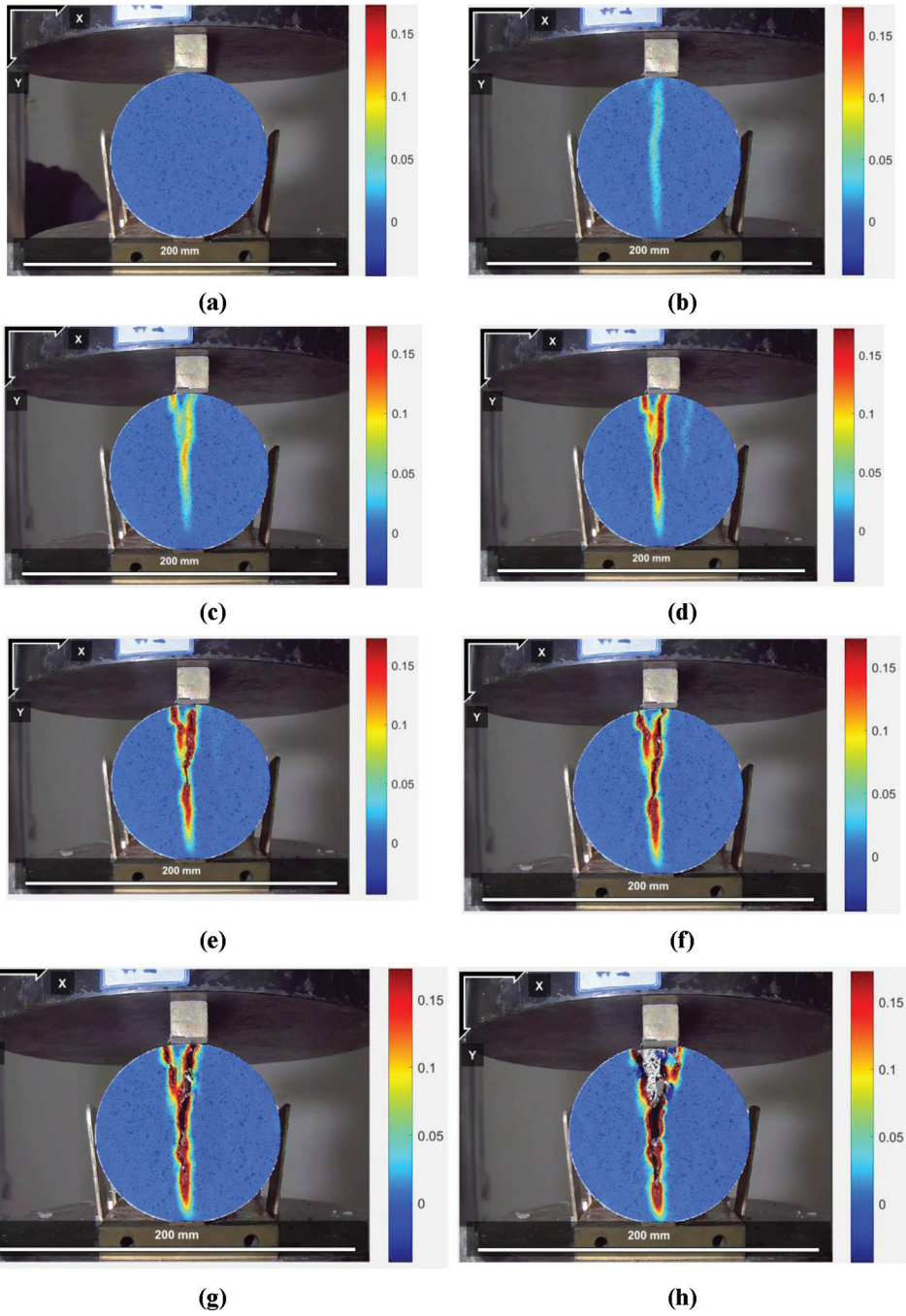

Fig. 14—Crack propagation in concrete.

the I1.25R1.25 mixture sample. This illustration serves as an exemplification of crack propagation throughout the various samples at eight distinct points. Nevertheless, while comparing the specimens of FRC with those of plain concrete at the same point, it was noted that the dimensions of the primary crack in FRC were comparatively lower in terms of length and width when compared to plain concrete. Moreover, Fig. 15 represents the effect of fiber content and hybridization on crack properties, using DIC analysis. While analyzing FRC samples with varying volume contents, it was observed that FRC samples with a greater volume content (0.5%) exhibited a reduction in the length and width of the main crack, as can be seen in Fig. 15. Furthermore, while comparing recycled mixture design samples with hybrid mixture design samples with equivalent volume content and at the same point, it was seen that the implementation of the hybrid method resulted in a considerable reduction in crack length and width parameters in the recycled mixture design. The results of this study highlight the efficacy of employing a hybrid mixture design strategy in reducing both the length and width of cracks, as compared to exclusively using recycled materials. The observed consistency in the propagation pattern of cracks across all specimens offers useful insights into the behavior of the studied materials when subjected to tensile pressure. Moreover, the notable decrease in crack sizes seen in FRC samples emphasizes the improved crack resistance supplied by the inclusion of fibers. The findings presented in this study enhance comprehension of crack

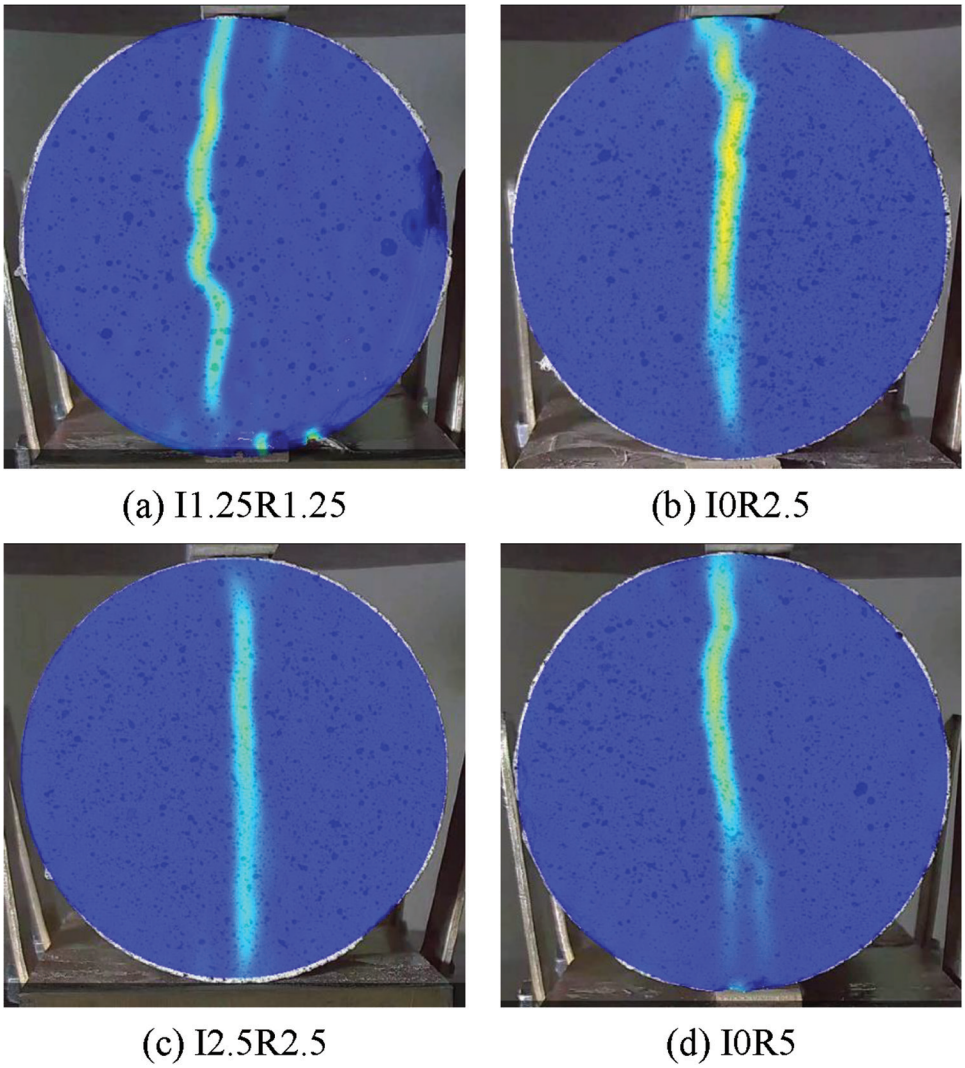

Fig. 15—Effect of fiber content and hybridization on crack properties.

propagation mechanisms in concrete structures and offer valuable insights for the development of optimum mixture designs that focus on enhancing durability and structural performance.

Tensile performance—The beginning of cracks generated by stress plays a crucial role as an entrance to the failure of concrete materials, hence presenting a significant risk to underground excavation operations and infrastructure facilities. Therefore, the precise estimation of crack initiation has significant importance in comprehending the deformation and stability characteristics of brittle materials. Moreover, it possesses substantial value in the realm of engineering design and practical applications.[16] The use of DIC is employed for analysis during the loading phase until failure. This study enables identification of three primary stages that characterize the behavior of the specimens. To begin with, the pre-peak phase of these stages demonstrates the magnitudes of strength and strain that are associated with the crack initiation. Second, the peak strength phase encompasses the distinctive characteristics of the material when it reaches its maximum strength. Finally, the post-peak phase represents a transition from a brittle mode to a more ductile behavior, which is especially noticeable in plain concrete samples, achieved through the inclusion of both single and hybrid steel fibers.

Pre-peak, peak, and post-peak tensile strength: Table 4, along with Fig. 16 and 17, provide a concise summary of the average tensile strength and corresponding stress and strain values, respectively, for all test specimens throughout the different phases. It is worth noting that points (b), (d), and (h) in Fig. 13 represent the pre-peak, peak, and post-peak stages in the I2.5R0 sample, respectively. The pre-peak phase, which indicates the beginning of cracking, demonstrates the potential of recycled fiber to postpone the initiation of cracks. At this particular stage, the tensile strength, indicated as I2.5R0 and I0R2.5, exhibits no significant disparity, as it maintains a value of 4.45 MPa. This observation is valid even when considering increasing volume percentages of fibers. Additionally, the tensile strength of the recycled fiber specimens I5R0 and I0R5, which demonstrate a strength of 5.3 MPa, stays constant. This important finding illustrates the similar performance of recycled fibers and industrial fibers in the pre-peak zone of FRC. It is noteworthy that the increase of the fiber volume content from 0.25 to 0.5% yields a 20% enhancement in strength, specifically in relation to the initial appearance of cracks. In

Table 4—Pre-peak, peak, and post-peak tensile strength and strain

Mixture description	Pre-peak		Peak		Post-peak	
	Strength, MPa	Strain, %	Strength, MPa	Strain, %	Strength, MPa	Strain, %
PC	3.82	0.007	3.92	0.007	0.78	0
I2.5R0	4.46	0.02	5.46	0.15	1.09	0.26
I1.25R1.25	5.04	0.057	5.18	0.13	1.04	0.24
I0R2.5	4.45	0.019	4.91	0.061	0.98	0.18
I5R0	5.31	0.064	6.78	0.16	1.36	0.31
I2.5R2.5	5.46	0.068	6.51	0.14	1.30	0.28
I0R5	5.33	0.041	6.28	0.08	1.26	0.21

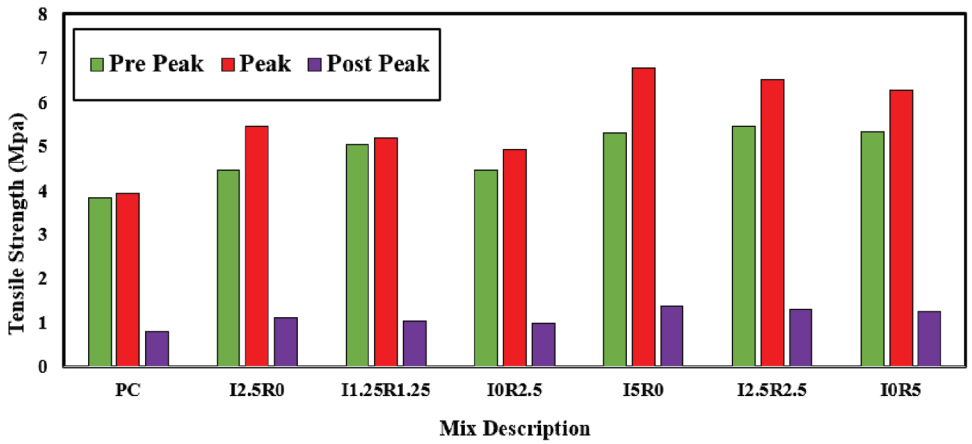

Fig. 16—Tensile strength at pre-peak, peak, and post-peak.

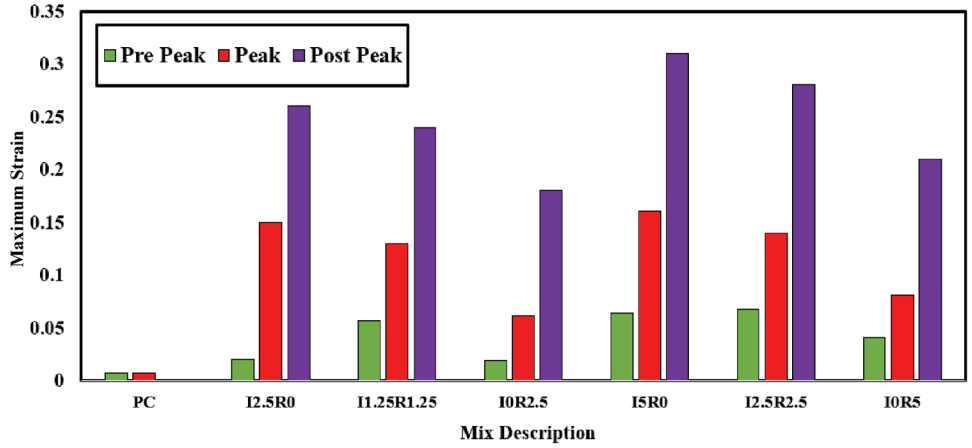

Fig. 17—Tensile strain at pre-peak, peak, and post-peak.

addition, the use of a hybrid mixture containing both recycled and industrial fibers, at varying levels of volume, has been observed to have a beneficial impact on increasing the strength associated with the initiation of cracks. The findings of this study highlight the benefits associated with the use of recycled fibers in FRC. The shown capacity of recycled fibers to effectively postpone the initial onset of cracks and exhibit comparable performance to industrial fibers during the pre-peak phase highlights their potential and feasibility for use in this specific application. Furthermore, the incorporation of recycled fibers, whether used alone or together with industrial fibers, improves the strength at the point where cracks first appear. The peak point parameters of the specimens were examined to determine the maximum level of peak strength. The mixture design that demonstrated the highest peak strength of 6.28 MPa among the other designs was the I5R0 mixture. This particular mixture indicated a strength gain of 1.6 times when compared to plain concrete. Consequently, the capabilities of industrial fibers have marginally exceeded those of recycled fibers. It is noteworthy that, across mixture designs with equivalent volume content, the mixture composed exclusively of industrial fibers had the highest peak strength, while the mixture that included recycled fibers exhibited the lowest peak strength. The drawbacks associated with the shape and appearance of recycled fibers, as mentioned in the SEM analysis section, were

further enhanced by implementing a hybrid strategy that incorporated both industrial and recycled fibers at equivalent volume content. In addition, a review of the recycled and hybrid mixture designs with varying volume content (I0R2.5 and I1.25R1.25, and I0R5 and I2.5R2.5) demonstrated peak strength enhancements of 1.3 and 1.6 times, correspondingly, when the recycled fiber was employed together with the hybrid approach. This observation shows the beneficial influence of incorporating recycled fibers in enhancing the peak strength of FRC. Nevertheless, it is crucial to acknowledge that, in the context of comparing peak strength with the strength associated with crack initiation, the influence of industrial fibers in this particular investigation exhibited a slightly more significant role at the peak point. The results of this study underscore the potential advantages of employing industrial fibers, particularly in regard to maximum strength, while also drawing attention to the notable enhancements achieved by incorporating recycled fibers through a hybrid methodology. The combined use of both types of fibers provides a potentially effective approach to enhancing the overall split tensile performance of FRC.

Pre-peak, peak, and post-peak tensile strain: The analysis of Fig. 16 reveals that plain concrete demonstrates an obvious bias toward brittle behavior. The incorporation of steel fibers, as examined in this study, significantly enhances the ductile behavior of the material, leading to a marked increase in strain capacity. It is worth mentioning that the specimens' ductility is improved in all three stages when the fiber volume content is increased from 0.25 to 0.5%. The comparison of stresses between recycled and industrial fibers during the pre-peak phase reaffirms earlier research findings, hence emphasizing the considerable potential of recycled fibers in preventing crack initiation. The maximum strain corresponding to peak strength appears to be 0.16 for the I5R0 mixture design, while the minimum strain value of 0.061 is attributed to the I0R2.5 mixture design. This discovery highlights the significance of employing industrial fibers at the peak point, as the presence of a hooked-end shape in industrial fibers improves fiber efficiency by facilitating interlocking. The aforementioned effect gets stronger during the post-peak region. The post-peak DIC analysis indicates that the rate at which recycled fibers are pulled off is higher when compared to that of industrial fibers alone. However, it is seen that industrial fibers exhibit a more favorable overall effect in the post-peak phase. The use of recycled fibers is widely accepted for its favorable characteristics, including its environmental sustainability and cost-effectiveness. However, relying exclusively on recycled fibers is considered inappropriate. Nevertheless, it is important to acknowledge that a hybrid strategy incorporating both types of fibers has the potential to mitigate a minimum of 50% of the drawbacks linked to recycled fibers, specifically in relation to the maximum strain. The mentioned discovery highlights the advantages of employing a hybrid approach to integrate the benefits of recycled and industrial fibers into FRC. The use of a hybrid technique serves to improve the ductility and overall performance of the composite material, so the inherent constraints associated with the exclusive use of recycled fibers are addressed.

CONCLUSIONS

This study focused on the split tensile behavior of recycled and hybrid fiber-reinforced concrete (FRC), examining microstructural and macroscopic properties. Scanning electron microscopy (SEM) analysis revealed that industrial fibers with hooked ends exhibited enhanced bonding, crack bridging, and crack deflection compared to recycled fibers. The presence of hooked ends promoted improved mechanical interlocking, resulting in shallower crack depths and a controlled crack pattern. Macroscopic analysis using digital image correlation (DIC) software demonstrated that recycled fibers delayed crack initiation and showed similar performance to industrial fibers in the pre-peak zone. The findings highlighted the advantages of using recycled fibers in FRC, as they effectively delayed crack onset and enhanced strength at the point of crack initiation. The hybridization of recycled fibers with industrial fibers was suggested as a strategy for improving mechanical performance, achieving cost savings, and using environmentally friendly materials in FRC. SEM analysis of the fiber interface transition zone (FITZ) revealed that industrial fibers had superior bonding characteristics due to their enhanced quality, homogeneity, and surface treatments. The presence of hooked ends in industrial fibers promoted better mechanical interlocking, crack bridging, and deflection, resulting in shorter crack depths. In contrast, recycled fibers exhibited reduced crack-bridging efficiency and deeper crack penetration due to their irregular forms and variations in aspect ratios. The hybrid approach incorporating both recycled and industrial fibers showed a beneficial impact on increasing the strength associated with crack initiation. Finally, the classification of the study's findings can be summarized as follows:

1. Microstructural analysis revealed that industrial fibers with hooked ends exhibited enhanced bonding, mechanical interlocking, crack bridging, and crack deflection compared to recycled fibers. Also, the presence of hooked ends in industrial fibers resulted in shallower crack depths, demonstrating their superior performance.

2. Recycled fibers significantly delay the initial occurrence of cracks and perform comparably to industrial fibers in the pre-peak phase when compared with plain concrete, highlighting their potential for application in this context. Additionally, the use of recycled fibers, either alone or with industrial fibers, strengthens the material precisely where cracks begin to form.

3. The increase in fiber content from 0.25 to 0.5% resulted in a 20% enhancement in strength, particularly in relation to the initial appearance of cracks.

4. The hybridization of recycled fibers with industrial fibers in both high-volume percentage (I2.5R2.5) and low-volume percentage (I1.25R1.25) mixtures is a recommended strategy for enhancing mechanical performance, achieving cost savings, using environmentally friendly materials, reducing crack dimensions compared to using solely recycled fibers, and increasing strength associated with crack initiation in FRC.

AUTHOR BIOS

Tohid Asheghi Mehmandari *is a PhD graduate in civil engineering from Amirkabir University of Technology, Tehran, Iran, and currently a Research Scholar at Morgan State University, Baltimore, MD. He is also a member of the ACI Iran Chapter. His research interests include experimental and numerical analysis of fiber-reinforced concrete, with a particular focus on the use of recycled and hybrid reinforced concrete in tunnel linings.*

ACI member **Mehdi Shokouhian** *is an Associate Professor at Morgan State University. He received his PhD in civil engineering from Tsinghua University, Beijing, China in 2015. He is an advisor for the ACI Morgan State University Student Chapter. His research interests include conducting comprehensive research that integrates experimental and analytical approaches, focusing on innovative structural designs and high-performance materials.*

Meysam Imani *is an Assistant Professor at Amirkabir University of Technology, where he received his PhD in civil engineering in 2011. His research interests include the numerical design of concrete tunnel linings.*

Kong Fah Tee *is an Associate Professor at King Fahd University of Petroleum and Minerals, Dhahran, Saudi Arabia. His research interests include structural health monitoring, reliability, and sustainable concrete materials.*

Ahmad Fahimifar *is a Professor and former President at Amirkabir University of Technology. He received his PhD in civil engineering from Newcastle University, Newcastle upon Tyne, UK, in 1990. His research interests include the analysis of tunnel linings using fiber-reinforced concrete.*

ACKNOWLEDGMENTS

The authors would like to express their gratitude to FARATAV Company for providing the steel fibers used in this research.

REFERENCES

1. Mehta, K. P., "Reducing the Environmental Impact of Concrete," *Concrete International*, V. 23, No. 10, Oct. 2001, pp. 61-66.

2. Aveston, J.; Cooper, G. A.; and Kelly, A., "Single and Multiple Fracture: The Properties of Fibre Composites," *The Properties of Fibre Composites*, IPC Science and Technology Press, Ltd. Teddington, UK, 1971, pp. 15-26.

3. Li, V. C., and Wu, H.-C., "Conditions for Pseudo Strain-Hardening in Fiber Reinforced Brittle Matrix Composites," *Applied Mechanics Reviews*, V. 45, No. 8, 1992, pp. 390-398. doi: 10.1115/1.3119767

4. Chin, S. C.; Tee, K. F.; Tong, F. S.; Doh, S. I.; and Gimbun, J., "External Strengthening of Reinforced Concrete Beam with Opening by Bamboo Fiber Reinforced Composites," *Materials and Structures*, V. 53, No. 6, 2020, p. 141. doi: 10.1617/s11527-020-01572-y

5. Mastali, M.; Dalvand, A.; Sattarifard, A. R.; Abdollahnejad, Z.; and Illikainen, M., "Characterization and Optimization of Hardened Properties of Self-Consolidating Concrete Incorporating Recycled Steel, Industrial Steel, Polypropylene and Hybrid Fibers," *Composites Part B: Engineering*, V. 151, 2018, pp. 186-200. doi: 10.1016/j.compositesb.2018.06.021

6. Asokan, P.; Osmani, M.; and Price, A. D., "Assessing the Recycling Potential of Glass Fibre Reinforced Plastic Waste in Concrete and Cement Composites," *Journal of Cleaner Production*, V. 17, No. 9, 2009, pp. 821-829. doi: 10.1016/j.jclepro.2008.12.004

7. Foti, D., "Use of Recycled Waste Pet Bottles Fibers for the Reinforcement of Concrete," *Composite Structures*, V. 96, 2013, pp. 396-404. doi: 10.1016/j.compstruct.2012.09.019

8. Hesami, S.; Salehi Hikouei, I.; and Emadi, S. A. A., "Mechanical Behavior of Self-Compacting Concrete Pavements Incorporating Recycled Tire Rubber Crumb and Reinforced with Polypropylene Fiber," *Journal of Cleaner Production*, V. 133, 2016, pp. 228-234. doi: 10.1016/j.jclepro.2016.04.079

9. Mastali, M.; Dalvand, A.; and Sattarifard, A., "The Impact Resistance and Mechanical Properties of Reinforced Self-Compacting Concrete with Recycled Glass Fibre Reinforced Polymers," *Journal of Cleaner Production*, V. 124, 2016, pp. 312-324. doi: 10.1016/j.jclepro.2016.02.148

10. McIntosh, J.; Gharehbaghi, K.; Tee, K. F.; De Luca, A.; and Taylor, J. S., "Viability Rubric of Fibre-Reinforced Polymer Composites for Civil Infrastructure Applications," *Infrastructure Asset Management*, V. 11, No. 2, 2024, pp. 78-87. doi: 10.1680/jinam.23.00009

11. Caggiano, A.; Gambarelli, S.; Martinelli, E.; Nisticò, N.; and Pepe, M., "Experimental Characterization of the Post-Cracking Response in Hybrid Steel/Polypropylene Fiber-Reinforced Concrete," *Construction and Building Materials*, V. 125, 2016, pp. 1035-1043. doi: 10.1016/j.conbuildmat.2016.08.068

12. Caggiano, A.; Xargay, H.; Folino, P.; and Martinelli, E., "Experimental and Numerical Characterization of the Bond Behavior of Steel Fibers Recovered from Waste Tires Embedded in Cementitious Matrices," *Cement and Concrete Composites*, V. 62, 2015, pp. 146-155. doi: 10.1016/j.cemconcomp.2015.04.015

13. Martinelli, E.; Caggiano, A.; and Xargay, H., "An Experimental Study on the Post-Cracking Behaviour of Hybrid Industrial/Recycled Steel Fibre-Reinforced Concrete," *Construction and Building Materials*, V. 94, 2015, pp. 290-298. doi: 10.1016/j.conbuildmat.2015.07.007

14. Neocleous, K.; Maxineasa, S.G.; Dumitrescu, L.; Themistocleous, K.; Taranu, N.; and Hadjimitsis, D, "D1. 6 Preliminary LCA. Anagennisi Project, Anagennisi: Innovative Use of all Tyre Components in Concrete," 2014.

15. Aydin, A. C., "Self Compactability of High Volume Hybrid Fiber Reinforced Concrete," *Construction and Building Materials*, V. 21, No. 6, 2007, pp. 1149-1154. doi: 10.1016/j.conbuildmat.2006.11.017

16. Hsie, M.; Tu, C.; and Song, P., "Mechanical Properties of Polypropylene Hybrid Fiber-Reinforced Concrete," *Materials Science and Engineering A*, V. 494, No. 1-2, 2008, pp. 153-157. doi: 10.1016/j.msea.2008.05.037

17. Shu, X.; Graham, R. K.; Huang, B.; and Burdette, E. G., "Hybrid Effects of Carbon Fibers on Mechanical Properties of Portland Cement Mortar," *Materials & Design*, V. 65, 2015, pp. 1222-1228. doi: 10.1016/j.matdes.2014.10.015

18. Asheghi Mehmandari, T.; Shokouhian, M.; Imani, M.; and Fahimifar, A., "Experimental and Numerical Analysis of Tunnel Primary Support Using Recycled, and Hybrid Fiber Reinforced Shotcrete," *Structures*, V. 63, 2024, p. 106282. doi: 10.1016/j.istruc.2024.106282

19. Asheghi Mehmandari, T.; Fahimifar, A.; and Asemi, F., "The Effect of the Crack Initiation and Propagation on the P-Wave Velocity of Limestone and Plaster Subjected to Compressive Loading," *AUT Journal of Civil Engineering*, V. 4, No. 1, 2020, pp. 55-62.

20. Balogun, O. P.; Alaneme, K. K.; Adediran, A. A.; Oladele, I. O.; Omotoyinbo, J. A.; and Tee, K. F., "Evaluation of the Physical and Mechanical Properties of Short Entada Mannii-Glass Fiber Hybrid Composites," *Fibers*, V. 10, No. 3, 2022, p. 30. doi: 10.3390/fib10030030

21. Zare, P.; Fahimifar, A.; Zabetian, S.; and Asheghi, T., "Experimental Assessment of Damage and Crack Propagation Mechanism in Heterogeneous Rocks," *5th International Conference on Applied Research in Science and Engineering*, University of Amsterdam, Amsterdam, the Netherlands, 2020.

22. Golewski, G. L., "Estimation of the Optimum Content of Fly Ash in Concrete Composite Based on the Analysis of Fracture Toughness Tests Using Various Measuring Systems," *Construction and Building Materials*, V. 213, 2019, pp. 142-155. doi: 10.1016/j.conbuildmat.2019.04.071

23. Golewski, G. L., "Energy Savings Associated with the Use of Fly Ash and Nanoadditives in the Cement Composition," *Energies*, V. 13, No. 9, 2020, p. 2184. doi: 10.3390/en13092184

24. Golewski, G. L., and Sadowski, T., "A Study of Mode III Fracture Toughness in Young and Mature Concrete with Fly Ash Additive," *Diffusion and Defect Data, Solid State Data. Part B, Solid State Phenomena*, V. 254, 2016, pp. 120-125. doi: 10.4028/www.scientific.net/SSP.254.120

25. Abdul Samad, A. A.; Ali, N.; Mohamad, N.; Jayaprakash, J.; Tee, K. F.; and Mendis, P., "Shear Strengthening and Shear Repair of 2-Span Continuous RC Beams with CFRP Strips," *Journal of Composites for Construction*, ASCE, V. 21, No. 3, 2017, p. 04016099. doi: 10.1061/(ASCE)CC.1943-5614.0000756

26. Diamond, S., and Huang, J., "The ITZ in Concrete–A Different View Based on Image Analysis and SEM Observations," *Cement and Concrete Composites*, V. 23, No. 2-3, 2001, pp. 179-188. doi: 10.1016/S0958-9465(00)00065-2

27. Adili, E., and Kheyroddin, A., "Fiber Interfacial Transition Zone Concept for Steel Fiber-Reinforced Concrete by SEM Observation," *Journal of Applied Research and Technology*, V. 19, No. 4, 2021, pp. 294-307. doi: 10.22201/icat.24486736e.2021.19.4.1024

28. Němeček, J., "Mikromechanické vlastnosti cementových kompozitů," master's thesis, Czech Technical University in Prague, Prague, Czech Republic, 2017, 72 pp. (in Czech)

29. Němeček, J.; Králík, V.; Šmilauer, V.; Polívka, L.; and Jäger, A., "Tensile Strength of Hydrated Cement Paste Phases Assessed by Micro-Bending Tests and Nanoindentation," *Cement and Concrete Composites*, V. 73, 2016, pp. 164-173. doi: 10.1016/j.cemconcomp.2016.07.010

30. Němeček, J.; Králík, V.; and Vondřejc, J., "Micromechanical Analysis of Heterogeneous Structural Materials," *Cement and Concrete Composites*, V. 36, 2013, pp. 85-92. doi: 10.1016/j.cemconcomp.2012.06.015

31. Zacharda, V.; Němeček, J.; and Štemberk, P., "Micromechanical Performance of Interfacial Transition Zone in Fiber-Reinforced Cement

Matrix," *IOP Conference Series. Materials Science and Engineering*, V. 246, 2017, p. 012018. doi: 10.1088/1757-899X/246/1/012018

32. Asheghi Mehmandari, T.; Mohammadi, D.; Ahmadi, M.; and Mohammadifar, M., "Fracture Mechanism and Ductility Performances of Fiber Reinforced Shotcrete under Flexural Loading Insights from Digital Image Correlation (DIC)," *Insight-Civil Engineering*, V. 7, No. 1, 2024, p. 611. doi: 10.18282/ice.v7i1.611

33. Ündül, Ö.; Amann, F.; Aysal, N.; and Plötze, M., "Micro-Textural Effects on Crack Initiation and Crack Propagation of Andesitic Rocks," *Engineering Geology*, V. 193, 2015, pp. 267-275. doi: 10.1016/j.enggeo.2015.04.024

34. Mohammadifar, M.; Asheghi Mehmandari, T.; and Fahimifar, A., "Parametric and Sensitivity Analysis on the Effects of Geotechnical Parameters on Tunnel Lining in Soil Surrounding," *Journal of Structural and Construction Engineering*, V. 11, No. 8, 2024, pp. 5-17.

35. ASTM C150/C150M-17, "Standard Specification for Portland Cement," ASTM International, West Conshohocken, PA, 2017.

36. ASTM C136/C136M-19, "Standard Test Method for Sieve Analysis of Fine and Coarse Aggregates," ASTM International, West Conshohocken, PA, 2019.

37. FARATAV Company, "STEEL FIBER Macro 5D/35/B Data Sheet," Tehran, Iran, 2022, https://construfiber.com/images/Data_sheet/STEEL-FIBER/Macro/5D/35/B/5D3588BA.pdf. (last accessed Jan. 29, 2025)

38. ASTM C138/C138M-17a, "Standard Test Method for Density (Unit Weight), Yield, and Air Content (Gravimetric) of Concrete," ASTM International, West Conshohocken, PA, 2017.

39. ASTM C143/C143M-12, "Standard Test Method for Slump of Hydraulic-Cement Concrete," ASTM International, West Conshohocken, PA, 2012.

40. Blaber, J.; Adair, B.; and Antoniou, A., "Ncorr: Open-Source 2D Digital Image Correlation Matlab Software," *Experimental Mechanics*, V. 55, No. 6, 2015, pp. 1105-1122. doi: 10.1007/s11340-015-0009-1

ACI MATERIALS JOURNAL TECHNICAL PAPER

Title No. 122-M09

Assessing Durability Characteristics of Basalt Fiber and Slag-Based Cementitious Composite

by Alein Jeyan Sudhakar and Bhuvaneshwari Muthusubramanian

Past researchers have concentrated on the durability characteristics of textile-reinforced cementitious composites with quartz and silica sand. However, to make it easily available for construction, this study explores the durability characteristics of cementitious composites (CC) with the available manufactured sand before applying it to textile reinforcement. It is more important to study the durability characteristics as the main aim of application is to construct thin structures without coarse aggregate. Thus, the durability and microstructural characteristics of basalt fiber (BF)-reinforced fine-grained CC incorporated with ground-granulated blast-furnace slag (GGBS) as a partial substitution of cement (BFRFGC) were studied. The CC were exposed to different exposure conditions, such as acidic environment, alkaline environment, and elevated temperature. Then, their visual appearance and change in weight and strength were studied as per the codal provisions at several exposure ages. In addition, microstructural studies were also performed at different exposure conditions and were compared with the specimens before exposure. The BFRFGC showed 61.93% and 27.58% lower strength and weight change than controlled fine-grained CC (CFGC) under extreme conditions (that is, exposure to sulfuric acid). Also, the results from microstructural studies reveal that BF and BFRFGC are resistant to all these conditions. Subsequently, BFRFGC has superior resistance under various exposure conditions and excellent durability characteristics.

Keywords: basalt fiber (BF); cementitious composite (CC); durability; ground-granulated blast-furnace slag (GGBS); microstructure; strength.

INTRODUCTION

The construction industry focuses on creating thin, light structures with good mechanical and thermal performance using sustainable building materials. Also, the aggressive climatic change due to urbanization and exposure of structures along coast lines increases the necessity to evaluate durability characteristics to ensure structures' longer life. As per ACI 201.2R-08,[1] concrete should show excellent resistance when subjected to chemical attack and different temperature changes. For example, when concrete is exposed to seawater, the rate of attack is slow, and when it is exposed to acid, its rate of attack is rapid. Hence, to determine the effect of concrete when subjected to two different rates of attack, the durability characteristics in acidic and alkaline environments are considered the most important. The alkalinity increases the internal stresses of the concrete, thereby reducing its mechanical characteristics and, in turn, affecting its serviceability. Using locally accessible agricultural and industrial waste resources has shown promise in resolving developing nations' economic and environmental issues. Yet, employing natural coarse aggregate depletes resources; this research aids in protecting it as well as the construction of thin, light, and complicated structures. The inclusion of admixtures improves the performance of the binder material. Instead of coarse aggregate, fine aggregate with a size of less than 2 mm (0.07 in.) is used to make fine-grained cementitious composites (FGCC). Shrinkage fractures are caused when a higher cement concentration is needed to achieve greater strength in the absence of coarse aggregate. The appropriate dispersion of fibers inside the matrix can prevent this. By packing tightly, the materials' fineness minimizes the amount of air voids in the matrix. Compared to normal concrete, it also has higher tensile strength and strain.[2] The fabrication of textile-reinforced composites makes extensive use of these FGCC. It aids in the building of delicate and intricate structures. Sand's smaller grain size lowers air spaces and creates an adequate binding between the yarns in textile reinforcement, improving strength properties.[3] It has enhanced durability, minimizes corrosion, and resists permeability through the voids.[4] The finer particles easily impregnate the yarns and strengthen the bond between the matrix and textile fiber. Due to their fineness, FGCC are more workable.[5] The use of fibers improves and strengthens the effectiveness of the binder.[6] This matrix has greater shrinkage cracks due to the higher amount of cement used in its preparation than other matrixes. However, this problem can be solved by using enough fibers or nano dispersants.[7] To create FGCC, the raw ingredients must be carefully selected depending on necessity.[8]

Although fiber-reinforced concrete (FRC) has been studied before, it is often employed because of its excellent flexural properties. The yarn count and the length of the distributed fiber influence its behavior. Basalt fibers (BF), created from igneous basalt rock, are now widely used in domestic and worldwide concrete structures.[9] Cementitious composites (CC) have been the subject of significant research over the past 10 years, producing ductile, strong, and energy-absorbing composites with high compressive and tensile strengths and ductility.[10] BF have received significant interest from the composites sector due to their exceptional mechanical and thermal properties and chemical stability.[11,12] Because of its lower cost, BF finds numerous uses in the building and polymer industries.[13,14] BF, which is

ACI Materials Journal, V. 122, No. 2, March 2025.

MS No. M-2023-372.R3, doi: 10.14359/51745597, received September 29, 2024, and reviewed under Institute publication policies.

made from rocks, can endure temperatures as high as 1500°C (2732°F). BF can improve flexural toughness and postpone the onset of cracks when added to the concrete mixture. Moreover, the fiber changes the failure type from brittle to ductile.[15] After quenching, ground-granulated blast-furnace slag (GGBS), which is produced as a by-product of the steel, can be used in the concrete industry by partially replacing cement. As a result, less cement is used, less energy is required, less money is spent, and constructions are more durable.[16] Compared to cement, GGBS has finer particles, a larger surface area, and contains more silica.[17,18] Early in the curing process, the rate of hydration is lower.[19] The FGCC aids in the development of complex, thin, and lightweight building materials.[20] In this concern, an FGCC is developed in this study as a matrix for textile reinforcement.

RESEARCH SIGNIFICANCE

It is evident from the literature that FGCC can be used as a matrix for textile reinforcements and is mainly prepared with quartz or siliceous sand as a fine aggregate due to its fineness, but it is costly. BF has excellent resistance to different environmental conditions. As GGBS induces the dilution effect, it may help improve durability aspects; hence, it was chosen in this study in addition to BF. The BF- and GGBS-based matrix showed greater performance in terms of mechanical and thermal characteristics than the previous studies. It is desired to know about the durability aspects of any cementitious matrix before applying it in the field. The literature on manufacturing an FGCC matrix with conventionally available fine aggregate is limited. Furthermore, there is a lag in studying the performance of BF and GGBS as a combination in FGCC with regard to its durability aspect. Thus, this paper focuses on the compressive strength of FGCC with BF as an additive and GGBS as a partial replacement for cement. Then, its effect on appearance, weight, strength, and difference in microstructural characteristics when exposed to acidic and alkaline environments was evaluated by exposing it directly to sulfuric acid, seawater, and temperature.

Table 1—Basic material characteristics

Properties	Cement	GGBS	Fine aggregate	HRWRA
Standards	IS 12269:2013[21]	IS 16714:2018[22]	IS 383:2016[23]	IS 9103:1999 (2018)[24]
Specific gravity	3.1	2.96	2.74	1.18
Grading of M-sand	—	—	Zone III	—
Density, kg/m^3	1420	1200	1790	1173
Fineness, m^2/kg	324	415	—	—

MATERIALS AND MIXTURE

Raw materials

The raw materials for preparing FGCC include cement, fine aggregate, GGBS, chopped BF, and high-range water-reducing admixture (HRWRA). Quartz or silica sand is the most used raw material in preparing the cementitious matrix due to its fineness. However, due to its scarce availability and cost, in this study, fine aggregate (M-Sand) of less than 2 mm (0.07 in.) was used. The basic characteristics of the raw materials used conform to standards and are given in Table 1. A chopped BF of 12 mm (0.47 in.) in length and an aspect ratio of 706 was used in this study. It possesses a tensile strength of 3.56 GPa (0.516 Mpsi) and an elastic modulus of 87 GPa (12.62 Mpsi).

Mixture proportions

The mixture proportions for FGCC were decided based on the trial-and-error method. In the optimized trial batch, chopped BF of 12 mm (0.47 in.) was dispersed as an additive by 0.4% to the volume of the matrix.[25] The percentage addition of BF and GGBS was decided from the previous research studies as it gave better mechanical and thermal characteristics, as reported.[25,26] The mixture details of the cementitious matrix are given in Table 2.

EXPERIMENTAL PROGRAM

ACI 201.2R-08[1] says any concrete material can be affected due to temperature changes and aggressive environments (acids, chemicals, and seawater). So, in this paper, the durability characteristics of FGCC when subjected to different environmental conditions are evaluated. The durability properties are studied only for the sample—which performed well in mechanical and thermal characteristics, as found from previous studies—and compared with controlled fine-grained CC (CFGC).[25,26]

Specimen preparation

The durability characteristics of FGCC were studied from cubic samples with 70.6 mm (2.78 in.) dimensions. Initially, the dry mixture of BF-reinforced fine-grained CC incorporated with GGBS as a partial substitution of cement (BFRFGC) was prepared by adding fine aggregate, cement, and GGBS. After proper mixing, the 12 mm (0.47 in.) chopped BF was dispersed in the mixture and again dry-mixed carefully. Then, after thorough mixing, water was added to the dry mixture little by little, and a proper mixture was made. Then, HRWRA of 1% to the cement weight was mixed with 10% of the water content required and mixed thoroughly. After proper mixing, the matrix was placed in the greased molds

Table 2—Mixture proportions of CC

Mixture	Ingredients, kg/m^3					
	Cement	GGBS	Fine aggregate	Water	HRWRA	BF
CFGC	478.5	—	1656.25	215.29	4.78	—
BFRFGC	382.8	95.7	1656.25	215.29	4.78	1.91

and allowed to set for 24 hours; after that, the cube specimens were demolded and cured by immersing them in water for approximately 28 days. The CFGC was prepared using the same process without the addition of GGBS and BF. After 28 days of curing, the specimens were air-dried and initially weighed. Then, they were placed in different environmental conditions. The flow diameter and density of the CFGC and BFRFGC were 175 mm (6.89 in.) and 2201 kg/m^3 (137.4 lb/ft^3), and 166 mm (6.54 in.) and 2186 kg/m^3 (136.47 lb/ft^3), respectively. The fragments collected from the specimens after checking their strength were crushed, sieved, washed in ethanol to stop further hydration reactions, and then used for microstructural analysis.

Preparation of acid medium

Acid attack is the primary source of chemical deterioration of any structure. So, the chemical resistance of FGCC was studied as per ASTM C267-01.[27]

Table 3—Specifications of seawater

Parameters	Values
Appearance	Turbid
Color	Light blueish
Odor	Foul smell
Appearance	Turbid
pH	8.10
Total hardness, mg/L	7600
Total alkalinity, mg/L	225
Chlorides, mg/L	2377.63
Sodium, mg/L	557.44
Calcium, mg/L	893.10
Potassium, mg/L	104.19

Seawater medium

Structures near the seashore may be easily affected due to the alkalinity of seawater. So, the effect of the alkalinity of the CC was studied by exposing it directly to seawater. Seawater was collected from the nearest beach in Kovalam, Chennai, India. The detailed specifications of seawater collected are given in Table 3. The seawater was changed at every inspection period as per ASTM C267-01.[27]

Temperature

The structure should withstand the specified load during fire and fire stream testing and prevent the passage of fire for an extended period as per Part 4 of the National Building Code of India.[28] In this paper, the durability characteristics of CFGC and BFRFGC upon exposure to different environmental conditions such as acid, seawater, and temperature at 200°C (392°F) were evaluated through physical and microstructural observations.

RESULTS AND DISCUSSION

The effect of FGCC when directly exposed to acid, seawater, and temperature is discussed in detail in this section through physical observations and different microstructural characteristics.

Effect of GGBS on cementitious matrix

The compressive strength of FGCC increased with the age of curing. The strength increased for the GGBS-based matrix with the higher curing ages as higher GGBS content induced a dilution effect at the early ages. The compressive strength for both matrixes at different days of curing is shown in Fig. 1. The compressive strength increased by 29.34% for the BFRFGC at 90 days of water curing. According to Sobia et al.,[29] the slow reactivity of GGBS contributed to an increase in the concrete's compressive

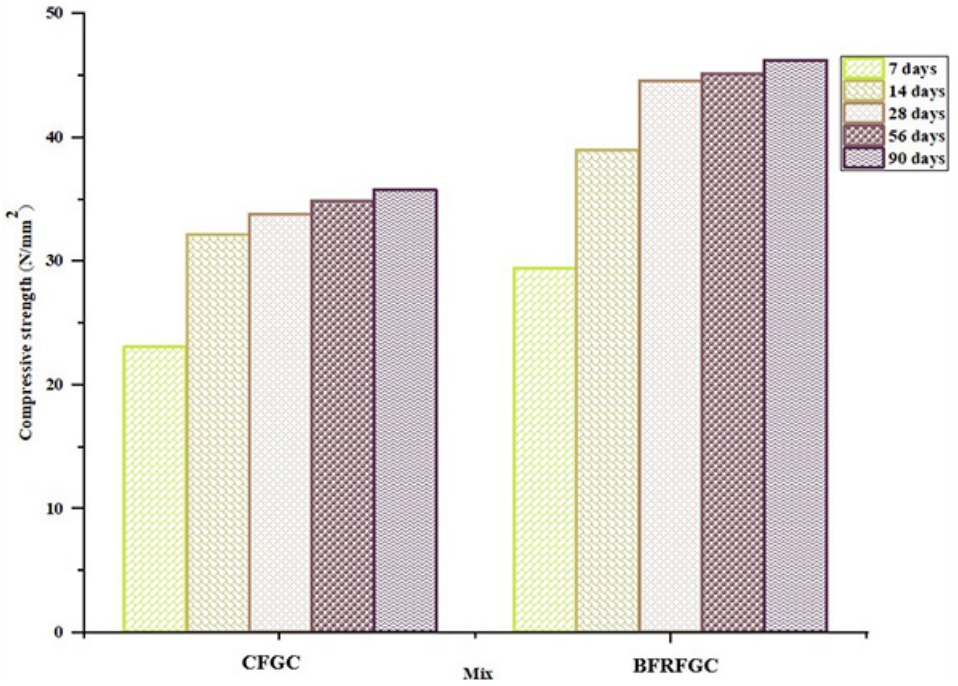

Fig. 1—Compressive strength of CC.

strength with prolonged curing. A similar trend was also observed in this study. The higher GGBS content in the cementitious matrix was attributed to the dilution effect and slowdowns of the pozzolanic reaction in the early ages due to higher silica content, but it started to react over time and improved the compressive strength. The fineness of GGBS also plays a major role in this reaction.[30,31] In addition to this, the bridging effect of fibers in the matrix also helped to improve the strength characteristics of the matrix without GGBS. Replacing cement with 20% GGBS in combination with 0.4% BF helped achieve higher compressive strength.

Effect of acid

When exposed directly or indirectly to any acid environment, the specimens degrade in strength and other aspects. Thus, the effect of 5% sulfuric acid-exposed samples was evaluated based on appearance, strength, and change in weight.

Visual appearance—The CFGC and BFRFGC specimens were placed in an acid medium after 28 days of water curing. The outer surface of the CFGC and BFRFGC specimens exposed to sulfuric acid started to disintegrate. On continuous exposure, the color of the specimens changed to light brown. The dehydration of the hydration products on exposure to sulfuric acid is given in Eq. (1) and (2).

$$Ca(OH)_2 + H_2SO_4 \rightarrow CaSO_4 \cdot 2H_2O \quad (1)$$

$$3CaOAl_2O_3 \cdot 12H_2O + 3(CaSO_4 \cdot 2H_2O) + 14H_2O \rightarrow 3CaO.Al_2O_3.3CaSO_4 \cdot 32H_2O \quad (2)$$

$$Fe^{2+} + 2OH^- \rightarrow Fe(OH)_2 \quad (3)$$

The calcium hydroxide present in the specimens in the reaction with sulfuric acid led to the formation of gypsum. The gypsum, on further reaction with the calcium aluminates, formed ettringite, as shown in Eq. (2), leading to the disintegration of the sides. The bulging of sides noticed in the BFRFGC was due to ettringite formation, leading to the specimens' volumetric expansion, as shown in Eq. (2). When GGBS is used in the cementitious matrix as a partial replacement of cement, the rate of hydration of the matrix is slow and its hydration rate increases over time due to its slow reacting nature. A higher rate of hydration that takes place over time leads to the formation of calcium-silicate-hydrate (C-S-H) and is known as the secondary hydration reaction, which helps to decrease the rate of degradation of the cementitious matrix. Thus, the rate of disintegration of BFRFGC specimens was slow compared with CFGC due to the secondary hydration reaction that occurs due to the addition of GGBS. The ferric present in the specimen in the reaction forms the ferric oxide (Eq. (3)), causing a light brown color[32,33] on the surfaces of the specimens when exposed to sulfuric acid.[34] Wang et al.[32] studied the erosion of BF concrete with sulfuric acid, and the disintegration of the specimen was observed with color change upon continuous exposure. Madhuri and Srinivasa Rao[33] studied the performance of slag concrete when exposed to sulfuric acid, and the disintegration of specimens was found with a change in color and the appearance of coarse aggregates. Thus, the color change was due to the precipitation of ferric oxide, and the specimens disintegrated along the sides with continuous exposure, as shown in Fig. 2. However, the disintegration was less in BFRFGC than in CFGC due to the secondary hydration reactions that take place when cement is partially substituted with GGBS.

Change in weight—As shown in Fig. 3, when the CFGC and BFRFGC were exposed to sulfuric acid, the reduction in the weight of the specimens was observed at different inspection periods. The percentage weight loss was lower in the BFRFGC specimens than in the CFGC specimens. The maximum weight loss of approximately 6.745% and 5.11% was observed in the CFGC and BFRFGC specimens at 84 days of exposure to sulfuric acid. The BFRFGC showed 24.18% lower weight loss than CFGC at 84 days of exposure. Khan et al.[35] studied the performance of BF-reinforced concrete with coarse aggregate under different environmental conditions, and they observed a weight reduction with the increase in days of exposure. However, the weight reduction was less than conventional concrete specimens. Tanwar et al.[36] studied the performance of GGBS-based concrete with coarse aggregate exposed to sulfuric acid; the weight gain of the specimens was observed up to 7 days of curing, and then a weight reduction was observed. The results obtained in this study were contradictory to those obtained by Tanwar et al.[36] and similar to Khan et al.,[35] as a reduction in the weight of the samples was observed upon continuous exposure to sulfuric acid. The weight reduction was due to the disintegration of the specimens, which was caused by the formation of ettringite, as given in Eq. (2), which causes internal pressure, leading to volumetric expansion of the specimen, causing deterioration upon continuous exposure to sulfuric acid. The weight reduction was lower in the BFRFGC due to the secondary hydration reaction that takes place due to the GGBS. The rate of disintegration was higher as specimens exposed to acid experienced a rapid attack. Thus, when BF and GGBS were added, it gave better resistance to weight reduction than the CFGC.

Compared to the optimized mixture, the percentage weight loss was smaller for specimens with BF and GGBS. After 84 days of exposure to sulfuric acid, the largest weight loss percentages of approximately 6.745% and 5.11% were noticed in the CFGC and BFRFGC. The specimens' degradation from continuous exposure to sulfuric acid was the cause of the weight loss. In their study of BF-reinforced concrete with coarse aggregate under various environmental circumstances, Khan et al.[35] found that as the number of curing days increased, the weight of the concrete decreased. However, compared to examples made of standard concrete, the weight decrease was less.

Change in strength—The change in compressive strength of the CFGC and BFRFGC specimens when exposed to sulfuric acid was studied, and the failure images are shown in Fig. 4. The CFGC shows more spalling and crushing upon testing than the BFRFGC. Figure 5 indicates the compressive strength reduction of CFGC and BFRFGC when exposed to sulfuric acid at different inspection periods.

Fig. 2—Visual appearance of specimens at different days of exposure in sulfuric acid medium.

As shown in Fig. 5, when CFGC and BFRFGC are exposed to sulfuric acid, a reduction in compressive strength occurs. The BFRFGC showed less of a reduction in compressive strength than the CFGC. The maximum loss of compressive strength of approximately 26.96% and 14.21% was found in the CFGC and BFRFGC, respectively, when exposed continuously to sulfuric acid. The BFRFGC showed a 47.25% lower change in weight than CFGC. From the results obtained, the BFRFGC showed better resistance to acid than the CFGC. The reduction in strength is due to the decalcification of calcium silica hydra-gel. Thus, when BF and GGBS are added to the matrix, they give better resistance to strength reduction than the CFGC.

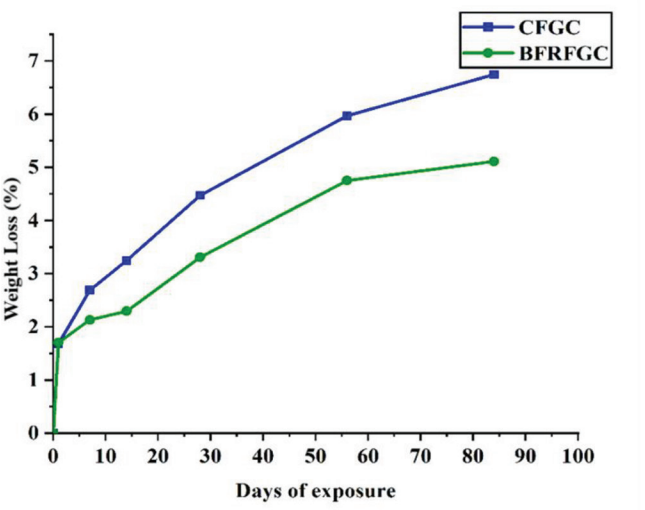

Fig. 3—Loss of weight of FGCC with exposure to sulfuric acid.

Fig. 4—Failure of specimens in compression when exposed to sulfuric acid for 84 days.

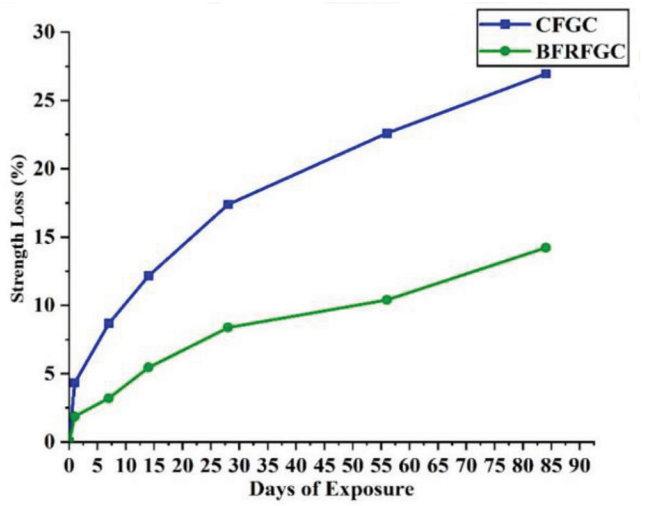

Fig. 5—Loss of compressive strength of specimens when exposed to sulfuric acid.

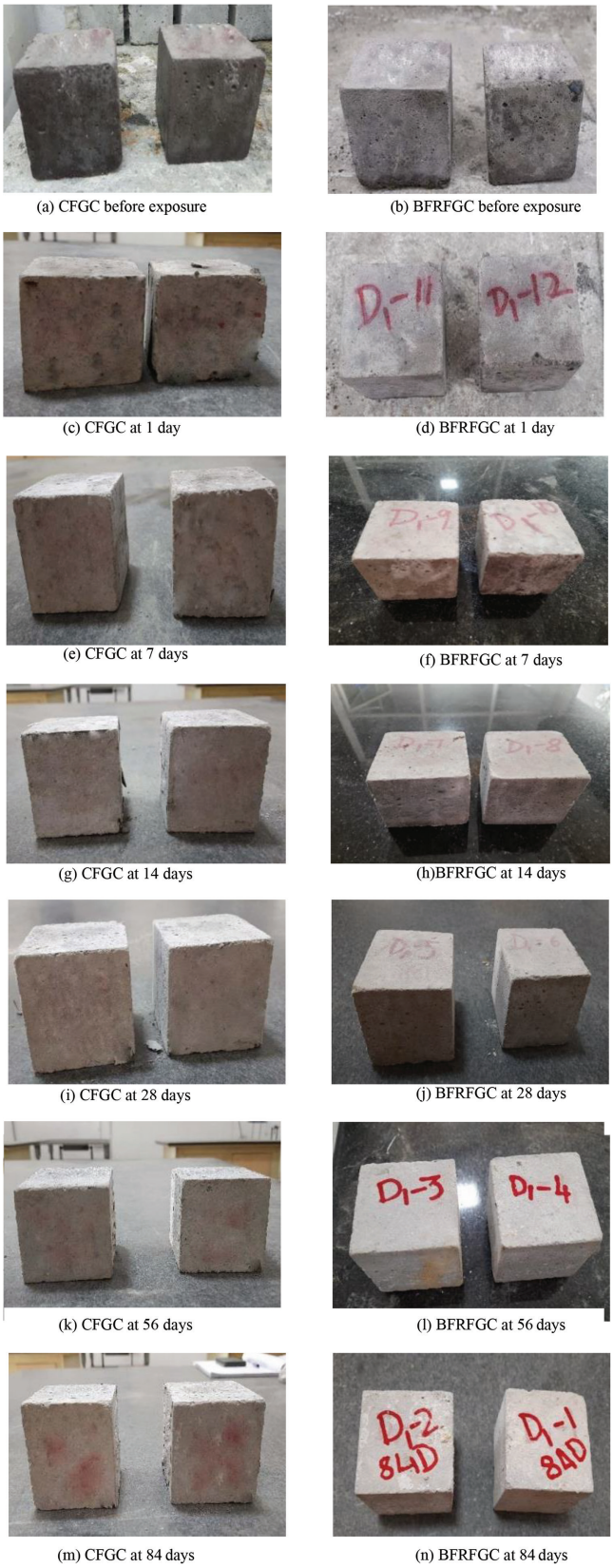

Fig. 6—Visual appearance of specimens at different days of exposure in seawater medium.

Effect of seawater

Structures near coastal areas or submarine structures are exposed to alkaline conditions either directly or indirectly. The visual inspections of the specimens after exposure to seawater, change in weight, and change in strength at the required days are performed as per ACI 201.2R-01.[37]

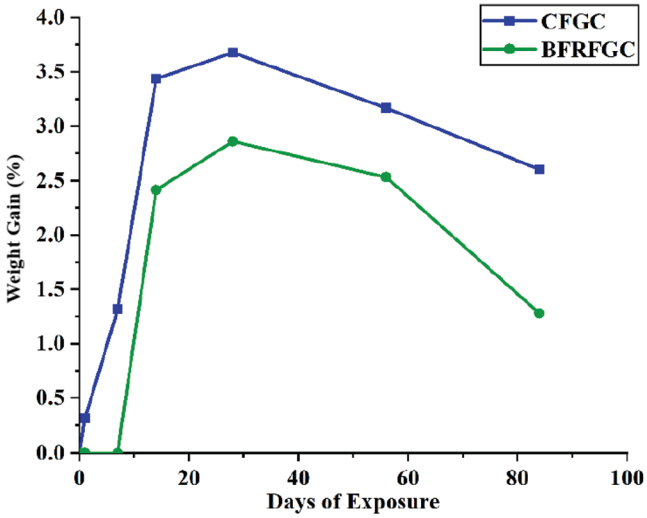

Fig. 7—Percentage change in weight of specimens when exposed to seawater.

Visual appearance—The CFGC and BFRFGC specimens were inspected visually at 1, 7, 14, 28, 56, and 84 days of exposure to salt water directly and are shown in Fig. 6(a) to (g).

$$3C_3A(CaSO_4).12H_2O + 2CaCl_2 + 16H_2O \rightarrow C_3A(CaSO_4)_3.32H_2O + 2C_3A(CaCl_2).10H_2O \quad (4)$$

As shown in Fig. 6(a) to (n), the specimens started to change color to white due to the crystallization of salt particles at the sides of the specimens. The salt was found in both the CFGC and BFRFGC, and no physical damage or deterioration of the specimens was detected. Wang et al.[32] studied the performance of concrete with GGBS under a seawater exposure environment and found that the samples with GGBS showed better resistance to corrosion than conventional samples. The results obtained in this study for BFRFGC without coarse aggregate showed similar performance as found in the literature, and no erosion of the sample was found. When the specimens were exposed to direct seawater, the calcium hydrates reacted with chlorine and formed Friedel's salt, as given in Eq. (4). This salt blocked the pores, thus reducing the chlorine permeability and resulting in salt crystallization. In the BFRFGC, due to the presence of GGBS and its fineness, the permeability was less, leading to more crystallization of salt particles on the surface. Thus, the BFRFGC showed better resistance to seawater, and a change in color to white was observed due to the salts settled at the sides of the specimen.

Change in weight—As shown in Fig. 7, exposing the CFGC and BFRFGC to seawater resulted in increased weight of the specimens at different inspection periods. The percentage gain in weight was less for the BFRFGC specimens than for the CFGC specimens. A weight gain of approximately 2.6% and 1.27% was found for the CFGC and BFRFGC at 84 days of direct exposure to seawater. The BFRFGC showed a lower weight gain of 51.15% than CFGC at 84 days of exposure

(a) CFGC (b) BFRFGC

Fig. 8—Failure of specimens in compression when exposed to seawater for 84 days.

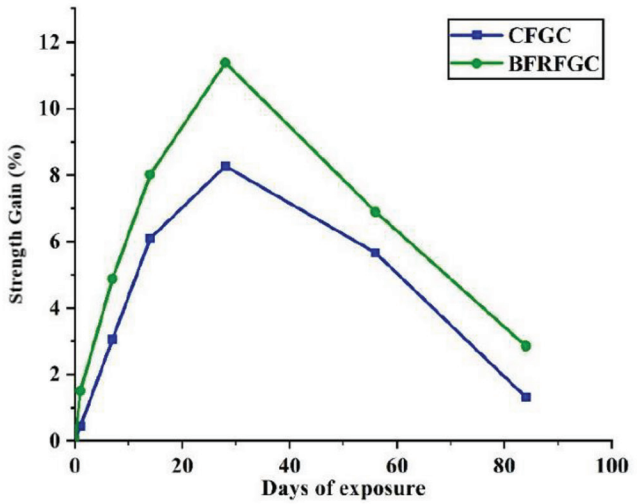

Fig. 9—Percentage change in compressive strength of specimens when exposed to seawater.

to seawater. Wang et al.[32] studied concrete performance with GGBS under a seawater exposure environment. A gain in weight was observed at the initial stages of exposure, with a reduction in the mass of the specimen at the later stages upon continuous exposure. The durability characteristics of Huijun et al.[38] on concrete exposed to seawater environments show a reduction in weight upon continuous exposure. The referred literature shows contradictory results. The results obtained in this work on CC were similar to those obtained by Wang et al.,[32] even without coarse aggregate. The weight gain was noticed at the initial ages due to the slow attack of seawater. The most common phase present in the portland cement was monosulfoaluminate, which, when exposed to seawater, reacts with the chlorine present in it, leading to the formation of ettringite and resulting in weight gain at initial ages. With continuous seawater exposure, the concentration of chloride ions increases in the specimen, leading to the direct phase transformation of monosulfoaluminate to Friedel's salt.[39] This process of dissolution results in volumetric expansion of the specimen, leading to its disruption and resulting in reduced weight at later ages. Thus, from the aforementioned results, it was clear that exposure to seawater had less of an effect on the BFRFGC compared to the CFGC.

Change in strength—The change in the strength of the CFGC and BFRFGC specimens when exposed to seawater continuously was studied and is shown in Fig. 8. Not much difference in failure mode between the two matrixes was noted. Figure 9 indicates the improved compressive strength of the CFGC and BFRFGC when exposed to direct seawater at different inspection periods. Figure 9 shows that when the CFGC and BFRFGC were exposed to seawater, their compressive strengths increased. The gain in strength was observed until 28 days of exposure, and it started to decrease on further exposure. The BFRFGC showed a higher gain in compressive strength than the CFGC.

A gain in compressive strength of approximately 1.31% and 2.85% was found in the CFGC and BFRFGC, respectively, when exposed directly to seawater for 84 days. The BFRFGC showed a 54.03% higher strength gain than the CFGC at 84 days of exposure to seawater. From the results obtained, it was clear that BFRFGC shows better resistance to seawater than CFGC. Jau and Tsay[40] studied the resistance of slag-based concrete to seawater and observed more of a reduction in compressive strength than CFGC when exposed to seawater. The weight gain was due to the formation of ettringite at the initial ages of exposure by spending the calcium hydroxide, as discussed in the previous section. BFRFGC showed more weight gain than CFGC due to the secondary hydration reactions that take place due to the presence of GGBS. The higher concentration of chloride ions suppressed the dissolution of monosulfoaluminate due to the ion-exchange mechanism. Thus, from the aforementioned results, it was clear that BFRFGC, when exposed to a marine environment, shows good resistance compared with CFGC.

Effect of temperature

The CFGC and BFRFGC specimens were evaluated when exposed to the elevated temperature of 200°C (392°F) for 2, 4, and 6 hours, for which the visual appearance of the specimen and the change in weight and strength were evaluated.

Visual inspection—Figures 10(a) to (h) show that when the CFGC and BFRFGC were exposed to a temperature of 200°C (392°F) for 2, 4, and 6 hours, hairline cracks were observed in the CFGC with a color change to pale. No physical damage was observed in the BFRFGC specimen, but the color started to pale. Alaskar et al.[41] studied the performance of BF concrete under higher temperatures, and a slight color variation was observed, and cracks were found on the surfaces. The results obtained in this study are contradictory to the referred literature. The change of color to pale was due to the loss of capillary water present in the specimen.

Change in weight—The change in weight of the CFGC and BFRFGC specimens when subjected to the elevated temperature of 200°C (392°F) was studied. As shown in Fig. 11, the weight of the CFGC and BFRFGC specimens reduced with the duration of exposure. The BFRFGC showed less of a reduction in weight than the CFGC. After exposure, a reduction in weight of approximately 2.9% and 2.44% was observed for the CFGC and BFRFGC, respectively.

The results show that the BFRFGC showed better resistance to the temperature than the CFGC, with a lower weight loss of 15.92% compared to the CFGC. Li et al.[42] studied the properties of concrete with GGBS at elevated

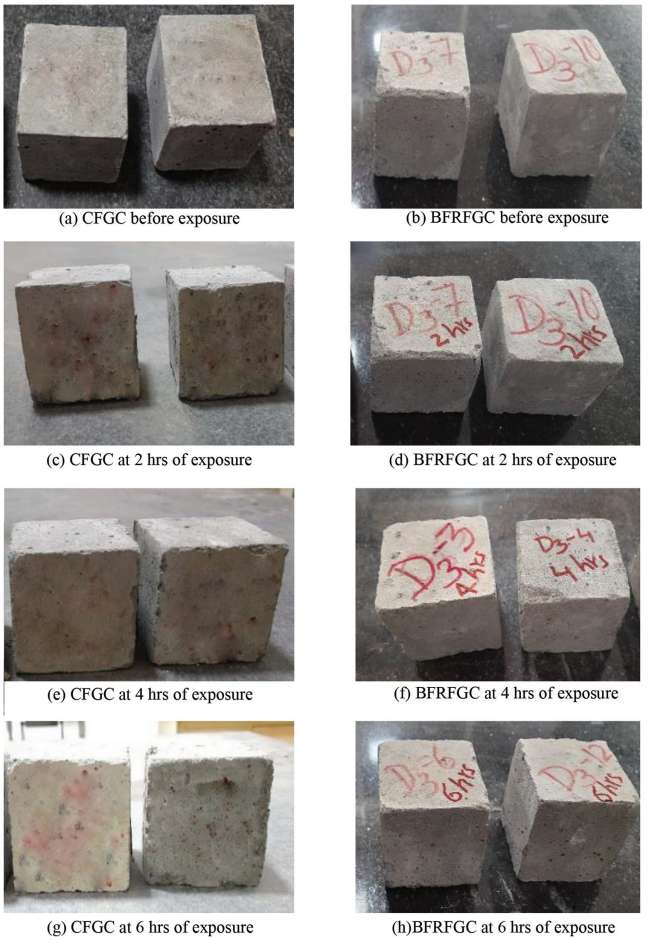

Fig. 10—Visual appearance of specimens exposed to 200°C (392°F).

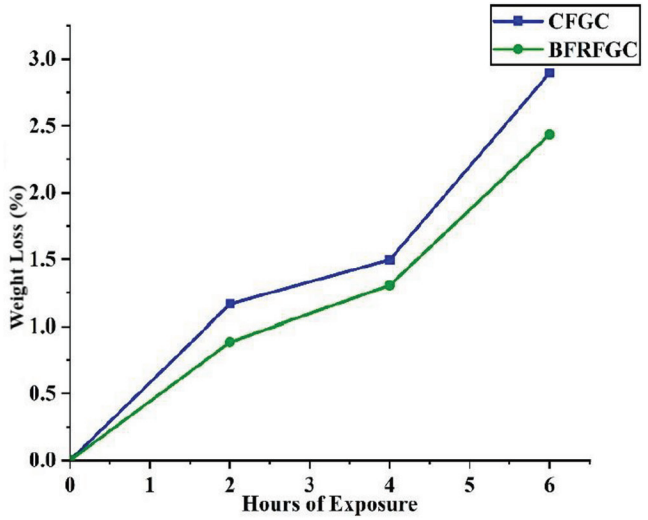

Fig. 11—Percentage loss of weight of specimens when exposed to elevated temperature.

temperatures and found that the weight reduction upon exposure to elevated temperature was identical to the present study. When specimens are exposed to temperature, the free water in the specimen evaporates first, and on continuous exposure, the decomposition of phases starts, leading to weight loss. However, in the case of the BFRFGC, the

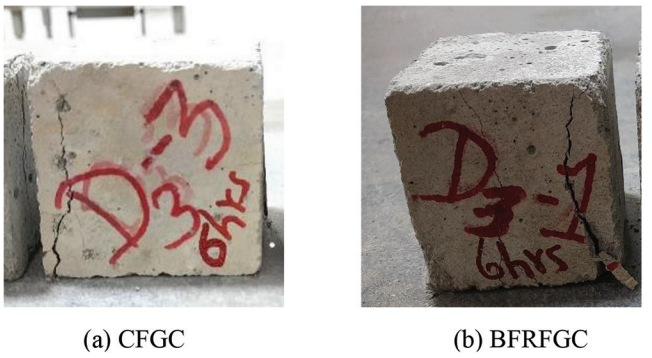

Fig. 12—Failure of specimens in compression when exposed to 200°C (392°F) for 6 hours.

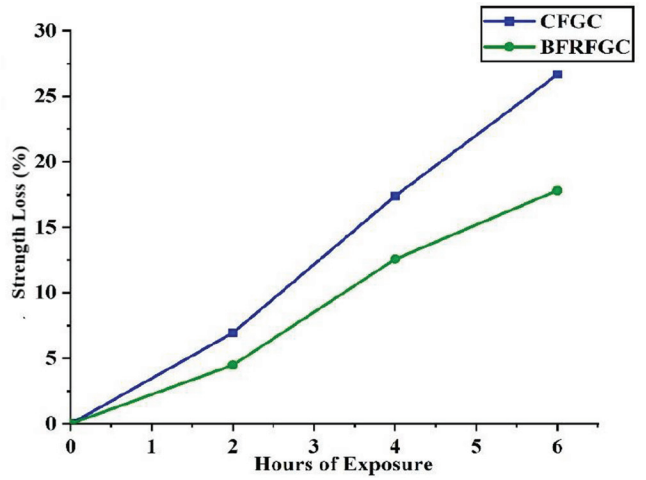

Fig. 13—Percentage loss of strength of specimens when exposed to elevated temperature.

weight loss was less than the CFGC due to the acceleration of secondary hydration reactions on exposure to higher temperatures. Thus, it was clear that the BFRFGC showed better resistance to the temperature effect than the CFGC.

Change in strength—The loss of strength of the BFRFGC specimen when subjected to the elevated temperature of 200°C (392°F) was studied, and the failure mode of both the matrixes after 6 hours of exposure is shown in Fig. 12. The failure mode obtained for both the matrix specimens was the same. Figure 13 indicates the weight gain of the CFGC and BFRFGC when different durations of exposure were studied. As shown in Fig. 13, the compressive strength of the CFGC and BFRFGC specimens reduced with the duration of exposure. The BFRFGC showed a 33.21% reduction in compressive strength compared to the CFGC. The maximum reduction in compressive strength observed for the CFGC and BFRFGC was approximately 26.65% and 17.8%, respectively. The results clearly show that the BFRFGC showed better resistance to temperature than the CFGC. Alaskar et al.[41] studied the properties of concrete with BF at elevated temperatures. A decrease in compressive strength was observed, but it showed better resistance when compared with concrete without fiber content and was similar to the current study for CC. The reduction in strength was due to the dehydration of water in C-S-H, and it started to decompose. GGBS is rich in silica content and takes time

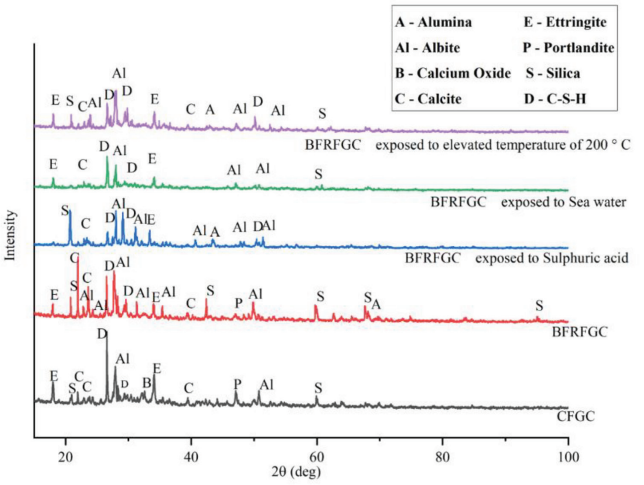

Fig. 14—XRD analysis of FGCC samples at different conditions.

to start the hydration process. However, when GGBS was used as a partial replacement for cement, the cement content initially started the hydration reaction, and the GGBS started to react slowly. When the specimen was exposed to higher temperatures, the hydration reaction started to react due to the GGBS content—that hydration reaction is called secondary hydration, and it led to higher strength than the CFGC. However, when the specimen was exposed continuously to a higher temperature, the water content responsible for the hydration started to dehydrate, resulting in strength reduction.

Microstructural characteristics

The microstructural characteristics were observed for the CFGC and BFRFGC samples at atmospheric and different exposure conditions through X-ray diffraction (XRD), Fourier-transform infrared spectroscopy (FTIR), thermogravimetric analysis (TGA), and scanning electron microscopy (SEM) with energy-dispersive X-ray spectroscopy (EDS).

X-ray diffraction—The XRD analysis was carried out for the CFGC and BFRFGC after 28 days of water curing and for the BFRFGC after being exposed to sulfuric acid and seawater for 84 days and elevated temperature of 200°C (392°F) for 6 hours, as shown in Fig. 14. C-S-H, calcite, silica, portlandite, alumina, and albite were the major phases present in the samples. Ettringite and calcium oxide were the minor peaks observed in the FGCC samples. C-S-H was the primary element responsible for strength and durability characteristics. The significant peaks found for different samples with 2θ values of 26.56, 29.8, and 50.1 degrees represent the presence of C-S-H.

The peaks at 23.9 and 27.9 degrees indicate the presence of albite, while the peaks at 20.9 and 60.1 degrees were due to the presence of silica. The peaks at 18.1 and 34.1 degrees indicate the ettringite formation, while the minor peaks at 23 and 39.5 degrees were due to the presence of calcite. The peaks at 28.1 and 23.9 degrees were formed due to the presence of alumina. The peaks obtained at 32.2 and 42.9 degrees represent the phases of calcium oxide and

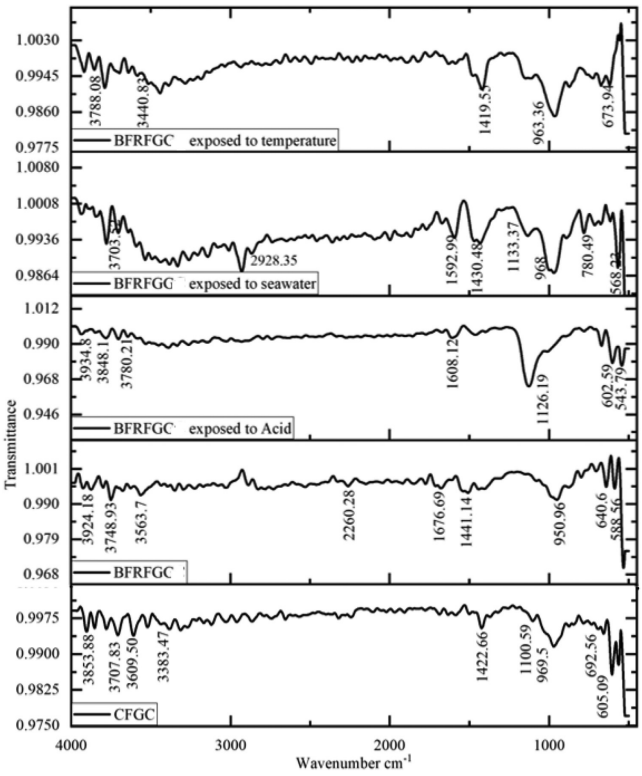

Fig. 15—FTIR analysis of FGCC samples at different conditions.

alumina, respectively. The intensity of the XRD peaks was reduced for samples exposed to sulfuric acid, seawater, and elevated temperature compared to the CFGC and BFRFGC samples.

The degree of crystallinity was 14.46%, 18.13%, 23.5%, 19.06%, 16.18%, and 13.22% for the CFGC and BFRFGC samples when exposed to sulfuric acid, seawater, and elevated temperature, respectively. Munjal et al.[43] and Yalçınkaya and Çopuroğlu[44] studied the effect of GGBS as a partial replacement of cement in concrete under different curing conditions and GGBS on ultra-high-performance concrete and found C-S-H, calcite, and portlandite were the significant elements present, similar to the current study on CC. The degree of crystallinity was found to increase based on CH. The degree of crystallinity reduces when exposed to different environmental conditions. This confirms the change in the weight and strength of the BFRFGC when exposed to different environmental conditions, as discussed earlier. The degree of crystallinity was reduced by exposing the samples to different environmental conditions.

Fourier-transform infrared spectroscopy—The FTIR analysis was performed to identify the bonds present in the samples, and the degree of carbonation can be identified from the graph. The FTIR analysis was carried out for the CFGC and BFRFGC after 28 days of water curing and for the BFRFGC after being exposed to sulfuric acid, seawater for 84 days, and an elevated temperature of 200°C (392°F) for 6 hours and is shown in Fig. 15. The bonds present in the sample are identified from the infrared (IR) spectrum chart. The bonds obtained between wave numbers 3500 to 3200 cm^{-1} are strong intermolecular O-H bonds.

The prominent peak of all the samples was found in the range of 1200 to 900 cm^{-1} and indicated the presence of C-S-H in the matrix, which is the primary cause of the increase in strength. The second significant peak was found between the wave range of 1300 to 1550 cm^{-1} and was responsible for the carbon bond, and the peaks in the range of 500 to 600 cm^{-1} were due to the anhydrous calcium silicate bond.

The degree of carbonation can be found from FTIR analysis without using the phenolphthalein indicator. The samples here were not exposed to accelerated carbonation in the chamber, but the natural degree of carbonation in atmospheric conditions was studied. The BFRFGC sample exposed to sulfuric acid for 84 days had higher carbonation than the other samples. The degree of carbonation was in the higher hierarchical order of BFRFGC, CFGC, sample exposed to seawater, sample exposed to elevated temperature, and sample exposed to concentrated sulfuric acid. The BFRFGC and CFGC showed the same degree of carbonation. Similarly, the samples exposed to seawater had the same degree of carbonation and were slightly higher than the BFRFGC and CFGC. Also, the samples exposed to elevated temperatures were in the same range. However, the degree of carbonation was remarkably higher in the case of BFRFGC exposed to sulfuric acid for 84 days. Not much variation in the intensity of peaks was found for other bonds. Tanwar et al.[36] studied the performance of GGBS-based concrete. They found that the transmittance and wavelength of samples, even after exposure to acid, almost remained the same as the current study on CC. The carbonic aggregates in the matrix, in the reaction with sulfuric acid, formed carbon dioxide, which controls the formation of gypsum. Thus, the FTIR curve of BFRFGC exposed to sulfuric acid showed a higher degree of carbonation.

Thermogravimetric analysis—Simultaneous thermogravimetric/derivative thermogravimetric/ differential thermal analysis (TG/DTG/DTA) was performed for the CC using Bhatty's method.[45] Figure 16(a) indicates the mass loss of samples at different phases of decomposition. The DTA and DTG curves shown in Fig. 16(b) and (c) represent the decomposition of phases and the type of reaction (endothermic or exothermic). The four stages of mass loss of the samples are confirmed in Fig. 16(a). The first stage of mass loss was from 30 to 140°C (86 to 284°F), indicating the evaporation of free capillary water present in the sample.[46] The next stage of mass loss occurred between 140 to 440°C (284 to 824°F) due to the dehydration of the hydration phases such as calcium alumina silica gel.[47] The subsequent stage of mass loss was between 440 to 680°C (824 to 1256°F), which was due to the dehydroxylation of portlandite.[48] The next stage of mass loss was due to the decarbonation of calcite to calcium oxide between 680 to 900°C (1256 to 1652°F). The mass loss of the CC specimens at the different stages is given in Table 4. The reduction in mass of 14.84%, 12.76%, 12.28%, 8.65%, 8.22%, and 7.73% was observed for the BFRFGC and CFGC samples exposed to acid, seawater, and temperature, respectively.

As shown in Table 4, significant mass loss was due to the evaporation of free water. As shown in Fig. 16(a) and

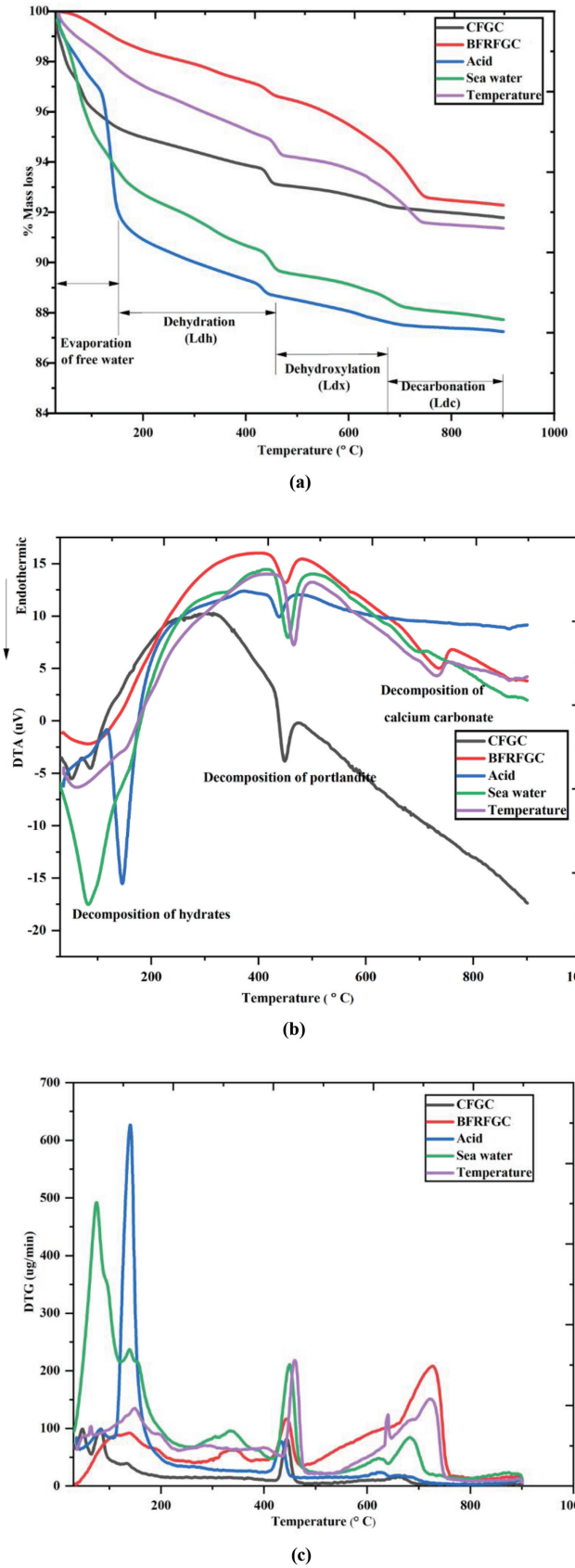

Fig. 16—(a) TGA of FGCC samples at different conditions; (b) DTA of FGCC samples at different conditions; and (c) DTG analysis of FGCC samples at different conditions.

Table 4—Mass loss at different phases of TGA

Sample	% weight loss		
	Ldh	Ldx	Ldc
CFGC	4.63	1.49	1.2
BFRFGC	1.1	1.68	1.74
BFRFGC exposed to acid	7.88	2.81	1.26
BFRFGC exposed to seawater	6.31	3.02	1.54
BFRFGC exposed to temperature	2.28	2.43	1.57

Note: Ldh is dehydration; Ldx is dehydroxylation; and Ldc is decarbonation.

(b), the mass loss was lower for BFRFGC and higher for BFRFGC exposed to sulfuric acid and seawater. The DTG curve obtained for all the samples is shown in Fig. 16(c). The first endothermic peak in Fig. 16(c) between 140 and 440°C (284 and 824°F) indicates the hydrates' decomposition and free water's evaporation. The second endothermic peak is in the range of 440 to 680°C (824 to 1256°F). The third endothermic peak from 680 to 900°C (1256 to 1652°F) represents the dehydration of $Ca(OH)_2$ due to the decarbonation of calcium carbonates. However, the intensity of the peak varied in all the samples. The peak shown between 100 and 200°C (212 and 392°F) in Fig. 16(a) to (c) is due to the evaporation of free water and decomposition of ettringite.

The simultaneous TG/DTA/DTG analysis showed that the mass loss was low in BFRFGC but increased when subjected to sulfuric acid and seawater. The mass loss percentages were contrary to the research findings by Snehal and Das[49] on CC exposed to acid, alkali, and chloride environments incorporating nanosilica particles. As the mass loss obtained by BFRFGC was less compared to the reported study, it confirmed the resistance of BF and GGBS to different environmental conditions. The GGBS content leads to the secondary hydration reaction as GGBS reacts slowly, and this improves the thermal stability of the cementitious matrix. The mass loss was lower for specimens subjected to elevated temperatures than for samples exposed to sulfuric acid and seawater. This confirms that BFRFGC was thermally more stable.

Scanning electron microscopy with energy-dispersive X-ray spectroscopy—The SEM images with EDS obtained for the CFGC and BFRFGC samples exposed to different environments are shown in Fig. 17(a) to (e). From the SEM images, it was clear that the CFGC shown in Fig. 17(a) contained shrinkage and voids. Further, with BF addition and by substituting GGBS partially instead of cement, the voids were reduced and are clear in Fig. 17(b), and the binding between the matrix and BF was confirmed from the interfacial transition zone (ITZ).

The BFRFGC specimens, after exposure to different environmental conditions, such as sulfuric acid, seawater, and elevated temperature, are shown in Fig. 17(c) to (e), and no damage to the fiber was noticed. When BFRFGC was exposed to sulfuric acid voids, cracks were observed, as shown in Fig. 17(c). The formation of cracks was due to the internal pressure caused by volumetric expansion by ettringites, as discussed earlier. Also, when the BFRFGC was exposed to seawater, cracks and ettringite phases were noticed, as shown in Fig. 17(d). No damage was found in BF exposed to seawater. The cracks were generated due to the volumetric expansion caused by ettringite formation. The ettringite phases disintegrated slowly, as seawater exposure is a slow attack. Similarly, when BFRFGC was exposed to temperature, voids and broken ettringite needles were discovered, as shown in Fig. 17(e). It indicates the decomposition of C-S-H when subjected to temperature. No damage in BF proves its thermal resistance. The results obtained through the SEM images confirm the observations of durability characteristics discussed earlier. This proves the high resistance of BF and BFRFGC to different environmental conditions.

From the EDS, calcium and silica were significant elements in the samples. The silica content increased, and a reduction in calcium was observed in the case of the BFRFGC compared with CFGC. When the specimens were exposed to different environmental conditions, there was a variation in calcium and silica contents. The calcium content increased when the sample was exposed to sulfuric acid, and silica was reduced. In a sample continuously exposed to seawater, the calcium, oxygen, and silica contents were reduced with higher iron content. In addition to these elements, chlorine was present in the sample, which was continuously exposed directly to seawater. No variation in elemental composition was found for the sample exposed to elevated temperatures. The increase in silica content in the BFRFGC was due to the higher silica content in the GGBS. The calcium-to-silica ratio in the CC helps to understand the strength characteristics of the sample. The low calcium-to-silica ratio indicated the formation of C-S-H, resulting in higher strength. The EDS results in Fig. 17 confirm the strength characteristics explained earlier. However, environmental conditions, such as acid exposure and elevated temperature, did not affect the elemental composition. However, the seawater-exposed sample showed higher iron content and chlorine due to the permeability of salt in the seawater.

CONCLUSIONS

It is desired to study the durability aspects of any construction material before applying it practically. The durability characteristics of cementitious composites (CC) with basalt fiber (BF) and ground-granulated blast-furnace slag (GGBS) were studied with exposure to acidic and alkaline environments and elevated temperatures. The following conclusions are drawn from the results obtained.

1. The fine-grained cementitious composites (FGCC) with 0.4% BF and 20% GGBS as partial replacement of cement showed approximately 29% higher strength.

2. The durability strength characteristics of BF-reinforced fine-grained CC incorporated with GGBS as a partial substitution of cement (BFRFGC) were 61.87%, 31.65%, and 39.8%, respectively, better with exposure to sulfuric acid, seawater, and a temperature of 200°C (392°F) compared with CFGC, which proves the better resistance to different environmental conditions.

3. The change in color of specimens with continuous exposure to sulfuric acid was due to the formation of ferric

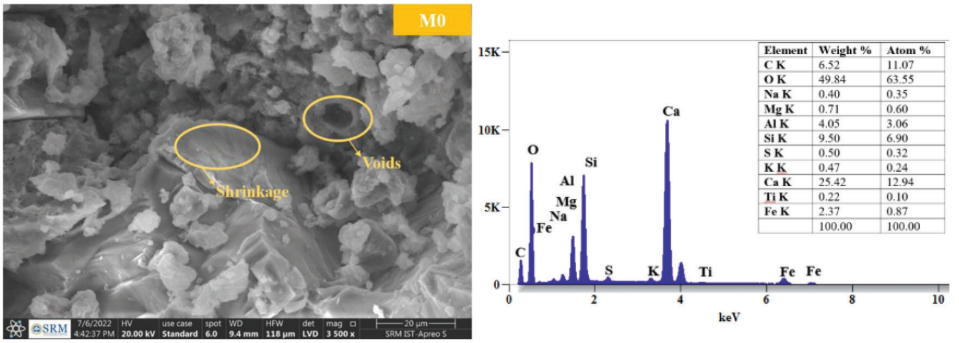

(a)CFGC

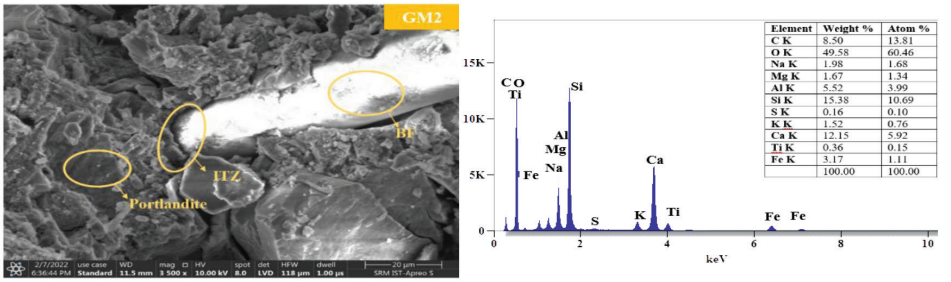

(b) BFRFGC

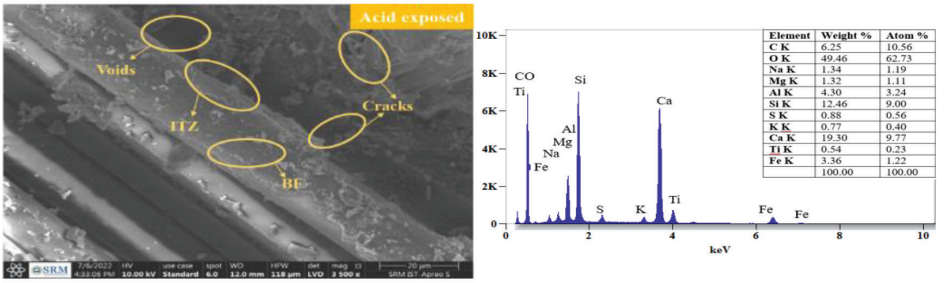

(c) BFRFGC after 84 days of exposure to Sulphuric acid

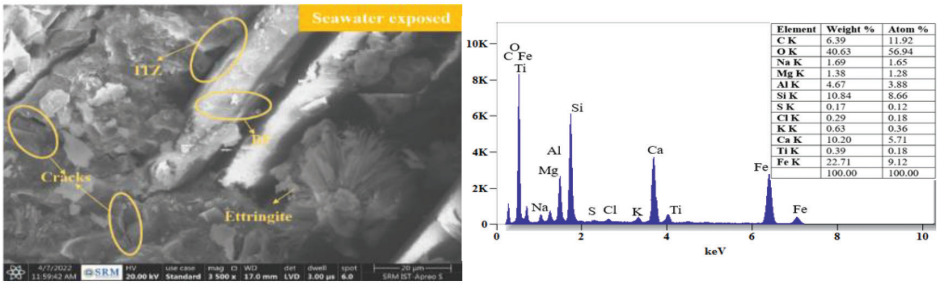

(d) BFRFGC after 84 days of exposure to Seawater

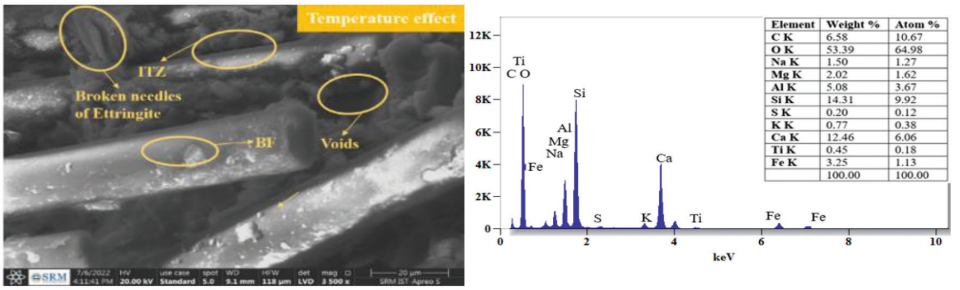

(e) BFRFGC after exposed to elevated temperature

Fig. 17—SEM with EDS images of FGCC.

oxide, and salt crystallization and deposits on the sides of specimens in the case of seawater.

4. The microstructural characteristics prove the reason for the better durability properties of BFRFGC.

5. Also, the lower impregnation of chlorides into the specimen when exposed to seawater confirmed the reduced voids.

From the overall observations, BFRFGC showed good resistance to the acidic and alkaline environments and exposure to higher temperatures. The improvement in durability characteristics was mainly due to the addition of GGBS, as it induces the dilution effect in the matrix and reacts slowly under different conditions, which induces the secondary hydration reaction. Thus, by using BF and GGBS in combination with the cementitious matrix, its durability characteristics can be improved.

AUTHOR BIOS

Alein Jeyan Sudhakar *received her PhD from SRM Institute of Science and Technology, Chennai, Tamil Nadu, India. Her research interests include textile-reinforced sandwich composites.*

Bhuvaneshwari Muthusubramanian *is an Assistant Professor in the Department of Civil Engineering at SRM Institute of Science and Technology with 10 years of teaching experience. She has published several journal articles and patents. Recently, she contributed as one of the authors in the record-breaking book for the thickest book and most authors in a single book in the* Asia Book of Records *and* India Book of Records.

DECLARATION OF CONFLICTING INTERESTS

The author(s) declared no potential conflicts of interest with respect to the research, authorship, and/or publication of this paper.

REFERENCES

1. ACI Committee 201, "Guide to Durable Concrete (ACI 201.2R-08)," American Concrete Institute, Farmington Hills, MI, 2008, 49 pp.

2. Chen, B.; Du, L.; Yuan, J.; Sun, X.; Pathirage, M.; Sun, W.; and Feng, J., "A Experimental Study on Engineered Cementitious Composites (ECC) Incorporated with *Sporosarcina pasteurii*," *Buildings*, V. 12, No. 5, May 2022, Article No. 691. doi: 10.3390/buildings12050691

3. Markou, I., "Effect of Grain Shape and Size on the Mechanical Behavior of Reinforced Sand," *Procedia Engineering*, V. 143, 2016, pp. 146-152. doi: 10.1016/j.proeng.2016.06.019

4. Zajceva, L.; Lucyk, E.; Latypova, T.; Latypov, V.; Fedorov, P.; and Salamanova, M., "Influence of the Type of Aggregate from Industrial Waste on Corrosion Resistance of Modified Fine-Grained Concrete," *Buildings*, V. 11, No. 8, Aug. 2021, Article No. 352. doi: 10.3390/buildings11080352

5. Brockmann, T., "Mechanical and Fracture Mechanical Properties of Fine Grained Concrete for TRC Structures," *Advances in Construction Materials 2007*, C. U. Grosse, ed., Springer, Berlin, Germany, 2007, pp. 119-129. doi: 10.1007/978-3-540-72448-3_12

6. Klyuev, S.; Klyuev, A.; and Vatin, N., "Fine-Grained Concrete with Combined Reinforcement by Different Types of Fibers," *MATEC Web of Conferences*, V. 245, 2018, Article No. 03006. doi: 10.1051/matecconf/201824503006

7. Lukutsova, N. P.; Soboleva, G. N.; Golovin, S. N.; Chivikova, E. V.; and Ogloblina, E. V., "Fine-Grained High-Strength Concrete," *Materials Science Forum*, V. 945, Feb. 2019, pp. 131-135. doi: 10.4028/www.scientific.net/MSF.945.131

8. Fediuk, R.; Pak, A.; and Kuzmin, D., "Fine-Grained Concrete of Composite Binder," *IOP Conference Series: Materials Science and Engineering*, V. 262, 2017, Article No. 012025. doi: 10.1088/1757-899X/262/1/012025

9. Haido, J. H., "Flexural Behavior of Basalt Fiber Reinforced Concrete Beams: Finite Element Simulation with New Constitutive Relationships," *Structures*, V. 27, Oct. 2020, pp. 1876-1889. doi: 10.1016/j.istruc.2020.08.005

10. Scholzen, A.; Chudoba, R.; and Hegger, J., "Thin-Walled Shell Structures Made of Textile-Reinforced Concrete: Part I: Structural Design and Construction," *Structural Concrete*, V. 16, No. 1, Mar. 2015, pp. 106-114. doi: 10.1002/suco.201300071

11. Dhand, V.; Mittal, G.; Rhee, K. Y.; Park, S.-J.; and Hui, D., "A Short Review on Basalt Fiber Reinforced Polymer Composites," *Composites Part B: Engineering*, V. 73, May 2015, pp. 166-180. doi: 10.1016/j.compositesb.2014.12.011

12. Smarzewski, P., "Comparative Fracture Properties of Four Fibre Reinforced High Performance Cementitious Composites," *Materials*, V. 13, No. 11, June 2020, Article No. 2612. doi: 10.3390/ma13112612

13. Hong, L.; Chen, Y. D.; Li, T. D.; Gao, P.; and Sun, L. Z., "Microstructure and Bonding Behavior of Fiber-Mortar Interface in Fiber-Reinforced Concrete," *Construction and Building Materials*, V. 232, Jan. 2020, Article No. 117235. doi: 10.1016/j.conbuildmat.2019.117235

14. Manimaran, A.; Pravinkumar, S.; Ravichandran, P. T.; and Ramasubramani, R., "Experimental Investigation on the Flexural Behaviour of Basalt Fibre Reinforced Polymer Rebar Concrete," *Materials Today: Proceedings*, V. 50, Part 3, 2022, pp. 353-357. doi: 10.1016/j.matpr.2021.08.268

15. Jalasutram, S.; Sahoo, D. R.; and Matsagar, V., "Experimental Investigation of the Mechanical Properties of Basalt Fiber-Reinforced Concrete," *Structural Concrete*, V. 18, No. 2, Apr. 2017, pp. 292-302. doi: 10.1002/suco.201500216

16. Oner, A., and Akyuz, S., "An Experimental Study on Optimum Usage of GGBS for the Compressive Strength of Concrete," *Cement and Concrete Composites*, V. 29, No. 6, July 2007, pp. 505-514. doi: 10.1016/j.cemconcomp.2007.01.001

17. Kumar, V. R. P.; Gunasekaran, K.; and Shyamala, T., "Characterization Study on Coconut Shell Concrete with Partial Replacement of Cement by GGBS," *Journal of Building Engineering*, V. 26, Nov. 2019, Article No. 100830. doi: 10.1016/j.jobe.2019.100830

18. Krishnaraj, L., and Ravichandran, P. T., "Characterisation of Ultra-Fine Fly Ash as Sustainable Cementitious Material for Masonry Construction," *Ain Shams Engineering Journal*, V. 12, No. 1, Mar. 2021, pp. 259-269. doi: 10.1016/j.asej.2020.07.008

19. Ganesh Babu, K., and Sree Rama Kumar, V., "Efficiency of GGBS in Concrete," *Cement and Concrete Research*, V. 30, No. 7, July 2000, pp. 1031-1036. doi: 10.1016/S0008-8846(00)00271-4

20. Alein, J. S., and Bhuvaneshwari, M., "Textile-Reinforced Concrete Sandwich Panels: A Review," *ACI Structural Journal*, V. 119, No. 5, Sept. 2022, pp. 207-216. doi: 10.14359/51734899

21. IS 12269:2013, "Ordinary Portland Cement, 53 Grade — Specification," Bureau of Indian Standards, New Delhi, India, 2013, 14 pp.

22. IS 16714:2018, "Ground Granulated Blast Furnace Slag for Use in Cement, Mortar and Concrete — Specification," Bureau of Indian Standards, New Delhi, India, 2018, 11 pp.

23. IS 383:2016, "Coarse and Fine Aggregate for Concrete — Specification," Bureau of Indian Standards, New Delhi, India, 2016, 22 pp.

24. IS 9103:1999 (Reaffirmed 2018), "Concrete Admixtures — Specification," Bureau of Indian Standards, New Delhi, India, 2018.

25. Sudhakar, A. J., and Muthusubramanian, B., "Development of Basalt Fiber Reinforced Fine-Grained Cementitious Composites for Textile Reinforcements," *Journal of Composites Science*, V. 6, No. 12, Dec. 2022, Article No. 396.

26. Sudhakar, A. J., and Muthusubramanian, B., "Thermal Characteristics of Fine Grained Concrete with Various Percentages of Basalt Fiber and GGBS," *Journal of Thermal Analysis and Calorimetry*, V. 148, No. 12, June 2023, pp. 5217-5233. doi: 10.1007/s10973-023-12011-9

27. ASTM C267-01, "Standard Test Methods for Chemical Resistance of Mortars, Grouts, and Monolithic Surfacings and Polymer Concretes," ASTM International, West Conshohocken, PA, 2001, 6 pp.

28. Bureau of Indian Standards, "National Building Code of India: Part 4: Fire and Life Safety," New Delhi, India, 2016.

29. Sobia, A. Q.; Hamidah, M. S.; Azmi, I.; and Rafeeqi, S. F. A., "Elevated Temperature Resistance of Ultra-High-Performance Fibre-Reinforced Cementitious Composites," *Magazine of Concrete Research*, V. 67, No. 17, Sept. 2015, pp. 923-937. doi: 10.1680/macr.14.00134

30. Ahmad, J.; Kontoleon, K. J.; Majdi, A.; Naqash, M. T.; Deifalla, A. F.; Ben Kahla, N.; Isleem, H. F.; and Qaidi, S. M. A., "A Comprehensive Review on the Ground Granulated Blast Furnace Slag (GGBS) in Concrete Production," *Sustainability*, V. 14, No. 14, July 2022, Article No. 8783. doi: 10.3390/su14148783

31. Saranya, P.; Nagarajan, P.; and Shashikala, A. P., "Eco-Friendly GGBS Concrete: A State-of-The-Art Review," *IOP Conference Series: Materials Science and Engineering*, V. 330, 2018, Article No. 012057. doi: 10.1088/1757-899X/330/1/012057

32. Wang, D.; Ma, Y.; Kang, M.; Ju, Y.; and Zeng, C., "Durability of Reactive Powder Concrete Containing Mineral Admixtures in Seawater Erosion Environment," *Construction and Building Materials*, V. 306, Nov. 2021, Article No. 124863. doi: 10.1016/j.conbuildmat.2021.124863

33. Madhuri, G., and Srinivasa Rao, K., "Performance of Alkali-Activated Slag Concrete Against Sulphuric Acid Attack," *Asian Journal*

of Civil Engineering, V. 19, No. 4, June 2018, pp. 451-461. doi: 10.1007/s42107-018-0028-1

34. Chintalapudi, K., and Pannem, R. M. R., "Enhanced Chemical Resistance to Sulphuric Acid Attack by Reinforcing Graphene Oxide in Ordinary and Portland Pozzolana Cement Mortars," *Case Studies in Construction Materials*, V. 17, Dec. 2022, Article No. e01452. doi: 10.1016/j.cscm.2022.e01452

35. Khan, M.; Cao, M.; Chu, S. H.; and Ali, M., "Properties of Hybrid Steel-Basalt Fiber Reinforced Concrete Exposed to Different Surrounding Conditions," *Construction and Building Materials*, V. 322, Mar. 2022, Article No. 126340. doi: 10.1016/j.conbuildmat.2022.126340

36. Tanwar, V.; Bisht, K.; Kabeer, K. I. S. A.; and Ramana, P. V., "Experimental Investigation of Mechanical Properties and Resistance to Acid and Sulphate Attack of GGBS Based Concrete Mixes with Beverage Glass Waste as Fine Aggregate," *Journal of Building Engineering*, V. 41, Sept. 2021, Article No. 102372. doi: 10.1016/j.jobe.2021.102372

37. ACI Committee 201, "Guide to Durable Concrete (ACI 201.2R-01)," American Concrete Institute, Farmington Hills, MI, 2001, 41 pp.

38. Huijun, W.; Diao, Z.; and Fan, K., "Study on Durability of Non-dispersible Concrete in Seawater Environment," *International Journal of Structural Integrity*, V. 11, No. 3, 2020, pp. 443-452. doi: 10.1108/IJSI-07-2019-0066

39. Yoon, S.; Ha, J.; Chae, S. R.; Kilcoyne, D. A.; Jun, Y.; Oh, J. E.; and Monteiro, P. J. M., "Phase Changes of Monosulfoaluminate in NaCl Aqueous Solution," *Materials*, V. 9, No. 5, May 2016, Article No. 401. doi: 10.3390/ma9050401

40. Jau, W.-C., and Tsay, D.-S., "A Study of the Basic Engineering Properties of Slag Cement Concrete and Its Resistance to Seawater Corrosion," *Cement and Concrete Research*, V. 28, No. 10, Oct. 1998, pp. 1363-1371. doi: 10.1016/S0008-8846(98)00117-3

41. Alaskar, A.; Albidah, A.; Alqarni, A. S.; Alyousef, R.; and Mohammadhosseini, H., "Performance Evaluation of High-Strength Concrete Reinforced with Basalt Fibers Exposed to Elevated Temperatures," *Journal of Building Engineering*, V. 35, Mar. 2021, Article No. 102108. doi: 10.1016/j.jobe.2020.102108

42. Li, Q.; Yuan, G.; Xu, Z.; and Dou, T., "Effect of Elevated Temperature on the Mechanical Properties of High-Volume GGBS Concrete," *Magazine of Concrete Research*, V. 66, No. 24, Dec. 2014, pp. 1277-1285. doi: 10.1680/macr.14.00142

43. Munjal, P.; Hau, K. K.; and Cheng, C. H. A., "Effect of GGBS and Curing Conditions on Strength and Microstructure Properties of Oil Well Cement Slurry," *Journal of Building Engineering*, V. 40, Aug. 2021, Article No. 102331. doi: 10.1016/j.jobe.2021.102331

44. Yalçınkaya, Ç., and Çopuroğlu, O., "Hydration Heat, Strength and Microstructure Characteristics of UHPC Containing Blast Furnace Slag," *Journal of Building Engineering*, V. 34, Feb. 2021, Article No. 101915. doi: 10.1016/j.jobe.2020.101915

45. Bhatty, J. I., "Hydration versus Strength in a Portland Cement Developed from Domestic Mineral Wastes — A Comparative Study," *Thermochimica Acta*, V. 106, Sept. 1986, pp. 93-103. doi: 10.1016/0040-6031(86)85120-6

46. Liu, C.-T., and Huang, J.-S., "Fire Performance of Highly Flowable Reactive Powder Concrete," *Construction and Building Materials*, V. 23, No. 5, May 2009, pp. 2072-2079. doi: 10.1016/j.conbuildmat.2008.08.022

47. Narattha, C.; Thongsanitgarn, P.; and Chaipanich, A., "Thermogravimetry Analysis, Compressive Strength and Thermal Conductivity Tests of Non-autoclaved Aerated Portland Cement–Fly Ash–Silica Fume Concrete," *Journal of Thermal Analysis and Calorimetry*, V. 122, No. 1, Oct. 2015, pp. 11-20. doi: 10.1007/s10973-015-4724-8

48. Yun, T. S.; Jeong, Y. J.; and Youm, K.-S., "Effect of Surrogate Aggregates on the Thermal Conductivity of Concrete at Ambient and Elevated Temperatures," *The Scientific World Journal*, V. 2014, No. 1, 2014, Article No. 939632. doi: 10.1155/2014/939632

49. Snehal, K., and Das, B. B., "Acid, Alkali and Chloride Resistance of Binary, Ternary and Quaternary Blended Cementitious Mortar Integrated with Nano-Silica Particles," *Cement and Concrete Composites*, V. 123, Oct. 2021, Article No. 104214. doi: 10.1016/j.cemconcomp.2021.104214

ACI MATERIALS JOURNAL TECHNICAL PAPER

Title No. 122-M10

Impressed Current Cathodic Protection with Near-Surface-Mounted Titanium Retrofit Bars

by Amanda K. Slawinski, Christopher Higgins, and O. Burkan Isgor

Titanium alloy bars (TiABs) have recently been accepted as a structural material for near-surface-mounted retrofit (NSMR) of reinforced concrete structural elements. This paper shows that TiABs in NSMR applications can be used simultaneously as anodes in impressed current cathodic protection (ICCP) to prevent corrosion of the existing reinforcement. Following a successful proof-of-concept study performed for small-scale prisms, dual-purpose TiABs were used as longitudinal and shear reinforcements to retrofit large-size structural beams. Prior to structural tests, the specimens were investigated to characterize the TiAB functionality within the ICCP system. During ICCP, cathodic potentials were in the expected linear region of the cathodic polarization curve of the steel reinforcing bars, and the 100 mV potential shift (decay) criterion following shutoff was satisfied upon the interruption of the protection current. The applied current and potential to achieve the required cathodic potentials were stable and were satisfactorily maintained while achieving the structural retrofit requirements.

Keywords: cathodic protection; corrosion; reinforcement; reinforcing bar; retrofit; steel; titanium.

INTRODUCTION

Strengthening reinforced concrete structures using the near-surface-mounted retrofit (NSMR) technique is an established approach in structural engineering practice.[1,2] Besides conventional fiber-reinforced polymer-based retrofitting materials, in recent years, titanium alloy bars (TiABs) have been shown to effectively and economically increase shear and flexural strength of existing reinforced concrete structures.[2,3]

Titanium is a widely used anode in impressed current cathodic protection (ICCP) systems to mitigate reinforcement corrosion issues in existing structures.[4] In these ICCP systems, ASTM Grade 1 or 2 titanium is typically used as anodes in the form of embedded welded wire reinforcement, strips, or discrete anodic bars.[5] These titanium anodes are often coated with mixed metal oxides (MMOs) such as iridium oxide or ruthenium oxide to increase their efficiency, stability, and durability.[6] In conventional ICCP systems, titanium anodes only serve to provide the necessary impressed current to protect the existing reinforcement from corrosion and do not provide any structural benefits. The use of TiABs as an NSMR material creates the unique opportunity for a multi-functional (dual-purpose) solution that can provide immediate capacity restoration, and when integrated into an ICCP system, can also mitigate future reinforcement corrosion issues in existing structures, which is the focus of this paper.

The opportunity to use TiABs that combine strengthening with corrosion protection offers the potential for achieving multiple objectives for restoration of corrosion damaged infrastructure. Although TiABs have been shown to perform well for retrofitting applications, their efficacy in providing the necessary cathodic protection has not been studied when they are used as an NSMR material. Present design and construction guidelines are available for strengthening bridges with NSMR-TiABs,[7] and the chemical and physical characteristics of TiABs for use in NSMR applications are prescribed in ASTM B1009-18.[8] Typically, TiABs that are used as NSMR material are made up of the Ti-6Al-4V alloy, which corresponds to ASTM Grade 5.[8] Because TiABs are not specifically developed for ICCP applications, they are not MMO coated. The lack of surface coating might have implications with respect to their ICCP performance and durability and requires further investigation.

Another challenge with using NSMR-TiABs as anodes in ICCP applications is related to the installation procedures that are developed for the NSMR applications. In a typical NSMR application, TiABs are installed in the grooves cut into the surface of structural elements and bonded to the concrete substrate with epoxy resins.[7] Because embedment in epoxy electrically isolates the TiAB from the surrounding materials, epoxy-embedded TiABs cannot function as anodes to impress current that can protect the existing reinforcement from corrosion. Therefore, an alternative installation procedure and mounting material are needed for ICCP applications. In this work, non-shrink conductive grouts were developed to maintain electrical conductivity at the interfaces between the ICCP anode and the protected reinforcement. Another important consideration is the electrical connectivity to the TiAB anodes within the ICCP system.

The main objective of this paper is to address the major challenges associated with using dual-purpose TiAB anodes in NSMR/ICCP applications. The paper first reports on the electrically conductive structural grout developed for the NSMR/ICCP application. Next, small-scale prism tests were used to study the ICCP parameters in different TiAB and installation settings. Finally, the ICCP performance of TiAB anodes is presented from their use as NSMR-TiABs for the structural retrofit of a large-scale beam undergoing active corrosion.

RESEARCH SIGNIFICANCE

The annual cost of corrosion in civil infrastructure in the United States is estimated at over $25 billion, and a large proportion is ascribable to corrosion of the embedded

ACI Materials Journal, V. 122, No. 2, March 2025.

MS No. M-2024-191.R1, doi: 10.14359/51745598, received December 18, 2024, and reviewed under Institute publication policies.

reinforcing steel in concrete. Approximately 15% of over 600,000 bridges in the United States are identified as structurally deficient, many due to corrosion issues. NSMR is an established technique to retrofit structurally deficient bridges and other structures, but the proposed approach described here allows structural TiABs to be used for a secondary purpose as ICCP anodes. This dual-purpose application has the potential to revolutionize how structurally deficient structures can simultaneously be strengthened and protected from further corrosion.

EXPERIMENTAL INVESTIGATION

Materials

Electrically conductive structural grout (ECSG)—Two commercially available high-strength grouts were selected as options for installing TiABs in surface grooves of structural elements. Non-shrink grouts were required to satisfy both the structural (NSRM) and electrical connectivity (ICCP) requirements. The commercial grouts were designed for repair applications and readily available from commonly known and accessible manufacturers. The grouts were chosen for their sulfate resistance in marine environments, freezing-and-thawing resistance, fluid consistency over a 30-minute working time, high placement versatility, and their recommended use for the placement of anchors and dowels.

Carbon fibers (CFs) were incorporated in the grout mixtures based on volume percentage to increase electrical conductivity of the grouts.[9,10] The use of CFs in a cementitious mixture required the addition of a dispersion agent to prevent fibers from clumping together. The dispersion agent used was methyl cellulose, which was added to the mixtures based on percent by weight of grout.[10] Carbon black (CB) was also considered as a material that could impact the electrical conductivity (or resistivity) of the grout, and it was combined with carbon fibers in the grout mixture by percent volume.[9] Variables considered in the grout design included the brand of commercial grout, CF content and fiber length, CB content, methyl cellulose content, and quantity of high-range water reducer (HRWR).

Three different CF lengths were used to determine the effect on both resistivity and compressive strength. All the CFs were unsized, milled polyacrylanitrile (PAN) fiber with a carbon content of 94% or greater in accordance with ASTM D5291-16.[11] They had a diameter of 7 to 9 microns and a tensile strength of 2.0 to 3.8 GPa (290 to 551 ksi). The NSMR design application for the grout prescribed the use of a 1 x 1 in. (25.4 x 25.4 mm) square groove and a 1/2 x 1/2 in. (13 x 13 mm) square groove for the placement of No. 5 and No. 2 TiABs, respectively.[7] Due to the small groove sizes, short CF lengths were considered more appropriate for the application. The fiber lengths ranged from 350 microns to 0.24 in. (6 mm). The recommended amount of CF content in concrete is less than 1% by total volume of grout.[10] This CF content recommended in existing research considers percentage volume for concrete, which includes large aggregates in its composition, so the volume percentage was adjusted for grout, by correcting for the absence of large aggregates. Volume percentages considered were 0.1, 0.2, and 0.4% for the carbon content in the grout mixture. Table 1 provides the details of the grout matrix based on CF size and content.

Both commercial grouts were first cast without the addition of any CFs to produce control samples to compare with baseline resistivities and compressive strengths. The grout exhibiting the lower resistivity was then mixed with CFs to observe their effect on the compressive strength and resistivity. The intention was to create a grout mixture that was both strong and had a low resistivity, thereby creating a conductive grout mixture to improve the performance of the ICCP system. For each test mixture, three grout cylinders measuring 4 in. (100 mm) diameter by 8 in. (200 mm) in height were cast to measure resistivity through a bulk resistivity test per ASTM C1876-19.[12] A total of six 2 in. (50 mm) grout cubes were cast to test compressive strength according to ASTM C109/C109M-16a.[13] Municipal tap water was used in all mixtures to replicate field conditions. All grout cylinders and cubes were cured in a fog room to create an idealized curing environment.

Methyl cellulose was used in all mixtures at a quantity of 0.2% by weight of the grout mixture. The addition of both the methyl cellulose and the CFs had an impact on the viscosity of the mixture when combined with water. To improve workability and ensure fluidity of the mixture, the addition of a HRWR admixture was also required. The commercial HRWR admixture used recommended a volume in the range of 2 to 12 fl oz per 100 lb (130 to 780 mL per 100 kg) of cementitious materials. The HRWR admixture was added to grout mixtures for applications in the prisms and beams at the maximum range of the recommendations.

After the combination that resulted in the lowest resistivity was determined, CB was added to that mixture to determine the influence on the grout resistivity. Two different quantities of CB were tested on the grout in combination with CFs to assess the change in resistivity and strength. CB was added at volume percentages of 0.16% and 0.30%. The best

Table 1—Carbon fiber content matrix for electrically conductive structural grouts

Commercial grout	Control (no fibers)	CFs			
		% CF by volume	MO	3 mm (0.118 in.)	Milled (350 μm)
1	1-C	0.1	1-CF-0.1-6	1-CF-0.1-3	1-CF-0.1-M
		0.2	1-CF-0.2-6	1-CF-0.2-3	1-CF-0.2-M
		0.4	1-CF-0.4-6	1-CF-0.4-3	1-CF-0.4-M
2	2-C	0.1	2-CF-0.1-6	2-CF-0.1-3	2-CF-0.1-M
		0.2	2-CF-0.2-6	2-CF-0.2-3	2-CF-0.2-M
		0.4	2-CF-0.4-6	2-CF-0.4-3	2-CF-0.4-M

Table 2—Properties of metal bars used in this study

Property	Grade 40 (280) steel (No. 4 [13M])	Grade 60 (420) steel (No. 9 [29M])	Ti-6Al-4V (No. 2 [6M])	Ti-6Al-4V (No. 5 [16M])
Nominal diameter, in. (mm)	0.50 (13)	1.125 (29)	0.25 (6)	0.625 (16)
Effective cross-sectional area, in.^{2} (mm^2)	0.20 (129)	1.00 (645)	0.049 (32)	0.31 (200)
Minimum yield stress, ksi (MPa)	40 (275)	60 (415)	130 (900)	130 (900)
Actual yield stress, ksi (MPa)	52 (359)	68 (476)	136.3 (984)	142.7 (984)
Actual tensile strength, ksi (MPa)	81 (558)	102 (703)	150 (1034)	154 (1062)
Nominal modulus of elasticity, ksi (GPa)	29,000 (200)	29,000 (200)	15,550 (107)	15,500 (107)
Elongation, %	28	15	20	19

Table 3—ICCP test prism concrete mixture proportions

w/c	0.55
Required concrete volume, ft^3	1.85
Water, lb/yd^3	419
Cement, lb/yd^3	618
Coarse aggregate, lb/yd^3	1239
Fine aggregate, lb/yd^3	1533
NaCl, lb/yd^3	15.3

Note: 1 lb/yd^3 = 0.593 kg/m^3; 1 ft^3 = 0.0283 m^3.

combination of materials was used in subsequent tests and is herein defined as the ERSG.

Reinforcing metals: Carbon steel reinforcing bar and TiABs—Conventional carbon reinforcing steel was used within the concrete elements as primary reinforcement. All longitudinal bars were Grade 60 (Grade 420) steel and size No. 9 (No. 29M) bars for both flexural tension and compression steel. Transverse steel was Grade 40 (Grade 280) steel and size No. 4 (No. 13M) bars for all stirrups. The TiABs correspond to ASTM B1009[8] Class 130 (having a minimum yield stress of 130 ksi [896 MPa]). The bars used for transverse bars were size No. 2 (No. 6M), and longitudinal bars were size No. 5 (No. 16M), as shown in Fig. 1. The physical properties of the metal bars used in this study, based on uniaxial tension tests per ASTM E8/E8M-16a[14] are shown in Table 2. Both sizes of TiABs were manufactured with surface deformations to enhance bond along the length of the bars.[15]

ICCP prisms—Two small-scale test prisms were designed and cast using an ordinary portland cement (OPC) concrete mixture with a 0.55 water-cement ratio (*w/c*). The mixing water contained 1.5% chlorides in the form of NaCl to ensure the active corrosion of the embedded steel reinforcing bars. The concrete mixture design closely matched the concrete properties that were widely used in bridges constructed during the mid-twentieth century. Type I/II cement was used. The test prisms were cast with an 8 x 6 x 18 in. (200 x 150 x 460 mm) profile. The mixture proportions are shown in Table 3.

The prisms were cast with two No. 9 Grade 60 (No. 29M Grade 420) and two No. 4 Grade 40 (No. 13M Grade 280) carbon steel bars protruding through one end of the concrete's surface so that an external electrical connection could be established between pieces of reinforcing bar. Reinforcing bar pieces were 18 in. (460 mm) in length and

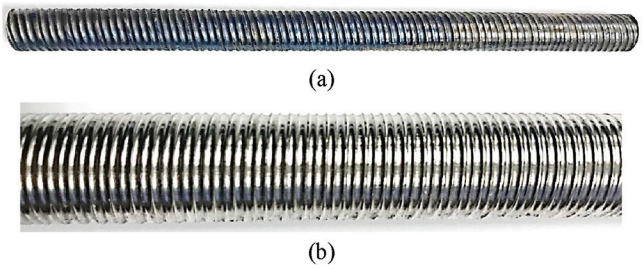

Fig. 1—TiAB profiles: (a) No. 2 (No. 6M) bar (diameter = 0.25 in. [6 mm]); and (b) No. 5 (No. 16M) bar (diameter = 0.625 in. [16 mm]).

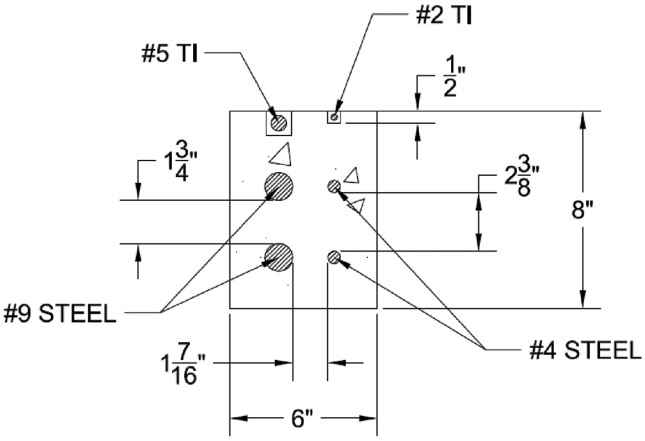

Fig. 2—Cross section of ICCP concrete test prism. (Note: Units in inches; 1 in. = 25.4 mm.)

extended approximately 1 in. (25.4 mm) beyond the end of the prism. Before the prisms were cast, the ends of the carbon steel bar were drilled and tapped. This permitted the electrical connection at the steel for ICCP. Fasteners were secured into the ends of the exposed reinforcing bar, and copper wire was wrapped tightly around the fasteners to externally connect the circuitry between pieces of bar in the prisms. This allowed ICCP to be applied to the system from outside of the specimen. The exposed ends of reinforcing bar were coated in epoxy. The cross section of the prism can be seen in Fig. 2.

After the prisms cured under wet burlap for 28 days, grooves were cut into the concrete for the NSMR-TiAB placement. The No. 5 (No. 16M) TiABs were cast into 1 x 1 in. (25.4 x 25.4 mm) grooves, and the No. 2 (No. 6M) TiABs were cast into 1/2 x 1/2 in. (13 x 13 mm) grooves

Table 4—Concrete mixture proportions from batch ticket (3 yd³)

Material	Design quantity, per yd³	Required	Batched	% Variation	% Moisture	Actual water, gal.
3/4 in. (19 mm) coarse aggregate	1741 lb	5342 lb	5290 lb	–0.97%	2.27% M	14
Sand	1392 lb	4428 lb	4420 lb	–0.19%	6.04% A	30
OPC	470 lb	1410 lb	1397 lb	–0.92%	—	—
Air-entraining admixture	1.40 oz.	4.20 oz.	4.00 oz.	–4.76%	—	—
Water-reducing admixture	23.50 oz.	70.50 oz.	68.00 oz.	–3.55%	—	—
Cold water	31 gal.	43 gal.	47 gal.	10.43%	—	47
NaCl	11.62 lb	34.9 lb	35.3 lb	+1.25%	—	—

Note: 1 lb = 0.454 kg; 1 oz = 29.57 mL; 1 L = 3.79 gal.

using the ECSG as the bonding agent. After the ECSG cured, ICCP was applied to the prisms so that the appropriate current range could be determined to achieve cathodic protection. In these tests, the prism concrete was determined to have a bulk resistivity of 3.77 kΩ-cm and the ECSG exhibited a bulk resistivity of 0.42 kΩ-cm.

Large-size beams with NSMR-TiAB and ICCP—OPC-based concrete for the NSMR-TiAB/ICCP beams was supplied by a local ready mix company. The concrete mixture design closely matched the concrete properties that were widely used in bridges constructed during the mid-twentieth century and as in the prism study described previously. The design concrete compressive strength was a minimum of 3300 psi (22.8 MPa). Mixing water included 1.5% chlorides in the form of NaCl to ensure the corrosion of the embedded reinforcing bars. The salt was mixed into batch water in the concrete truck; this produced active corrosion of the embedded steel. The proportions of the concrete mixture are reported in Table 4. Concrete beams cured under wet burlap for the first 14 days before formwork was removed and concrete grooves were cut. The concrete had a 28-day strength of 3387 psi (23.4 MPa), and a test-day strength of 3839 psi (26.5 MPa).[16] The bulk resistivity of the concrete was measured as 4.96 kΩ-cm from concrete cylinders cast with the beams. The ECSG had a 28-day compressive strength of 8600 psi (59.3 MPa)[13] and a bulk resistivity of 0.875 kΩ-cm.

Carbon steel reinforcing bar was used as internal reinforcement in the beams. Because the beams were designed to reflect the designs and details of aging highway bridges, the reinforcing steel needed to represent what are now-obsolete Intermediate Grade. This grade corresponds to modern Grade 40 (Grade 280) reinforcing bar. Smaller-diameter reinforcing steel bars are still available in Grade 40 (Grade 280) and these were used for the stirrups. Because larger diameters bars are no longer available at Grade 40 (Grade 280), the longitudinal reinforcing steel required the use of Grade 60 (Grade 420) bars, but smaller bar sizes were used to account for the higher strength. Stirrups were Grade 40 No. 4 (Grade 280 No. 13M) steel bars, and longitudinal bars were Grade 60 No. 9 (Grade 420 No. 29M) steel bars. To prevent anchorage failures, the steel longitudinal bars were detailed to have 90-degree hooks at the ends. The tails of the hooks were extended above the top of the beams to allow connection of the steel to the ICCP system.

For the ICCP application, electrical connections were required to both the reinforcing steel and the TiABs. Because the concrete was intentionally mixed with salt to produce a corrosive environment in the beam, external access to the steel was selected to prevent corrosion of wiring needed for the ICCP application. A potentiostat was attached to each of the flexural bars at the tail extension protruding above the concrete surface for cathodic protection. The reinforcing cages contained many individual bars that would generally be in direct contact with each other and tied together with bare steel tie wire. For this study, to isolate the participation of the flexural tension steel and stirrups, each of these components was electrically isolated and insulated from the others at their interfaces. Reinforcing bar cages were built using small pieces of nylon tubes placed around the longitudinal bars to insulate the longitudinal and transverse steel and prevent a direct connection between them. Plastic zip ties were used instead of traditional tie wire to construct the cage. The combination of nylon tubes and the zip ties maintained insulation between the individual reinforcing bars such that any applied current would be isolated to a single bar. The insulation of one bar from another allowed direct observation of how ICCP affected the different steel layers and groups, effectively allowing bars to be incorporated into or isolated from application of the ICCP. The reinforcing bar cages in the two beams connected the top No. 9 (No. 29M) steel bar to No. 4 (No. 13M) steel stirrups with tie wire to allow for the selective addition or exclusion of the stirrups and compression steel into the ICCP experiments.

The exposed ends of the longitudinal steel bars were drilled and tapped, allowing for an external connection between the steel and copper wires that were used to apply ICCP. While there was no external means of connection for the steel stirrups during casting, after the beams were fully cured, a small hole was drilled through the concrete cover to provide access to the side of a steel stirrup. The stirrup was drilled and tapped, and an electrical connection was established externally while ensuring that wired connections were not lost to corrosion within the beam. The longitudinal TiABs were drilled and tapped at the external side of the bar's hook, at the location of the bend, such that the connection protruded slightly from the side of the beam. Transverse TiABs were surface prepared for a crimped electrical connection just below the bend at the top of the bar hooks. Copper wires extended from the sides of the grouted grooves

for external connection between TiABs. A detail of such a connection is shown in Fig. 3.

Two concrete beams were designed as shown in Fig. 4 and 5. One specimen was designed to produce a flexural failure and deployed No. 5 (No. 16M) longitudinal TiABs. The other specimen was designed to produce a diagonal-tension (shear-dominated) failure and used No. 2 (No. 6M) transverse TiABs. These beams varied in span and reinforcing bar configurations. Both specimens were reinforced with TiABs using the NSMR technique. Typically, NMSR is undertaken by bonding the reinforcing material into surface-cut grooves using a structural adhesive like epoxy. The adhesive has the secondary effect of electrically isolating the NSMR from the underlying reinforcing steel. However, an ICCP system that uses the TiAB-NSMR as the anode must necessarily allow ions to flow between the surfaces of the reinforcing steel and anodes and therefore the TiABs cannot be electrically insulated. Instead, the ECSG was used to bond the TiABs into the saw cut grooves. Figure 6 shows the beams after the installation of the near surface mounted TiAB bars. These beams were tested structurally, and additional details of this structural program are presented elsewhere.[17]

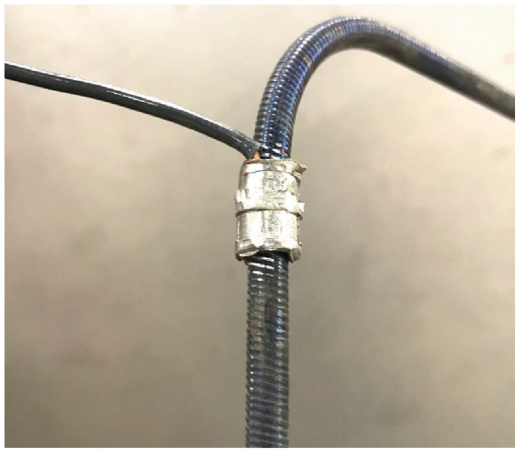

Fig. 3—Crimped No. 2 (No. 6M) TiAB electrical connection for ICCP.

Methods

Grout testing—Six cubes from each material combination were tested to failure, and the compressive loads were averaged to determine the grout strength. Grout cylinders were used to test resistivity to determine the influence of the different constituent materials and combinations. Resistivity was measured using a bulk resistivity test.[12] A mixture of standard dish soap and water was used to saturate sponges that were placed between the top and bottom surfaces of the concrete cylinders and the bulk resistivity testing apparatus. The testing equipment was compressed to the surface of the concrete and resistivity readings were taken.

ICCP testing of small-scale prisms—The open circuit half-cell potentials (HCPs) of the prism specimens were measured to determine the corrosion state of the embedded reinforcing bar. The HCP was measured using a high-impedance voltmeter and saturated calomel electrode (SCE)

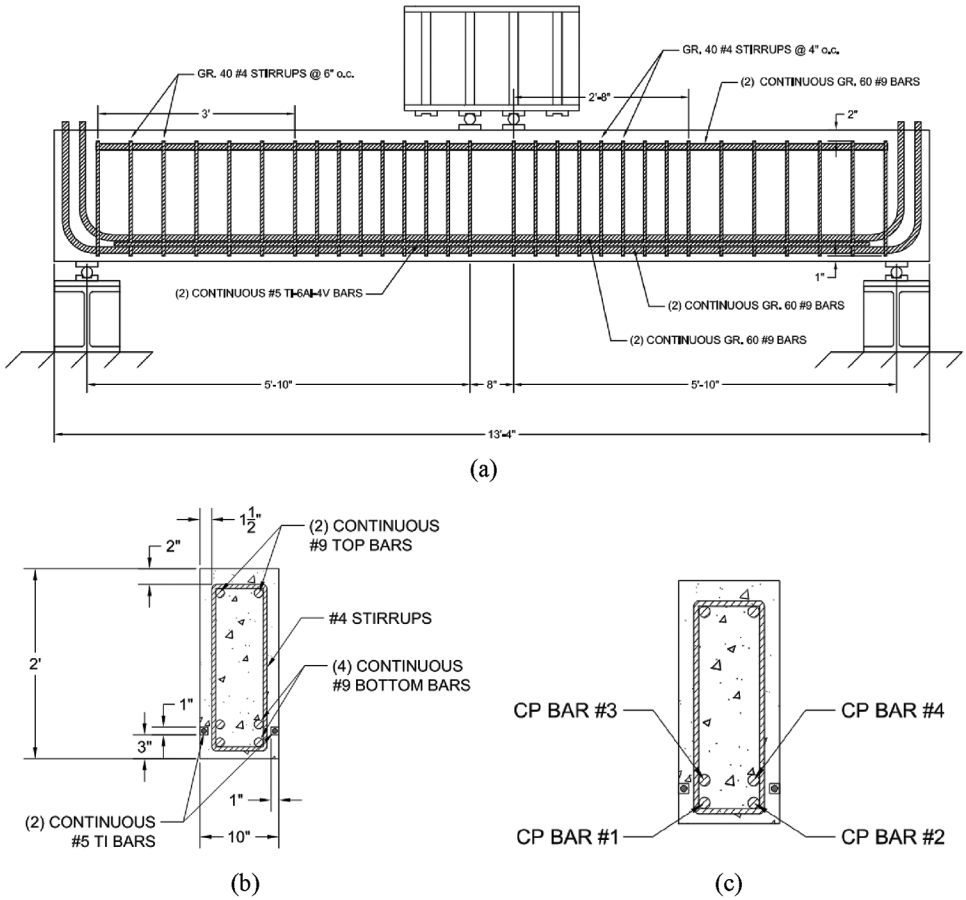

Fig. 4—Flexural beam: (a) span; (b) cross section; and (c) ICCP bar numbers. (Note: Units in inches; 1 in. = 25.4 mm.)

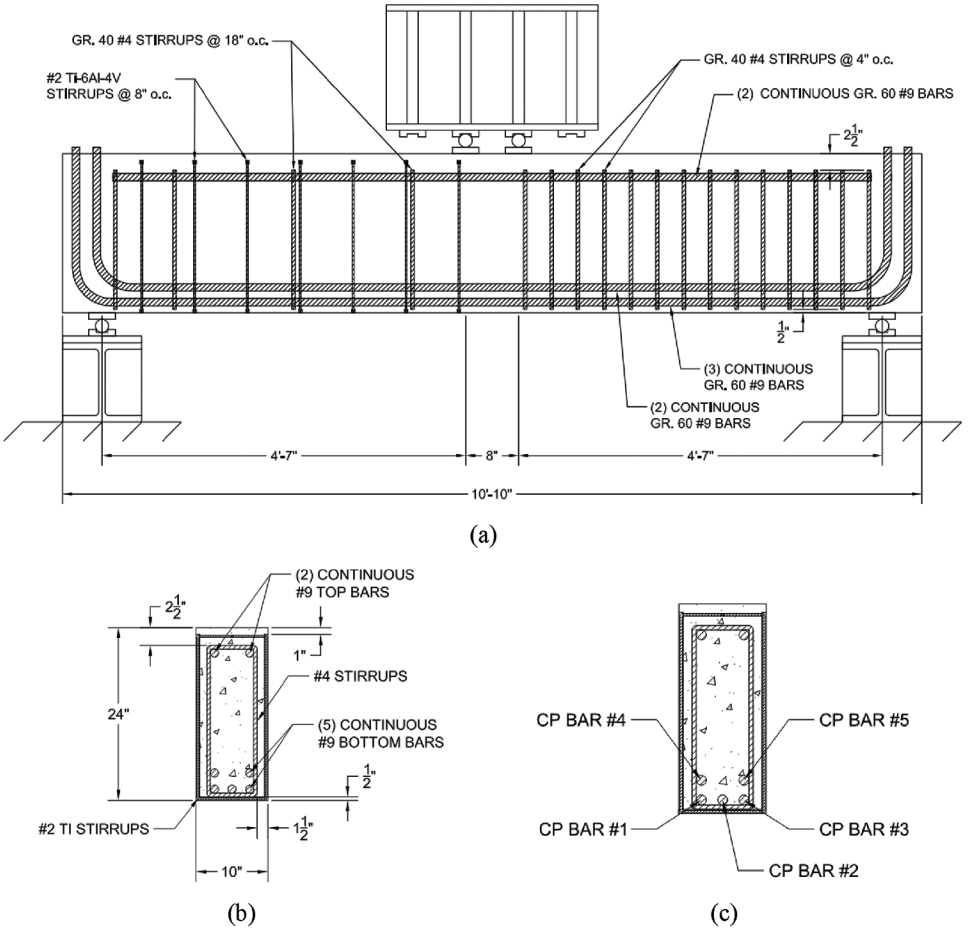

Fig. 5—Shear beam: (a) span; (b) cross section; and (c) ICCP bar numbers.

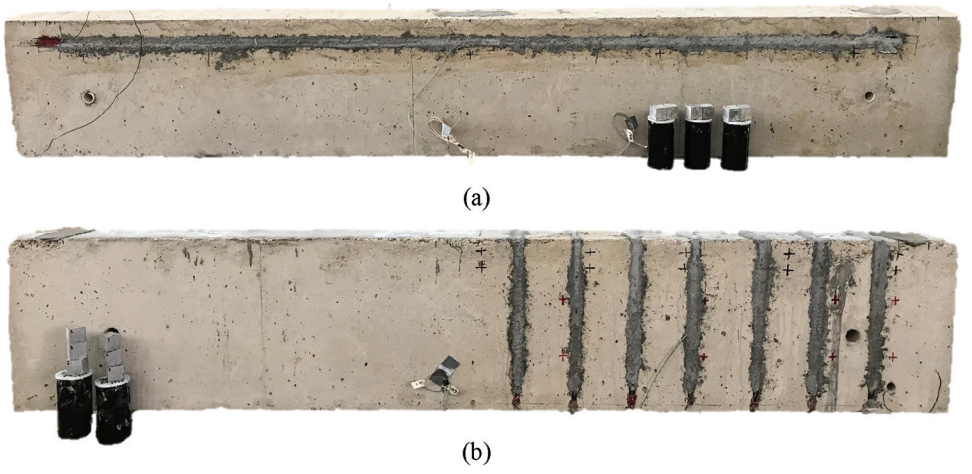

Fig. 6—(a) Flexural beam specimen with TiABs (inverted for ease of TiAB installation); and (b) shear beam specimen with TiABs (inverted for ease of installation).

following ASTM C876 guidelines.[18] It was expected that the premixed salts would cause active corrosion by introducing chlorides to the system.

In typical cathodic protection applications for reinforced concrete structures, the recommended current density to achieve cathodic protection potentials is typically in the range of 0.6×10^{-7} to 2.5×10^{-7} A/cm^2.[19,20] Because every system is different, a more scientific approach for choosing the current density can be used through the actual polarization curve of the system.[19] In this research, the latter approach is used, and anodic polarization scans of the embedded reinforcing bar were performed. The linear segment of the cathodic portion of the polarization curve is used as the range for the operating cathodic potential and corresponding current density in ICCP systems, as recommended by ICCP guidelines.[19] The polarization scans were performed using a stainless-steel plate counter electrode placed on the concrete surface above the measured reinforcing bar. A sponge that was saturated with a conductive solution was used between the counter electrode and the concrete surface. The polarization tests

were performed using a potentiostat, with an SCE reference electrode, the steel bar as the working electrode, and the stainless-steel plate as the counter electrode. Because these scans were performed using a stainless-steel counter electrode without the use of a grout, the required ICCP current was expected to be higher than the indicated range in the potentiodynamic scans. Therefore, some trial-and error ICCP runs were performed to fine-tune the ICCP applied current.

After the finalization of the applied current level, ICCP was run for 5 hours using the potentiostat. After the 5 hours of ICCP application, the cathodic current was switched off and the HCP were measured against the SCE at the surface of the concrete above a steel bar that spanned the length of the prism. HCPs were recorded at four points evenly spaced along the length of the prism at 10-minute intervals over a 4-hour period. These data were used to check the effectiveness of ICCP using the 100 mV polarization shift criterion, which states that a successful ICCP system would experience at least 100 mV of potential shift in 4 hours after the conclusion of the cathodic current application.[20,21]

ICCP testing of large-size NSMR-TiAB strengthened beams—Using the results from the prism tests, ICCP was applied to the large-size beam specimens, adjusting for the different surface areas of the reinforcing bars and TiABs within the beams. As with the prism tests, the HCPs of the beams were measured following ASTM C876 guidelines[18] to determine the corrosion state of the embedded reinforcing bar. The measurement locations are shown in Fig. A1 to A3 of the Appendix. Like the prisms, anodic polarization scans were performed to determine the linear segment of the cathodic portion of the polarization curve to decide the operating cathodic potential and the corresponding current density in the ICCP application. The polarization tests were performed for the No. 9 reinforcing bar at the bottom of the flexural beam using the potentiostat, SCE as the reference electrode, and a stainless-steel plate as the counter electrode, following a similar setup as the prism potentiodynamic scans.

The polarization test informed the cathodic potential to operate the ICCP setup, which was run for 5 hours. During the ICCP application, HCPs of the reinforcing bar were measured. After the 5 hours of ICCP, the cathodic current was turned off and the HCPs were measured and recorded at five locations along each No. 9 bar at 10-minute intervals over the course of 4 hours. This data was also used to assess the effectiveness of the ICCP using the 100 mV polarization shift criterion, which states that a successful ICCP system would experience at least 100 mV of potential shift in 4 hours after the conclusion of the cathodic current application.[20,21]

RESULTS AND DISCUSSION

Grout testing

Two commercial grouts were evaluated for compressive strength and bulk resistivity before any additions or modifications were made to the grout. The grout with the lower resistivity was selected for further steps of the experimental process. The two grout mixtures were cast following commercial instructions, and the observed properties are shown in Table 5.

Table 5—Commercial grout test results

Commercial grout	Average 28-day compressive strength, psi (MPa)	Average 28-day bulk resistivity, kΩ-cm
1	9532 (65.7)	15.36
2	10,008 (69)	4.65

Commercial Grout 2 had a substantially lower resistivity, so it was used to investigate the influence of different CF contents and sizes. Because the grout mixtures containing CFs required the addition of a dispersion agent (methyl cellulose), a control mixture was produced using only Commercial Grout 2 with methyl cellulose. The bulk resistivity for the grout with methyl cellulose was reduced to 3.56 kΩ-cm for a 23.4% reduction in resistivity compared to grout alone. The compressive strength of the mixture was 8886 psi (61.3 MPa), which corresponded to an 11.2% reduction in compressive strength compared to grout alone.

Variations of CF size and content were tested, and results are shown in Table A1 (in the Appendix). The addition of milled CFs did not substantially reduce the resistivity of the grout mixture. The most notable reduction in resistivity came from the mixture using 0.24 in. (6 mm) length fibers at 0.4% CF content. This combination of materials was used in subsequent experiments. The introduction of CB into the mixture did not produce a meaningful reduction in bulk resistivity. Only a 1% reduction was observed with the addition of CB compared to just CFs alone. CB is a challenging material to work with due to the very small particle sizes, so due to the cost/benefit balance, it was left out of the grout mixture in subsequent ICCP experiments. The final mixture consisted of Grout No. 2, methyl cellulose dispersion agent, 0.4% CF content with 0.24 in. (6 mm) long fibers, and HRWR agent, and is herein referred to as the ECSG which was used for all subsequent experiments. The ECSG was used in bond tests to assess bonding between TiABs and the concrete substrate, for the ICCP investigation in the prisms, as well as for the large-size beam tests that combined NSMR structural strengthening and ICCP applications. The bond tests are reported elsewhere.[17]

ICCP testing of small-scale prisms

Prior to running ICCP, HCP and polarization scans were conducted. The HCP of the embedded reinforcing bar was stable between –325 to –400 mV (SCE), which is indicative of active corrosion, as was expected from the corrosive environment produced by adding salt (in the form of NaCl) to the concrete mixture. The polarization scans are shown in Fig. 7. The linear segments of the cathodic zone of the polarization curves, as shown in Fig. 7, provide the cathodic potential range that should be targeted in the ICCP application. Although the No. 4 and 9 (No. 13M and 29M) bars showed slightly different polarization behavior, this range was found to be between –410 and –480 mV. Potentials lower than –480 mV caused the loss of linearity in the polarization curve. The corresponding current densities for the cathodic range were 1×10^{-6} to 7×10^{-6} A/cm^2, respectively. These current densities required larger ICCP currents in the ICCP of NSMR systems using TiAB anodes than

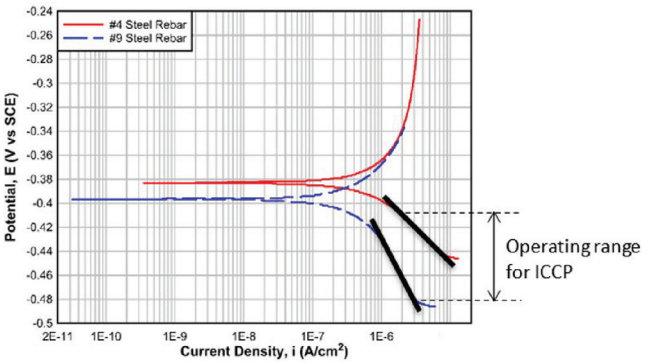

Fig. 7—Potentiodynamic scan of steel reinforcing bar in concrete prism.

expected from the potentiodynamic scans predicted (using stainless steel plates and conductive sponge) in Fig. 7. It is hypothesized that additional resistance was created by the conductive grout and the resistance of the grout-concrete interface that were not factors affecting the measurements in the potentiodynamic scan setup. Also, it is possible that because the TiAB bars were not MMO-coated, a larger operating ICCP current was needed. Nevertheless, the potentiodynamic scans provided in Fig. 7 offered a good starting point for selecting the ICCP current.

To fine-tune the ICCP current, several trials of ICCP applications were made. These runs are not presented here, but experimental data generated a better understanding and starting point for conducting ICCP on a larger scale. Although not shown here, additional attempts to run ICCP on the prisms started with the operating range shown in Fig. 7, which was also aligned with the recommended range in the literature. However, when these current densities were applied during ICCP, the 100 mV criterion was not satisfied. This could be attributed to a combination of factors including not having an MMO coating on the TiAB anodes, the resistance of the grout, as well as the resistance of the grout-concrete interface. After several trials, the operating current for the ICCP application was selected as 4.40 mA, which corresponded to a 1.67×10^{-5} A/cm^2 current density on the protected reinforcing bar surface, which is higher than ICCP current densities used in conventional cathodic protection of reinforced concrete structural elements.

ICCP started after 1 hour of HCP scans, which confirmed stable reinforcing bar corrosion at the open circuit conditions to verify that previous ICCP iterations did not affect the test. After HCP measurements, the ICCP application was initiated and sustained for 5 hours. During the ICCP application, HCP of the bars were measured, which indicated that reinforcing bar potentials ranged from –450 mV (SCE) to –550 mV (SCE), depending on the measurement location. Although the potentials at some of the measurement locations were lower than the aimed potentials in the linear segment of the cathodic portion of the polarization curve, they were stable and higher than the hydrogen evolution potentials. These stable potentials also indicate that electrical resistivity of the grout surrounding the TiAB did not change considerably, which suggests that chemistry of the grout remained unchanged. However, it is also acknowledged that

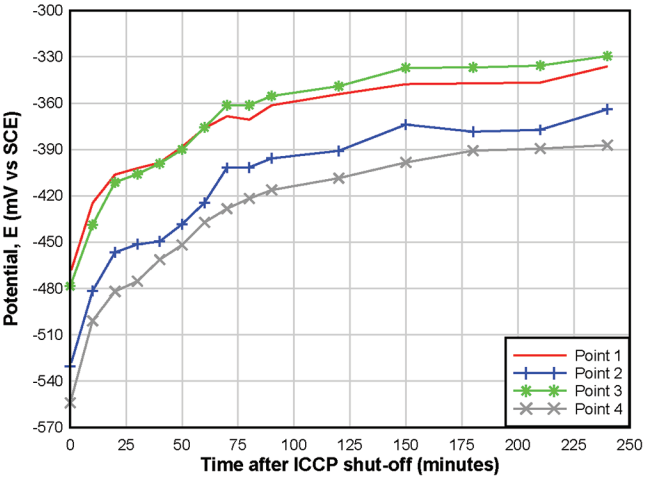

Fig. 8—Depolarization of No. 9 bars in test prism after ICCP is shut off.

these laboratory tests are rather short compared to field operations; therefore, long-term behavior should be investigated further in the future.

After 5 continuous hours, the ICCP was shut off, and potential shift was monitored through HCP measurements taken at the surface above each reinforcing bar in the prism. Measurements were taken every 10 minutes to record changes in HCP readings over the course of 4 hours to determine if the 100 mV criterion was met. The potential shift results after the termination of ICCP are shown in Fig. 8. As shown in this figure, for all bars, depolarization of at least 100 mV was observed within 4 hours. This observation indicates a successful ICCP outcome. The tests indicated that the applied current could have been reduced to lower the cathodic potentials below –485 mV (SCE) at some measurement points, which corresponded to the lower end of the ICCP operating range in the polarization scans, while still maintaining the 100 mV criterion.

ICCP testing of large-size structural beams

Prior to running ICCP, HCP and polarization scans were conducted for the large-size flexural and shear beam specimens. All HCP data showed that beams were actively corroding[22] (these scans are not shown for brevity). Figure 9 illustrates a typical polarization scan of a longitudinal bar in the flexural beam. The linear segment of the cathodic portion of the polarization curve, as shown in Fig. 9, provides the cathodic potential range that should be targeted in the ICCP application. Although different bars and different measurement locations showed slightly different polarization behavior, this range was found to be between –425 and –700 mV. Potentials lower than –725 mV caused the loss of linearity in the polarization curve. The corresponding current densities for this range are 1×10^{-7} to 4×10^{-7} A/cm^2, respectively. As with the prisms, these polarization scans were performed using a stainless-steel counter electrode that was placed on the concrete surface; therefore, in the ICCP application of NSMR systems using TiAB anodes (as in this work), the current required to produce these current densities on the reinforcing bar surface was expected to be higher. Nevertheless, the cathodic portion of the polarization curve

for the steel bar provided information about the lower end of the current range required to ensure cathodic protection. The prism data provided insight into the application of ICCP in the concrete substrate and the required current density for the 100 mV criterion to be met, which informed the ICCP experiments in the beams.

Prior to ICCP, it was confirmed that the bottom flexural tension reinforcing bars in both beams remained electrically isolated from each other. For the flexural beam specimen, the four longitudinal No. 9 (No. 29M) bars were externally connected with copper wire and attached to the potentiostat as the working electrode. The two longitudinal No. 5 (No. 16M) TiABs were connected externally with copper wire and attached to the potentiostat so that the current was applied to these bars as the counter electrode.

While bottom longitudinal reinforcing bars were isolated from the steel stirrups using nylon tubes and plastic zip ties, the top longitudinal bars and stirrups were tied together using standard tie wire so that the steel stirrups and top bars in the shear beam were electrically connected. An external connection was made to a steel stirrup that allowed for an additional ICCP experiment in the shear beam. Two ICCP experiments were performed in the shear beam. The first used the No. 2 (No. 6M) TiABs as the counter electrode, while the five externally connected bottom steel bars acted as the system's working electrode. The second used the externally connected No. 2 (No. 6M) TiABs as the counter electrode, while the steel stirrups and top bars acted as the working electrode.

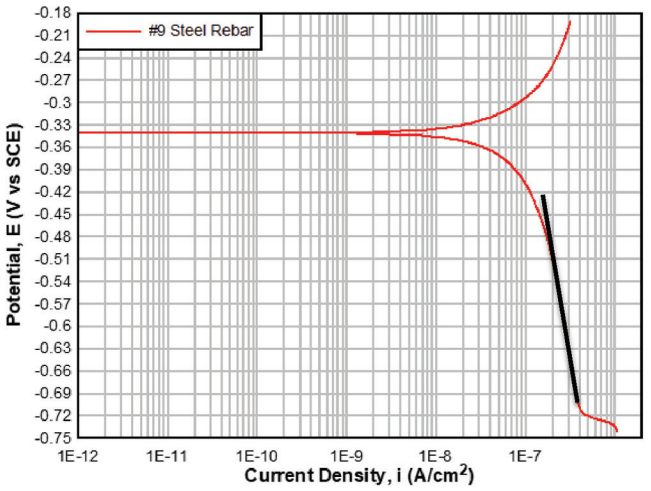

Fig. 9—Polarization scan of longitudinal reinforcing bar in flexural beam at selected measurement point. Other bars and measurement locations showed similar patterns; therefore, they are not shown.

In the flexural beam specimen, ICCP was conducted with an applied current of 143.9 mA, which translated to a current density of 8.28×10^{-6} A/cm^2 on the protected reinforcing bar surface. For the shear beam specimen, the applied current was 102.5 mA to protect the five No. 9 (No. 29M) bottom bars, which resulted in a current density of 5.62×10^{-6} A/cm^2 on the protected bar surface. An applied current of 55.5 mA was used to protect the four No. 4 (No. 16M) steel stirrups and the two No. 9 (No. 29M) top bars, which resulted in a current density of 1.11×10^{-5} A/cm^2 on the protected reinforcing bar surface in the shear beam specimen. The current densities varied for the different ICCP experiments. Based on polarization data in the beams, the anticipated required current density to cathodically protect the steel was on the order of 10^{-7} A/cm^2. Observed current densities were higher than anticipated to meet depolarization requirements. The differential observed herein was similar to that observed for the prism specimens and the theorized cause attributed to the same influences.

The applied currents were stable throughout the ICCP operation and did not require major adjustments to the applied potential as shown in Fig. 10, establishing that even without an MMO coating, TiAB bars were able to sustain the required current, and the ECSG was able to serve as a conductive medium between the TiAB anodes and concrete. Although the potentials at some of the measurement locations were lower than the aimed potentials in the linear segment of the cathodic portion of the polarization curve, they were stable and higher than the hydrogen evolution potentials. As in the case of prism tests, these stable potentials also indicate that electrical resistivity of the grout surrounding the TiAB did not change considerably, which suggests that chemistry of the grout remained unchanged. Furthermore, the structural testing after the completion of the ICCP study did not

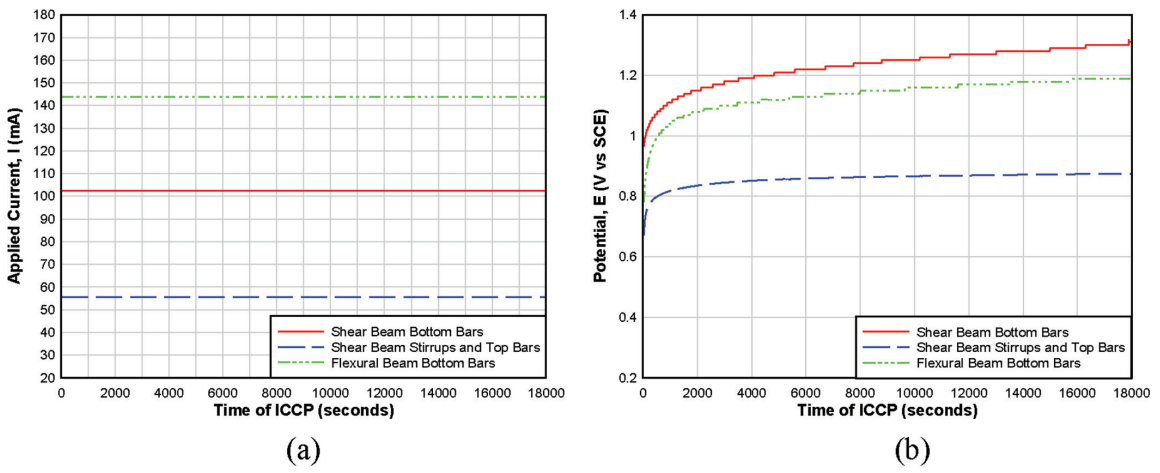

Fig. 10—(a) Applied current; and (b) resulting potential in flexural and shear beams during ICCP.

show any bond failure between TiAB and the ECSG. Further details on the structural testing can be found in the thesis by Slawinski.[17] However, it is also acknowledged that these laboratory tests are rather short compared to field operations. Long-term performance of TiAB bars in ECSG within ICCP systems, as well as the need for MMO coatings, will be investigated in the future.

In the flexural beam specimen, the longitudinal reinforcing bar and TiABs were placed close to each other over the length of the beam, such that the current density on the bar surface was expected to be relatively uniform. For the shear beam, the localized effects of ICCP could be observed based on the proximity of TiAB stirrups to both steel stirrups and longitudinal bars. If a steel stirrup was closer to a TiAB, it received increased protection, and similarly, longitudinal bars saw better protection at locations closer to TiABs than at locations between TiABs stirrups.

ICCP was performed for 5 hours on the flexural beam specimen. Once the system was turned off, HCP measurements were taken with the SCE at the surface of the concrete above the steel reinforcing bar. For the flexural beam, measurements were recorded at five points along the length of the four bottom longitudinal steel bars. The five points used for potential readings were evenly distributed between the ends of the beam as shown in Fig. A1. Measurements were taken every 10 minutes for 4 hours to observe the change in voltage over time. HCP readings were taken at the same locations along the beam for each reinforcing bar. Bars 1 and 3 were on the "front" face of the concrete beam, and bars 2 and 4 were on the "back" face. Bars 1 and 2 were the bottom layers of steel, and bars 3 and 4 were the second layer of steel. A diagram of the bar numbers for the flexural beam is shown in Fig. 4. As can be noted, based on the data recorded in Fig. 11(a) to (d), the 100 mV polarization shift requirement was met for each bar along all points of the beam, such that cathodic protection was achieved for the test conditions.

For the shear beam specimen, two different ICCP conditions were performed. First, the effect of ICCP on the steel longitudinal reinforcing bars was observed. Second, the effect of ICCP on the steel stirrups from the TiABs were measured. The TiAB stirrups were located on only one half of the beam, so measurements following both ICCP applications were only taken for the TiAB-reinforced half of the beam. The effect of ICCP was monitored on the longitudinal reinforcing bars, bars 1, 2, and 3 were the bottom steel, and bars 4 and 5 were in the second layer of steel. Bars 1 and 4 were located on the "front" face of the concrete, while 3 and 5 were located on the "back" face. A diagram of the bar numbers for the shear beam is shown in Fig. 5.

Measurement locations are depicted in Fig. A2, such that points 1 through 5 along the length of the longitudinal bar were evenly spaced along half of the length of the beam. The measurement locations varied in their distance to the TiABs. Point 5 was located towards the center of the beam

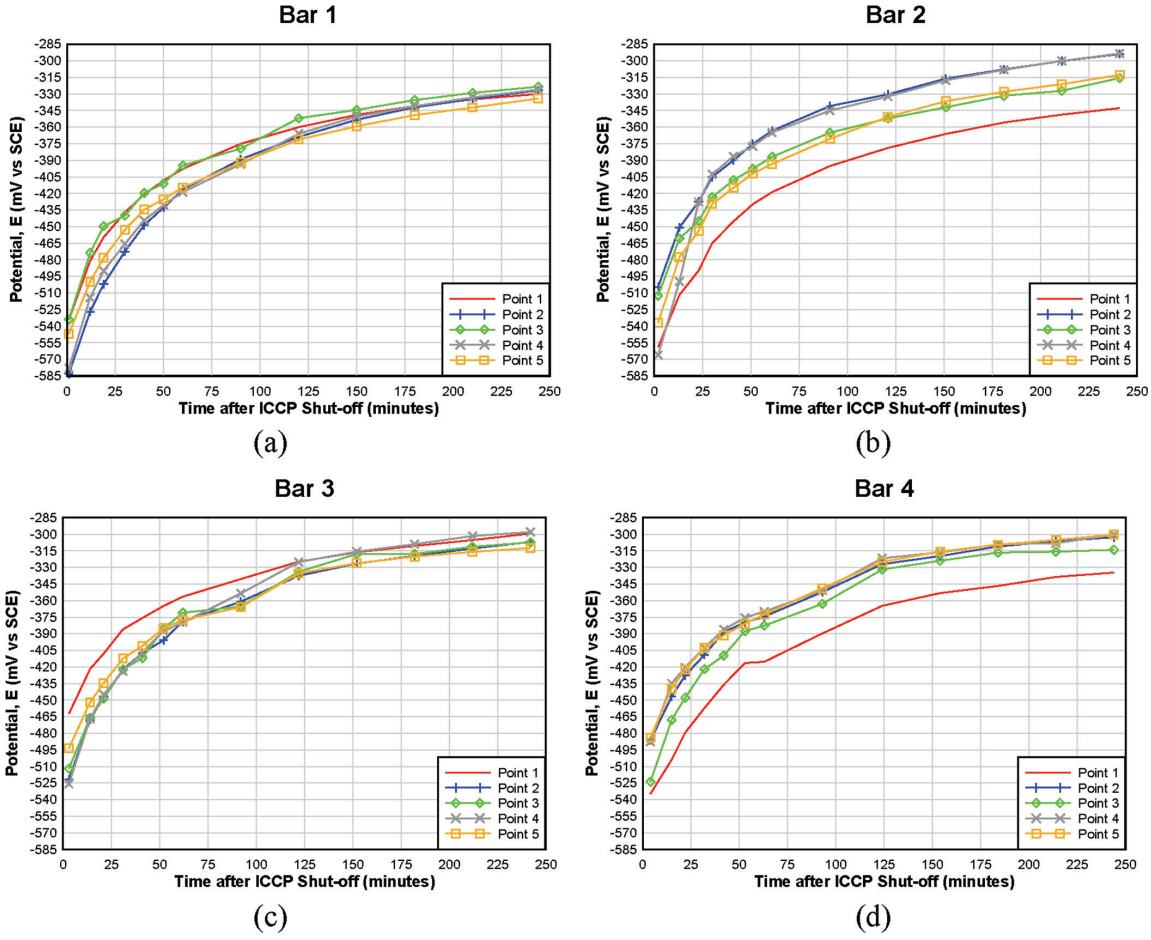

Fig. 11—Depolarization of longitudinal steel reinforcing bar within flexural beam after ICCP is shut off.

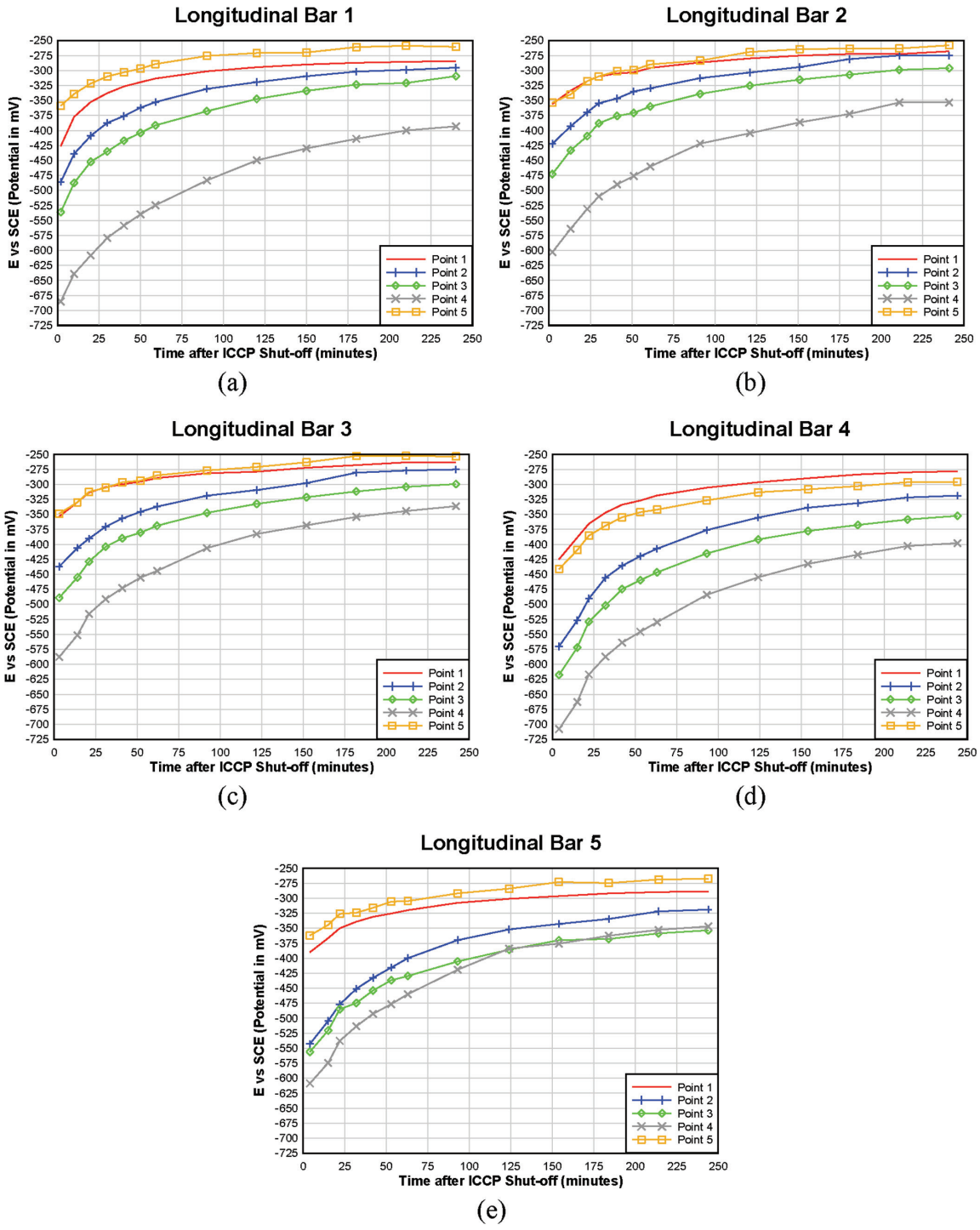

Fig. 12—Depolarization of longitudinal steel reinforcing bar in shear beam after ICCP is shut off.

beyond the last TiAB stirrup and, as expected, that location saw the smallest change in potential after ICCP was terminated. HCP results after stopping ICCP are shown in Fig. 12. Both the transverse steel and TiAB stirrups were discretely located, which meant that the distance from the steel to the TiAB varied between adjacent stirrups based on the steel stirrup number. Stirrup number increased from the end of the beam in towards the center of the beam. Point 1 started at the top of the beam on the "front" face of the concrete, and the number increased as the location along the stirrup wrapped around the base of the beam and up the "back" face of the concrete. Points 1 and 2 were located on the "front" face of the concrete, point 3 was centered between the "front" and "back" faces of the concrete at the beam soffit, and points 4 and 5 were located on the "back" face of the concrete beam. Bar locations and stirrup numbers are shown in Fig. 5 and 9. Half-cell potential measurements were recorded and the corresponding results for the 100 mV Polarization can be seen in Fig. 13.

Experiments performed on both the flexural and shear beam specimens demonstrate that the 100 mV criterion was met, thereby proving that ICCP can be achieved with ASTM B1009 Class 130 TiABs in NSMR applications. Both No. 5 (No. 16M) longitudinal TiABs and No. 2 (No. 6M) transverse

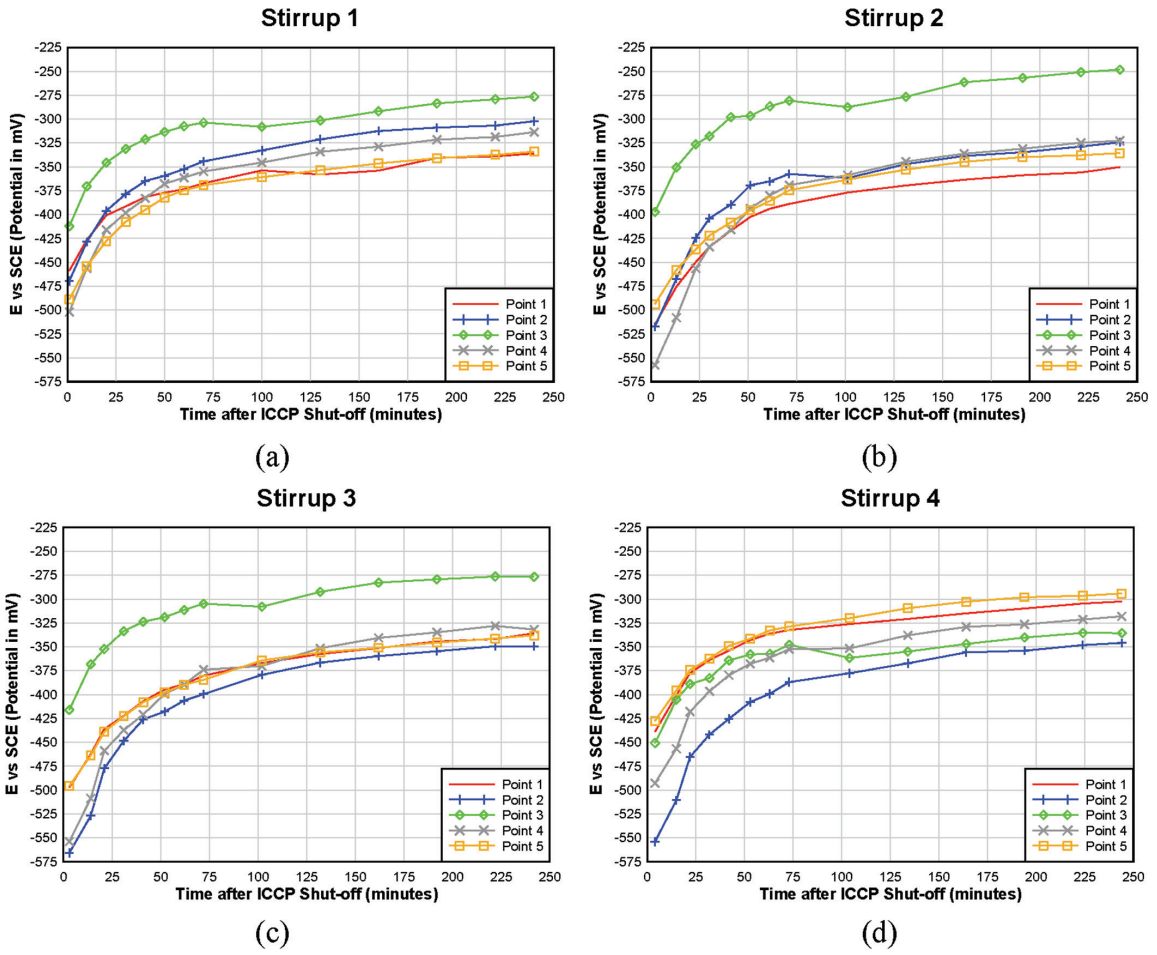

Fig. 13—Depolarization of transverse bars in shear beam after ICCP is shut off.

TiABs were able to locally protect the steel reinforcing bars in the concrete beam specimens. The installation of a consumable structural element provides a unique obstacle that requires further investigation to monitor the impact on the structural strength of the reinforced structural element over time to ensure the expected lifetime. These experimental results show for the first time that NSMR TiABs can be used as anodes in an ICCP system, and this research creates an opening for additional studies to explore this further. Studies performed thus far have only explored short-term ICCP application, and because ICCP systems are typically in place for approximately 20 or more years, additional research is needed to establish the long-term durability and performance of this dual-purpose application. There are several items that must be explored in future research to develop a more robust knowledge of this multifunctional application. While TiABs are impervious to corrosion in conventional applications, the long-term corrosive behavior of the TiABs in ICCP systems requires further study to ensure designs can achieve the expected service life. It is recommended that an understanding of TiAB corrosion products in the TiAB/grout interface, local acidification, as well as the changes in electrochemical behavior of the grout and the impact on the bond with the ECSG be properly evaluated. Another area of interest is the exploration of MMO coatings for TiABs. Because TiABs are not specifically developed for ICCP applications, they are not MMO-coated.[23] MMO coatings for TiABs require development and could improve ICCP performance and delay consumption of the anode. Once the questions about the long-term performance of the ICCP process are resolved, the proposed dual purpose NSMR-ICCP application has the potential to revolutionize how structurally deficient structures can simultaneously be strengthened and protected from further corrosion. The financial feasibility of using TiAB-based NSMR systems has already been proven in field applications. In a report by the Oregon Department of Transportation,[24] it was shown that using TiAB-based NSMR process is approximately 30% cheaper than using CFRP-based NSMR. With the added advantage of ICCP, the proposed dual-purpose system has significant financial and operational advantages over conventional NSMR techniques.

CONCLUSIONS

Titanium alloy bars (TiABs) have the potential to serve a dual purpose in a combined near-surface-mounted retrofit (NSMR) and impressed current cathodic protection (ICCP) application. While structural retrofit applications using TiABs as a NSMR material has been standardized,[8] prior work has only considered epoxy bonding of the material that would electrically isolate the TiABs from the surrounding concrete. This study, for the first time, developed new materials and approaches to deploy TiABs as a NSMR material that can be used to both strengthen and preserve existing reinforced concrete elements. The experimental results reported here demonstrated that cathodic protection of steel reinforcement

in reinforced concrete beams can be achieved using TiABs in an electrically conductive structural grout (ECSG).

The research showed that an ECSG containing 0.24 in. (6 mm) long carbon fibers (CFs) at a CF content of 0.4% by volume provided the necessary electrical properties for ICCP while satisfying structural requirements of the NSMR application. Of the two commercial grouts that were tested, the grout selected had a control resistivity 69.7% lower than the alternative. The 0.24 in. (6 mm) long CFs at a CF content of 0.4% volume exhibited the largest drop in resistivity among the experimental results. The lower resistivity increases the efficiency of the ICCP system across material interfaces. The ECSG was also shown to meet the bond strength requirements prescribed by the AASHTO design guide.[7,17]

Prism tests confirmed the feasibility of the ICCP setup using TiAB anodes and the ECSG in the NSMR application. The prism tests helped fine-tune the ICCP parameters, including the applied current required to cathodically protect the reinforcing steel, and the results informed the large-size beam specimens with ICCP installations.

TiAB anodes were used to retrofit both longitudinal reinforcement in a beam that was designed to fail in flexure (flexural beam specimen), and transverse reinforcement in a beam that was designed to fail in diagonal-tension (shear beam specimen). In both applications, it was found that ICCP of the NSMR with TiABs setups were feasible and cathodic potentials could be maintained in the linear region of the cathodic polarization curve of the embedded reinforcing steel.

The applied current and potential to achieve the required cathodic potentials were stable, and their stability was not challenging to maintain during the ICCP application. However, ICCP was only conducted for a relatively short period of time, and the required applied currents were higher than those typically used in conventional ICCP of reinforced concrete elements of similar dimensions and reinforcing bar detailing. This was attributed to the resistivity of the conductive grout, resistance of the grout-concrete interface, and the fact that TiAB anodes were not mixed metal oxide (MMO) coated. More research is needed for the long-term performance of these dual-purpose ICCP systems. However, this study provides a major advancement toward real-life applications by proving the concept of using dual-purpose TiAB anodes for NSMR/ICCP applications.

AUTHOR BIOS

Amanda K. Slawinski *is a Structural Designer at Consor Engineers based out of Kailua-Kona, HI. She received her BS in civil engineering from Cornell University, Ithaca, NY, and her MS in civil engineering from Oregon State University, Corvallis, OR. Her research interests include concrete durability, corrosion of steel in concrete, and evaluation and rehabilitation of structures.*

ACI member **Christopher Higgins** *is the Cecil and Sally Drinkward Professor of Structural Engineering in the School of Civil and Construction Engineering at Oregon State University. He received his BS from Marquette University, Milwaukee, WI; his MS from The University of Texas at Austin, Austin, TX; and his PhD from Lehigh University, Bethlehem, PA. His research interests include evaluation and rehabilitation of structures.*

O. Burkan Isgor, *FACI, is a Professor in the School of Civil and Construction Engineering at Oregon State University. He received his BS from Boğaziçi University, Istanbul, Turkey, and his MS and PhD from Carleton University, Ottawa, ON, Canada. He is a member and past Chair of ACI Committee 222, Corrosion of Metals in Concrete, and a member of ACI Committees 236, Material Science of Concrete, and 365, Service Life Prediction. He received the 2021 and 2023 ACI Wason Medal for Materials Research, 2022 ACI Sustainability Award, and 2023 ACI Concrete International Award. His research interests include corrosion of steel in concrete, service life modeling of concrete, and thermodynamic modeling of cementitious systems.*

ACKNOWLEDGMENTS

The authors wish to express their gratitude and sincere appreciation to J. Perryman Sr., company leadership, technical staff, and J. Adkins of The Perryman Company, Houston, PA, for supporting this research work and for fabricating the TiABs used in the study. Material donations were provided by Asbury Carbons, Five Star Products, and BASF Solutions. Additional funding for this work was provided by the U.S. Department of Transportation through the Coastal Research and Transportation Education (CREATE) Center, a BIL UTC, under Grant No. 69A3552348330. Any opinions, findings, and conclusions or recommendations expressed are those of the authors and do not necessarily reflect the views of the individuals, companies, or federal agencies.

REFERENCES

1. Parvin, A., and Shah, T. S., "Fiber Reinforced Polymer Strengthening of Structures by Near-Surface Mounting Method," *Polymers*, V. 8, No. 8, 2016, p. 298 doi: 10.3390/polym8080298

2. Higgins, C., and Barker, L., "Methods for Strengthening Reinforced Concrete Bridge Girders Containing Poorly Detailed Flexural Steel Using Near-Surface Mounted Metallics," FHWA-OR-RD-16-02, Oregon Department of Transportation, Salem, OR, 2015, 154 pp.

3. Higgins, C.; Amneus, D.; and Barker, L., "Shear and Flexural Strengthening of Reinforced Concrete Beams with Titanium Alloy Bar," *Proceedings of the 2nd World Congress on Civil, Structural, and Environmental Engineering (CSEE'17)*, Barcelona, Spain, 2017.

4. TM0294-2016, "Testing of Embeddable Impressed Current Anodes for Use in Cathodic Protection of Atmospherically Exposed Steel-Reinforced Concrete," NACE International, Houston, TX, 2016.

5. Segan, E. G.; Bukowski, J.; and Kuma, A., "Titanium Anodes in Cathodic Protection," *Report* CERL-TR-M-303, U. S. Army Construction Engineering Research Laboratory, Champaign, IL, 1982, 29 pp.

6. ISO 19097-1, "Accelerated Life Test Method of Mixed Metal Oxide Anodes for Cathodic Protection — Part 1: Application in Concrete," International Organization for Standardization (ISO), Geneva, Switzerland, 2018, 14 pp.

7. AASHTO, "Guide for Design and Construction of Near-Surface Mounted Titanium Alloy Bars for Strengthening Concrete Structures," American Association of State Highway and Transportation Officials, Washington, DC, 2020, 48 pp.

8. ASTM B1009-18, "Standard Specification for Titanium Alloy Bars for Near Surface Mounts in Civil Structures," ASTM International, West Conshohocken, PA, 2018.

9. Sun, M.; Wu, Y.; Li, B.; and Zhang, X., "Deicing Concrete Pavement Containing Carbon Black/Carbon Fiber Conductive Lightweight Concrete Composites," *ICTIS*, V. 2011, 2011, pp. 662-668. doi: 10.1061/41177(415)84

10. Sassani, A.; Ceylan, H.; Kim, S.; Gopalakrishnan, K.; Arabzadeh, A.; and Taylor, P. C., "Influence of Mix Design Variables on Engineering Properties of Carbon Fiber-Modified Electrically Conductive Concrete," *Construction and Building Materials*, V. 152, 2017, pp. 168-181. doi: 10.1016/j.conbuildmat.2017.06.172

11. ASTM D5291-16, "Standard Test Methods for Instrumental Determination of Carbon, Hydrogen, and Nitrogen in Petroleum Products and Lubricants," ASTM International, West Conshohocken, PA, 2016.

12. ASTM C1876-19, "Standard Test Method for Bulk Electrical Resistivity or Bulk Conductivity of Concrete," ASTM International, West Conshohocken, PA, 2019.

13. ASTM C109/C109M-16a, "Standard Test Method for Compressive Strength of Hydraulic Cement Mortars (Using 2-in. or [50-mm] Cube Specimens)," ASTM International, West Conshohocken, PA, 2016.

14. ASTM E8/E8M-16ae1, "Standard Test Methods for Tension Testing of Metallic Materials," ASTM International, West Conshohocken, PA, 2016.

15. Mohammed, M. T.; Khan, Z. A.; and Siddiquee, A. N., "Surface Modifications of Titanium Materials for developing Corrosion Behavior in Human Body Environment: A Review," *Procedia Materials Science*, V. 6, 2014, pp. 1610-1618. doi: 10.1016/j.mspro.2014.07.144

16. ASTM C39/C39M-18, "Standard Test Method for Compressive Strength of Cylindrical Concrete Specimens," ASTM International, West Conshohocken, PA, 2018.

17. Slawinski, A. K., "Dual Purpose Utilization of Titanium Alloy Bars for Impressed Current Cathodic Protection and Near Surface Mounted Retrofit In Reinforced Concrete Beams," MS thesis, Oregon State University, Corvallis, OR, 2022.

18. ASTM C876-15, "Standard Test Method for Corrosion Potentials of Uncoated Reinforcing Steel in Concrete," ASTM International, West Conshohocken, PA, 2015.

19. ACI Committee 222, "Guide to Protection of Reinforcing Steel in Concrete Against Corrosion (ACI 222-19)," American Concrete Institute (ACI), Farmington Hills, MI, 2019, 60 pp.

20. DNV-RP-B401, "Recommended Practice: Cathodic Protection Design," Det Norske Veritas Group, 2021, 70 pp.

21. Glass, G., "Technical Note: The 100-mV Potential Decay Cathodic Protection Criterion," *Corrosion*, V. 55, No. 3, 1999, pp. 286-290. doi: 10.5006/1.3283989

22. Jones, D. A., *Principles and Prevention of Corrosion*, second edition, Prentice-Hall, Inc., Upper Saddle River, NJ, 1996, 572 pp.

23. Funahashi, M., and Wu, H., "What You Need to Know about MMO Coated Metal Anodes," *NACE - International Corrosion Conference Series*, 2013.

24. Knudtsen, J., and Higgins, C., "Application of Titanium Alloy Bars for Strengthening Reinforced Concrete Bridge Girders (Part A: Shear)," FHWA-OR-RD-18-01, Oregon Department of Transportation, Salem, OR, 2017, 150 pp.

APPENDIX A

Table A1—Effect of CF addition to Commercial Grout 2

Carbon fiber content, % volume	Carbon fiber size, mm	Average 28-day compressive strength, psi (MPa)	Average 28-day bulk resistivity, kΩ-cm	% Change in average 28-day compressive strength	% Change in average 28-day bulk resistivity
0.1	~0.350 (milled)	8356 (57.6)	5.27	–17%	13%
	3	6296 (43.4)	3.48	–37%	–25%
	6	6987 (48.2)	4.22	–30%	–9%
0.2	~0.350 (milled)	8425 (58.1)	2.37	–16%	–49%
	3	8561 (59)	0.40	–14%	–91%
	6	9214 (63.5)	2.28	–8%	–51%
0.4	~0.350 (milled)	8963 (61.8)	1.86	–10%	–60%
	3	9279 (64)	0.29	–7%	–94%
	6	8744 (60.3)	0.16	–13%	–96%

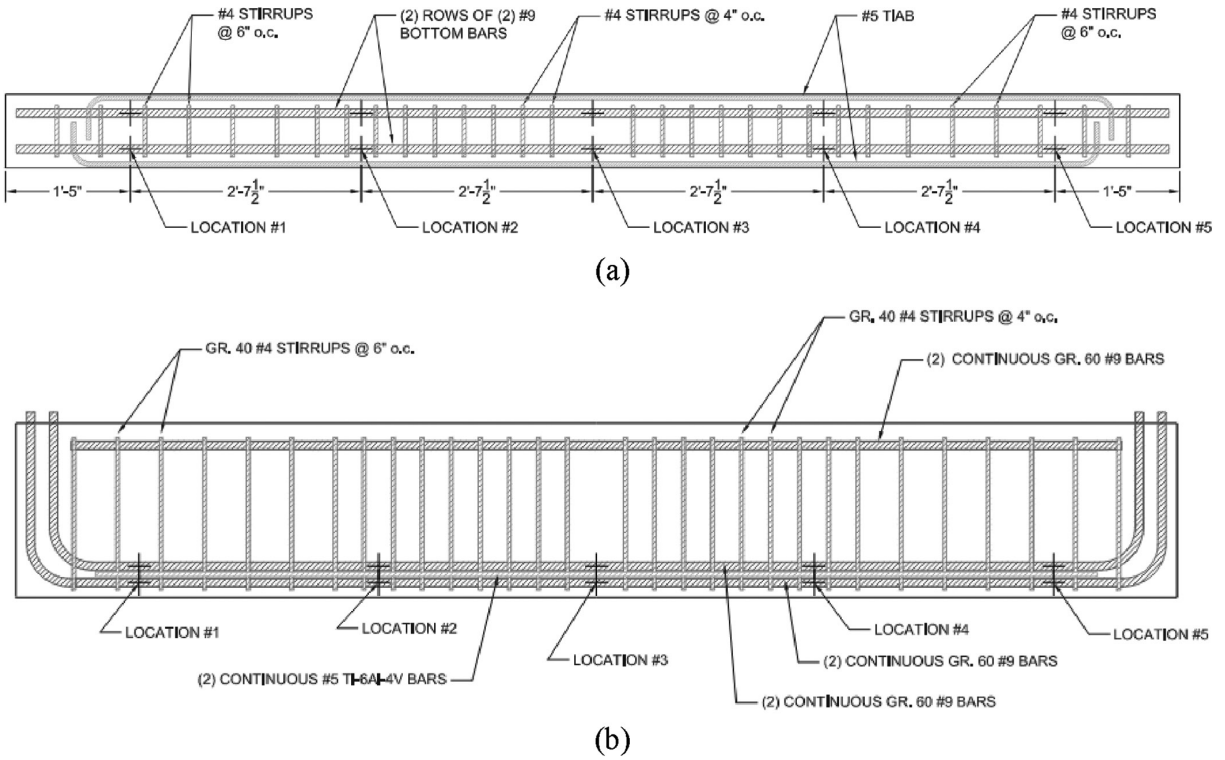

Fig. A1—HCP measurement locations in flexural beam: (a) top view; and (b) side view.

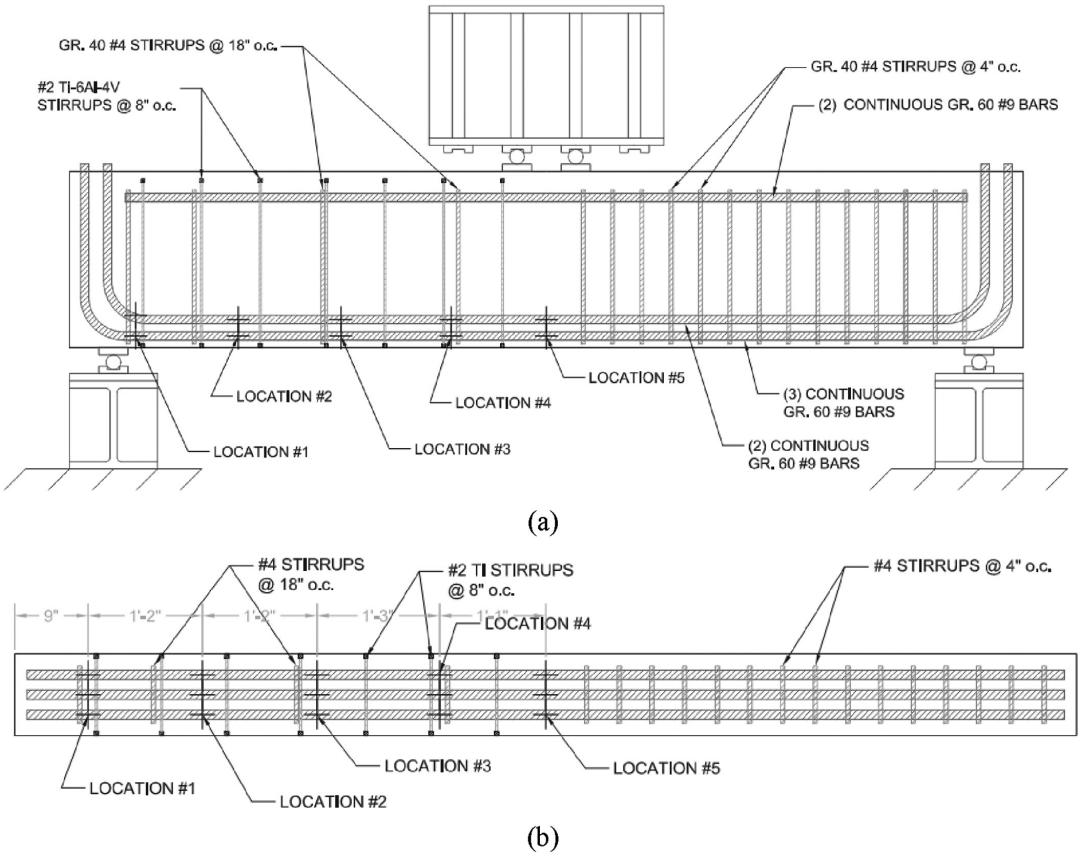

Fig. A2—HCP measurement locations in shear beam (bottom bars CP): (a) side view; and (b) top view.

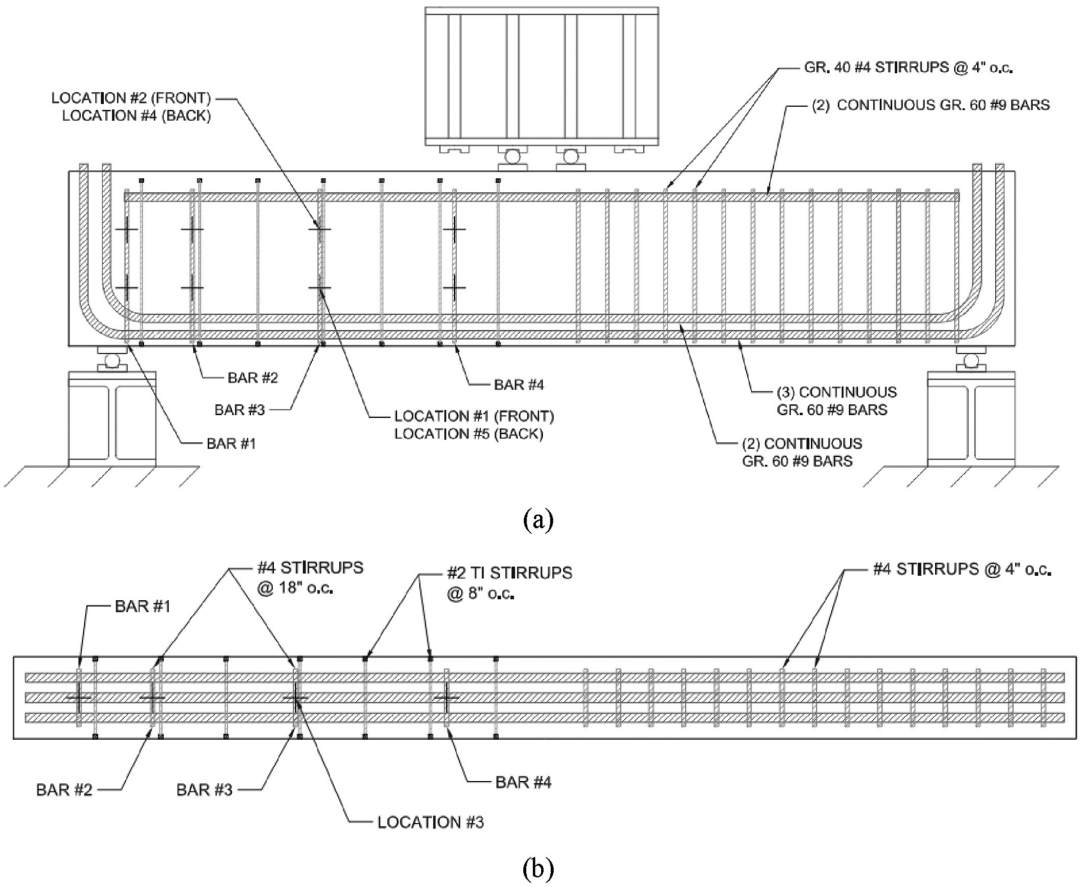

Fig. A3—HCP measurement locations in shear beam (stirrup CP): (a) side view; and (b) top view.

JOIN AN ACI Chapter!

The American Concrete Institute has Chapters and Student Chapters located throughout the world. Participation in a local chapter can be extremely rewarding in terms of gaining greater technical knowledge and networking with leaders in the concrete community.

Because chapters are distinct and independent legal entities, membership includes both ACI members and non-ACI members and is made up of a diverse blend of architects, engineers, consultants, contractors, educators, material suppliers, equipment suppliers, owners, and students—basically anyone interested in concrete. Many active ACI members initially became involved in ACI through their local chapter. In addition to technical programs and publications, many chapters sponsor ACI Certification programs, ACI educational seminars, project award recognition programs, and social events with the goal of advancing concrete knowledge.

To find a chapter near you, go to: https://www.concrete.org/getinvolved/chapters.aspx

---

Student Chapters

Join or form an ACI Student Chapter to maximize your influence, knowledge sharing, and camaraderie! ACI has 240+ student chapters located throughout the world, each providing opportunities for students to:

- Connect with their peers and participate in concrete-related activities such as: student competitions, ACI Conventions, ACI Certification Programs, ACI Educational Seminars, local chapter meetings, social events, and community service projects;
- Network with members of local chapters, many of whom have been in the industry for decades and can help to develop professional relationships and offer career advice;
- Win recognition for their universities through the University Award; and
- Learn about the many scholarships and fellowships offered by the ACI Foundation and by ACI's local chapters.

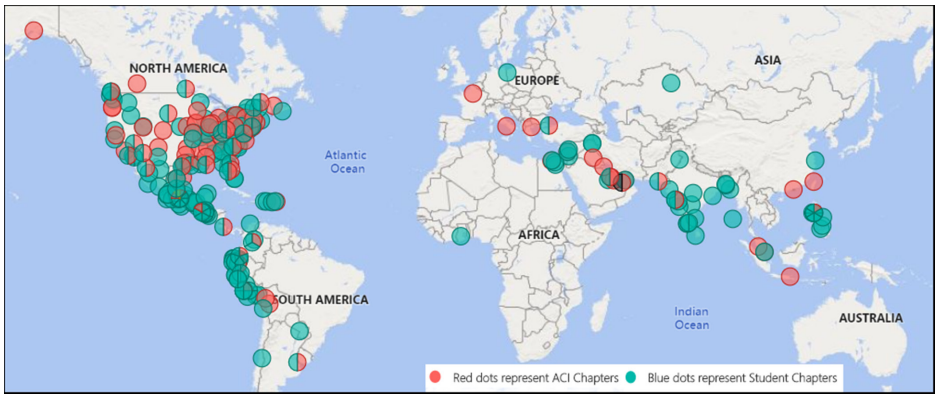

ACI MATERIALS JOURNAL TECHNICAL PAPER

Title No. 122-M11

Mechanical Behavior of Textile Concrete under Uniaxial Tensile Tests: Experimental Study

by J. Rizzo, E. S. Bastos, L. A. Reginato, P. M. Lazzari, and L. C. P. da Silva Filho

Through uniaxial tensile tests, the mechanical behavior of bone-shaped concrete reinforced with glass textile and carbon textile impregnated with epoxy resin was verified using a stress-strain response curve. It was observed that elements reinforced with glass fabric presented different mechanical responses depending on the textile reinforcement rate. In samples with two layers of glass fabric, three stages were formed, as predicted in the literature. In the specimens reinforced with only one layer, the structural incapacity of the element was observed. For samples reinforced with carbon textile, there were problems with slipping and spalling caused by the concentration of stress at the ends of the piece. Even so, it was possible to clearly determine the three stages in the curve response of the material. The stresses experimentally obtained in the elements reinforced with carbon textile obtained results approximately five times greater than those of the glass fabric.

Keywords: carbon textile; glass textile; mechanical behavior; textile concrete.

INTRODUCTION

The research and development of sustainable and environmentally friendly products is a prominent challenge in most areas of academic research. In civil engineering, the techniques used in the construction of structural elements have undergone relatively few technological advances compared to other fields, such as the mechanical industry.

Textile concrete, also known as textile-reinforced concrete (TRC) or fiber-reinforced polymer (FRP), is an innovative construction material consisting of a high-resistance, fine-grained cementitious matrix and textile fabrics capable of resisting the tensile forces that occur upon fracture of the concrete.[1]

The cement matrix where the textile reinforcement is arranged is formed by a high-mechanical-resistance fluid mortar, which can fill the tissue strands without requiring externally induced vibration. However, as it presents characteristics resembling high-performance concrete (HPC), the literature has named the cement matrix as a fine concrete.[2,3] This explains the fact that several scientific studies carried out in different countries name this composite material as a textile concrete.[4-12]

In general, concretes used in conjunction with textile reinforcement exhibit high mechanical resistance. Moreover, the combination of ultra-high-performance concrete (UHPC)[13,14] and HPC[10,15] with textile reinforcement can further enhance the mechanical performance of the structure.

According to Scheerer et al.,[16] research into textiles being used as reinforcement in construction began in the 1980s in Germany and the United Kingdom. Based on the authors, in the 1990s, Japan and Israel began studies on this material.

Through in-depth and comprehensive investigations, Germany has established itself as a world leader in textile concrete research.[16] Several structural elements made of this composite material have already been built in this country, such as bridges,[17-19] façades,[20] and innovative shell-shaped structures.[4,21]

Between 1999 and 2013, Dresden University of Technology and RWTH Aachen University worked together to evaluate the mechanical properties of TRC through the projects "DFG CRC 528" and "DFG CRC 532," funded by the German Research Foundation.[22,23] These studies observed that concrete reinforced with carbon textile presents great potential for use in the construction industry.[23]

The textile concrete walkway installed in 2007 in Allgäu, Germany, called "Kempten," was built in U-shaped segments with a thickness of 30 mm (1.18 in.). It was reinforced with four layers of alkali-resistant glass textile, and its segments were secured by steel bars. Accounting for the recent material developments, the four layers of glass textile could be replaced by just two layers of carbon textile impregnated with epoxy resin. This way, the work carried out to produce the structure could be reduced by half, making the bridge more cost-effective.[17]

In 2015, in Albstadt, Germany, the first pedestrian bridge that consisted of just two layers of carbon textile impregnated with epoxy resin was built.[24,25] This structure did not need lateral stiffeners and steel bars like the Kempten bridge mentioned previously. Consequently, this bridge, with a span of 15.5 m (610.23 in.), was built in a monolithic format, requiring just a few days to carry out the production process.

To verify the potential of TRC through its mechanical properties, RILEM Technical Committee 232-TDT[26] explain that direct tensile tests are the most adequate. According to Rawat et al.,[5] the mechanical behavior of textile concrete directly depends on the shape, geometry, type of fiber, and properties of the fabric. The mechanical behavior of textile concrete differs from that of conventional concrete. Because textile concrete lacks the ability for plastic deformation, these structures do not exhibit plastic behavior prior to rupture.[3,27] Thus, the behavior of textile concrete during uniaxial tests

ACI Materials Journal, V. 122, No. 2, March 2025.

MS No. M-2024-227.R2, doi: 10.14359/51745606, received December 22, 2024, and reviewed under Institute publication policies.

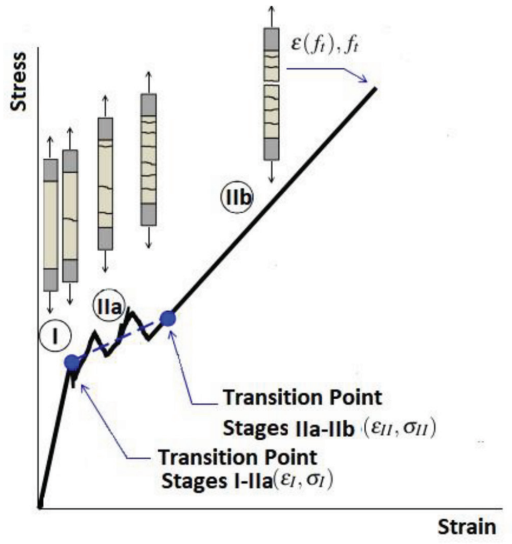

Fig. 1—Transition points between stages of textile concrete (adapted from De Santis et al.[28]).

can be divided into three parts: Stages I, IIa, and IIb. These are identified, respectively, by the elastic behavior of the matrix, cracking of the matrix and stress redistribution to the textile fabric, and load transfer to the textile fabric.

To assist in understanding the mechanical behavior of textile concrete, De Santis et al.[28] identified the transition points between the stages of the composite material. As indicated in Fig. 1, the transition between Stages I and IIa is identified by the stress (σ_I) and strain (ϵ_I) values. The intersection of the points that coincide with the end of Stage IIa and the beginning of Stage IIb are called tension (σ_{II}) and deformation (ϵ_{II}). The rupture of the structure is marked by the points corresponding to the peak of the curve, with the maximum stress and strain being f_t and ϵ_t, respectively.

It is worth mentioning that De Santis et al.[28] identified the last stage as Stage III. However, German research by Jesse,[27] Molter,[29] Kulas,[22] and Voss[3] refers to this stage as IIb. To standardize the nomenclature of the technical elements of this study, the authors of this research chose to name the last stage on the stress-strain response curve as IIb, as adapted in Fig. 1.

Several parameters were analyzed during the research on this composite material, such as the use of different types of cement matrixes,[10,30-32] the binding capacity between the textile and the matrix,[33] textile concrete under a harsh freezing-and-thawing environment,[34] the type of textiles,[9,11,31,35,36] textile pre-stretch,[37] the addition of short fibers in concrete,[8,38-42] textile impregnation techniques,[9,15,43] and test methods.[7,26,28]

Mattarollo et al.[10] carried out studies evaluating the mechanical behavior and mode of rupture with one layer of carbon and basalt textile in an HPC inorganic matrix. In this research, the authors also evaluated the addition of short steel fibers to concrete. Through tests carried out on 24 samples, it was found that the carbon textile reached high strength values, and it was observed that the textile pulled out of the concrete during its rupture.

Colombo et al.[11] analyzed three different glass textiles under uniaxial tension tests, in which they evaluated the effects of geometry, position, area of textile reinforcement, curing method, and strain rate. The researchers identified that in the case of the sample reinforced with one layer of fabric, called "F1-1," Stages II and IIb did not occur, with only a few visible cracks forming in the structure and no pattern of multiple cracks typical of concrete textile.

Preinstorfer et al.[15] verified the cracking behavior of different carbon textiles in a cementitious matrix through 144 direct tensile tests. The authors evaluated smooth carbon textiles and those with a sand coating layer, varying the concrete coverage between 5 and 30 mm (0.19 and 1.18 in.), and the geometry of the fiber strands. Regardless of the textile surface, longitudinal cracks were observed in tests with concrete coverage starting at 15 mm (0.59 in.). Textiles with sand coating showed greater interlock with the concrete, resulting in thinner and smaller cracks. In these textiles, longitudinal cracks occurred at low load levels around the entire specimen, with no displacement of the concrete upon rupture. In uncoated textiles, longitudinal cracks formed in later load stages, favoring the appearance of concrete spalling.

Ortolan[36] investigated two alkali-resistant glass textiles from a Brazilian textiles company. In the direct tensile test, the author analyzed that, for composites reinforced with just one layer of both textiles, the constitutive law of the mechanical behavior of the textile concrete was not verified because the three stages of the stress-strain response curve were not formed.

De Santis et al.[28] carried out a series of direct tensile tests to assist in the specifications of these tests, such as the geometry, development, curing process, experimental configurations, and measurement methods, among others. According to the authors, there are three failure modes for textile concrete. Rupture mode "A" is characterized by occurring close to the claw area, with rupture of the textile; "B" is in the middle of the sample; and "C" is in the gripper area due to the slipping of the textile on the concrete.

Considering the importance of investigating more sustainable materials for civil construction, experimental research was carried out through direct tensile tests of concrete reinforced with epoxy resin-impregnated carbon textile obtained from a German reinforcement manufacturing company and Brazilian glass textile from the aforementioned Brazilian textiles company. In this research, the mechanical behavior of the samples was evaluated through the stress-strain response curves.

RESEARCH SIGNIFICANCE

The comparison between the German carbon textile, which is considered among the most modern produced worldwide, and the glass textile available in Brazil aims to understand the differences between these two technologies and verify, through experimental analysis, the properties of these materials, adapted to the Brazilian inputs present in the cement matrix developed in this study.

EXPERIMENTAL INVESTIGATION

Cementitious matrix

The cement matrix used in this research was developed according to the concrete dosage method created by Christ.[44] Using this technique, it was possible to find the best proportions of materials in the mixture, resulting in higher values of tension and compressive strength of the concrete, allowing great workability. This method worked with the parameters of the components analyzed, according to the Andreasen and Andersen packing method.

The first step was to determine the theoretical packing curve of the materials using the Funk and Dinger equation. The range of diameters chosen was from 0.3 to 400 μm (1.1811×10^{-5} to 0.015748 in.). The percentage passing in each diameter was calculated as indicated in Christ[44] to obtain the theoretical packing curve of the mixture.

This curve was considered a reference in terms of comparison with the mixture packing curve, obtained through the quantities of materials in each analyzed diameter. Using the mixture packing curve, the packing deviation index was found. In this context, the mixture with lower values was chosen to obtain better compaction and, therefore, a packing curve closer to the theoretical packing.

Thus, using the tool in Microsoft Excel developed by Christ,[44] the theoretical packing and mixing curves were found. Through an iteration of the quantities of materials, the mixture with the lowest packing deviation index value, equal to 114.2, was chosen. Figure 2(a) shows the theoretical packing curve and the chosen mixture. The proportions of materials chosen for the fine concrete in this study are shown in Table 1.

Table 1—Mixture design of concrete

Component	Content, kg/m^3
Cement	471.26
Active silica	113.1
Fly ash	358.16
Calcium carbonate	334.59
Sand (0 to 400 μm)	966.08
Water-binder ratio	263.9
HRWRA	28.28
Viscosity modifier	9.43
Air detrainer	9.43

Note: HRWRA is high-range water-reducing admixture; 1 kg/m^3 = 0.06 lb/ft^3.

Thin concrete was cast into cylindrical specimens measuring 5 cm (1.9685 in.) in diameter and 10 cm (3.93701 in.) in height to evaluate the compressive strength according to ABNT NBR 5739:2018[45] and elastic modulus according to ABNT NBR 8522-1:2021.[46] All samples were arranged in a humid chamber, with relative air humidity equal to 98%. After 28 days of curing, mechanical tests were carried out, resulting in an average compressive strength of 80.07 MPa (11.61 ksi), average tensile strength of 4.5 MPa (0.65 ksi), and elastic modulus of 31.16 GPa (4519.37 ksi).

These results showed that the application of the dosing method created by Christ[44] resulted in a fine concrete with ideal characteristics to be used together with textile reinforcement, such as fluidity capacity and workability, as demonstrated in Fig. 2(b), and high mechanical resistance. The values of compressive strength, tension, and modulus of elasticity are in line with the results for thin concrete presented in the literature.[9,10,11,32]

Textile reinforcement

The textile reinforcements selected for the research were the alkali-resistant glass textile from the Brazilian company and the carbon textile with epoxy resin impregnation available from the German company, as presented in Fig. 3. It is worth mentioning that the textiles used in this research are donations provided by the mentioned companies, without disclosing the value of the product.

The glass textile has a cross-sectional area of one fiber strand equal to 1.8 mm^2 (0.0027 in.^{2}) and an axial distance between the grids of 10 mm (0.39 in.), according to the characterization carried out by Dalazen[47] in the LEME laboratory at the Federal University of Rio Grande do Sul in Brazil. To verify its load capacity, a mechanical tensile test was carried out on a warp filament of the aforementioned fabric, in accordance with the parameters of ASTM D885/D885M-10A(2014)e1.[48] In this test, the average textile tension found was 566.72 MPa (82.19 ksi).

According to information obtained by the manufacturing company, the glass textile is impregnated with an acrylic resin that has no structural function and is only used to avoid failures in the weaving of the material during its use.

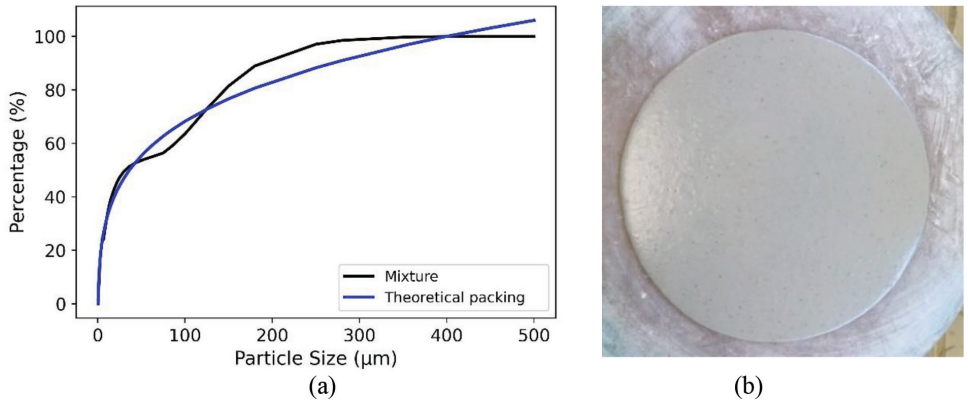

Fig. 2—(a) Theoretical packing and packing of mixture; and (b) appearance of fine concrete. (Note: 1 μm = 3.937 × 10^{-5} in.)

However, this resin can help with the connection capacity between the filaments, promoting the mechanical capacity of the material. Therefore, this textile was considered to be of the impregnated type.

The German carbon textile has a cross-sectional area of one fiber strand equal to 0.9 mm^2 (0.001395 in^2.), an axial distance between the grids of 21 mm (0.82 in.), a textile tensile strength of 4000 N/mm^2 (580.151 ksi), and is impregnated with epoxy resin, with a structural function.

Mechanical behavior of composite material

The evaluation of the mechanical behavior of the TRC was carried out using the direct tensile test, following recommendations from RILEM Technical Committee 232-TDT[26] and De Santis et al.[28] The tensile test model was chosen by adapting the Hinzen[2] test.

The dimensions of the test piece were selected according to Hinzen,[2] adapting the width of the sample to 55 mm (2.16 in.), to use three individual warp filaments of the carbon textile and four warp filaments of the glass textile, in addition to the thickness of 9.5 mm (0.37 in.), as demonstrated in Fig. 4(a), for the evaluation of one and two layers of both textiles. Because textile concrete is a relatively new material in the civil industry, there are still no standards that recommend the minimum reinforcement value for this material. Hence, further research is needed to evaluate these materials.

It should be mentioned that this work was limited to the analysis of only one layer of carbon textile reinforcement due to the limitation of the gripper's mechanical capacity. Furthermore, different sample thicknesses were not considered due to the limitation of resources available for the production of shapes and grippers.

The choice of the dog-bone shape was based on references from German research such as Hinzen,[2] Jesse,[27] Molter,[29] Voss,[3] and Kulas,[22] which are studies that evaluate the mechanical tensile behavior of textile concrete pieces. These dimensions are in accordance with the minimum values recommended by RILEM Technical Committee 232-TDT.[26]

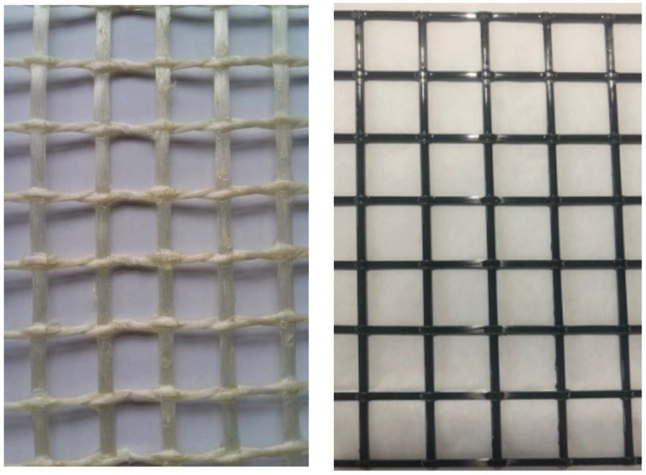

Fig. 3—(a) Glass textile; and (b) carbon textile.

Preparation of samples for tensile test

The bone-shaped forms, used as a reference for the specimen molds, were made of steel. After mixing the fine concrete, the lamination technique was used to insert the textile reinforcement into the mixture, in accordance with RILEM Technical Committee 232-TDT's[26] guidelines.

In this technique, the first layer of concrete (Fig. 4(b)) was placed, followed by the layer of carbon or glass textile, applying a small pressure to make it better "adhered" to the cement matrix. Afterward, this procedure was repeated until all layers of the samples were produced. As the concrete is self-consolidating, there was no need for subsequent vibration. It is worth mentioning that the thickness of the thin concrete was controlled using a measuring ruler, as demonstrated in Fig. 4(b).

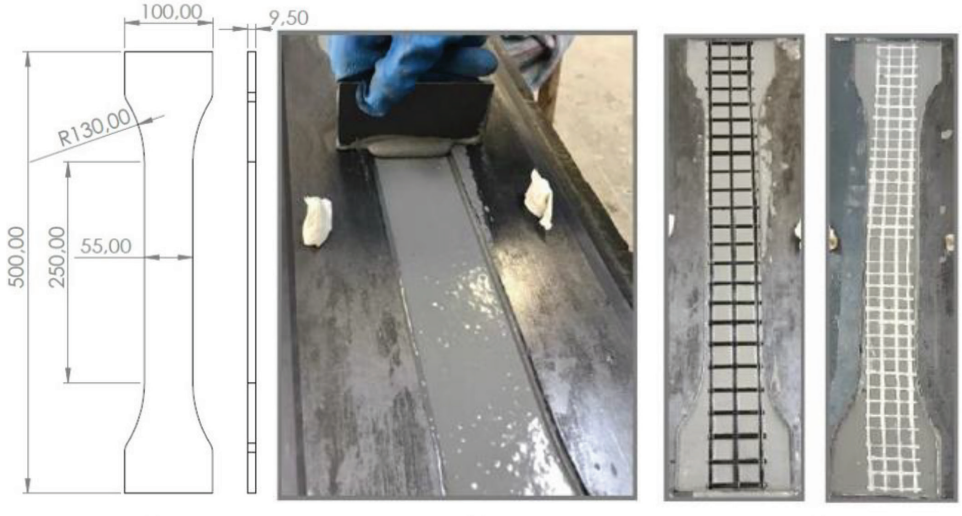

Fig. 4—(a) Dimensions (in mm) of test piece; (b) first concrete layer; and (c) carbon and glass textile layers. (Note: 1 mm = 0.04 in.)

Fig. 5—(a) Failure of sample; and (b) LVDT fixed in sample.

Technical test procedure

Direct tensile tests were carried out on samples aged 28 days in a tension machine with a capacity of 100 kN (22,480.9 lbf) and a displacement rate of 1 mm/min (0.04 in./min). According to RILEM Technical Committee 232-TDT's[26] specifications, a thin rubber layer of 1 mm (0.04 in.) was placed between the steel plates and the test piece to avoid excessive load concentrations in the location during the procedure. In this test, the samples were analyzed until their respective ruptures.

To improve rigidity in the extreme areas of the bone piece and contribute to uniform stress distributions in the element, two layers of carbon blanket with epoxy resin were fixed on each face of the piece, as shown in Fig. 5(a). A linear variable differential transformer (LVDT) with a 10 mm (0.4 in.) cursor was fixed to one side of the sample to check the displacement of the tested material (Fig. 5(b)).

Experimental test variables

The direct tensile test was carried out according to the following items: a) four samples of thin concrete with one layer of alkali-resistant glass textile; b) four samples of thin concrete with two layers of alkali-resistant glass textile; and c) four samples of thin concrete reinforced with one layer of carbon textile.

In total, 11 samples were analyzed in this experimental study. One sample (CTG14), in which a layer of Brazilian glass fabric was used, had to be disregarded due to failure to read the LVDT during the technical test procedure. Specimens reinforced with two layers of carbon textile were tested, but due to the high resistance achieved by the material, the fitting pin in the tension machine ended up breaking, making it impossible to complete the analyses for inclusion

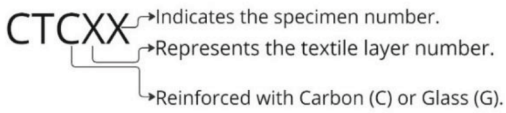

Fig. 6—Sample identification scheme.

in this paper. The scheme adopted for naming the samples verified in the tests can be seen in Fig. 6.

The specimens were placed in a humid chamber in the LEME laboratory, which has a moisture content of 98%, until the age of 21 days. The face of the samples in contact with the surface was covered with canvas to maintain the hydration of the concrete and reduce the probability of it shrinking. Seven days before the rupture test, the carbon blankets were fixed with the epoxy resin on the extreme faces of the specimens to improve the rigidity in these areas of the parts.

Table 2 shows the fiber cross-sectional area of one fiber strand ($A_{tex,i}$); the number of fiber strands used in each test body, represented by the letter "n"; the total area of the cross section of the textile fiber strands ($A_{tex,n}$); and finally, the percentage of textile reinforcement (ρ) of each sample analyzed, as named by Preinstorfer et al.[15]

EXPERIMENTAL RESULTS AND DISCUSSION

The experimentally generated data were analyzed on the Jupyter Notebook platform, in Python programming language, where the stress-strain curves response of the samples was generated. To prevent possible errors in the results derived from the variation in the thickness of the thin concrete, the stresses of the thin concrete samples reinforced with glass and carbon textiles were calculated by dividing the force by the total area of the cross section of the textile fiber strands ($A_{tex,n}$), according to De Santis et al.'s[28] technical

specifications. Regarding deformations, the displacements obtained through the LVDT were divided by the initial length of the measurable area of each part, turning these values into percentages for reading purposes on the graph.

For all the tensile tests, tables with the transition points between the stages, the maximum stress and strain, and the rupture mode were added, as recommended by De Santis et al.,[28] in addition to the respective averages and coefficient of variation values of these parameters.

Concrete reinforced with one layer of glass textile

In the three test specimens reinforced with just one layer of Brazilian glass textile, the formation of Stage I was clearly observed, characterized by its linear-elastic behavior and without the formation of cracks in the thin concrete. The rupture of all samples occurred in the measurable area, as shown in Fig. 7. The type of rupture is characterized as type "B," according to De Santis et al.[28] In Fig. 8, the stress-strain curves response of samples CTG11, CTG12, and CTG13 are represented, respectively.

As stated by Jesse,[27] with the formation of the first crack in the matrix, Stage IIa begins, with deformation ϵ_I and tension σ_I being the transition points between Stages I and IIa.[28] In the three tests, after the formation of the first crack, a drop in force was observed with an increase in deformation, followed by an increase in this force until the emergence of a new crack, as specified by Jesse.[27] In CTG11 and CTG12, only two cracks were formed in Stage IIa. Another particularity found in these samples is that it was not possible to clearly identify the formation of Stage IIb, where the cracking phase ends and the structure ruptures. This behavior was also verified by Ortolan,[36] who did not identify the three stages in his samples reinforced with one layer of Brazilian glass textile.

In this sense, the same stress and strain values (σ_{II} and ϵ_{II}) of the transition points from Stage IIa to Stage IIb were considered for these samples, which is equivalent to the rupture values (f_t and ϵ_t), as demonstrated in Table 3.

However, in sample CTG13, it was possible to identify Stage IIb after the formation of the third crack in the composite material, as demonstrated in Fig. 8(c). This behavior may have occurred due to the fact that there is a greater bond between the cement matrix and the textile reinforcement.

Table 2—Textile reinforcement parameters

Samples	$A_{tex,i}$, mm^2	n	$A_{tex,n}$, mm^2	ρ, %
CTG11	1.8	4	7.2	1.38
CTG12	1.8	4	7.2	1.38
CTG13	1.8	4	7.2	1.38
CTG21	1.8	8	14.48	2.77
CTG22	1.8	8	14.48	2.77
CTG23	1.8	8	14.48	2.77
CTG24	1.8	8	14.48	2.77
CTC11	1.81	3	5.43	1.04
CTC12	1.81	3	5.43	1.04
CTC13	1.81	3	5.43	1.04
CTC14	1.81	3	5.43	1.04

Note: 1 mm^2 = 0.00155 in.^{2}.

Concrete reinforced with two layers of glass textile

In the tests in which the thin concrete was reinforced with two layers of glass textile, it was possible to clearly verify the formation of the three stages in all samples. Multiple cracks were also formed in Stage IIa. In Stage IIb, for samples CTG21, CTG22, and CTG23, small load drops were identified in the material, called diffuse cracks by Jesse.[27] As discussed in the theoretical framework of this study, Bruckermann[49] justified these load drops by the occurrence of transverse contraction of the textile.

Samples CTG21, CTG22, and CTG4 showed rupture within the measurable area of the specimens, which can be characterized as a type "B" rupture. In CTG23, the rupture of the textile occurred in the claw area, classified as type "A." Its curves with the mechanical behavior of each test are shown in Fig. 9, and the rupture of the samples is shown in Fig. 10. It is important to highlight that the descending branch was not represented in the curves in Fig. 9, to focus on the three stages that are analyzed in textile concrete elements.

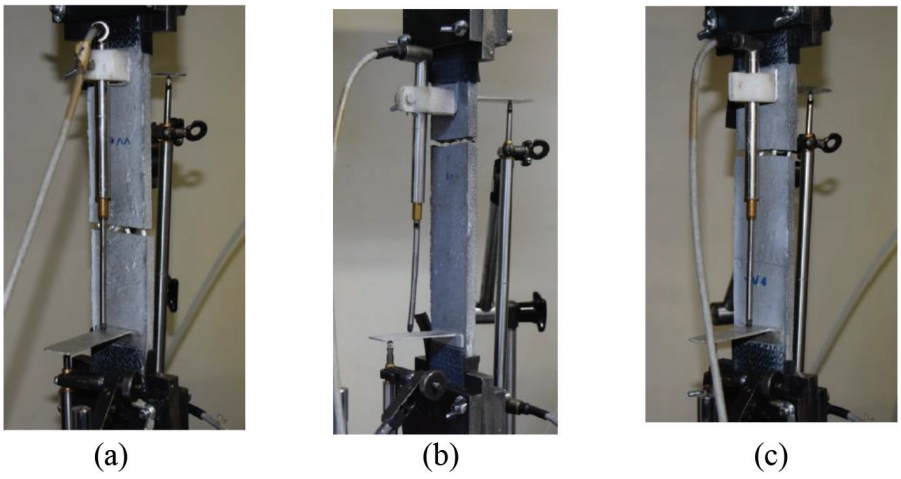

Fig. 7—Rupture of samples reinforced with one layer of glass textile: (a) CTG11; (b) CTG12; and (c) CTG13.

Table 3—Test results with one layer of glass textile

Samples	ϵ_I, %	ϵ_{II}, %	σ_I, N/mm^2	σ_{II}, N/mm^2	f_t, N/mm^2	ϵ_t, %	Rupture mode
CTG11	0.0198	0.977	412	443	443	0.977	B
CTG12	0.0361	0.761	367	439	439	0.761	B
CTG13	0.0468	0.639	372	377	441	1.32	B
Average	0.034	0.792	383.66	419.66	441	1.01	—
CV, %	32.43	17.63	5.24	7.19	0.37	22.58	—

Note: CV is coefficient of variation; 1 N/mm^2 = 0.145038 ksi.

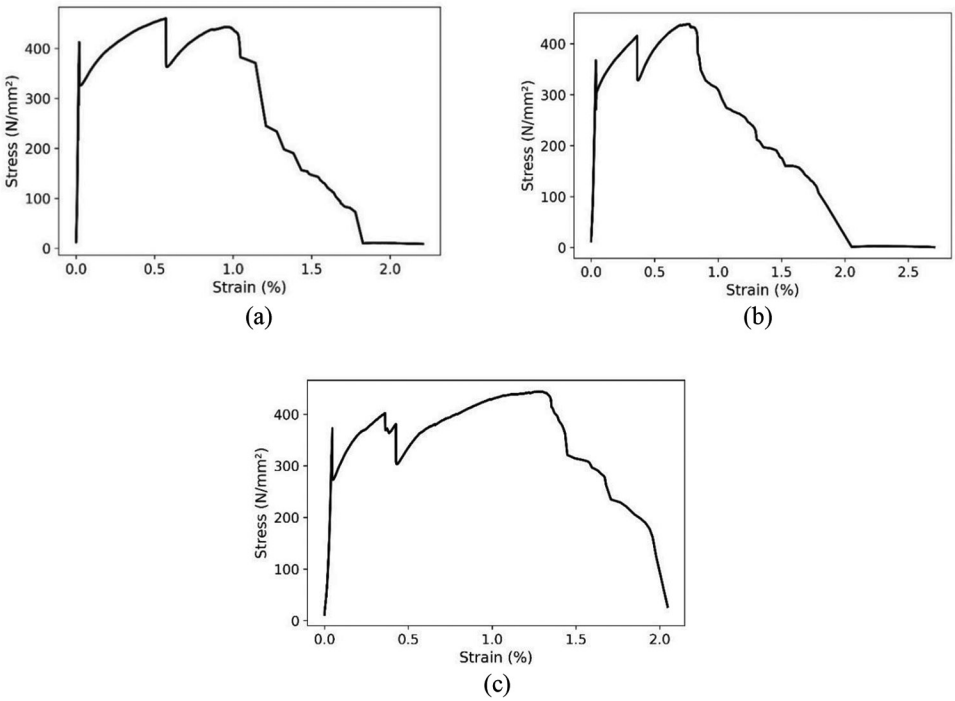

Fig. 8—Stress-strain response curves of samples reinforced with one layer of glass textile: (a) CTG11; (b) CTG12; and (c) CTG13. (Note: 1 N/mm^2 = 0.145 ksi.)

Table 4 lists all the results of this analysis. The maximum stress values (f_t) of the samples were very close, with a coefficient of variation of 1.36%. The CTG21 sample stood out in terms of maximum rupture stress, reaching a value of 550 N/mm^2 (79.77 ksi). The CTG24 sample was the one that obtained the highest Stage IIa stress (σ_I), which consequently generated a higher quality of connection between the textile reinforcement and the cement matrix, resulting in the highest deformation value of rupture (ϵ_{II}) among all analyzed samples.

Concrete reinforced with one layer of carbon textile

In all tests, the three stages of cracking of the textile concrete were formed, as shown in Fig. 11. However, due to reaching high values of force, failure was observed close to the claw area, between the measurable area and the rigid area created by the carbon blanket, as highlighted in red in Fig. 12, with the slippage of the textile reinforced in the cement matrix. In this context, according to De Santis et al.,[28] this type of rupture can be classified as type "C."

The stress concentration generated during the tensile test, caused by the high mechanical capacity of the carbon textile, influenced the formation of longitudinal cracks in the region of the claw where the rupture occurred. This behavior was also verified by Donnini et al.[35] and Preinstorfer et al.[15] As the carbon textile impregnated with epoxy resin is smooth, there was less bonding between the textile and the thin concrete, which combined with high values of force, caused the fabric to slide in the cement matrix and subsequent spalling of the concrete, as shown in sample CTC13 in Fig. 12(b).

In CTC12, a nonlinear formation of the composite material was observed in Stage I. According to Jesse,[27] Voss,[3] and Kulas,[22] this result may have occurred due to possible predeformations or shrinkage cracks caused on the sample side, which is directly exposed to air during the curing process of fine concrete. This explains the high value of the coefficient of variation from strain ϵ_I, demonstrated in Table 5. In CTC11, CTC12, and CTC13, diffuse cracks were observed in Stage IIb, caused by load drops during the tensile test.

The maximum stress of the CTC11, CTC12, CTC13, and CTC14 samples averaged 2575.0 N/mm^2 (373.47 ksi), with a coefficient of variation of just 4.31% between them, as shown in Table 5. In the rupture deformation, ϵ_t, an average value of 1% was obtained, with a coefficient of variation of 9.57%.

In general, the tests carried out with the carbon textile showed cracks throughout the measurable area of the test

Table 4—Test results with two layers of glass textile

Samples	ϵ_I, %	ϵ_{II}, %	σ_I, N/mm^2	σ_{II}, N/mm^2	f_t, N/mm^2	ϵ_t, %	Rupture mode
CTG21	0.0309	0.412	172	304	550	1.32	B
CTG22	0.0502	0.672	106	306	530	1.37	B
CTG23	0.0552	0.6	153	315	545	1.39	A
CTG24	0.0827	0.806	214	329	541	1.7	B
Average	0.054	0.622	161.25	313.5	541.5	1.44	—
CV, %	33.81	22.85	24.05	3.14	1.36	10.34	—

Note: 1 N/mm^2 = 0.145038 ksi.

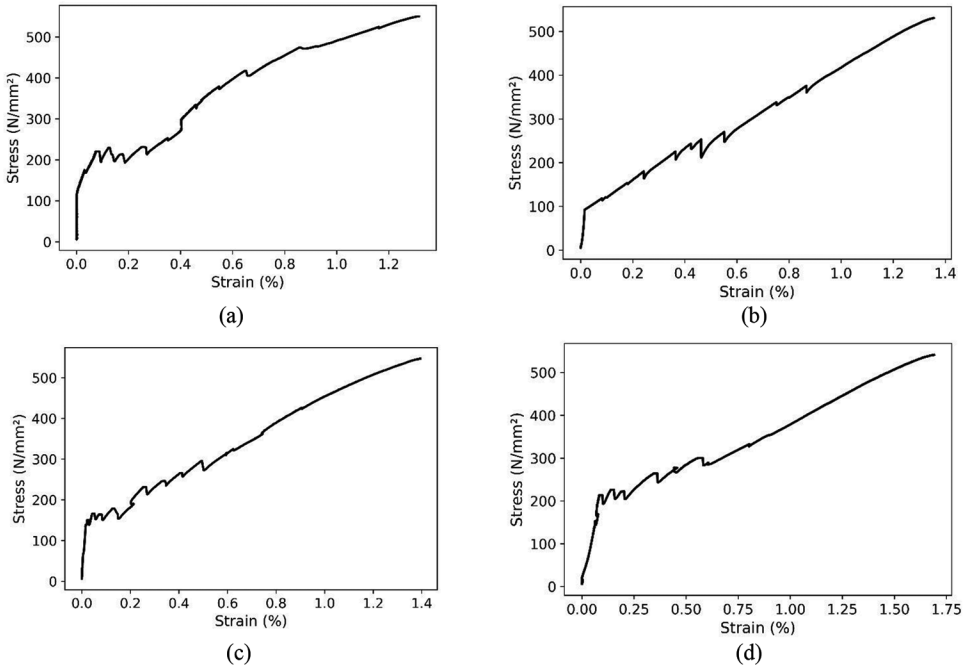

Fig. 9—Stress-strain response curves of samples reinforced with two layers of glass textile: (a) CTG21; (b) CTG22; (c) CTG23; and (d) CTG24. (Note: 1 N/mm^2 = 0.145 ksi.)

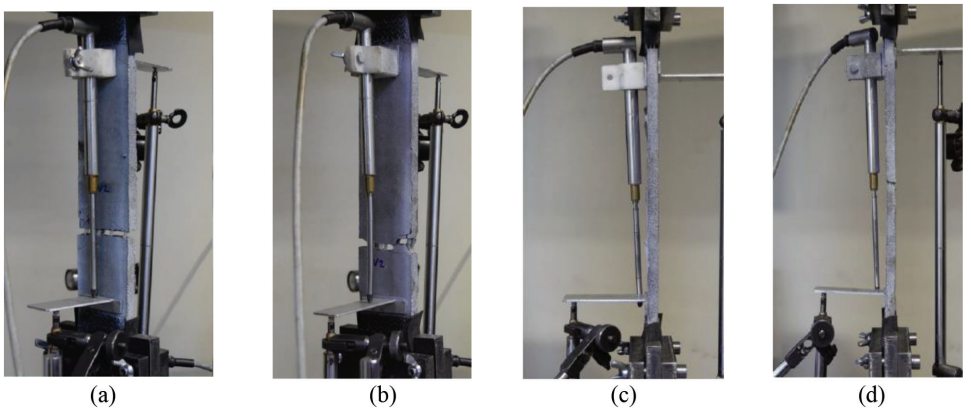

Fig. 10—Rupture of samples reinforced with two layers of glass textile: (a) CTG21; (b) CTG22; (c) CTG23; and (d) CTG24.

specimens, verifying that the stress distribution during the test occurred appropriately.

Comparison of experimental results of carbon and glass textiles

In terms of mechanical response, the samples reinforced with two layers of Brazilian glass textile and those reinforced with German carbon textile presented the expected mechanical behavior through the stress-strain curve response for textile concrete elements, with the formation of Stages I, IIa, and IIb.

However, in the specimens in which only one layer of glass textile was used, a reinforcement percentage of 1.38%

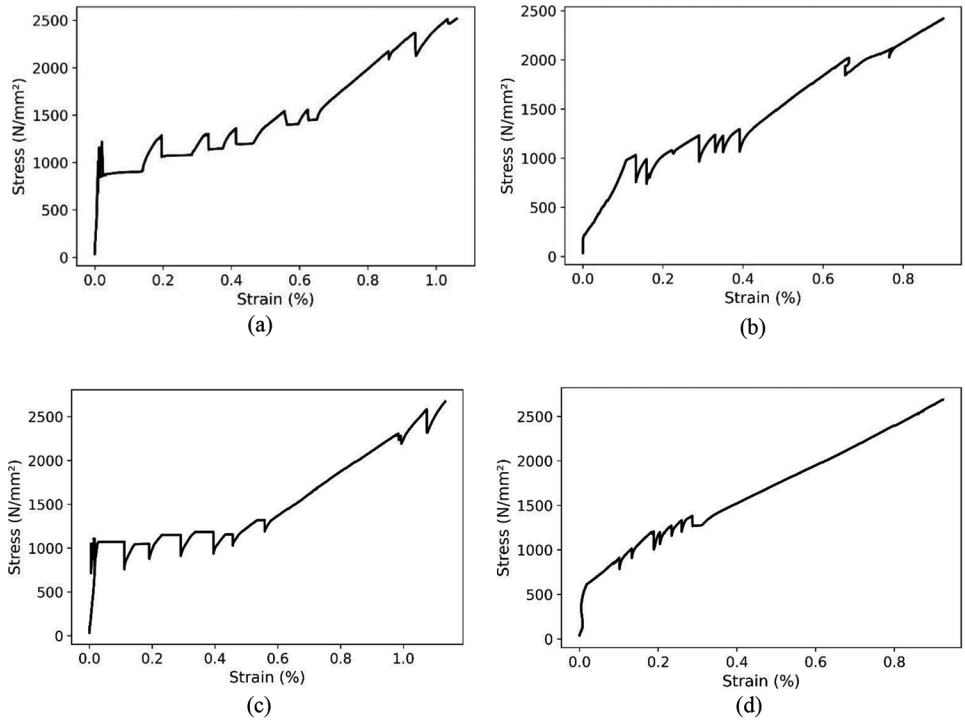

Fig. 11—Stress-strain response curves of samples reinforced with one layer of carbon textile: (a) CTC11; (b) CTC12; (c) CTC13; and (d) CTC14. (Note: 1 N/mm² = 0.145 ksi.)

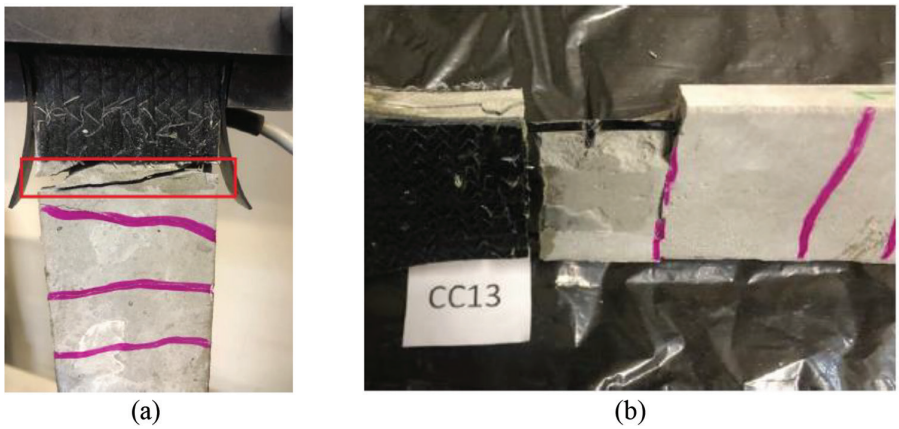

Fig. 12—Rupture of samples: (a) CTC11; and (b) CTC13.

was observed to be insufficient, as it was not possible to identify all stages for textile concrete elements.

The use of the claw type and "bone" sample shape in the tensile test favored the Brazilian glass fabric, as it resulted in better stress distribution during the tests. The samples reinforced with this material showed ruptures occurring in the measurement area without any sliding behavior of the test specimens.

For structures reinforced with carbon textile, due to the high mechanical capacity of this polymeric material, there was a concentration of stress in the part responsible for transmitting the efforts from the claw to the test piece, which favored the occurrence of ruptures close to the areas of the claw. Concrete spalling and textile slippage were also observed during the tests.

Regarding the reinforcement rate, with the increase in the number of layers for the glass textile, an increase in the number of cracks and a decrease in the average spacing between them was observed. In samples reinforced with two layers of the aforementioned textile (ρ = 2.77%), an average of seven cracks formed in the structural piece, while in tests in which one layer was used (ρ = 1.38%), only two cracks were formed on average. In the case of tests with one layer of carbon textile and a reinforcement rate of 1.04%, the average number of cracks observed in the structural part was equivalent to parts reinforced with two layers of glass textile (ρ = 2.77%). Figure 13 shows the crack pattern in each specimen reinforced with carbon textile.

Regarding the rupture stress (f_t), the samples reinforced with the German carbon textile reached values approximately five times higher than those reinforced with the Brazilian glass textile. This indicates that, compared to glass textiles, the use of rigid carbon textile reinforcement in structures can

Table 5—Test results with one layer of carbon textile

Samples	ϵ_I, %	ϵ_{II}, %	σ_I, N/mm^2	σ_{II}, N/mm^2	f_t, N/mm^2	ϵ_t, %	Rupture mode
CTG11	0.0122	0.661	1150	1560	2520	1.06	C
CTG12	0.11	0.45	981	1390	2420	0.9	C
CTG13	0.0144	0.641	1110	1470	2670	1.13	C
CTG14	0.0223	0.314	626	1290	2690	0.92	C
Average	0.039	0.051	966.75	1427.5	2575	1	—
CV, %	102.57	27.68	21.35	6.97	4.31	9.57	—

Note: 1 N/mm^2 = 0.145038 ksi.

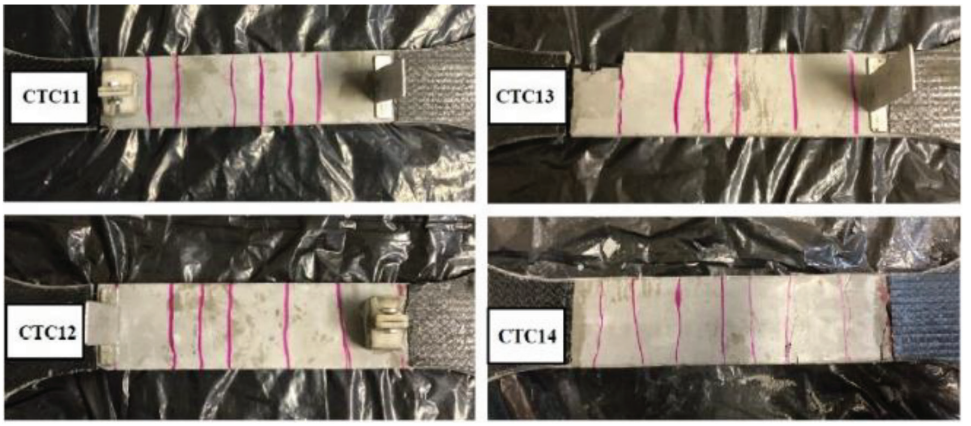

Fig. 13—Crack pattern in carbon-reinforced samples.

reduce their thickness and the number of textile layers by half, favoring the cost-benefit of using this material.

To visually exemplify the comparison between the two materials analyzed, Fig. 14 was generated with the curves resulting from the average of the experimentally obtained values of concrete reinforced with one layer of carbon textile reinforcement and two layers of glass textile. This figure highlights the high mechanical resistance achieved with carbon textiles. In the case of glass textiles, deformations reached higher values, as there was a better distribution of stresses due to the shape of the claw, as mentioned previously.

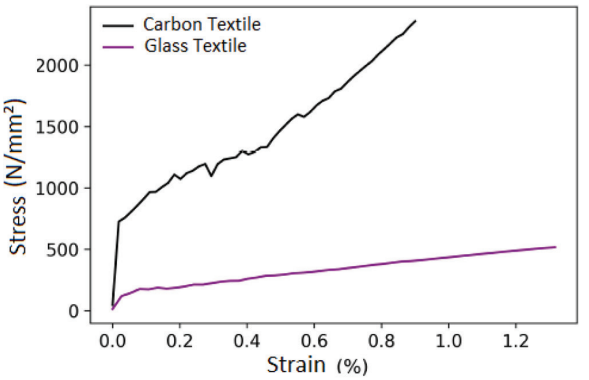

Fig. 14—Average stress-strain response curves of samples reinforced with two layers of glass textile and one layer of carbon textile. (Note: 1 N/mm^2 = 0.145 ksi.)

Comparison of resistances achieved experimentally and analytically

To compare the results of rupture stresses achieved experimentally and analytically, the analytical model used by Kulas[22] was considered for the analytical calculation of the tensile force of thin concrete elements reinforced with impregnated textiles.

The tensile strength of the carbon textile was 4000 N/mm^2 (580.151 ksi). For the glass textile, a mechanical test was carried out, and an average tensile strength of 566.72 N/mm^2 (82.19 ksi) was found. Considering this, the tensile force of both textiles analyzed was obtained according to Eq. (1)

$$F_{t,u} = A_{t,K} \cdot f_{t,K} \cdot k_v \cdot \left(1 - \frac{\alpha}{90°}\right)^2 + A_{t,S} \cdot f_{t,S} \cdot k_v \cdot \left(\frac{\alpha}{90°}\right)^2 \quad (1)$$

where $A_{t,K}$ and $A_{t,S}$ are the cross-sectional area of warp and weft, respectively; $f_{t,K}$ and $f_{t,S}$ are the tensile strength of the warp and weft textile mesh, respectively; k_v is the reduction factor equal to 0.84 due to lateral contraction of the strands; and α is the angle between the force and bending direction.

Equation (2) is an example of an analytical calculation for the case of a sample reinforced with two layers of glass textile, where the total cross-sectional area of the warp is 14.48 mm^2 (0.022 in.^{2}), the tensile strength of the warp is 566.72 N/mm^2 (82.19 ksi), the reduction factor is 0.84, and the angle between the force and bending direction is 0. The second part of this equation was disregarded, as the applied force is perpendicular to the weft thread direction.

$$F_{t,u} = 14.48 \cdot 566.72 \cdot 0.84 \cdot \left(1 - \frac{0}{90°}\right)^2 + 0 = 6893.12 \text{ N (1549.63 lbf)} \quad (2)$$

Thus, this value can be converted to tensile strength

$$f_t = \frac{6893.12\ \text{N}}{14.48\ \text{mm}^2} = 476.05\ \text{N/mm}^2\ (69.04\ \text{ksi}) \quad (3)$$

Table 6 lists the tensile strength (f_t) obtained experimentally and analytically from all samples presented in this study, in addition to the statistical analysis of error between the two selected values in percentage.

The samples reinforced with Brazilian glass textile presented results closest to the analytical calculation, with the samples with one layer (CTG11 to CTG13) having the lowest error values. In tests in which the thin concrete was reinforced with two layers of glass textile (CTG21 to CTVG4), it was observed that the rupture stresses obtained experimentally were higher than those from the analytical calculation. This indicates that for Brazilian glass textiles, the resistance reduction factor (k_v), equal to 0.84, considered in Eq. (1), can be disregarded due to the lateral contraction of the wicks.

The samples reinforced with German carbon textile with epoxy resin impregnation (CTC11 to CTC14) presented the highest error values, reaching 27.97% in the case of sample CTC12. In this case, the tension obtained experimentally could be even greater if there were greater adhesion between the textile reinforcement and the thin concrete and if the stresses were distributed more uniformly in the structural part.

CONCLUSIONS

In this work, experimental research was carried out to investigate the mechanical behavior obtained through uniaxial tensile tests of concrete structural parts reinforced with glass fabric, available in Brazil, and carbon fabric, produced in Germany.

In tests in which concrete parts reinforced with the Brazilian glass textile were evaluated, it was observed that the textile reinforcement of one layer was not sufficient to meet the element's structural issues. However, with two layers, the mechanical behavior obtained was excellent, demonstrating good bonding capacity between the fabric and the concrete, rupture within the measurable area, and adequate tension distribution.

The parts reinforced with the German carbon textile showed spalling of the concrete and slipping of the fabric. These phenomena suggest that there was a concentration of stress at the ends of the samples, corroborating the rupture of the structural element in regions close to the claw. However, even with these problems, it was observed that the mechanical behavior obtained through the stress-strain response curve occurred as expected for textile concrete elements, with the structure rupture on Stage IIb, as predicted in the literature.

Regarding the rate of reinforcement and cracking, it was observed that more cracks formed, with smaller spacing between them, as the rate of reinforcement with the glass textile in the analyzed structural element increased. In the samples reinforced with one layer of carbon textile, an average of seven cracks formed along the test piece, a value also found in the samples reinforced with two layers of Brazilian glass textile.

Table 6—Comparison of experimental and analytical tensile strengths

Samples	f_t experimental, N/mm^2	f_t analytical, N/mm^2	Error, %
CTG11	443	476.05	6.94
CTG12	439	476.05	7.78
CTG13	441	476.05	7.36
CTG21	550	476.05	15.53
CTG22	530	476.05	11.33
CTG23	545	476.05	14.48
CTG24	541	476.05	13.64
CTC11	2520	3360	25.00
CTC12	2420	3360	27.97
CTC13	2670	3360	20.53
CTC14	2690	3360	19.94

Note: 1 N/mm^2 = 0.145038 ksi.

In terms of mechanical resistance, the tensile strength of the concrete reinforced with carbon textile impregnated with epoxy resin was approximately five times greater than the tension of specimens reinforced with Brazilian fabric. With this result, it was observed that the German carbon textile achieves high mechanical resistance, which positively influences the reduction in the reinforcement rate, thickness, and weight of structures, which corroborates an economically viable project and its use in slender and innovative architectures.

From the results listed, it is concluded that both textiles analyzed in this research have great potential to be used in the construction industry, as in addition to offering structural capacity to the elements, they have concepts that encompass innovation, sustainability, and technology—characteristics that are essential for the sustainable development of current and future generations.

RECOMMENDATIONS

The authors provide the following recommendations for future research:

1. The authors recommend further investigation regarding Brazilian glass textile, evaluating its mechanical capacity based on the reinforcement of two or more layers because there was structural incapacity in the specimens reinforced with one layer.

2. For the specimens reinforced with German carbon textile, the authors suggest evaluating the mechanical behavior through a rectangular geometry, in addition to the increased thickness of the specimen.

AUTHOR BIOS

Joici Rizzo *received her master's in civil engineering, with a focus on structures, from the Federal University of Rio Grande do Sul (UFRGS), Porto Alegre, RS, Brazil, in 2023. She graduated in civil engineering from the University of Caxias do Sul (UCS), Caxias do Sul, RS, Brazil, in 2021. Her research interests include structural materials, with an emphasis on innovative and sustainable materials.*

Eduardo Stimamiglio Bastos *is a PhD Student in materials engineering in the Postgraduate Program in Mining, Metallurgical and Materials Engineering (PPGE3M) at UFRGS, where he works as a researcher at the Physical Metallurgy Laboratory (LAMEF). He received his master's in engineering and materials science from the postgraduate program (PGMAT) at UCS in 2018.*

Lucas Alexandre Reginato *received his PhD in 2020 and his postdoctorate in 2021 and 2023 in civil engineering from UFRGS. He is currently a Postdoctoral Fellow and Collaborating Professor at UFRGS in the area of inspection and conservation management of infrastructure works. His research interests include structures, experimental analysis, construction components, construction pathology, inspection, nondestructive testing, instrumentation and monitoring of structures, and recovery of reinforced concrete structures.*

Paula Manica Lazzari *is a Professor at UFRGS and a collaborating professor in the Postgraduate Program in Civil Engineering at UFRGS (PPGEC), where she received her PhD in civil engineering in 2016. Her research interests include analysis of concrete structures, numerical analysis, experimental analysis, and finite element modeling.*

Luiz Carlos Pinto da Silva Filho *is a Full Professor at UFRGS and Secretary of Innovation at Porto Alegre City Hall. He received his civil engineering degree from UFRGS in 1989; his master's in civil engineering/construction from the PPGEC at UFRGS in 1994; and his PhD in civil engineering/bridge maintenance from the University of Leeds, Leeds, UK, in 1998.*

ACKNOWLEDGMENTS

The authors of this research would like to thank the financial support granted by the Postgraduate Program in Civil Engineering (PPGEC) of the Federal University of Rio Grande do Sul (UFRGS) and Brazilian governmental research institutions (CAPES), as well as the companies Solidian and Texiglass for donating textiles.

REFERENCES

1. Hegger, J.; Will, N.; and Rüberg, K., "Textile Reinforced Concrete — A New Composite Material," *Advances in Construction Materials 2007*, C. U. Grosse, ed., Springer, Berlin, Germany, 2007, pp. 147-156.

2. Hinzen, M., "Einfluss von Kurzfasern auf die Frisch- und Festbeton-eigenschaften sowie das Tragverhalten von Textilbeton," PhD thesis, RWTH Aachen University, Aachen, NRW, Germany, 2014, 295 pp. (in German)

3. Voss, S., "Ingenieurmodelle zum Tragverhalten von Textilbewehrtem Beton," PhD thesis, RWTH Aachen University, Aachen, NRW, Germany, 2008, 246 pp. (in German)

4. Hegger, J.; Curbach, M.; Stark, A.; Wilhelm, S.; and Farwig, K., "Innovative Design Concepts: Application of Textile Reinforced Concrete to Shell Structures," *Structural Concrete*, V. 19, No. 3, June 2018, pp. 637-646. doi: 10.1002/suco.201700157

5. Rawat, P.; Liu, S.; Guo, S.; Zillur Rahman, M.; Yang, T.; Bai, X.; Yao, Y.; Mobasher, B.; and Zhu, D., "A State-of-the-Art Review on Mechanical Performance Characterization and Modelling of High-Performance Textile Reinforced Concretes," *Construction and Building Materials*, V. 347, Sept. 2022, Article No. 128521. doi: 10.1016/j.conbuildmat.2022.128521

6. Hartig, J.; Häußler-Combe, U.; and Schicktanz, K., "Influence of Bond Properties on the Tensile Behaviour of Textile Reinforced Concrete," *Cement and Concrete Composites*, V. 30, No. 10, Nov. 2008, pp. 898-906. doi: 10.1016/j.cemconcomp.2008.08.004

7. Schütze, E.; Lorenz, E.; and Curbach, M., "Test Methods for Textile Reinforced Concrete," *FERRO-11 and 3rd ICTRC—Proceedings of the 11th International Symposium on Ferrocement and 3rd International Conference on Textile Reinforced Concrete*, W. Brameshuber, ed., Aachen, NRW, Germany, 2015, pp. 307-318.

8. de Andrade Silva, F.; Butler, M.; Mechtcherine, V.; Zhu, D.; and Mobasher, B., "Strain Rate Effect on the Tensile Behaviour of Textile-Reinforced Concrete Under Static and Dynamic Loading," *Materials Science and Engineering: A*, V. 528, No. 3, Jan. 2011, pp. 1727-1734. doi: 10.1016/j.msea.2010.11.014

9. Valeri, P.; Fernàndez Ruiz, M.; and Muttoni, A., "Tensile Response of Textile Reinforced Concrete," *Construction and Building Materials*, V. 258, Oct. 2020, Article No. 119517. doi: 10.1016/j.conbuildmat.2020.119517

10. Mattarollo, G.; Randl, N.; and Pauletta, M., "Investigation of the Failure Modes of Textile-Reinforced Concrete and Fiber/Textile-Reinforced Concrete under Uniaxial Tensile Tests," *Materials*, V. 16, No. 5, Mar. 2023, Article No. 1999. doi: 10.3390/ma16051999

11. Colombo, I. G.; Magri, A.; Zani, G.; Colombo, M.; and di Prisco, M., "Erratum to: 'Textile Reinforced Concrete: Experimental Investigation on Design Parameters'," *Materials and Structures*, V. 46, No. 11, Nov. 2013, pp. 1953-1971. doi: 10.1617/s11527-013-0023-7

12. Yin, S.; Xu, S.; and Li, H., "Improved Mechanical Properties of Textile Reinforced Concrete Thin Plate," *Journal of Wuhan University of Technology-Materials Science Edition*, V. 28, No. 1, Feb. 2013, pp. 92-98. doi: 10.1007/s11595-013-0647-z

13. Mészöly, T.; Ofner, S.; and Randl, N., "Effect of Combining Fiber and Textile Reinforcement on the Flexural Behavior of UHPC Plates," *Advances in Materials Science and Engineering*, V. 2020, No. 1, Article No. 9891619.

14. Preinstorfer, P.; Huber, P.; Huber, T.; Kromoser, B.; and Kollegger, J., "Experimental Investigation and Analytical Modelling of Shear Strength of Thin-Walled Textile-Reinforced UHPC Beams," *Engineering Structures*, V. 231, Mar. 2021, Article No. 111735. doi: 10.1016/j.engstruct.2020.111735

15. Preinstorfer, P.; Yanik, S.; Kirnbauer, J.; Lees, J. M.; and Robisson, A., "Cracking Behaviour of Textile-Reinforced Concrete with Varying Concrete Cover and Textile Surface Finish," *Composite Structures*, V. 312, May 2023, Article No. 116859. doi: 10.1016/j.compstruct.2023.116859

16. Scheerer, S.; Schladitz, F.; and Curbach, M., "Textile Reinforced Concrete–from the Idea to a High-Performance Material," *FERRO-11 and 3rd ICTRC—Proceedings of the 11th International Symposium on Ferrocement and 3rd International Conference on Textile Reinforced Concrete*, W. Brameshuber, ed., Aachen, NRW, Germany, 2015, pp. 15-34.

17. Michler, H., "Segmentbrücke aus Textilbewehrtem Beton – Rottachsteg Kempten im Allgäu," *Beton- und Stahlbetonbau*, V. 108, No. 5, May 2013, pp. 325-334. doi: 10.1002/best.201300023

18. Hegger, J.; Goralski, C.; and Kulas, C., "Schlanke Fußgängerbrücke aus Textilbeton: Sechsfeldrige Fußgängerbrücke mit einer Gesamtlänge von 97 m," *Beton- und Stahlbetonbau*, V. 106, No. 2, Feb. 2011, pp. 64-71. doi: 10.1002/best.201000081

19. Curbach, M.; Graf, W.; Jesse, D.; Sickert, J.-U.; and Weiland, S., "Segmentbrücke aus Textilbewehrtem Beton: Konstruktion, Fertigung, Numerische Berechnung," *Beton- und Stahlbetonbau*, V. 102, No. 6, June 2007, pp. 342-352. doi: 10.1002/best.200700550

20. Raupach, M., and Morales Cruz, C., "Textile-Reinforced Concrete: Selected Case Studies," *Textile Fibre Composites in Civil Engineering*, T. Triantafillou, ed., Woodhead Publishing, Sawston, UK, 2016, pp. 275-299.

21. Scheerer, S.; Chudoba, R.; Garibaldi, M. P.; and Curbach, M., "Shells Made of Textile Reinforced Concrete – Applications in Germany," *Journal of the International Association for Shell and Spatial Structures*, V. 58, No. 1, Mar. 2017, pp. 79-93. doi: 10.20898/j.iass.2017.191.846

22. Kulas, C. H., "Zum Tragverhalten Getränkter Textiler Bewehrungselemente für Betonbauteile," PhD thesis, RWTH Aachen University, Aachen, NRW, Germany, 2013, 402 pp. (in German)

23. Beckmann, B.; Bielak, J.; Scheerer, S.; Schmidt, C.; Hegger, J.; and Curbach, M., "Standortübergreifende Forschung zu Carbonbetonstrukturen im SFB/TRR 280," *Bautechnik*, V. 98, No. 3, Mar. 2021, pp. 232-242. doi: 10.1002/bate.202000116

24. Rempel, S.; Kulas, C.; Will, N.; and Bielak, J., "Extremely Light and Slender Precast Pedestrian-Bridge Made Out of Textile Reinforced Concrete (TRC)," *High Tech Concrete: Where Technology and Engineering Meet: Proceedings of the 2017* fib *Symposium, held in Maastricht, The Netherlands, June 12-14, 2017*, D. A. Hordijk and M. Luković, eds., Springer, Cham, Switzerland, 2018, pp. 2530-2537.

25. Helbig, T.; Unterer, K.; Kulas, C.; Rempel, S.; and Hegger, J., "Fuß- und Radwegbrücke aus Carbonbeton in Albstadt-Ebingen: Die Weltweit erste Ausschließlich Carbonfaserbewehrte Betonbrücke," *Beton- und Stahlbetonbau*, V. 111, No. 10, Oct. 2016, pp. 676-685. doi: 10.1002/best.201600058

26. RILEM Technical Committee 232-TDT, "Recommendation of RILEM TC 232-TDT: Test Methods and Design of Textile Reinforced Concrete: Uniaxial Tensile Test: Test Method to Determine the Load Bearing Behavior of Tensile Specimens Made of Textile Reinforced Concrete," *Materials and Structures*, V. 49, No. 12, Dec. 2016, pp. 4923-4927.

27. Jesse, F., "Tragverhalten von Filamentgarnen in Zementgebundener Matrix," PhD dissertation, Dresden University of Technology, Dresden, Saxony, Germany, 2004, 366 pp. (in German)

28. De Santis, S.; Carozzi, F. G.; de Felice, G.; and Poggi, C., "Test Methods for Textile Reinforced Mortar Systems," *Composites Part B: Engineering*, V. 127, Oct. 2017, pp. 121-132. doi: 10.1016/j.compositesb.2017.03.016

29. Molter, M., "Zum Tragverhalten von Textilbewehrtem Beton," PhD dissertation, RWTH Aachen University, Aachen, NRW, Germany, 2005, 221 pp. (in German)

30. John, S. K.; Nadir, Y.; Girija, K.; and Giriprasad, S., "Tensile Behaviour of Glass Fibre Textile Reinforced Mortar with Fine Aggregate

Partially Replaced by Fly Ash," *Materials Today: Proceedings*, V. 27, Part 1, 2020, pp. 144-149. doi: 10.1016/j.matpr.2019.09.135

31. Saidi, M., and Gabor, A., "Experimental Analysis of the Tensile Behaviour of Textile Reinforced Cementitious Matrix Composites Using Distributed Fibre Optic Sensing (DFOS) Technology," *Construction and Building Materials*, V. 230, Jan. 2020, Article No. 117027. doi: 10.1016/j.conbuildmat.2019.117027

32. Zhang, M., and Deng, M., "Tensile Behavior of Textile-Reinforced Composites Made of Highly Ductile Fiber-Reinforced Concrete and Carbon Textiles," *Journal of Building Engineering*, V. 57, Oct. 2022, Article No. 104824. doi: 10.1016/j.jobe.2022.104824

33. Heins, K.; Kimm, M.; Olbrueck, L.; May, M.; Gries, T.; Kolkmann, A.; Ryu, G.-S.; Ahn, G.-H.; and Kim, H.-Y., "Long-Term Bonding and Tensile Strengths of Carbon Textile Reinforced Mortar," *Materials*, V. 13, No. 20, Oct. 2020, Article No. 4485. doi: 10.3390/ma13204485

34. Yin, S.-P.; Li, Y.; Jin, Z.-Y.; and Li, P.-H., "Interfacial Properties of Textile-Reinforced Concrete and Concrete in Chloride Freezing-and-Thawing Cycle," *ACI Materials Journal*, V. 115, No. 2, Mar. 2018, pp. 197-208.

35. Donnini, J.; Chiappini, G.; Lancioni, G.; and Corinaldesi, V., "Tensile Behaviour of Glass FRCM Systems with Fabrics' Overlap: Experimental Results and Numerical Modeling," *Composite Structures*, V. 212, Mar. 2019, pp. 398-411. doi: 10.1016/j.compstruct.2019.01.053

36. Ortolan, V. K., "Estudo de Matriz Cimentícia Reforçada com Fibra Têxtil para Uso em Painéis," PhD thesis, Universidade do Vale do Rio dos Sinos, São Leopoldo, RS, Brazil, 2021, 290 pp. (in Portuguese)

37. Gopinath, S.; Gettu, R.; and Iyer, N. R., "Influence of Prestressing the Textile on the Tensile Behaviour of Textile Reinforced Concrete," *Materials and Structures*, V. 51, No. 3, June 2018, Article No. 64. doi: 10.1617/s11527-018-1194-z

38. Butler, M.; Hempel, R.; and Schiekel, M., "The Influence of Short Glass Fibres on the Working Capacity of Textile Reinforced Concrete," *Proceedings of ICTRC'2006 - 1st International RILEM Conference on Textile Reinforced Concrete*, J. Hegger, W. Brameshuber, and N. Will, eds., Aachen, NRW, Germany, 2006, pp. 45-54.

39. Hinzen, M., and Brameshuber, W., "Load-Bearing Behaviour of Textile Reinforced Concrete with Short Fibres," *8th RILEM International Symposium on Fibre Reinforced Concrete: Challenges and Opportunities (BEFIB 2012)*, J. A. O. Barros, ed., Guimarães, Portugal, 2012, pp. 254-266.

40. Barhum, R., and Mechtcherine, V., "Effect of Short, Dispersed Glass and Carbon Fibres on the Behaviour of Textile-Reinforced Concrete Under Tensile Loading," *Engineering Fracture Mechanics*, V. 92, Sept. 2012, pp. 56-71. doi: 10.1016/j.engfracmech.2012.06.001

41. Barhum, R., and Mechtcherine, V., "Influence of Short Dispersed and Short Integral Glass Fibres on the Mechanical Behaviour of Textile-Reinforced Concrete," *Materials and Structures*, V. 46, No. 4, Apr. 2013, pp. 557-572. doi: 10.1617/s11527-012-9913-3

42. Gong, T.; Heravi, A. A.; Alsous, G.; Curosu, I.; and Mechtcherine, V., "The Impact-Tensile Behavior of Cementitious Composites Reinforced with Carbon Textile and Short Polymer Fibers," *Applied Sciences*, V. 9, No. 19, Oct. 2019, Article No. 4048. doi: 10.3390/app9194048

43. Mansur de Castro Silva, R., and de Andrade Silva, F., "Carbon Textile Reinforced Concrete: Materials and Structural Analysis," *Materials and Structures*, V. 53, No. 1, Feb. 2020, Article No. 17. doi: 10.1617/s11527-020-1448-4

44. Christ, R., "Proposição de um Método de Dosagem para Concretos de Ultra Alto Desempenho (UHPC)," PhD thesis, Universidade do Vale do Rio dos Sinos, São Leopoldo, RS, Brazil, 2019, 154 pp. (in Portuguese)

45. ABNT NBR 5739:2018, "Concreto — Ensaio de Compressão de Corpos de Prova Cilíndricos," Associação Brasileira de Normas Técnicas, Rio de Janeiro, RJ, Brazil, 2018, 13 pp.

46. ABNT NBR 8522-1:2021, "Concreto Endurecido — Determinação dos Módulos de Elasticidade e de Deformação: Parte 1: Módulos Estáticos à Compressão," Associação Brasileira de Normas Técnicas, Rio de Janeiro, RJ, Brazil, 2021, 24 pp.

47. Dalazen, C. D. A., "Reforço à Flexão de Vigas em Concreto Armado com a Utilização de Argamassa Reforçada com têxteis de Carbono e de Vidro," master's thesis, Federal University of Rio Grande do Sul, Porto Alegre, RS, Brazil, 2021, 142 pp. (in Portuguese)

48. ASTM D885/D885M-10A(2014)e1, "Standard Test Methods for Tire Cords, Tire Cord Fabrics, and Industrial Filament Yarns Made from Manufactured Organic-Base Fibers (Withdrawn 2023)," ASTM International, West Conshohocken, PA, 2014.

49. Bruckermann, O., "Zur Modellierung des Zugtragverhaltens von Textilbewehrtem Beton," PhD thesis, RWTH Aachen University, Aachen, NRW, Germany, 2007, 198 pp. (in German)

ACI Faculty Network

Why Join the Faculty Network?

The Faculty Network is a support group for educators interested in ACI and the concrete industry. Members receive notifications about classroom resources, fellowships and scholarships, funding for research, online learning, and calls for papers and presenters.

Free 1-Year Educator Membership

ACI offers complimentary membership to teaching professionals who have not been an ACI member within the past 5 years.

Free Desk Copies

Faculty Network members can request a complimentary print or PDF copy of:

- ACI CODE-318 Building Code Requirements for Structural Concrete and Commentary (includes a free subscription to ACI 318 PLUS)
- ACI CODE-530 Building Code Requirements and Specification for Masonry Structures and Companion Commentaries
- ACI CODE-562 Assessment, Repair, and Rehabilitation of Existing Concrete Structures—Code and Commentary
- MNL-3(20) Guide to the Code for Assessment, Repair, and Rehabilitation of Existing Concrete Structures
- MNL-5(19) Contractor's Guide to Quality Concrete Construction, 4th Edition
- MNL-17(21) ACI Reinforced Concrete Design Handbook (available digitally with ACI 318 PLUS subscription)
- MNL-66(20) ACI Detailing Manual (available digitally with ACI 318 PLUS subscription)

Networking

ACI hosts a Faculty Network Reception twice a year during the ACI Concrete Conventions, giving an opportunity to exchange ideas and network.

aci 318PLUS+ Faculty Network members receive a complimentary annual subscription that provides users with convenient digital interactive access to ACI CODE-318-25, ACI CODE-318-19, the ACI Detailing Manual, and the numerous design examples in the ACI Reinforced Concrete Design Handbook. The platform allows professors to create custom user notes that can be distributed to the students to view alongside the Code. Student members are provided 1-year access to ACI 318 PLUS when they purchase their printed copy of ACI 318-25 or ACI 318-19 at the student price of $105 (plus shipping).

aci Professors' Workshop
Materials | Pavements | Structures
Sponsor: aci Foundation

The Professors' Workshop is designed to provide instructors in civil engineering, architecture, architectural engineering, materials science, and construction management programs the tools to engage students in the latest developments in concrete design, construction, and materials.

aci Foundation
Building the Future

The Concrete Research Council (CRC) seeks concrete research projects that further the knowledge and sustainability of concrete materials, construction, and structures in coordination with ACI Committees. Annual Request for Proposals (RFP) are received annually between August 1 and December 1.

aci
American Concrete Institute
Always advancing

ADVANCE YOUR CLASSROOM WITH ACI

JOIN OR RENEW TODAY! concrete.org/educatorsandresearchers

REVIEWERS IN 2024

In 2024, the individuals listed on these pages served as technical reviewers of papers offered for publication in ACI periodicals. A special "thank you" to them for their voluntary assistance in helping ACI maintain the high quality of its publication program.

A, Selva Ganesa Moorthi
IIT Madras
Chennai, Tamil Nadu, India

A, Suresh Kumar
Kalasalingam Academy of Research and Education
Krishnan Kovil, Tamil Nadu, India

A. Abbas, Waleed
University of Technology
Al-Sinaa Street, Baghdad, Iraq

Aaleti, Sriram
University of Alabama
Tuscaloosa, AL, United States

Abbas, Abdelgadir
Carleton University
Ottawa, ON, Canada

Abbas, Zainab
Babylon, Iraq

Abd El-Aleem, Saleh
Fayoum University- Faculty of Science
El-Fayoum, Egypt

Abd Elrahman, Mohamed
TU Berlin
Berlin, Germany

Abd Elrazek, Mostafa
Assiut, Egypt

Abdalla, Hany
College of Technological Studies
Shuwaikh, Kuwait

Abdalla, Jamal
American University of Sharjah
Sharjah, United Arab Emirates

Abdallah, Amr
University of Manitoba
Winnipeg, MB, Canada

Abdel Shafy, Yasser
El Mina High Technology Institute
Beni Suef, Egypt

Abdelazim, Waseem
Universite de Sherbrooke
Sherbrooke, QC, Canada

Abd-Elfatah, Sahar
Higher Institute for Engineering and Technology
Alexandria, Egypt

Abdelgader, Hakim
Tripoli University
Tripoli, Libyan Arab Jamahiriya

Abdelkader, Ahmed
Horus University
Mansoura, Egypt

Abdellatef, Mohammed
University of New Mexico
Albuquerque, NM, United States

Abdulla, Nwzad
University of Salahaddin
Erbil, Iraq

Abdullah, Ahmad
Aswan University
Sahary City, Aswan, Egypt

Abdullah, Saman
University of California, Los Angeles
Los Angeles, CA, United States

Abdul-Razzaq, Khattab
University of Diyala
Diyala, Iraq

Abed, Ziyad
University of Technology - Iraq
Baghdad, Baghdad, Iraq

Abejide, Samuel
Walter Sisulu University - Buffalo City Campus
East London, Eastern Cape, South Africa

Abellan-García, Joaquin
Universidad del Norte
Barranquilla, Colombia

Abo-Shadi, Nagi
Robert Englekirk Inc.
Santa Ana, CA, United States

Abouhussien, Ahmed
GE-Hitachi Nuclear Energy International, LLC
Markham, ON, Canada

Abousnina, Rajab
University of Southern Queensland
Toowoomba, QLD, Australia

REVIEWERS IN 2024

Abu Obeidah, Adi
Piscataway, NJ, United States

Abu Taqa, Ala
Qatar University
Doha, Qatar

Abu Yosef, Ali
Pivot Engineers
Austin, TX, United States

Abu-Abaileh, Adham
GSG Consultants Inc.
Schaumburg, IL, United States

Abubakri, Shahriar
Rowan University
Glassboro, NJ, United States

Abuzeid, Al-Tuhami
Badr for Consulting and Retrofitting
Ciro, Nasr City, Egypt

Acarturk, Cansu
University of Colorado Boulder
Boulder, CO, United States

Acton, Katherine
University of Saint Thomas
St. Paul, MN, United States

Acun, Bora
UBC Okanagan
Kelowna, BC, Canada

Adak, Dibyendu
National Institute of Technology Meghalaya
Shillong, Meghalaya, India

Addai Boateng, Anthony
The Ohio State University
Columbus, OH, United States

Adinkrah-Appiah, Kwadwo
Sunyani Polytechnic
Sunyani, Ghana

Afif, Rahma
Arab International University (AIU), Faculty of Civil Engineering, Syria
Daraa Governorate, Syrian Arab Republic

Agarwal, Pankaj
Indian Institute of Technology Roorkee
Roorkee, Uttarakhand, India

Agrawal, Unnati
Nagpur, Maharashtra, India

Agustiningtyas, Rudi
Ministry of Public Works and Public Housing
Bandung, Indonesia

Ahani, Elshan
Sahand University of Technology
Tabriz, Islamic Republic of Iran

Ahmad, Seleem
Zagazig University Faculty of Engineering
Zagazig, Egypt

Ahmadi, Jamal
University of Science of Technology
Tehran, Islamic Republic of Iran

Ahmadi Nedushan, Behrooz
Yazd University
Yazd, Yazd, Islamic Republic of Iran

Ahmed, Afaf
Sohar College of Applied Sciences
Sohar, Oman

Ahmed, Ahmed A.
Oregon State University
Corvallis, OR, United States

Ahmed, Ehab A.
Toronto Metropolitan University
Toronto, ON, Canada

Ahmed, Mohamed
Université de Sherbrooke
Sherbrooke, QC, Canada

Ahmed, Mshtaq
King Saud University
Riyadh, Riyadh, Saudi Arabia

Ahn, Seong Ryong
Seoul National University
Seoul, Seoul, Republic of Korea

Akalin, Ozlem
PLUSTECHNO Ltd
İstanbul, Turkey

Akbarzadeh Bengar, Habib
University of Mazandaran
Babolsar, Islamic Republic of Iran

Akiyama, Hiroshi
The Zenitaka Corporation
Tokyo, Japan

Akkaya, Yildir
Istanbul Teknik Universitesi
Istanbul, Maslak, Sariyer, Turkey

Akram, Rameez
University of Engineering and Technology Taxila
Taxila, Pakistan

Alalaily, Hossam
Memorial University of Newfoundland
St. John's, NL, Canada

Alam, A. K. M. Jahangir
Bangladesh University of Engineering and Technology
Dhaka, Bangladesh

Al-Ani, Moustafa
Auckland, New Zealand

Albuquerque, Albéria
Federal Institute of Technological Education of Mato Grosso
Cuiabá, Mato Grosso, Brazil

Alcocer, Sergio
Institute of Engineering, UNAM
Mexico, DF, Mexico

Aldawsari, Salem
Florida State University
Tallahassee, FL, United States

Aldwaik, Mais
Russeifa, Zarqa, Jordan

Alexandre, Pierre
Université de Cergy-Pontoise
Cergy-Pontoise, France

Alghossoon, Abdullah
The Hashemite University
Shafa Badran/Amman, Amman, Jordan

Al-Hadithi, Abdulkader
University of Anbar
Ramadi, Al-Anbar, Iraq

Al-Hamd, Rwayda Kh. S.
Baghdad, Iraq

Ali, Majid
Capital University of Science and Technology
Islamabad, Pakistan

Ali, Shehroze
NFC Institute of Engineering and Fertilizer Research
Faisalabad, Punjab, Pakistan

Al-Kamal, Mustafa
Al-Nahrain University
Baghdad, Iraq

Alkerwei, Rana
Mustansiriyah University
Baghdad, Iraq

Alkhairi, Fadi
Dar Omran
Amman, Jordan

Al-Khateeb, Baha'a
University of Notre Dame
South Bend, IN, United States

Al-Mahaidi, Riadh
Swinburne University of Technology
Melbourne, VIC, Australia

Almuhsin, Bayrak
University of Technology
Karrada, Baghdad, Iraq

Al-Nasra, Moayyad
American University of Ras Al Khaimah School of Engineering
Ras Al Khaimah, United Arab Emirates

Al-Obaidey, Shubbar
University of Technology
Al-Sinaa Street, Baghdad, Iraq

Alqaisi, Shokry
Ibb University
Ibb, Yemen

Al-Rubaye, Salam
University of Nebraska-Lincoln
Lincoln, NE, United States

Al-Sabawy, Abdalkader
Olathe, KS, United States

Alshannaq, Ammar
Yarmouk University Hijjawi Faculty for Engineering Technology
Irbid, Jordan

Alshehri, Saad
SABIC
Jubail Industrial City, East Province, Saudi Arabia

Alsiwat, Jaber
Saudi Consulting Services
Riyadh, Saudi Arabia

Altabey, Wael
Alexandria University
Alexandria, Egypt

Al-Tersawy, Sherif
Higher Technological Instituite
10th of Ramadan City, Sharqia, Egypt

AL-Thairy, Haitham
University of Al-Qadisiyah College of Engineering
Al Diwaniyah, Qadisiyyah Province, Iraq

REVIEWERS IN 2024

Al-Tikrite, Ahmed
Tikrit University
Tikrit, Iraq

Al-Zuheriy, Ahmed
University of Technology Iraq
Baghdad, Baghdad, Iraq

Amir, Sana
Delft University of Technology
Delft, South Holland, Netherlands

Ammasi, Arun Kumar
Vellore Institute of Technology - Chennai Campus
Chennai, Tamil Nadu, India

Andriolo, Francisco
Andriolo Ito Engenharia S/C Ltda
Sao Carlos, Sao Paulo, Brazil

Angulski da Luz, Caroline
Universidade Tecnologica Federal do Parana
Pato Branco, Parana, Brazil

Arafa, Ahmed
Universite de Sherbrooke
Sherbrooke, QC, Canada

Araghi, Hassan
Azad University of South Tehran
Karaj, Tehran, Islamic Republic of Iran

Aras, Murat
Bilecik Şeyh Edebali University
Bilecik, Bilecik, Turkey

Araujo, Guilherme
State University of Campinas Faculty of Technology
Limeira, Brazil

Arce, Gabriel
Virginia Transportation Research Council
Charlottesville, VA, United States

Arcine, Maicon de Freitas
Universidade Federal de São Carlos
Sao Carlos, São Paulo, Brazil

Asadian, Alireza
Concordia University
Montreal, Quebec, Canada

Ashish, Deepankar Kumar
Yonsei University
Seodaemun-gu, Seoul, Republic of Korea

Assaad, Joseph
University of Balamand
Balamand, Lebanon

Attiyah, Ali
University of Kufa
Kufa, Iraq

Awasthi, Siddharth
WSP USA
Los Angeles, CA, United States

Awida, Tarek
SQC International Consultant
Kuwait, Kuwait, Kuwait

Aycardi, Luis
Proyectistas Civiles Asociados
Miami, FL, United States

Aydin, Ertug
Lefke Avrupa Universitesi
Lefke, Cyprus

Ayoub, Muhammad
University of Wollongong
Fairy Meadow, NSW, Australia

Aziiz, Shafan
National Research and Innovation Agency Republic of Indonesia
Surabaya, East Java, Indonesia

Aziz, Omar
Salahaddin University- Hawler
Erbil, Kurdistan Region, Iraq

B S, Meenakshi
KPRIET
Coimbatore, India

B S, Sindu
Structural Engineering Research Centre CSIR
Chennai, India

Bacinskas, Darius
Vilnius Gediminas Technical University
Vilnius, Lithuania

Bae, Baek Il
Hanyang Cyber University
Seoul, Seoul, Republic of Korea

Bahekar, Prasad
Visvesvaraya National Institute of Technology
Nagpur, Maharashtra, India

Bahij, Sifatullah
King Fahd University of Petroleum and Minerals
Dhahran, Dammam, Saudi Arabia

Bajwa, Muhammad
University of Wisconsin Madison
Madison, WI, United States

Balapour, Mo
Susmax
Philadelphia, PA, United States

Balouch, Sana
University of Dundee
Dundee, United Kingdom of Great Britain and Northern Ireland

Bandelt, Matthew
New Jersey Institute of Technology
Newark, NJ, United States

Banerji, Srishti
United States

Bartos, Peter
University of the West of Scotland
Paisley, Scotland, United Kingdom of Great Britain and Northern Ireland

Baty, James
Concrete Foundations Assoc
Mount Vernon, IA, United States

Bawono, Ali Aryo
TUM Create
Singapore, Singapore

Beglarigale, Ahsanollah
Okan Universitesi
Istanbul, Turkey

Bektas, Fatih
Minnesota State University Mankato
Mankato, MN, United States

Benaicha, Mouhcine
AMU
Marseille, France

Benítez, Pablo
Universidad Nacional de Itapúa
Encarnacion, Itapúa, Paraguay

Benmokrane, Brahim
University of Sherbrooke
Sherbrooke, QC, Canada

Bento, Ricardo
PUC Minas em Pocos de Caldas
Pocos de Caldas, Minas Gerais, Brazil

Bentz, Evan
University of Toronto
Toronto, ON, Canada

Bertero, Raul
Universidad de Buenos Aires
Buenos Aires, Argentina

Beyene, Mengesha
Turner-Fairbank Highway Research Center
McLean, VA, United States

Bharadwaj, Keshav
Indian Institute of Science
Bangalore, Karnataka, India

Bhargava, Kapilesh
Bhabha Atomic Research Centre
Mumbai, Maharashtra, India

Bhat, Dhanalakshmi
Manipal Institute of Technology
Udupi District, Karnataka, India

Bhogayata, Ankur
Marwadi Education Foundation's Group of Institutions
Rajkot, Gujarat, India

Bhojaraju, Chandrasekhar
St Joseph Engineering College
Mangalore, Karnataka, India

Bilek, Vlastimil
ZPSV a.s.
Brno, Czech Republic

Bilir, Turhan
İstanbul University-Cerrahpaşa
İstanbul, Turkey

Billah, AHM Muntasir
University of Calgary
Calgary, AB, Canada

Bischoff, Peter
University of New Brunswick
Fredericton, NB, Canada

Blandón Valencia, John
National University of Colombia Medellin
Medellin, Antioquia, Colombia

Blikharskyy, Yaroslav
Lviv Polytechnic National University
Lviv, Ukraine

Bonacci, John
Karins Engineering Group
Sarasota, FL, United States

Borzovič, Viktor
Slovak University of Technology, Faculty of Civil Engineering
Bratislava, Slovakia

Boulfiza, Moh
University of Saskatchewan
Saskatoon, SK, Canada

REVIEWERS IN 2024

Boulifa, Ridha
Mohamed Cherif Messaadia University Souk-Ahras
Souk-Ahras, Algeria

Bouzid, Haytham
Universite Ibn Khaldoun Tiaret
Tiaret, Algeria

Bouzid, Latifa
Oran, Algeria

Brahma, Abdelmalek
Universite Saad Dahlab Blida
Blida, Algeria

Brena, Sergio
University of Massachusetts
Amherst, MA, United States

Brenkus, Natassia
The Ohio State University
Columbus, OH, United States

Brewe, Jared
Palatine, IL, United States

Bui, Linh
Tokyo City University
Setagaya-ku, Japan

Burak Bakir, Burcu
Orta Dogu Teknik Universitesi
Ankara, Turkey

C, Akin
KCG College of Technology
Chennai, India

Calderon, Victor
Walter P Moore
Washington, DC, United States

Campos, Claudia
Universidade Federal Fluminense
Rio de Janeiro, Rio de Janeiro, Brazil

Cano Barrita, Prisciliano
Instituto Politécnico Nacional/CIIDIR Unidad Oaxaca
Oaxaca, OA, Mexico

Canpolat, Orhan
Yildiz Technical University
Istanbul, Esenler, Turkey

Capozucca, Roberto
Faculty of Engineering
Ancona, Italy

Carloni, Christian
Case Western Reserve University
Cleveland, OH, United States

Carlton, Aerik
Exponent
Warrenville, IL, United States

Carpio, Víctor
Escuela Politécnica Nacional
Quito, Pichincha, Ecuador

Carrette, Jordan
University of Manitoba
Winnipeg, MB, Canada

Cascudo, Oswaldo
Universidade Federal de Goias
Goiânia, GO, Brazil

Castillo, Rodrigo
University at Buffalo
Buffalo, NY, United States

Chang, Jeremy
Holmes NZ
Christchurch, New Zealand

Chao, Shih-Ho
The University of Texas at Arlington
Arlington, TX, United States

Chaunsali, Piyush
Indian Institute of Technology Madras
Chennai, India

Chen, Chunhong
Zhenjiang, Jiangsu, China

Cheng, Jianwei
China University of Mining and Technology
Xuzhou, Jiangsu, China

Cheng, Min-Yuan
National Taiwan University of Science and Technology
Taipei, Taiwan, China

Chhom, Amnoth
Novosibirsk State University of Architecture and Civil Engineering
Novosibirsk, Russian Federation

Chiker, Tarek
Universite de Jijel
Jijel, Algeria

Chitty, Francisco
Florida International University College of Engineering & Computing
Miami, FL, United States

Cho, Soon-Ho
Gwangju University
Gwangju, Republic of Korea

Choi, Chang-Sik
Hnayang University
Seoul, Republic of Korea

Chowdhury, Sharmin
Bogazici University
Istanbul, Turkey

Chun, Sung-Chul
Incheon National University
Incheon, Republic of Korea

Cifuentes, Gustavo
Universidade do Estado de Santa Catarina
Joinville, Santa Catarina, Brazil

Cladera, Antoni
University of the Balearic Islands
Palma, Balearic Islands, Spain

Cleland, Ned
Blue Ridge Design Inc.
Winchester, VA, United States

Climent, Miguel
University of Alacant
Alacant, Spain

Coleman, Zachary
Fort Lauderdale, FL, United States

Conforti, Antonio
University of Brescia
Brescia, Brescia, Italy

Correal, Juan
Universidad de los Andes
Bogota, Cundinamarca, Colombia

Dadsetan, Sina
Master Builders Solutions Admixtures US LLC
Brampton, ON, Canada

Dadvar, Sayyed Ali
University of Sherbrooke
Sherbrooke, QC, Canada

Daugevičius, Mykolas
Vilnius Gediminas Technical University
Vilnius, Lithuania

Dauji, Saha
Bhabha Atomic Research Centre
Mumbai, Maharashtra, India

Deb, Arghya
Indian Institute of Technology, Kharagpur
Kharagpur, West Bengal, India

DeFord, Harvey
Florida Department of Transportation
Gainesville, FL, United States

Degtyarev, Vitaliy
Home
Lexington, SC, United States

Delalibera, Rodrigo
University of São Paulo
São Carlos, São Paulo, Brazil

Demis, Sotiris
University of Patras
Patra, Greece

Desai, Vijay
Central Water and Power Research Station
Pune, Maharashtra, India

Dhole, Rajaram
Katy, TX, United States

Dhonde, Hemant
University of Houston
Houston, TX, United States

Do, Quang
The University of Queensland
Brisbane, QLD, Australia

Dogan, Unal
Istanbul Technical University
Istanbul, Turkey

Dogra, Purnima
Thapar Institute of Engineering and Technology
Patiala, Punjab, India

Dolan, Charles
University of Wyoming
Laramie, WY, United States

Domaneschi, Marco
Politecnico di Torino
Torino, Piedmont, Italy

Dong, Jiangfeng
Sichuan University
Chengdu, China

Dong-Qiu, Lan
Beijing University of Technology
Beijing, Beijing, China

REVIEWERS IN 2024

Donmez, Abdullah
Istanbul Teknik Universitesi
Istanbul, Turkey

Drury, Jonathan
Simpson Gumpertz & Heger Inc.
Waltham, MA, United States

Du, Lianxiang
The University of Alabama at Birmingham
Birmingham, AL, United States

Du, Yingang
Anglia Ruskin University
Chelmsford, United Kingdom of Great Britain and Northern Ireland

Duanmu, Xiangyong
Shanghai, Shanghai, China

Dundar, Cengiz
Cukurova University
Adana, Turkey, Turkey

Dwairi, Hazim
The Hashemite University
Zarqa, Zarqa, Jordan

Dyba, Marcin
Tadeusz Kosciuszko Cracow University of Technology Faculty of Civil Engineering
Krakow, Lesserpoland, Poland

Dymond, Ben
Northern Arizona University
Flagstaff, AZ, United States

Eid, Fatma
Menoufia University
Shebin El-Kom, Egypt

El Sayed, Mohamed
NTH Consultants Ltd.
Northville, MI, United States

El-Ariss, Bilal
United Arab Emirates University
Al Ain, United Arab Emirates

El-Dash, Karim
College of Technological Studies
Kuwait, Kuwait

El-Gendy, Mohammed
Winnipeg, MB, Canada

El-Hassan, Hilal
United Arab Emirates University Faculty of Engineering
Al Ain, United Arab Emirates

Eljadei, Abdelatee
Personal
Pittsburgh, PA, United States

El-Maaddawy, Tamer
United Arab Emirates University
Al-Ain, Abu Dhabi, United Arab Emirates

Elmasry, Mohamed Ihab
Arab Academy for Science Technology and Maritime Transport College of Engineering and Technology
Alexandria, Egypt

Elnady, Mohamed
Mansoura University
Vancouver, BC, Canada

El-Refaie, Sameh
El-Gama City, Mataria, Cairo, Egypt

El-Salakawy, Ehab
University of Manitoba
Winnipeg, MB, Canada

El-Sayed, Ahmed
University of Sherbrooke
Sherbrooke, QC, Canada

Eltahawy, Reham
Ain Shams University
Cairo, Egypt

Eng, Tian Zi
Nanjing University of Aeronautics and Astronautics
Nanjing, China

Erdil, Elif Firuze
Akdeniz Universitesi
Antalya, Turkey

Etman, Emad
El-Mahalla El-Kobra, Egypt

Ewis, Ahmed
Cairo, Egypt

Fadaee, Mostafa
Concordia University Department of Building Civil and Environmental Engineering
Montreal, QC, Canada

Faleschini, Flora
University of Padova
Padova, Italy

Fan, Shengxin
Nanyang Technological University
Singapore, Singapore

Fanella, David
Concrete Reinforcing Steel Institute
Schaumburg, IL, United States

Fantilli, Alessandro Pasquale
Politecnico di Torino
Torino, Italy

Fares, Ali
Sultan Qaboos University College of Engineering
Muscat, Oman

Fargier, Luis
Kiewit Infrastructure Engineers
Englewood, CO, United States

Farivar, Behzad
University of Arkansas Fayetteville
Fayetteville, AR, United States

Farrag, Sharef
Rutgers University
Piscataway, NJ, United States

Farzam, Masood
Structural Engineering
Tabriz, Islamic Republic of Iran

Fatemi, Hassan
Montreal, QC, Canada

Fattuhi, Nijad
Birmingham, United Kingdom of Great Britain and Northern Ireland

Ferche, Anca-Cristina
Austin, TX, United States

Fernandes, Fernando Antonio da Silva
Federal University of Pará - Campus Salinópolis - Faculty of Engineering
Salinópolis, Pará, Brazil

Fernandez Montes, David
Madrid, Spain

Fiset, Mathieu
Université du Québec à Chicoutimi
Chicoutimi, QC, Canada

Fitik, Birol
Hochschule fur Technik Stuttgart
Stuttgart, Germany

Folino, Paula
University of Buenos Aires
Buenos Aires, Argentina

Franco-Lujan, Victor
Tecnologico Nacional de Mexico
Mexico, DF, Mexico

Franklin, Miguel
Construcforms ltda
New York, NY, United States

French, Catherine
University of Minnesota
Minneapolis, MN, United States

Frosch, Robert
Purdue University
West Lafayette, IN, United States

Fu, Tengfei
Fuzhou, Fujian, China

Gąćkowski, Roman
Czestochowa University of Technology
Czestochowa, Poland

Galić, Mirela
University of Split Faculty of Civil Engineering Architecture and Geodesy
Split, Dalmatia, Croatia

Gallandorm, Edith
PCI
Chicago, IL, United States

Gan, Dan
Chongqing, China

Ganesan, N.
National Institute of Technology
Calicut, India

Gao, Lubin
Federal Highway Administration
Washington, DC, United States

Gao, Peng
Hefei University of Technology
Hefei, China

Garcia Troncoso, Natividad Leonor
ESPOL
Guayaquil, Ecuador

Gayed, Ramez
University of Calgary
Calgary, AB, Canada

Genikomsou, Aikaterini
Queen's University
Kingston, ON, Canada

REVIEWERS IN 2024

Ghahremannejad, Masoud
The University of Texas at Arlington
Arlington, TX, United States

Ghanem, Hassan
Beirut Arab University
Tripoli, Lebanon

Ghannoum, Wassim
The University of Texas at Austin
Austin, TX, United States

Gheni, Ahmed
Komar University of Science and Technology
Sulaymania, Iraq

Ghiami Azad, Amir Reza
University of Tehran
Boston, MA, United States

Ghimire, Krishna
Kansas State University
Manhattan, KS, United States

Giduquio, Marnie
National Taiwan University of Science and Technology
Taipei, Taiwan, China

González, Javier
University of Basque Country
Bilbao, Basque Country, Spain

Grandić, Davor
University of Rijeka
Rijeka, Croatia

Guades, Ernesto
University of Guam
Mangilao, Guam

Guan, Bowen
Xi'an, China

Guan, Garfield
Cambridge
Cambridge, United Kingdom of Great Britain and Northern Ireland

Guerrero, Hector
UNAM
Coyoacan, DF, Mexico

Gujar, Pratik
Indian Institute of Technology Madras
Chennai, Tamil Nadu, India

Gujar, Pratik
Texas State University
San Marcos, TX, United States

Gunasekara, Chamila
RMIT University City Campus
Melbourne, VIC, Australia

Guner, Serhan
University of Toledo
Toledo, OH, United States

Guo, Honglei
Wuhan Polytechnic University
Wu Han City, Hu Bei Province, China

Habib, Mohammad
MH and Associates
Tampa, FL, United States

Hadje-Ghaffari, Hossain
John A. Martin & Assoc.
Los Angeles, CA, United States

Han, Baoguo
Dalian University of Technology
Dalian, China

Han, Sun-Jin
Jeonju University
Jeonju, Republic of Korea

Harajli, Mohamed
American University of Beirut
Beirut, Lebanon

Harries, Kent
University of Pittsburgh
Pittsburgh, BA, United States

Hartmann, David
Fort Worth, TX, United States

Hassan, Maan
University of Technology
Baghdad, Baghdad, Iraq

Hassan, Mostafa
University of Connecticut
Storrs, CT, United States

Hassan, Wael
University of Alaska Anchorage
Anchorage, AK, United States

Hassanein, Ahmed
Université de Sherbrooke
Sherbrooke, QC, Canada

Hedegaard, Brock
University of Minnesota Duluth
Duluth, MN, United States

Helmy, Huda
Applied Science international
Durham, NC, United States

Hernandez, Eddisson
Instituto Politecnico Nacional/CIIDIR-Oaxaca
Oaxaca, OA, Mexico

Hernández, Ernesto
University of Canterbury
Christchurch, New Zealand

Hoskere, Vedhus
University of Houston
Houston, TX, United States

Hosseini, Seyed Mohammad
University of Sherbrooke
Sherbrooke, QC, Canada

Hoult, Neil
Toronto, ON, Canada

Hu, Bo
The University of Arizona
Tucson, AZ, United States

Hu, Jiong
University of Nebraska-Lincoln
Omaha, NE, United States

Hu, Nan
South China University of Technology
Guangzhou, Guangdong, China

Hu, Zhong-Wei
Nanjing, China

Huang, Weitao
Foshan, China

Huang, Xiaobao
Oakland University
Rochester, MI, United States

Huang, Yuan
Hunan University
Changsha, Hunan, China

Huber, Patrick
Vienna University of Technology
Vienna, Austria

Hurtado, Pablo E.
Simpson Gumpertz & Heger Inc.
Atlanta, GA, United States

Hussain, Zahid

Huts, Andriy
Politechnika Rzeszowska im Ignacego Lukasiewicza
Rzeszow, Poland

Hwang, Hyeon Jong
Seoul National University
Seoul, Republic of Korea

Hwang, Shyh-Jiann
National Taiwan University
Taipei, Taiwan, China

Ibrahim, Dr. Tamer
Menofia, Egypt

Ibrahim, Taha
Faculty Of Engineering, Benha University
Cairo, Egypt, Egypt

Ichinose, Toshikatsu
Meijo University
Nagoya, Aichi, Japan

Idrees, Maria
University of Engineering and Technology Lahore
Lahore, Punjab, Pakistan

Idrisi, Amir Hussain
Michigan Technological University
Houghton, MI, United States

Ilki, Alper
Istanbul Technical University
Istanbul, Turkey

Immanuel, Sophia
National Institute of Technology Tiruchirappalli
Tiruchirappalli, Tamil Nadu, India

Ioannou, Sokrates
Higher Colleges of Technology
Abu Dhabi, United Arab Emirates

Isik, Ercan
Bitlis Eren Universitesi
Bitlis, Turkey

Ismail, Fouad
Florida International University
Miami, FL, United States

Ismail, Kamaran
The University of Sheffield
Sheffield, United Kingdom of Great Britain and Northern Ireland

Ismail, Mohamed
Memorial University of Newfoundland
St. John's, NL, Canada

REVIEWERS IN 2024

Jagad, Gaurav
Sardar Vallabhbhai National Institute of Technology
Surat, Gujarat, India

Jahami, Ali
University of Balamand Faculty of Engineering
El-Koura, Lebanon

Jaiswal, Ankit
Visvesvaraya National Institute of Technology
Nagpur, Maharastra, India

Janssen, Donald
Seattle, WA, United States

Javed, Ali
Florida International University
Miami, FL, United States

Jazaei, Robabeh
Slippery Rock University of Pennsylvania
Slippery Rock, PA, United States

Jensen, Elin
Lawrence Technological University
Southfield, MI, United States

Jeyaprakash, Maheswaran
St Xavier's Catholic College of Engineering
Chunkankadai, Tamil Nadu, India

Jiang, Hua
McDermott International Inc.
Plainfield, IL, United States

Jiang, Jinyang
Southeast University
Nanjing, China

Jiang, Liying
Jensen Hughes Inc.
Lexington, MA, United States

Ju, Hyunjin
Nazarbayev University
Nur-Sultan, Kazakhstan

Kabashi, Naser
Faculty of Civil Engineering and Architecture
Pristina, Kosovo, Albania

Kalliontzis, Dimitrios
University of California System
San Diego, CA, United States

Kamde, Deepak
Indian Institute of Technology Madras
Chennai, TN, India

Kan, Yu-Cheng
Chaoyang University of Technology
Taichung County, Taiwan, China

Kanakubo, Toshiyuki
University of Tsukuba
Tsukuba, Japan

Kang, Thomas
Seoul National University
Seoul, Republic of Korea

Kankam, Charles
Kwame Nkrumah University of Science & Technology
Kumasi, Ghana

Kanta Rao, Velidandi
Central Road Research Institute
New Delhi, Delhi, India

Kaya, Osman
Mugla Sitki Kocman University
Mugla, Turkey

Keane, Patrick
United States

Kellouche, Yasmina
Universite Hassiba Benbouali de Chlef
Chlef, Algeria

Kenel, Albin
Hochschule Luzern Technik und Architektur
Horw, Lucerne, Switzerland

Khalil, Nariman
University of Balamand
Kelhat, Koura, Lebanon

Khaliq, Wasim
National University of Sciences and Technology
Islamabad, ICT, Pakistan

Khan, Sadaqat Ullah
NED University of Engineering and Technology
Karachi, Sindh, Pakistan

Khanzadeh Moradllo, Mehdi
Temple University
Philadelphia, PA, United States

Khatib, Milad
ISSEA-Cnam Lebanon
Beirut, Lebanon

Kim, Chulgoo
Seoul National University
Seoul, Republic of Korea

Kim, InSung
Degenkolb Engineers
San Francisco, CA, United States

Kim, Taehwan
University of New South Wales
Sydney, NSW, Australia

Kirgiz, Mehmet
Istanbul Universitesi-Cerrahpasa
Istanbul, Turkey

Kopiika, Nadiia
University of Birmingham
Birmingham, United Kingdom of Great Britain and Northern Ireland

Krstulovic-Opara, Neven
ExxonMobil Production Co
Houston, TX, United States

Kulkarni, Abhijit
Pune, Maharashtra, India

Kumar, Mayank
NIT Kurukshetra Haryana
Kurukshetra, Haryana, India

Kupwade-Patil, Kunal
Massachusetts Institute of Technology
Cambridge, MA, United States

Kwan, Albert
The University of Hong Kong
Hong Kong, China

Kytinou, Violetta
Democritus University of Thrace School of Engineering
Xanthi, Greece

Laco, Jan
D-Phase a.s.
Bratislava, Slovakia

Lantsoght, Eva
Delft University of Technology
Delft, Netherlands

Lee, Chang Hoon
Cornell University
Ithaca, NY, United States

Lee, Chung-Sheng
UCSD
La Jolla, CA, United States

Lee, Deuckhang
Chungbuk National University
Cheongju, Republic of Korea

Lee, Hung-Jen
National Yunlin University of Science and Technology
Douliou, Taiwan

Lee, Michael
Dallas, TX, United States

Lekshmi, Sreedevi
Indian Institute of Technology Bombay
Mumbai, India

Lequesne, Rémy
University of Kansas
Lawrence, KS, United States

Li, Bing
Nanyang Technological University
Singapore, Singapore

Li, Faping
Wuhan, China

Li, Fumin
China University of Mining and Technology
Xuzhou, Jiangsu, China

Li, Genfeng
Chongqing University of Arts and Sciences
Chongqing, China

Li, Ning
Tianjin University
Tianjin, Tianjin, China

Li, Wei
Wenzhou University
Wenzhou, Zhejiang, China

Li, Yi-An
National Chung Hsing University
Taichung, Taiwan, China

Lim, Malcolm
MLim Consulting Inc.
Buffalo Grove, IL, United States

LIU, Chengqing
Southwest Jiaotong University
Chengdu, Sichuan, China

Liu, Jing
Railway Engineering Research Institute
Beijng, Beijng, China

Liu, Junshan
Terra Engineering Ltd.
Chicago, IL, United States

REVIEWERS IN 2024

Liu, Kai-Wei (Victor)
Prairie View A&M University
Prairie View, TX, United States

Liu, Leping
Nanning, China

Liu, Peng
Changsha, China

Liu, Xuejian
The University of Texas at Arlington
Arlington, TX, United States

Liu, Zhengyu
Iowa State University of Science and Technology
Ames, IA, United States

Liu, Zhu
Arlington, MA, United States

Lizarazo Marriaga, Juan
Universidad Nacional de Colombia - Sede Bogotá
Bogota, Colombia

Lobo, Colin
National Ready Mixed Concrete Association
Silver Spring, MD, United States

Lowes, Laura
University of Washington
Seattle, WA, United States

Lubell, Adam
Read Jones Christoffersen Ltd
Vancouver, BC, Canada

Luo, Dayou
Iowa State University
Ames, IA, United States

Lutomirska, Marta
Warsaw University of Technology Faculty of Civil Engineering
Warszawa, Poland

Mahdy, Mohamed
Faculty of Engineering, Masoura University
Mansoura, Dakhlia, Egypt

Maheswaran, Chellapandian
Mepco Schlenk Engineering College
Sivakasi, Tamil Nadu, India

Mahfouz, Ibrahim
Cairo, Egypt

Majeed, Hozan
Salahaddin University - Erbil
Erbil, Iraq

Mander, John
Texas A&M University
College Station, TX, United States

Mari, Antonio
Universitat Politecnica de Catalunya
Barcelona, Barcelona, Spain

Marikunte, Shashi
Southern Illinois University
Carbondale, IL, United States

Martinez Andino, Marcos
Desimone Consulting Engneers
Atlanta, GA, United States

Mata, Luis
University of Toledo
Toledo, OH, United States

Matta, Fabio
University of South Carolina
Columbia, SC, United States

McCall, W.
Concrete Engineering Consultants
Charlotte, NC, United States

Milestone, Neil
Callaghan Innovation
Lower Hutt, New Zealand

de Miranda Moraes, Crislayne
Instituto Federal do Pará
Belém, Pará, Brazil

Mirrashid, Masoomeh
Abu Dhabi University
Abu Dhabi, United Arab Emirates

Mirzaee, Alireza
Shiraz, Islamic Republic of Iran

Mishra, Dhanada
KMBB College of Engg and Tech
Khordha, Odisha, India

Mishra, Geetika
Drexel University
Philadelphia, PA, United States

Mitrofanov, Vitalii
Center for Advanced Design Methods of Concrete Structures
Poltava, Ukraine

Mogili, Srinivas
Indian Institute of Technology Delhi
New Delhi, Delhi, India

Mohammed, Tarek
Islamic University of Technology
Gazipur, Dhaka, Bangladesh

Mohee, Fai
TMBN Extrados Inc.
Toronto, ON, Canada

Montoya Coronado, Luis Alberto
Palma, Spain

Moretti, Marina
National Technical University of Athens
Athens, Greece

Mostafa, Mostafa M. A.
Al-Azhar University - Assiut Branch
Qena, Egypt

Mostofinejad, Davood
Isfahan University of Technology
Isfahan, Islamic Republic of Iran

Motter, Christopher
Washington State University
Pullman, WA, United States

Moutassem, Fayez
American University of Ras Al Khaimah
Ras Al Khaimah, United Arab Emirates

MS, Sandeep
Muthoot Institute of Technology and Science
Cochin, Kerala, India

Muciaccia, Giovanni
Politecnico di Milano
Milan, Italy

Mullins, Gray
University of South Florida
Tampa, FL, United States

Murcia-Delso, Juan
Universitat Politècnica de Catalunya - BarcelonaTech
Barcelona, Spain

Murkute, Pratik
VCS Enginering Inc.
Tampa, FL, United States

Murray, Cameron
University of Arkansas Fayetteville
Fayetteville, AR, United States

Murray, Polly
University of Alaska Anchorage
Anchorage, AK, United States

Musselman, Eric
Villanova University
Villanova, PA, United States

Mutsuddy, Rupak
Bangladesh University of Engineering and Technology
Dhaka, Bangladesh

N, Pannirselvam
SRM Institute of Science and Technology
Kanchipuram, Tamil Nadu, India

Nabavi, Seyed Esrafil
Rezvanshahr, Islamic Republic of Iran

Nair, Sooraj
United States Gypsum Corp
Libertyville, IL, United States

Nalon, Gustavo
Universidade Federal de Viçosa
Vicosa, Minas Gerais, Brazil

Namakiaraghi, Parsa
Philadelphia, PA, United States

Narayanan, Subramanian
Gaithersburg, MD, United States

Naser, M. Z.
Clemson University
Clemson, SC, United States

Navarro-Gregori, Juan
Universitat Politecnica de Valencia
Valencia, Valencia, Spain

Nazarimofrad, Ebrahim
Bu-Ali Sina University
Hamedan, Islamic Republic of Iran

Nguyen, Hai
Huntington, WV, United States

Nguyen, Tan
Ton Duc Thang University
Ho Chi Minh City, Viet Nam

Nili, Mahmoud
Bu-Ali Sina University
Hamedan, Islamic Republic of Iran

Nishiyama, Minehiro
Kyoto University
Kyoto, Japan

Noor-E-Khuda, Sarkar
Central Queensland University
Perth, WA, Australia

REVIEWERS IN 2024

Noviari Wibowo, Yosi
Institut Teknologi Sepuluh Nopember
Surabaya, East Java, Indonesia

Nowak-Michta, Aneta
Cracow University of Technology
Cracow, Poland

Nzambi, Aaron
Universidade Federal do Pará
Belem, Pará, Brazil

Ojha, Parmanand
National Council for Cement and Building Materials
Ballabgarh, HR, India

Okumus, Pinar
University at Buffalo
Buffalo, NY, United States

Orakcal, Kutay
Bogazici University
Istanbul, Bebek, Turkey

Orta, Luis
ITESM
Zapopan, JA, Mexico

Ortiz, Albert
Universidad del Valle
Cali, Valle del Cauca, Colombia

Othman, Nor Hazurina
Universiti Tun Hussein Onn Malaysia
Batu Pahat, Johor, Malaysia

Ou, Yu-Chen
National Taiwan University
Taipei, Taiwan, China

Oukaili, Nazar
University of Baghdad
Baghdad, Iraq

Oundhakar, Abhijeet
Invictus Consultancy Services
Navi Mumbai, Maharashtra, India

Ousalem, Hassane
Takenaka Corporation - Research and Development Institute
Inzai, Chiba, Japan

Ozturk, Onur
Cornell University
Ithaca, NY, United States

Pacheco, Alexandre
Universidade Federal do Rio Grande do Sul (UFRGS)
Porto Alegre, RS, Brazil

Pacheco, Jose
MJ2 Consulting
Chicago, IL, United States

Palieraki, Vasiliki
National Technical University of Athens
Athens, Zografou, Greece

Pan, Wang Fook
SEGi University
Petaling Jaya, Selangor, Malaysia

Panchmatia, Parth
Kansas State University
Manhattan, KS, United States

Pandit, Poornachandra
Manipal Institute of Technology
Manipal, India

Pantazopoulou, Stavroula
York University - Keele Campus
Toronto, ON, Canada

Parsekian, Guilherme
UFSCar
Sao Carlos, Brazil

Pattaje, Karthik
Wiss, Janney, Elstner Associates, Inc.
Northbrook, IL, United States

Paulson, Conrad
Wiss, Janney, Elstner Associates, Inc.
Pasadena, CA, United States

Peng, Fei
Hunan University
Changsha, China

Perceka, Wisena
Parahyangan Catholic University Faculty of Engineering
Bandung, West Java, Indonesia

Perez Caldentey, Alejandro
Universidad Politécnica de Madrid
Madrid, Madrid, Spain

Persson, Bertil
Bara, Sweden

Piccinin, Roberto
Hilti, Inc.
Tulsa, OK, United States

Pincheira, Jose
University of Wisconsin
Madison, WI, United States

Proestos, Giorgio
North Carolina State University
Raleigh, NC, United States

Pugliaro, Andrea
Senior Materials and Laboratory Engineer (Civil and Geotechnical)
Savona, Italy

Putra Jaya, Ramadhansyah
Universiti Teknologi Malaysia
Gambang, Pahang, Malaysia

Qissab, Musab
Al-Nahrain University
Baghdad, Iraq

Quintana Gallo, Patricio
Czech Technical University in Prague
Praha, Czech Republic

Rafi, Muhammad
NED University of Engineering and Technology
Karachi, Sindh, Pakistan

Ragheb, Wael
Alexandria University
Windsor, ON, Canada

Rahal, Khaldoun
Kuwait University
Safat, Kuwait

Rajbanshi, Soumi
Indian Institute of Technology Guwahati
Guwahati, Assam, India

Ramanathan, Sivakumar
University of Miami - Coral Gables Campus
Coral Gables, FL, United States

Ramaswamy, Ananth
Indian Institute of Science
Bangalore, Karnataka, India

Ramirez Garcia, Alberto
University of Arkansas
Fayetteville, AR, United States

Ramirez, Julio
Purdue University
West Lafayette, IN, United States

Rashad, Alaa
Housing and Building National Research Center
Giza, Egypt

Rautenberg, Jeffrey
Wiss, Janney, Elstner Associates, Inc.
Emeryville, CA, United States

Razaqpur, A. Ghani
McMaster University
Hamilton, ON, Canada

Reese, Garth
Raba Kistner
San Antonio, TX, United States

Ridha, Maha (Lianne)
Melbourne, VIC, Australia

Rieder, Klaus
Unterschleissheim, Germany

Rodrigues, Conrado
Federal Centre for Technological Education in Minas Gerais, CEFET-MG
Belo Horizonte, Minas Gerais, Brazil

Rodriguez, Mario
National Autonomous University of Mexico
Mexico, DF, Mexico

Rojas-Leon, Matias
University of California, Los Angeles
Los Angeles, CA, United States

Ross, Brandon
Clemson University
Clemson, SC, United States

Russo, Gaetano
University of Udine
Udine, Udine, Italy

Saeed, Yasir
Portland State University
Portland, OR, United States

Safiuddin, Md.
George Brown College
Toronto, ON, Canada

Sahoo, Kirtikanta
Rourkela, India

Said, Shwan
Erbil, Iraq

Salib, Sameh
Markham, ON, Canada

Sanaei Ataabadi, Hossein
Yasouj University
Yasouj, Kohgiluyeh and Boyerahmad, Islamic Republic of Iran

Santos, Daniel
University of Sao Paulo Polytechnic School
Sao Paulo, Sao Paulo, Brazil

REVIEWERS IN 2024

Santos, Jose
University of Madeira
Funchal, Portugal

Santos, Sérgio
SBS Engineering Consultancy
Goiânia, Goiás, Brazil

Sapp, James
ATMI Precast
Aurora, IL, United States

Sarkar, Manas
Zhejiang University
Hangzhou, Zhejiang, China

Sarkhosh, Reza
The Hague, South-Holland, Netherlands

Sarkis Fernandez, Ana Isabel
Vancouver, BC, Canada

Sato, Yuichi
Kyoto University
Kyoto, Kyoto, Japan

Sayed Ahmed, Mahmoud
Toronto Metropolitan University
Toronto, ON, Canada

Seco, Laura
Coimbra, Portugal

Semelawy, Mohamed
Western University
London, ON, Canada

Sengupta, Amlan
Indian Institute of Technology Madras
Chennai, Tamil Nadu, India

Sennour, Larbi
Consulting Engineers Group
San Antonio, TX, United States

Sezen, Halil
The Ohio State University
Columbus, OH, United States

Shabana, Islam
University of Sherbrooke
Sherbrooke, QC, Canada

Shafigh, Payam
Wenzhou University of Technology
Wenzhou, Zhejiang, China

Shang, Ziduan
Shanghai Nuclear Engineering Research and Design Institute
Shanghai, China

Sharifzad, Shayan
The University of Texas at Arlington College of Engineering
Arlington, TX, United States

Shayan, Ahmad
ARRB Group
Vermont South, VIC, Australia

Shehata, Medhat
Toronto Metropolitan University
Toronto, ON, Canada

Sheikh, Shamim
University of Toronto
Toronto, ON, Canada

Shekarchi, William
Austin, TX, United States

Shen, Yin
Tongji University
Shanghai, China

Sherman, Matthew
Simpson Gumpertz & Heger Inc.
Melrose, MA, United States

Shi, Caijun
Hunan University
Changsha, Hunan, China

Shi, Zhongqi
National Science and Technology Institute of Urban Safety
Shenzhen, Guangdong, China

Shivali, Ram
Central Soil and Materials Research Station
New Delhi, India

Shumuye, Eskinder Desta
Shenzhen University College of Civil and Transportation Engineering
Shenzhen, GD, China

Siddique, Mohammad
Bangladesh University of Engineering and Technology
Dhaka, Bangladesh

Silfwerbrand, Johan
KTH Royal Institute of Technology
Stockholm, Sweden

Singh, Harvinder
Guru Nanak Dev Engineering College
Ludhiana, Punjab, India

Singh, Navdeep
Jalandhar, Punjab, India

Smadi, Mohammad
Jordan University of Science and Technology
Irbid, Jordan

Sneed, L.
University of Illinois Chicago
Chicago, IL, United States

Soares, Renan
Universidade Federal de Pernambuco
Recife, Pernambuco, Brazil

Sobolev, Konstantin
University of Wisconsin-Milwaukee
Milwaukee, WI, United States

Solanki, Pranshoo
United States

Soltani, Masoud
Tarbiat Modares University
Tehran, Tehran, Islamic Republic of Iran

Sonkusare, Hemantkumar
G H Raisoni College of Engineering
Nagpur, Maharashtra, India

Souza, Rafael
Universidade Estadual de Maringá
Maringá, Paraná, Brazil

Souza, Wallace
Universidade Federal do Maranhão
São Luís, Maranhão, Brazil

Spinella, Nino
University of Catania Faculty of Engineering
Catania, Italy

Spyridis, Panagiotis
Institute for Structural Engineering
Vienna, Austria

Stanton, John
University of Washington
Seattle, WA, United States

Stengel, Thorsten
Hochschule für Angewandte Wissenschaften München
Munchen, Germany

Stojadinovic, Bozidar
Swiss Federal Institute of Technology
Zurich, Switzerland

Stucchi, Fernando
University of Sao Paulo Polytechnic School
Adamantina, SP, Brazil

Sun, Tao
Wuhan, China

Surehali, Sahil
Arizona State University
Tempe, AZ, United States

Suryawanshi, Yogesh
JSPM's Imperial College of Engineering and Research Wagholi
Pune, Maharashtra, India

T., Hemalatha
CSIR-Structural Engineering Research Centre
Chennai, Tamil Nadu, India

Tabkhi Wayghan, Amir Reza
Carleton University Faculty of Engineering and Design
Ottawa, ON, Canada

Tabsh, Sami
American University of Sharjah
Sharjah, United Arab Emirates

Tajaddini, Abbas
University of Bath Faculty of Engineering and Design
Bath, United Kingdom of Great Britain and Northern Ireland

Takase, Yuya
Muroran Institute of Technology
Muroran, Hokkaido, Japan

Tang, Chao-Wei
Cheng-Shiu University
Niaosong District, Kaohsiung City, Taiwan, China

Tang, Fujian
Dalian University of Technology
Dalian, Liaoning, China

Tanner, Jennifer
University of Wyoming
Laramie, WY, United States

Tarawneh, Ahmad
The Hashemite University
Zarqa, Jordan

Tariq, Samia
University of Engineering and Technology, Lahore
Lahore, Punjab, Pakistan

Tatiraju, Ramanjaneyulu
North Dakota State University
Fargo, ND, United States

Tavio
Sepuluh Nopember Institute of Technology (ITS)
Surabaya, East Java, Indonesia

REVIEWERS IN 2024

Tawfic, Yasser
Minia University
Minia, Minia, Egypt

Terzioglu, Tevfik
Parsons Corporation
Raleigh, NC, United States

Thokchom, Suresh
Manipur Institute of Technology
Imphal, Manipur, India

Thorstensen, Rein Terje
University of Agder
Grimstad, Norway

Tian, Ying
University of Nevada, Las Vegas
Las Vegas, NV, United States

Tiecher, Francieli
IMED
Passo Fundo, Brazil

Tohidi, Mosleh
University of West London
London, United Kingdom of Great Britain and Northern Ireland

Tomlinson, Douglas
University of Alberta
Edmonton, AB, Canada

Tore, Erkan
Balikesir University
Balikesir, Balikesir, Turkey

Tran, Mien
Ho Chi Minh City University of Technology
Ho Chi Minh City, Viet Nam

Tregger, Nathan
GCP Applied Technologies Inc.
Cambridge, MA, United States

Tripathi, Avinaya
Arizona State University
Tempe, AZ, United States

Turgut, Paki
Inonu Universitesi
Malatya, Turkey

Turk, Ahmet Murat
Istanbul Kultur University
Istanbul, Turkey

Ueda, Naoshi
Kansai University
Suita, Osaka, Japan

Ul Haq, Inzimam
Korea Advanced Institute of Science and Technology
Daejeon, Republic of Korea

Umipig, Jorge
Vistaland & Lifescapes Inc.
Mandaluyong City, Metro Manila, Philippines

Unal, Mehmet
METU
Ankara, Turkey

Ungermann, Jan
RWTH Aachen University
Aachen, Germany

Uzal, Burak
Abdullah Gul University
Kayseri, Turkey

Vaddey, Naga Pavan
CTLGroup
Skokie, IL, United States

Varela-Rivera, Jorge
Universidad Autonoma de Yucatan
Merida, YU, Mexico

Wagner, Elizabeth
Wiss, Janney, Elstner Associates, Inc.
Northbrook, IL, United States

Wahrhaftig, Alexandre
Federal University of Bahia
Salvador, Bahia, Brazil

Wang, Ben
University of Houston
Houston, TX, United States

Wang, Dun
Research Institute of Structural Engineering & Disaster Reduction, Tongji University
Shanghai, China

Wang, Hongze
Inner Mongolia University of Technology
Hohhot, Inner Mongolia, China

Wang, Penggang
Qingdao University of Technology
Qingdao, China

Wang, Shuwei
Qinzhou, Guangxi, China

Wan-Wendner, Roman
Ghent University
Ghent, Belgium

Wardhono, Arie
The State University of Surabaya
Surabaya, Jawa Timur, Indonesia

Wegner, Leon
University of Saskatchewan College of Engineering
Saskatoon, SK, Canada

Wei-Jian, Yi
Changsha, China

Weng, Pu-Wen
National Center for Research on Earthquake Engineering
Taipei, Taipei, Taiwan, China

Werner, Anne
SIUE
Edwardsville, IL, United States

Winnefeld, Frank
EMPA
Duebendorf, Switzerland

Wondimu, Temesgen
Addis Ababa Science and Tech. University
Addis Ababa, Ethiopia

Wu, Chao
Wuhan University of Technology
Wuhan, Hubei, China

Wu, Haikuan
Chengdu, China

Wu, Teng
University at Buffalo, The State University of New York
Buffalo, NY, United States

Wu, Yu-You
Foshan University
Foshan, Guangdong, China

Xi, Xun
University of Strathclyde
Glasgow, Scotland, United Kingdom of Great Britain and Northern Ireland

Xia, Jin
Zhejiang University
Hangzhou, Zhejiang, China

Xiang, Tianyu
Chengdu, Sichuan, China

Xie, Guoshuai
Wuhan University
Wuhan, Hubei, China

Xie, Tianyu
RMIT University
Melbourne, VIC, Australia

Xu, Aimin
ARRB Group
Melbourne, VIC, Australia

Yang, Datian
Nan'an District, Chongqing, China

Yang, Deqiang
Inner Mongolia University of Technology
Hohhot, Inner Mongolia, China

Yang, I-Tung
National Taiwan University of Science and Technology
Taipei, Taiwan, China

Yang, Keun-Hyeok
Kyonggi University
Suwon, Kyonggi-do, Republic of Korea

Yang, Rick
SNC-Lavalin Engineers and Constructors Inc.
Houston, TX, United States

Yang, Shuyan
Yinchuan City, China

Yang, Sung Chul
Hongik University
Mapo-gu, Republic of Korea

Yassein, Mohamed
Abu Dhabi, Abu Dhabi, United Arab Emirates

Yasso, Samir
University of Mosul
Mosul- Bartella, Nineveh, Iraq

Yekrangnia, Mohammad
Shahid Rajaee Teacher Training University
Tehran, Islamic Republic of Iran

Yepez, Fabricio
Universidad San Francisco de Quito
Quito, Pichincha, Ecuador

Yi, Yousun
The University of Texas at Austin
Austin, TX, United States

Yin, Shiping
China University of Mining and Technology
Xuzhou, China

YK, Guru
Indian Institute of Science
Bangalore, India

REVIEWERS IN 2024

Yoon, Young-Soo
Korea University
Seoul, Republic of Korea

Yousefpour, Hossein
Babol Noshirvani University of Technology
Babol, Mazandaran, Islamic Republic of Iran

Youssef, Ahmed
Cairo University
Giza, Giza, Egypt

Yu, Jing
The University of Hong Kong
Hong Kong, Hong Kong, China

Yuan, Qiang
Central South University
Changsha, China

Zandparsa, Kumars
California State University, Long Beach
Long Beach, CA, United States

Zapata, Luis
Universidad Industrial de Santander
Bucaramanga, Santander, Colombia

Zega, Claudio
CONICET
La Plata, Argentina

Zhang, Lihe
LZhang Consulting & Testing Ltd
Delta, BC, Canada

Zhang, Qian
Nanjing, China

Zhang, Qin
Dalian University of Technology
Dalian, Liaoning, China

Zhang, Wei
Tsukuba Daigaku
Tsukuba, Japan

Zhang, Xuejian
Changchun, China

Zhao, Haitao
Hohai University
Nanjing, China

Zhao, Xingzhuang
University of Maryland at College Park
College Park, MD, United States

Zheng, Herbert
Gammon Construction Limited
Hong Kong, Hong Kong, China

Zheng, Yulong
Jiangsu University
Zhenjiang, China

Zhou, Binbin
The National Prestress Engineering Research Center
Nanjing, Jiangsu, China

Zhou, Wei
Harbin Institute of Technology
Harbin, China

ARE YOU A RESEARCHER?

SIGN UP FOR ORCID TODAY!

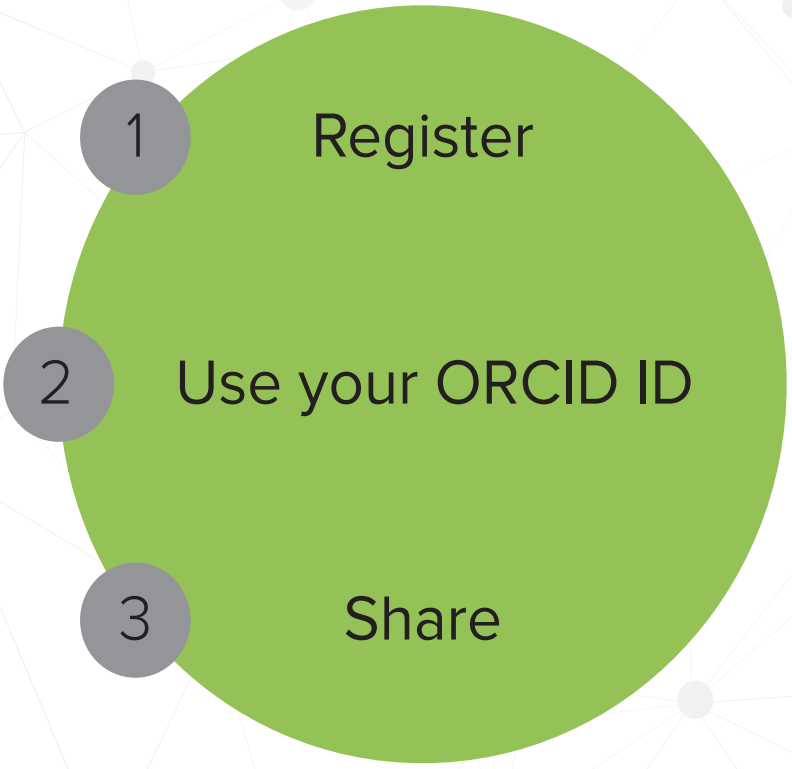

ORCID provides a digital identifier that distinguishes you from every other researcher and, through integration in key research workflows such as manuscript and grant submission, supports automated linkages between you and your professional activities, ensuring that your work is recognized.

ORCID services are FREE and it's as easy as **1-2-3**.

WWW.ORCID.ORG

aci Foundation

Building the Future

We're Building the Future

OUR MISSION

We make strategic investments in ideas, research, and people to create the future of the concrete industry.

Through its councils and programs, the ACI Foundation helps to keep the concrete industry at the forefront of advances in material composition, design, and construction.

OUR FOCUS

- Identifying technologies and innovations which provide needed solutions for the concrete industry
- Seeking concrete research projects that further the knowledge and sustainability of concrete materials, construction, and structures
- Supporting our future concrete innovators and leaders by administering fellowships and scholarships
- Helping honorably discharged veterans with our Veterans Rebate for ACI Certification program

www.acifoundation.org

ACI MATERIALS JOURNAL

The American Concrete Institute (ACI) is a leading authority and resource worldwide for the development and distribution of consensus-based standards and technical resources, educational programs, and certifications for individuals and organizations involved in concrete design, construction, and materials, who share a commitment to pursuing the best use of concrete.

Individuals interested in the activities of ACI are encouraged to explore the ACI website for membership opportunities, committee activities, and a wide variety of concrete resources. As a volunteer member-driven organization, ACI invites partnerships and welcomes all concrete professionals who wish to be part of a respected, connected, social group that provides an opportunity for professional growth, networking, and enjoyment.

American Concrete Institute